Development and experimental validation of a new in-situ geotechnical test - Cyclic CPT, with emphasis on identifying liquefiable soils

Ankit Sharma

THÈSE

Pour obtenir le grade de

DOCTEUR DE L'UNIVERSITÉ GRENOBLE ALPES

École doctorale : I-MEP2 - Ingénierie - Matériaux, Mécanique, Environnement, Energétique, Procédés, Production
Spécialité : 2MGE : Matériaux, Mécanique, Génie civil, Electrochimie
Unité de recherche : Laboratoire Sols, Solides, Structures et Risques

Développement et validation expérimentale d'un nouvel essai géotechnique in-situ - CPT cyclique, avec l'accent mis sur l'identification des sols liquéfiables

Development and experimental validation of a new in-situ geotechnical test - Cyclic CPT, with emphasis on identifying liquefiable soils

Présentée par :

Ankit SHARMA

Direction de thèse :

Bruno CHAREYRE MAITRE DE CONFERENCES HDR, Université Grenoble Alpes	Directeur de thèse
Luc SIBILLE MAITRE DE CONFERENCES, Université Grenoble Alpes	Co-encadrant de thèse
Christophe DANO MAITRE DE CONFERENCES, UNIVERSITE GRENOBLE ALPES	Co-encadrant de thèse

Rapporteurs :

Marcos Arroyo ALVAREZ DE TOLEDO
PROFESSEUR ASSOCIE, Universitat Politècnica de Catalunya
Phillipe REIFFSTECK
DIRECTEUR DE RECHERCHE, Université Gustave Eiffel

Thèse soutenue publiquement le **16 décembre 2022**, devant le jury composé de :

Bruno CHAREYRE MAITRE DE CONFERENCES HDR, Grenoble INP	Directeur de thèse
Marcos Arroyo ALVAREZ DE TOLEDO PROFESSEUR ASSOCIE, Universitat Politècnica de Catalunya	Rapporteur
Fabrice EMERIAULT PROFESSEUR DES UNIVERSITES, Grenoble INP	Président
Phillipe REIFFSTECK DIRECTEUR DE RECHERCHE, Université Gustave Eiffel	Rapporteur

Contents

ABSTRACT

With rapidly growing projects in remote, unexplored sites, finding time and cost efficient methods to identify the potential risks at these sites is becoming imperative. Furthermore, these risks have to be studied for the project's entire life cycle to decide the project viability and often the project design.

This research focuses on developing a new geotechnical test to assess such risks. The test is called **Cyclic CPT** test and uses a mechanical Gouda tip with no embedded sensors. This tip, combined with a cyclic loading module developed by Equaterre Company, enables stress and displacement control of the tip. A robust tip makes this test much more durable and cost-effective, while the possibility to have a stress controlled test, makes it possible to apply a cyclic loading on the tip and therefore on the soil layer.

The current research work focuses on physical modelling of the **Cyclic CPT** test inside a newly built calibration chamber on clean Fontainebleau GA39 sand from Sibelco. This thesis introduces the different steps involved in the **Cyclic CPT** test and the information extracted from them. During the application of uniform stress cycles, the displacement measurement of the tip enables the calculation of stiffness parameters. It is attempted to study the changes of these stiffness parameters during cyclic loading. The dependency of these changes on different conditions of vertical stress, saturation and density is also discussed.

Results from the in-situ campaign are used to demonstrate the possibility and ease of performing this test. At the site, the Cyclic CPT tests are done close to a conventional cone penetration test with pore pressure measurement (CPTu). Robertson method is used to find the Soil Behaviour Index from the CPTu measurements. Further, Boulanger and Robertson methods are used to find the liquefaction resistance of layers at different depth. The analysis of the CPTu data is done using a python code developed during this research work (py-CPT).

Finally, based on the experiences from this research work, the input parameters for future tests and an interpretation methodology to use the results from this test is discussed.

Chapter 1

1. Introduction to in-situ testing and soil liquefaction studies

Civil engineering is the second-oldest engineering discipline after military engineering. It is defined as the engineering discipline that deals with the design, construction, and maintenance of the environment around us, including public works such as roads, bridges, canals, dams, airports, sewerage systems, pipelines, structural components of buildings, and railways.

Geotechnical engineering is a part of civil engineering that deals with acquiring and analysing information about materials of the earth's crust. It also incorporates using this information to solve engineering problems, design engineering works, predict ground response to natural hazards like earthquakes, and make the earth's crust more suitable for human activities.

Geotechnical engineers depend on several tests to perform these tasks. These geotechnical tests are expected to provide a detailed understanding of ground conditions, without which no foundation should be built. In-situ geotechnical tests are often the most precise and cost-effective solution to define these ground conditions. However, most of these in-situ tests conventionally estimate the static properties of in-situ soil to monotonous loading and rely on correlations for predicting the response of the soil to repeated disturbances like the one caused by an earthquake.

Cone Penetration Testing (CPT) is one of the most widely used in-situ geotechnical tests in large portions of the globe. Its repeatability, high speed and relative ease have made it a prevalent option among geotechnical engineers. This test relies on data from several sensors like pore pressure sensor, friction sleeve sensor, tip resistance etc. Using the data from these sensors, the user generally relies on correlations between the measurements and soil properties. However, this test has its limitations and applies a load different to those experienced by soil in real-world events like an earthquake, thus leaving the scope of further research and development.

1.1 Context and objectives of this research work

This PhD aims to develop a new geotechnical test called a "**Cyclic CPT**" and takes place in *3SR Laboratory* in partnership with *Equaterre*. The 3SR laboratory and Equaterre collaborated first in 2015 for the PhD thesis titled : "In-situ identification of liquefiable soils by cyclic static penetrometer: physical and numerical modelling "(Sadrabadi 2019) and also in 2018 for a master thesis titled : "Probing liquefiable soils by cyclic cone penetration"(Celeste 2018). Encouraged by the results of these projects, Equaterre and 3SR decided to start a new PhD that focuses on developing this new cyclic CPT test. This

test was first envisaged by Pierre Riegel from Equaterre (Reigel 2017). This thesis details the progress made towards developing this **Cyclic CPT** test. This new in-situ geotechnical test aims to provide an alternative to current geotechnical tests for assessing liquefaction susceptibility, being a cost-effective and robust option. During this thesis, it was attempted to refine the test methodology and ensure its correct application during field and laboratory experiments. For this, the physical modelling of the **Cyclic CPT** test is done on clean industrial sand inside a calibration chamber. The calibration chamber, the associated loading device and a pluviator for the sand sample preparation were conceptualized during this research work. The field equipment is also refined.

Then, an attempt is made to perform the test under different conditions of vertical stress, saturation and density inside the calibration chamber. The effect of these conditions on the results of the **Cyclic CPT** test is studied, and the interpretation methodology used is explained. During this research, Sibelco's "Fontainebleau GA39" is used for preparing samples at different conditions inside the calibration chamber. During this research, an experimental campaign is also undertaken to characterize the mechanical properties of this sand. In future, it is envisaged to study the liquefaction susceptibility of this sand using established tests like cyclic triaxial testing or CPTu (Cone Penetration Testing with pore pressure and friction sleeve measurements) in well-controlled laboratory conditions and compare the result with the one obtained from the **Cyclic CPT** testing.

This thesis is divided into six chapters. The current chapter introduces soil investigation, liquefaction, methods and challenges to predict liquefaction. It also explains the new **Cyclic CPT** test, the steps involved and information extracted from each step. Chapter 2 of this thesis details the characterization tests performed on Fontainebleau GA39 sand. It also introduces the sample preparation methods and the calibration chamber testing. Chapter 3 of this thesis details the results of the calibration chamber testing undertaken till now. Chapter 4 discusses the tests done in-situ while developing the equipment. It also shows the results of the CPTu analysis using a python code "py-CPT" developed during this research work. Chapter 5 suggest the input parameters for field testing and highlights the suitability of the **Cyclic CPT** test for studying liquefaction susceptibility. Finally, Chapter 6 details the perspective of this research work.

1.2 Soil Investigation

Soil is a challenging engineering material whose properties vary not only in both horizontal and vertical directions but also at the same location with different environmental conditions and time. Therefore, investigating soil for any geotechnical application is a challenging task. Various objectives of any soil investigation for a civil engineering project are: (BS 5930:2015)

- To help choose the best site.
- To establish the suitability of the site and environment for the concerned project.
- To aid in the design of both temporary and permanent structures.
- To help choose the best construction method.
- To predict the soil and surrounding changes due to a new project.

Methods utilized for soil investigation depend on the expected load and the importance of the project. However, all methods can be broadly classified into three broad categories:

1. Open Trial Pits: limited to small projects and shallow excavations
2. Sub Surface Sounding: May involves going to different depths (Standard Penetration Test (SPT), Cone Penetration Test (CPT), Pressuremeter test etc.) or performing tests from the surface (geophysical tests) to indirectly measure key properties of the underlying strata and thus construct a 3D map of the subsoil.
3. Exploratory Borings: Involve retrieving samples of a small cross-section from shallow to deep depths and using them for laboratory testing to find the soil properties.

The laboratory experiments rarely simulate the field conditions. It is also often extremely difficult or expensive to retrieve undisturbed samples, especially for coarse grained soils with little cohesion. Remoulded and disturbed samples often demonstrate properties quite different from their original behaviour. Therefore we mostly rely on in-situ testing for common engineering applications. Moreover, in recent history, the rapid spread of human civilization and continuous growth of all the public works to scales never seen before and to previously unexplored sites has made it mandatory to construct on challenging ground conditions. As such, it is imperative to develop methods to record and measure soil properties by in-situ techniques that can give reliable results in a short time frame and at a low cost.

Most in-situ tests study soil's response to applied disturbances. The disturbance can vary from a penetrating tube or cone, shear waves etc. The difference in behaviour to the applied disturbance/loading helps to distinguish the type of sub-surface material and their state of density and stress.

However, with these in-situ tests, the drainage conditions are not clearly identified, and often the effective stress path applied during the testing may not be able to reproduce design conditions. Another challenge to in-situ tests is that they do not constitute homogeneous mechanical tests. They rather constitute complex boundary value problem in themselves. The response of any particular kind of soil depends on many conditions, including the in-situ stress state and the boundary conditions. As such the intrinsic soil parameters cannot be measured directly. Consequently, the analyses of these in-situ results become very challenging and require expertise and a large data set before reliable

co-relations are formed (Lancellotta 2009). Few of the widely used in-situ tests that are also referenced in Eurocode 7: “Ground investigation and testing" are discussed below:

1.2.1 Pressuremeter tests : PMT

The pressuremeter test PMT, is a test done to measure the in-situ deformation of soil and soft rock caused by the expansion of a cylindrical, flexible membrane under pressure. The original concept of the pressuremeter dates back to Kogler 1933, who developed a device consisting of a rubber bladder clamped at both ends and lowered in a pre-bored hole. Without knowledge of Kogler's work, a French researcher Ménard (1957) developed a much improved pressure meter (PMT), which has been widely used in engineering practice for more than half a century (Benoit and Howie 2014). A schematic of conventional PMT setup is as shown in Figure 1.1(right) from Ali et al 2012. Pressuremeter has a probe containing a cylindrical, flexible membrane which is inserted into the ground either into a pre-formed borehole or by self-boring or by full displacement pushing. Once at a predetermined depth, the membrane is expanded under pressure, and readings of pressure and volume changes are recorded until a maximum expansion for the particular device is reached. As such, we obtain a stress-strain curve that can be used to extract soil properties which in turn may be used in the analytical design of the geotechnical structures. The two main parameters derived from a test in a soil layer are E-Modulus called pressuremeter modulus and limit pressure which by convention is the pressure at which the volume of the expanded cavity doubles. This information can be used to predict the bearing capacity and settlement of foundations, including piles (Briaud and Gerald 1983).

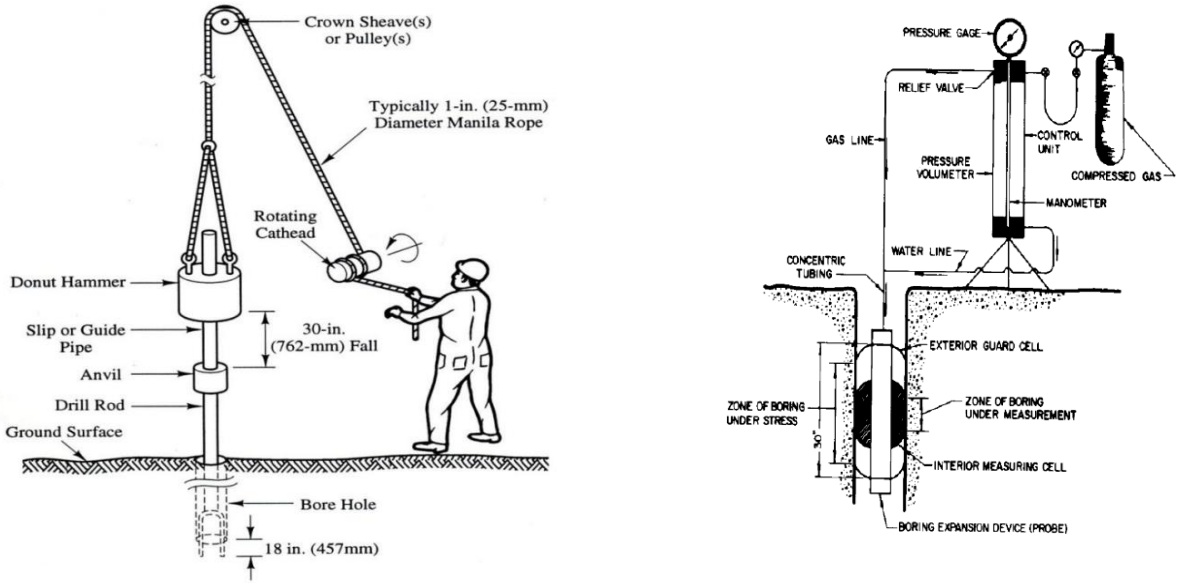

Figure 1.1 Conventional Setup for Standard Penetration Testing (left, from Sarker and Abedin, 2015) and Pressuremeter Testing (right, from Ali et al 2012)

1.2.2 Standard Penetration Testing: SPT

SPT is an in-situ dynamic test that, till recent history, was one of the most widely used subsurface exploration drilling tests. It is mostly used to determine coarse soils' strength and deformation properties. The test procedure is described in ISO 22476-3. In 1902 Colonel Charles R. Gow, owner of the Gow Construction Co. in Boston (USA), began making exploratory borings using 1-inch diameter drive samplers. During the late 1920s and early 1930s, the procedure was standardized by Harry Mohr, one of Gow's engineers. He used a slightly bigger split spoon drive sampler and recorded the number of blow counts per 30.48 cm of penetration. He used a 45.72 cm deep sample round with a 5.08 cm outside diameter while recovering a 3.49 cm diameter sample. The impact was provided by a 63.5 kg hammer dropping 76.2 cm. A schematic of standard SPT test is as shown in Figure 1.1(left) from Sarker and Abedin 2015. In 1947, Terzaghi helped Harry Mohr to develop correlations between bearing capacity and blow counts for sand. The first SPT correlations appeared in "Soil Mechanics in Engineering Practice (1st Ed.)" by Terzaghi and Peck, published in 1948. Over time standardized SPT corrections were introduced to account for variability caused by the efficiency of the hammer, the geometry of the sampler (tip), the length of the rod and also corrections to account for the effect of overburden stress, ageing, particle size etc. (Skempton 1986). This corrected and normalized blow count could be related to the bearing capacity of the soil, resistance of liquefaction using empirical relationships and can be read out from charts.

1.2.3 Flat dilatometer test : DMT

Prof. Marchetti invented the first dilatometer blade in 1974 at the L'Aquila University in Italy. This test consists of a steel blade having a thin and expandable membrane mounted on its surface. The blade is connected to the control-measurement unit by pneumatic wire used to transfer gas pressure exerted on the membrane. The test consists of measuring the pressures required when the membrane is in contact with the surrounding soil, when the displacement in the centre of the membrane reaches 1.10 mm and also the pressure required after the controlled return of the membrane to the position of the first measurement. Using the DMT, dilatometer modulus, horizontal stress index, and coefficient characterizing the water flow conditions of the soil are obtained (Crapps 2006). This information can be used to determine the soil profile and history of stress conditions and to estimate values like undrained shear strength, coefficient of the at-rest earth pressure, over-consolidation stress and deformation modulus.

1.2.3 Field vane test : FVT

The field vane test is carried out with a rectangular vane consisting of four plates fixed at 90 angles to each other, pushed into the soil to the desired depth and rotating until a cylindrical surface in the soil fails by shearing.
A conventional setup for FVT test is represented in Figure 1.2 from Ameratunga et. al. 2016.The torque applied for this is recorded and gives a measure of the shear resistance of the soil. After significant rotation, the soil can be considered remoulded, and remoulded shear strength parameters can also be calculated. A perceived advantage of the FVT is its theoretical model for data interpretation, i.e. lower bound limit analysis for well-defined failure planes. The basic output consists of undrained shear strength (s_{uv}) for undisturbed conditions. Undrained shear strength for remoulded (or "residual") (s_{ur}) conditions can also be obtained. Eventually, the strength sensitivity is defined by $S_t = s_{uv}/s_{ur}$. Empiricism is still required to link this output with the parameter values required for common geotechnical calculation models. These models generally include simplifications so that factors such as strength anisotropy and time-dependency are accounted for only in an approximate manner (Peuchen and Mayne 2007).

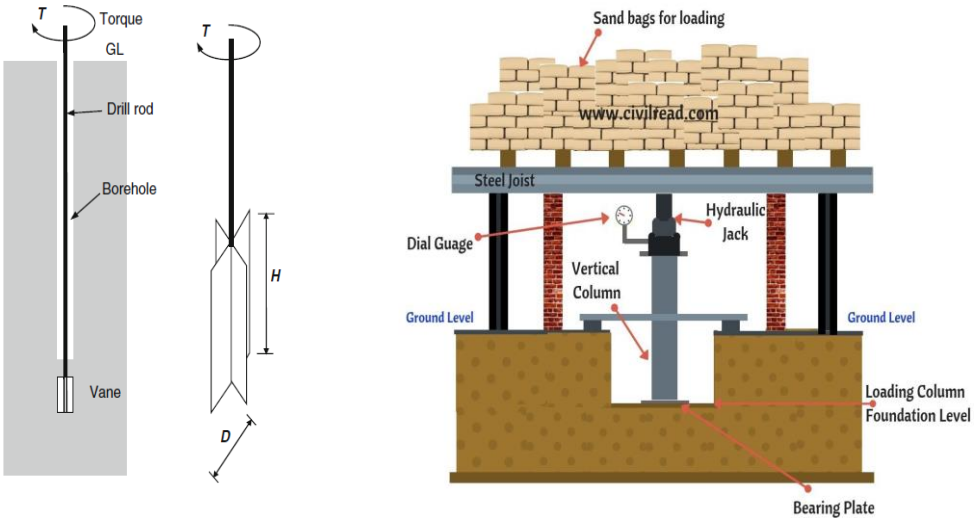

Figure 1.2 Conventional setup for FVT(left – from Ameratunga et. al. 2016) and PLT(right – from Civilread.com)

1.2.5 Plate loading test : PLT

PLT is an in-situ test done generally to find the ultimate bearing capacity of the soil and the probable settlement under a given load. In this test, the vertical deformation is recorded while progressively increasing the load applied on a plate placed on a levelled surface at a depth of concern. At a particular load, the settlement starts increasing rapidly. The total load divided by the area of the plate can be used as the ultimate bearing capacity of the soil at that depth. If there is a uniform soil layer with sufficient depth and the size of the plate is comparable to the foundation planned, the same bearing capacity can be

used directly for the design of the foundation. However, to compute undrained shear strength, the PLT should be conducted at a constant rate of penetration which is fast enough to prevent any drainage. Young's modulus of elasticity and modulus of subgrade reaction can also be estimated using the PLT.

1.2.6 Cone Penetration Testing

The first CPT apparatus dates from 1932, the so-called Barentsen-apparatus. This device was named after civil servant Mr Pieter Barentsen, who was the first to perform a CPT test for a road in the vicinity of Gouda. He did this by pushing a 10 cm cone manually into the ground using his own bodyweight. He was the one who invented a way to accurately measure the resistance of the soil reacting to the conical tip. He inserted an inner rod into the CPT sounding tube and pushed this inner rod annually on the interior part of the conical tip. The soil resistance was read out by means of a hydraulic measuring head provided with a pressure gauge. Consequently, in 1938, Goudsche Machinefabriek and Peter Barentsen got the first patent of cone penetration testing in the field and also became the first manufacturer of CPT equipment on an industrial scale. In 1959, GMF Gouda introduced the first hydraulic pushing rigs for 10 tonnes and later also 20 tonnes capacity. In 1965, H.K.S. Begemann improved the Dutch cone and added an extra sliding shaft for measuring the sleeve friction, resulting in the friction jacket cone, also known as Begemann Cone. In 1970's electric cone penetrometers with strain gauged measuring bodies became more reliable and popular and are widely used to date. Nowadays, cones are equipped with sensors capable of measuring the pore pressure, temperature, electrical resistance, dangerous chemical content etc. Various empirical relationships have been formed that connects the measurements of these sensors to the soil properties. A more detailed discussion of CPTu's use to find soil properties and liquefaction susceptibility can be found in Chapter 4 of this document.

1.2.7 Scope for a new geotechnical test for liquefaction prediction

Conventional pressuremeter test, flat dilatometer test, field vane test and the plate load test are traditionally used to estimate the static properties of in-situ soil and are not apt to be used for predicting soil response to cyclic seismic shear load. Similarly, Standard and Cone Penetration tests even with their benefits of rapid testing and well established correlations for predicting the soil resistance to liquefaction, do not study the stiffness degradation possible with cyclic loading. Attempts have been made to use cyclic pressuremeter tests to do this and have shown positive results for the assessment of stiffness degradation of soil by in-situ cyclic loading. (Kamura and Kazama 2020, Karagiannopoulos 2020). Similarly, attempts have been made to add to information extracted from the conventional CPT by performing tests like incremental loading on the

cone (Reiffsteck et al. 2009) and by using vibrational loading on the cone. (Moon et al. 2013).

Using CPT is much more cost effective then a pressure meter test which requires a much bigger borehole. However, methods of applying incremental load on the tip and applying vibrational loading, applies a load much different to the seismic event. This leaves room for development of new geotechnical tests that are better suited for the task of studying liquefaction susceptibility.

1.3 Soil liquefaction

Liquefaction is observed in saturated, cohesionless, loose and undrained soils under monotonic, transient or repeated disturbances. Under such circumstances, the soil, unable to contract faces an increase in pore pressure leading to decreasing effective stress and, consequently, an early and easy failure of the ground leading to large deformations.
Hazen 1920 used the term "liquefies" to describe the Calaveras Dam rupture of 1918 in California. The term liquefaction is believed to be used first by Terzaghi in 1925 and appears in a famous publication by Terzaghi and Peck in 1948. However, the subject is much older than this. The first documented proof of liquefaction is in Weesp city of northern Netherlands, where flow slides were observed in the approach of a railway bridge triggered by vibrations from a passing train in 1918. This incident is considered the start of practical soil mechanics in the Netherland. The phenomenon linked to liquefaction, sand boils, known as craterlets at that time, has been reported as back as 1906 after the San Francisco earthquake. The first plausible basic mechanism explaining the sand boils was given by Housner 1958. This phenomenon and its mechanism are still a subject of research(Scott and Zuckerman 1964, Muir and Scott 1979, Youd 1999, Cudmani 2014).

1.3.1 Major Liquefaction events

A few of the major events in recent history that led to the study of liquefaction in greater detail and brought it up as a major challenge for geotechnical engineers are discussed here.

Niigata Earthquake :

Niigata is a city on the west coast of Japan and lies on the bank of river Shinano, where it meets the sea. The city has nearly 30 m of alluvial deposits. On June 16, 1964, an earthquake of 7.6 magnitude hit the city. The epicenter of the earthquake was offshore, just 56 km from the city. The city witnessed the uplifting of buried underground structures, sand flows and mud volcanoes. These effects were observed to continue for as long as 20 minutes after the shaking due to the earthquake had stopped. This city's photo of a building tilting by 80^{o} is iconic and used widely to demonstrate the effects of

liquefaction (Figure 1.3). Many researchers studied this site to understand better the phenomenon observed. Idriss and Seed 1968 discuss in detail the liquefaction phenomenon observed in Niigata. Later on, Idriss and Seed 1971 and 1983. characterized the earthquake loading in terms of Cyclic Stress Ratio (CSR) and resistance to liquefaction by a factor called Cyclic Resistance Ratio (CRR), which are used even till date for finding out liquefaction probability at a site. Iwasaki et al. 1978 studied this earthquake and also used data from previous earthquakes to use the blow counts from standard penetration testing to calculate the CRR. Over the years, many scientists have improved his empirical relationships to account for all variables. A similar approach was later developed for CPTu tests too. Iwasaki also calculated the "factor of liquefaction resistance" (F), also called the safety factor to indicate if the soil layer is prone to liquefaction or not.

$$F = \frac{R}{L} \qquad \textit{Eq. 1.1}$$

where R is the in-situ resistance (or undrained cyclic strength) of a soil element to dynamic loads and L is the dynamic load induced in the soil element by seismic motion. A value less than one would indicate susceptibility to liquefaction for a particular layer. Ishihara and Koga 1981 studied two sites of this city, one that had liquefied and the one that did not, during the earthquake in 1964. They performed laboratory tests and compared the results for the samples extracted from the two sites. The loading to be applied was decided by the reading of accelerometers during the earthquake, fixed in the basement of a building near the liquefaction site. They calculated the safety factor as given in equation 1.1 and demonstrated that the site where liquefaction occurs had a safety factor less than 1 for a depth between 3 to 13 m while the other sand had safety of factor greater than 1 for almost the entire depth tested thus justifying no liquefaction during the earthquake in 1964. As such this earthquake is critical in giving liquefaction assessment the direction, which even to date, most of geotechnical engineers are following.

Figure 1.3 Damages caused by liquefaction events: Niigata Earthquake (Left) and Loma Earthquake(Right)

Loma Preita Earthquake

On October 17, 1989, a 6.9 magnitude earthquake hit parts of California, with an epicentre about 16 km northeast of Santa Cruz. Significant property damage in San Francisco's Marina District was witnessed due to the liquefaction of soil used to create waterfront land. Other effects included sand volcanoes, landslides and ground ruptures. This area is prone to liquefaction as it is built on superficial sand deposits that were used to fill the old lagoon in 1915. Also, the underlying soil layer leads to amplified ground motion, as was already seen in 1906. Therefore, the possibility of the occurrence of liquefaction was well known in the area. Also, other instrumentation to record and analyize the earthquake loading and the site response was installed in this area due to its susceptibility to earthquakes. Furthermore, a number of ground treatments to improve liquefaction resistance were done at sites of importance. Thus this earthquake allowed us to check the effect of these ground improvement techniques, evaluate soil density changes by in-situ testing before and after the earthquake, analyse the effect of site amplification and study the liquefaction-induced settlements and lateral movements. The study of damages also showed higher susceptibility in transition zones between liquefiable and non-liquefiable soils, i.e. the edges of the old lagoon in this area. Thus this event and the research that followed helped us understand liquefaction better with a large amount of data recorded before, after and during the event. According to the study done by Bardet and Kapuskar 1993 on the effects of this earthquake, 33% of sand boils observed were inside structural areas and 36% at the boundaries of these structures. However, most of these structures were un-damaged. Bardet suggested that liquefaction may have been beneficial to buildings in the center of the liquefied areas by decreasing the amplitude of the seismic shear stresses applied to the foundation.

Kobe Earthquake:

In the morning of January 17, 1995, Hanshin faced one of the most deadly earthquakes in Japan's recent history. The earthquake resulted in over 5500 confirmed deaths and as many as 35,000 seriously injured. In addition, approximately 300,000 people were left homeless (Figure 1.4(left), Soga 1998). One significant reason for the damages incurred was the occurrence of extensive soil liquefaction and lateral spreads of poorly compacted fill even when the earthquake's magnitude was recorded as 6.9 MW magnitude, which was not too extreme for the region. Kobe's harbour was also Japan's second largest port and faced widespread damage. Lateral spreads caused many concrete caisson quay walls in the port to displace as much as 5 m seaward and subside 1-2 m. Most of the port was made on 16-24 m filled soil, which was dumped over soft alluvial clay. The parts of the port that were formed on improved grounds by densifying the sand by vibro-rod and sand compaction piles faced lesser settlements. The effect of the sand improvement techniques on vertical displacement was studied and represented by Soga 1998 in Figure 1.4(right). He compared several sites on two islands of Kobe that faced liquefaction. The bar in the

figure showed the range of settlement observed, and the symbol represented the mean displacement. The number of measurement points, i.e. the number of sites, is marked on top of each bar. It can be clearly seen that much less settlement was observed at sites where ground improvement was made. Thus this earthquake showcased that just building earthquake-resistant structures is insufficient and highlighted the importance of studying the possibility of liquefaction and taking preventive action.

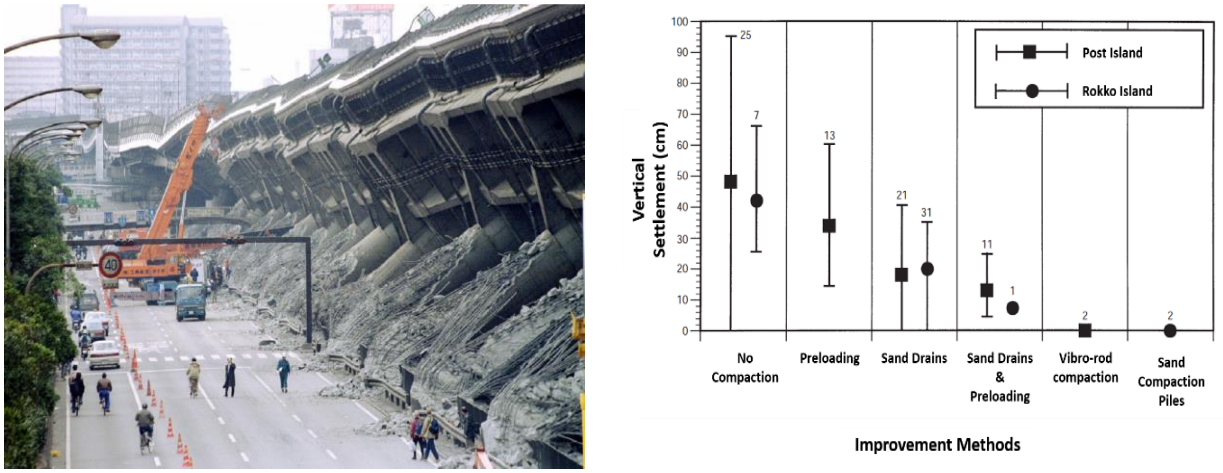

Figure 1.4 Damage caused by Kobe Earthquake (Left) and benefits of ground imporvement techniques observed at different sites during Kobe earthquake (Right – from Soga 1998)

Canterburry Earthquake:

On 4 September 2010, a 7.1 Magnitude earthquake struck the New Zealand South Island. Some damaging aftershocks followed the main event, the strongest of which was a magnitude 6.3 shock known as the Christchurch earthquake that occurred nearly six months later on 22 February 2011. Because this aftershock was centred very close to Christchurch, the second biggest city of New Zealand at that time and had a very shallow depth (5 km), it was much more destructive and resulted in the deaths of 185 people. The peak ground acceleration(PGA) measured was 1.26g for the earthquake in September 2010 while 2.2g for the February 2011 earthquake. There were three major earthquakes after this too. The total estimated damage bill was by $40 billion and liquefaction did more damage than the actual shaking of the ground due to the earthquake. As a result of the massive damage caused by the liquefaction of the ground in this city, a massive geotechnical investigation comprising more than 7,000 cone penetration tests, 1,000 boreholes, 800 monitoring wells and laboratory testing was carried out. The dataset gathered from these tests was used to characterise land vulnerability to the liquefaction hazard by comparing the existing published liquefaction vulnerability assessment tools of the Liquefaction Potential Index (LPI). It was used to calculate settlement indicator from predictive correlations (S) and were compared to the settlement observed and new

liquefaction severity number was developed which could help better understand the susceptibility to liquefaction. As such, this was one of the most concentrated and most extensive study on liquefaction carried out to date.(Potter et al. 2015)

Sulawesi Earthquake:

On 28 September 2018, a shallow, large earthquake struck the neck of the Minahasa Peninsula, Indonesia, with its epicentre located in the mountainous Donggala Regency of Central Sulawesi. Significant damage was caused by liquefaction. In what is considered the biggest liquefaction observed ever, Palu city was severely damaged. The suburbs of Balaroa and Petobo of this city sank in 3 meters-deep mud. In Petobo alone, 6,000 inhabitants are thought to have been buried by the mud out of total of 13000. It led to one of the most horrific sights where the land just vanished and turned to mud and caused submergence of large parts of the city, as shown in Figure 1.5.

Apart from this, liquefaction caused extensive damage to the coastal areas, and the gravity flow of the liquefied soil into the ocean caused multiple tsunamis. Some analysis shows that less than 20% of the tsunami height was related to the tectonic processes while the liquefied gravity flow and the resulting landslides into the water was the major contributor (Sassa and Takagawa 2019). An earlier report, (Widyaningrum 2012) had concluded that the majority area in Palu had a high potential for soil liquefaction.

Figure 1.5 Damage caused by liquefaction at Palu (Sulawesi) – From Reuters Images

However, no measures were taken, which highlights the importance of carrying out soil liquefaction studies and working on findings of the studies.

Liquefaction events not triggered by an earthquake:

For the occurrence of liquefaction, an earthquake is not the only triggering factor. Another cyclic or even static load has been seen to cause liquefaction based on the sand's state. Two famous events are **Nerlerk Berm** liquefaction and **Amauliaga I-65** island liquefaction. The former was caused by static liquefaction, and the same mechanism had also been observed in **Fort Peck Dam**, and man-made storage spills like **Aberfan** and **Merriespruit.**

Amauliaga I-65 island liquefaction event was caused by the cyclic loading caused by the continuous striking of large volumes of ice. The storm on 12th April 1986, caused nearly 900 cycles of horizontal loading in the frequency range of 0.5-2 Hz within 14 cycles, causing a large settlement of sand filled inside the core unit of the caisson-type drilling unit.

1.3.2 Soil prone to liquefaction

Conventionally clean and silty sands with low plasticity are considered prone to liquefaction. However, cases have been recorded where soils with clayey content (i.e. with a particle size less than .002 mm) also have liquefied. Such soils had less than 15% clayey content by weight, a liquid limit less than 35% and water contents greater than 90% of the liquid limit (Wang 1979).

Similarly, even in certain cases, gravely soils have been found prone to liquefaction. Gravely soils with their voids filled with finer particles or gravely soil layers surrounded by low permeable soils can also be susceptible to seismically induced pore pressures and, therefore, to liquefaction (Andrus 1994) .

1.3.3 Factors affecting a soil's liquefaction susceptibility

The same soil may be safe or susceptible to liquefaction based on its state and its environment. Few of the important factors affecting the chances of soil liquefaction in case of a cyclic loading are:

Density: The resistance to liquefaction of a soil increases with increasing density (Seed et al. 1975).
Age of deposit: The resistance to liquefaction increases with increase of a sustained load i.e. ageing (Finn 1981).

Initial state of stress: Higher the overburden pressure, more resistant is the soil to liquefaction (Campanella and Lim 1981).
Loading Characteristics: Earthquakes are the most common loading causing liquefaction events. Earthquake's epicentre's distance greater than 500 kilometers and a magnitude less than 5.2 have rarely been found to cause liquefaction (Kuribayanshi and Tatsuoka 1975). Isolated horizontal shear loading waves has been found to be more dangerous than vertical ones in causing pore pressure generation(Puri 1984).

1.4 Liquefaction Potential Assessment

Preliminary assessments of susceptibility of a site to liquefaction is done based on historical, geological and compositional criterions. Information that aids the process of preliminary liquefaction potential assessment is: site topography, ground water level and its variations, soil profile and seismic history of the site.

"The liquefaction resistance of an element of soil depends on how close the initial state of the soil is to the state corresponding to "failure" and on the nature of the loading required to move it from the initial state to the failure state." (Kramer 1996)

Traditionally, liquefaction susceptibility is predicted using deterministic analysis for engineering applications. During the initials days of liquefaction prediction studies this deterministic analysis was done from the criteria on the grain size. Nowadays, deterministic liquefaction potential assessment is usually done using a Factor of safety(F) (Equation Eq. 1.1). To calculate "F", a number of methods have been used. They can be broadly categorized as analytical methods, physical modelling methods or empirical procedures.

1.4.1 Numerical Modelling Methods

Analytical methods use constitutive relationships for the different soil layer involved in a given engineering problem and their interaction to estimate the risk of liquefaction in an event of an earthquake. A crucial step in the elaboration of such numerical models is the determination of the soil mechanical properties required by the ad hoc constitutive relations. The determination of the cyclic mechanical properties rely generally on laboratory experiments like cyclic simple shear and cyclic tri-axial tests. However, determination of soil properties has its own limitations ranging from difficulties in preparing undisturbed samples, boundary and size effects and the inability of the tests to represent an actual earthquake loading correctly. The difficulties of performing representative laboratory experiments and the absence of constitutive models that can correctly predict the various aspects of soil behaviour while having a low computational cost make these approaches generally limited to research and critical projects.

1.4.2 Physical Modelling Methods

Physical modelling is a valuable method for engineering problems which are not easily solved by mathematical solutions. These methods involve making a small-scale model face the same loading as an actual event. However, the problem with these methods is replicating the same stress state. During liquefaction, soil exhibits stress and time-dependent loading response, challenging to mimic in small-scale models. Centrifuge testing can generate similar stresses and strains in the model. The prototype is often used to study scale models with prescribed soil property profiles and shaken with desired base input motion. However, the most significant disadvantages are the inability to model the effect of particle size and the inability to replicate the in-situ soil loading history and soil conditions, which play a crucial role in liquefaction resistance.

1.4.3 Empirical Procedures

In the absence of good Analytical and Physical modelling options for liquefaction studies, empirical methods have become widely accepted and are used in routine engineering applications for liquefaction potential assessment. Empirical procedures generally follow a cyclic stress approach in which the loading (L) is described in terms of cyclic shear stresses caused by an earthquake, and the resistance (R) is also quantified on the basis of the number of cycles of uniform amplitude stress cycles required to cause liquefaction. Historical data is used to define boundaries that separate loading events that caused liquefaction from those that did not (Figure 1.6). These boundaries are then defined empirically to predict the liquefaction susceptibility of a site having a certain value of resistance (R).

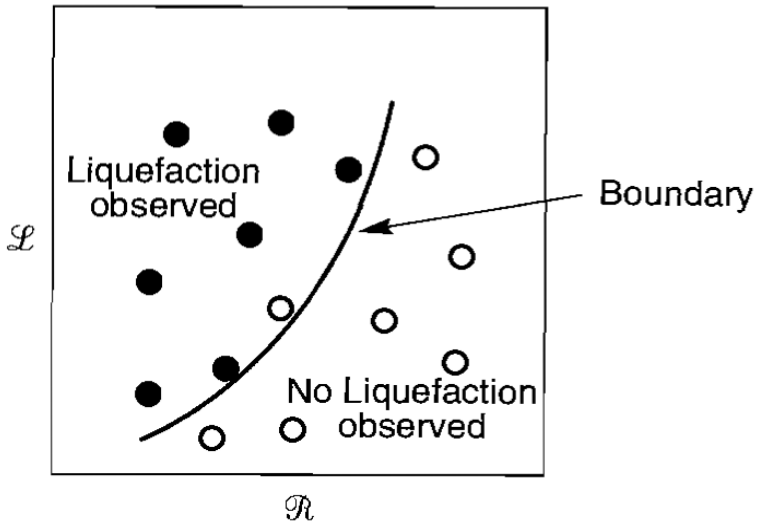

Figure 1.6 General form of graphs to predict liquefaction susceptibility from in-situ tests(from Kramer 1996).

Estimation of the Earthquake induced cyclic loading (L):

The irregular cyclic shear stresses caused by the earthquake are quantified in terms of uniform cycles with a given amplitude and number of cycles. This work was pioneered by H.B. Seed and his colleagues from the University of California at Berkeley.

- Amplitude: The shear stress caused by an earthquake is not constant and varies during an earthquake. This shear loading depends on the earthquake magnitude and the local ground response. However, in empirical procedures, it is common to represent the irregular cyclic shear loading with cycles of constant amplitude. This amplitude is a ratio of the maximum shear stress caused by the actual earthquake. A ratio of 0.65 was suggested by Seed et al. 1975.

- Number of cycles: Seed et al. 1975 studied a number of strong ground motions. The number of uniform stress cycles, with an amplitude of 0.65 times the peak shear stress (of the actual ground motion) required to cause an increase in pore pressure similar to the actual event, was plotted against the magnitude of the earthquake. The mean of this data is used to find the equivalent number of shear stress cycles of constant amplitude to represent the irregular shear loading caused by an earthquake of a given magnitude. (Figure 1.7)

As discussed, the earthquake loading for empirical methods is quantified using cyclic shear stresses. This cyclic shear stress on a soil layer is often normalized for effective vertical stress on that soil layer and is then known as Cyclic Stress Ratio (CSR). CSR values are calculated based on expected peak horizontal surface acceleration during the design earthquake (a_{max}). The acceleration at different depths can be calculated using a reduction factor value (r_d) for that depth level. Once we have the two values, the loading at any depth of concern can be found, as shown in equation 1.2. (Seed et al. 1975)

$$CSR = 0.65 \left(\frac{a_{max} * r_d}{g}\right)\left(\frac{\sigma_V}{\sigma_V'}\right) \qquad \text{Eq 1.2}$$

Where:

g is the acceleration due to gravity

σ_V and σ_V' represent total and effective vertical stress at depth of interest.

The factor 0.65, as discussed before, accounts for irregular nature of the earthquake loading.

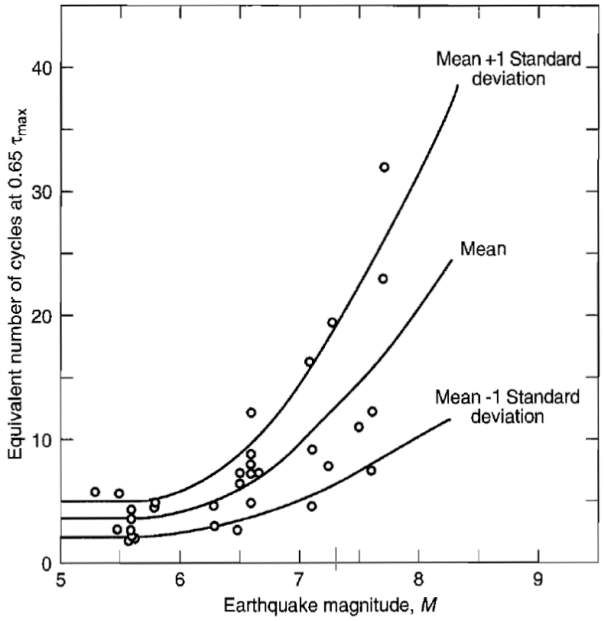

Figure 1.7 Number of equivalent uniform stress cycles for earthquakes of different magnitudes (From Seed et al. 1975)

Estimation of the in-situ liquefaction resistance:

The resistance of the soil at a given depth against cyclic pore pressure generation or accumulation of cyclic shear strain is found to predict liquefaction resistance. A common method to find liquefaction resistance is by performing laboratory experiments. As already discussed, the cyclic simple shear test and the cyclic triaxial test are the most commonly performed tests to assess liquefaction resistance.

However, it has been seen that this resistance of soil is also influenced by its fabric, history of prior seismic straining, over-consolidation ratio and lateral earth coefficient apart from the conventionally controlled parameters of density and confining stress conditions. *"These additional parameters are all functions of the depositional and historical environment of a soil deposit, and they tend to influence soil behaviour primarily at the low strain levels associated with the initiation of liquefaction. These low-strain effects are easily destroyed by sampling disturbance and are very difficult to replicate in reconstituted specimens. Because of these factors, characterization of liquefaction resistance by laboratory testing is extremely difficult and has been supplanted by methods based on in situ test results for many projects."* (Kramer 1996)

Whitman 1971 proposed one of the earliest methods to organize field observations concerning liquefaction and non-liquefaction events during actual earthquakes. The paper involved quantifying the earthquake loading causing liquefaction in terms of a loading parameter (L), e.g. Cyclic Stress Ratio (τ/σ_v) and using a resistance value (R)

calculated from an in-situ experiment. The liquefaction and non-liquefaction range defined with respect to these parameters are separated by a boundary that becomes a criterion for predicting liquefaction. (Figure 1.6). In the case of the use of CSR values as a loading parameter, this boundary is generally called Cyclic Resistance Ratio (CRR). Standard Penetration was the first test used to define a well-accepted CRR value using equivalent blow counts required for a given penetration(N_{eq}). However, CRR predictions from cone penetration testing are becoming increasingly popular and will be discussed later in section 4.2.3. The CRR measurement using SPT and CPT has a number of associated problems like the requirement of corrections for overburden stress, corrections for fine content and static stresses in the soil, corrections for different earthquake magnitudes etc. This, along with other uncertainties caused by the test equipment and procedure, make it necessary to be careful while using the empirical relations developed over a period of time. Also, local site conditions have to be studied and compared to those used for the development of empirical relationships and adjustments (if any) should be made. Also, in nature, the loading causing an actual liquefaction event is quite different from the one caused by SPT and conventional CPT tests.

All these shortcomings leave room for developing new geotechnical tests to predict liquefaction resistance.

1.5 Cyclic CPT test

Equaterre's experience in the geotechnical investigation in the Alpes encouraged them to find an alternative to the conventional CPTu tests. Apart from the problems mentioned in previous sections, the interbedded very soft layers of clays and silts between dense gravels and sands made it impossible to use high-precision CPTs with accurate friction and pore pressure measurements Also, the reliance of CPTu on empirical relationships and site adjustments required made it complex to be sure of the analysis using CPTu. To study liquefaction too, the practise involved relying on data gathered from a test that applies loading much different to those causing liquefaction in the soil. CPTu and SPT tests have worked to identify liquefaction because there is a correlation between soil properties involved in liquefaction sensitivity and those affecting results of these tests (compressibility and shear strength). However, these are correlations and not causations and can lead to errors in liquefaction susceptibility analysis.

With the aim to apply a loading on the soil closer to actual seismic events while keeping the benefits of conventional CPT testing, Equaterre came up with an ingenious method to apply cyclic loading on the robust and cheap mechanical Gouda tip. The tests involve penetrating to the depths of interest while measuring the tip resistance classically and then applying the **Cyclic CPT** test.

1.5.1 Equipment Used

For the new proposed **Cyclic CPT** test, Equaterre uses one of the oldest cone tips in CPT testing. It is a mechanical cone with a front sleeve that can move independently from the main body of the cone (Figure 1.8). This front sleeve is connected to the internal rods, while the main body of the cone is pushed via the external rods. During monotonous penetration, the external and internal rods move without any movement relative to each other (Figure 1.9). The internal and external rods' length is so selected that the front sleeve is always slightly open. This ensures that the force from the tip is transferred to internal rods, not external ones. Therefore the tip resistance can be measured using a force transducer pushed by the internal rod (Figure 1.10).

The internal rods are stacked over one another. During the **Cyclic CPT** test, a push on the internal rod will not cause any movement of the external rods but will cause the front sleeve to slide past the main body of the cone (Figure 1.10). Similarly, a cyclic compressive loading applied on the internal rod will be transferred to the cone tip and can cause the front sleeve to open (Figure 1.11).

In addition, the front sleeve is tapered in shape to minimize the effect of friction from the soil tested and ensure that the force transferred to the internal rods during penetration is the tip resistance (the force on the tip). There are no force, friction or pore pressure sensors at the tip level, and neither are any cables inside the tip. The tip force can be measured directly on the surface and is equal to the compressive load on the internal rods.

This cone tip avoids the problems of conventional CPTu, like loss of saturation of the pore pressure sensor, damage to the friction sleeve, the effect of temperature changes on measured tip resistance etc. This tip is also more robust and cheaper than the conventional cone tip. This tip can also be used to drill past very compact layers and removes the necessity of creating boreholes past these dense layers, saving time and money.

However, this also means that it is impossible to apply pore pressure correction on the measured tip resistance and use the existing charts of CPTu testing to define a Soil Behaviour Type (SBT), liquefaction susceptibility or any other soil property.

For the calibration chamber, a mini mechanical Gouda tip of 4 cm^2 cross-section($Ø = 2.25$ cm), as shown in Figure 1.8, is used, while for the field testing, the conventional cross-section of 10 cm^2 is used. During the initial testing, it was observed that there was negligible friction between the outer and inner sleeves. However, consequent testing showed that the sand grains were getting stuck between the two parts of the cone while closing the tip after one **Cyclic CPT** test, which affected the subsequent cyclic test results

as it became more difficult to open the tip. This necessitated cleaning the tip after every cyclic test, which was not practical. Therefore, a new modified cone tip (Figure 1.8) was proposed and manufactured. The new tip reduces sand grains getting stuck via an outer rubber cover between the front sleeve and the body of the cone. This rubber cover and an O-ring prevented the sand grains from getting stuck, and the requirement for cleaning the

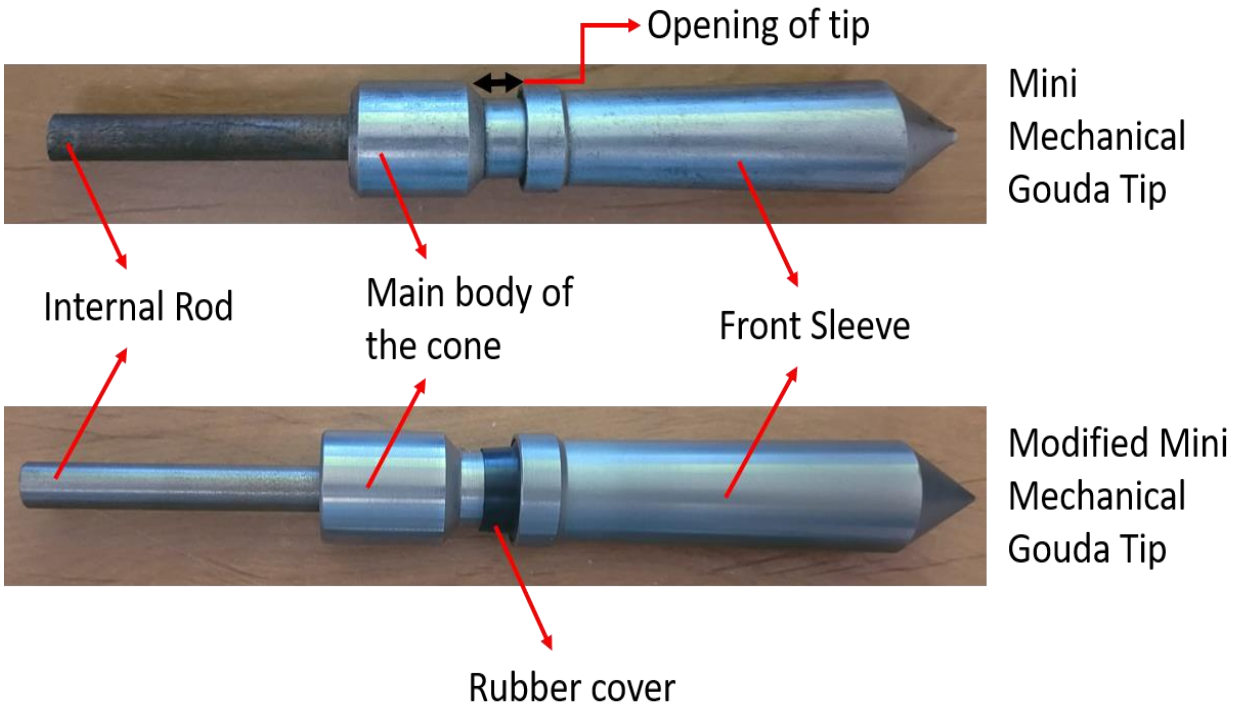

Figure 1.8 Mini Gouda Tip

tip after every test without increasing the friction between the two components. The material used for this cone was also treated to minimize friction and water adhesion.

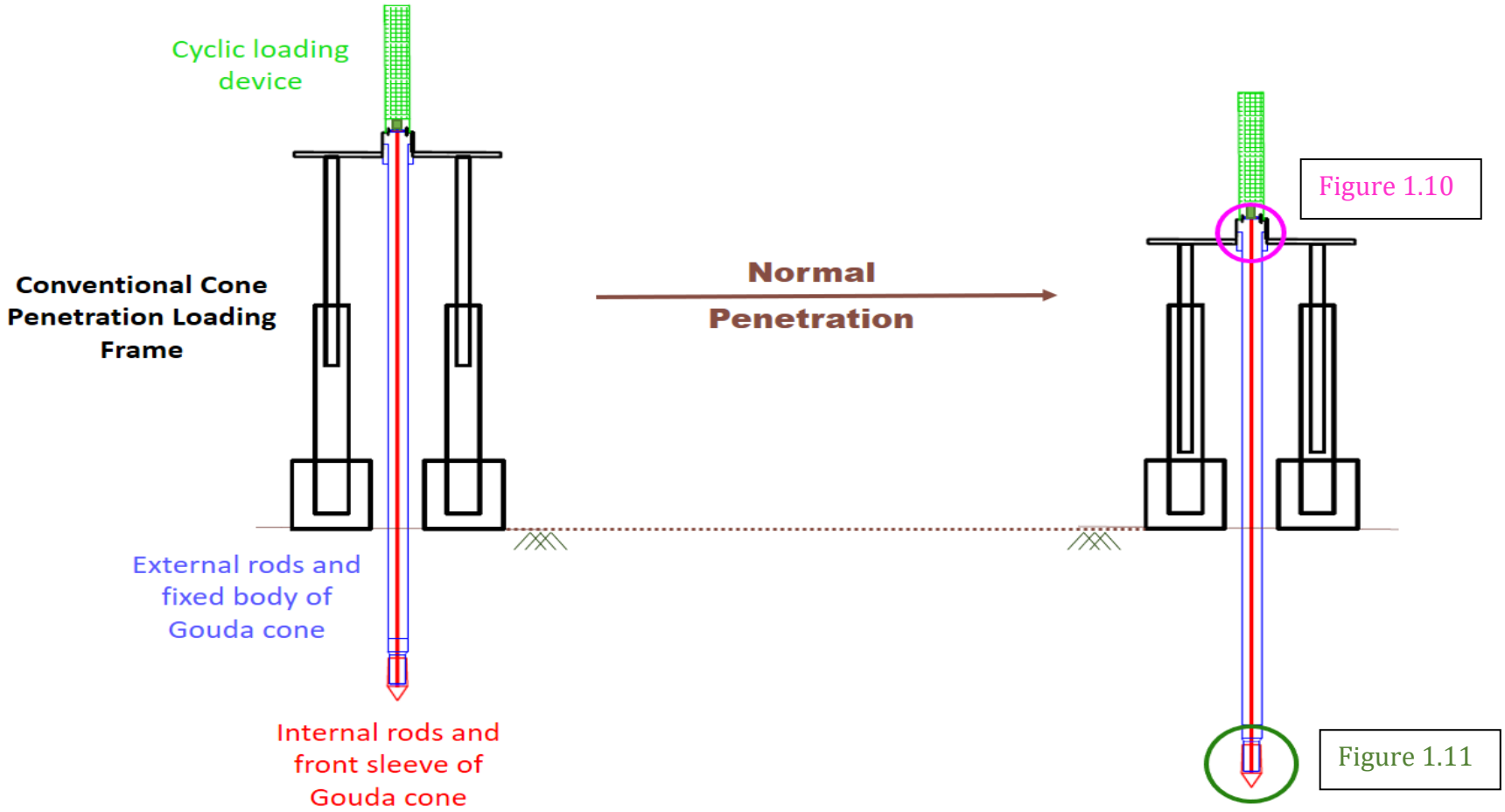

Figure 1.9 Representation of normal penetration of gouda cone using Equaterre's equipment

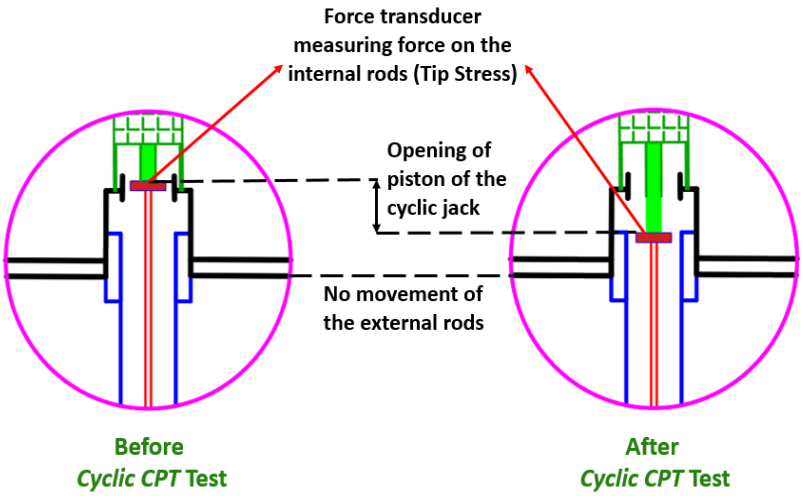

Figure 1.10 Application of Cyclic CPT test without moving the external rods

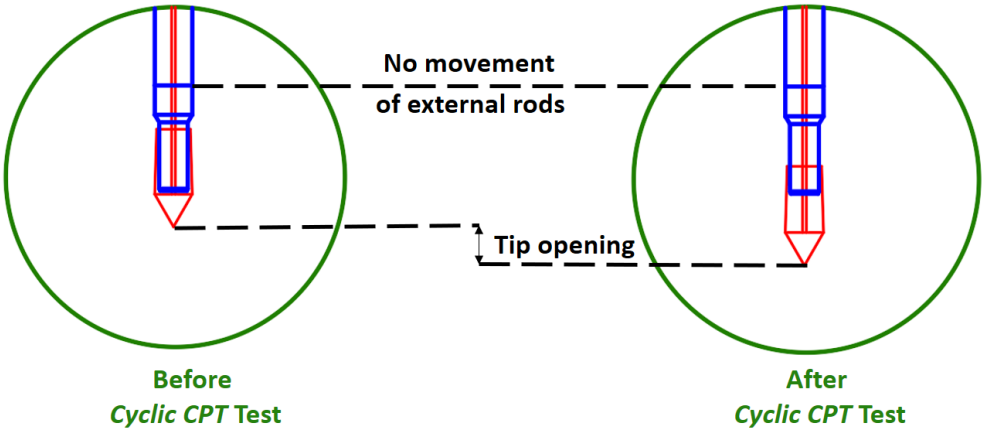

Figure 1.11 Opening of the Gouda tip during Cyclic CPT test

1.5.2 Test Methodology

The process implemented for the realisation of the **Cyclic CPT** test has been reconsidered in collaboration with Equaterre during this PhD. It can be best described as a combination of eight successive steps named A to H in the chronological sequence. There are two separate phases of loading (Steps A to D and Steps E to H). Each phase of loading is initiated by a monotonous tip penetration (Steps A and E) followed by a waiting period at constant force on the tip (Steps B and F). These steps are followed by application of stress controlled cycles (Steps C and G) and ended with another set of waiting periods (Steps D and H). The second set of loading (Steps E to H) tries to study the changes in behaviour caused by the first stage of **Cyclic CPT** test, which aims at gathering information about post-liquefaction strength. The entire process is as shown in Figure 1.12 and summarized in Table 1.1. The details of each step, the input parameters and key results are discussed in the following sections.

1.5.2.1 Step A – Monotonous Push:

The first step involves pushing the front sleeve of the cone by a small distance (1 cm) at a constant speed to measure the tip resistance. This maximum tip resistance measured during this time is saved as "TR#1".

Input Parameters:

Distance of push

In line with the methodology followed in the field and the limitation of just six centimetre of total displacement of cyclic jack (**VE**) in laboratory, **one centimetre** push was used for almost all cyclic tests performed in the lab.

Speed of push

Traditional CPT speed of 20 mm/s caused problems with the control during the **Cyclic CPT** test performed inside the calibration chamber and a **5 mm/s** penetration speed was used. This change should not cause any change of tip resistance in clean sand in which even the conventional CPTu test is considered drained.

Key Results:

Tip resistance

The key result is the maximum force (TR#1) required to penetrate the tip at the input speed to the input distance. This tip resistance is used in other steps: to control the constant force during STEP B, D, F and H; to control the maximum and min amplitude of cycles during STEP C and G. The range of tip resistance can give us an indication of soil type. Clay like soil have generally much lower tip resistance than sand type soil.

1.5.2.2 Step B – Application of Constant Force: A constant force, which is certain fraction of the TR1 is applied while the tip displacement is measured. This fraction is referred as $\alpha_{F,const.}$

Input Parameters:

Ratio of tip resistance to be applied as constant force ($\alpha_{F,const}$)

Values between 0.2 to 0.9 were tested during this research work. Closer the value is to the tip resistance, greater is the expected tip displacement.

Duration of loading

The time duration of applying the constant load is also an input. Generally a time period of 20 s was used for calibration chamber tests.

Maximum displacement of the tip

The maximum opening of the tip during these steps can be fixed. If this value is reached, the control moves to next step (Or the test is stopped in case of STEP H).

Key Results:

Displacement during constant load

The displacement of the tip during the application of constant load is recorded. The same value of $\alpha_{F,max}$ for different soils may result in different tip displacement and can be used to indicate the soil type.

Based on soil type we may see different tip displacement while applying similar percentage of tip resistance based on the penetration mechanism in play. Clay type soil may seem tip penetration during this step while sand type soil may see negligible tip resistance. An application of 0.6 times the tip resistance can also be used as a limit state load. This step is also useful to differentiate the displacement caused during the constant speed penetration and the one caused during the cyclic loading

1.5.2.3 Step C – Application of uniform stress cycles: Sinusoidal compressive stress cycles are applied on the tip without moving the external rods. The maximum and minimum amplitude of these stress cycles are decided based on the tip resistance recorded in step A (TR#1)

Input Parameters:

Maximum and the minimum amplitude ratio ($\alpha_{F,max}$ and $\alpha_{F,min}$)

These are the ratio of the tip resistance to be applied as maximum and minimum amplitudes of constant compressive stress cycles. In this research work, $\alpha_{F,max}$ values between 0.5 and 0.95 were tested while $\alpha_{F,min}$ values between 0.3 to 0.6 were tested. The closer the values of $\alpha_{F,max}$ are to 1, the easier it will be to open the tip during the

cyclic loading. Similarly, a lower value of $\alpha_{F,min}$ will result in larger range of force cycles.

Frequency of the cyclic loading

The cyclic jack (VE) is capable of applying a cyclic load between 0.1 to 5 Hz. During this research work, frequency range between 0.1 to 2 Hz was tested. This is an input that has to be done before starting the cyclic CPT test.

Time of cyclic loading

The maximum time of application of cyclic loading is also an input. Generally, a value of 180 s (3 minutes) was selected for the calibration chamber tests. For a smaller frequency a greater time period is selected as input for applying the same number of cycles.

Maximum tip opening during the cyclic loading

We can input the maximum opening of tip allowed during the cyclic loading. If the tip opens by this value, the control is directed to move on the next step

Key Results:

Displacement during cyclic loading

The only direct result is the displacement of the tip during the cyclic loading. From this, the displacement per number of cycles, the change of stiffness during cyclic loading can be derived to give information of the changes occurring during the test and help derive soil properties.

The displacement recorded can be used to observe the change of stiffness w.r.t. to number of cycles. A liquefaction like event will probably lead to sudden large change of observed stiffness.

1.5.2.4 Step D – Application of Constant Force: A constant force similar to Step B is applied. The inputs and results are also similar to Step B.

1.5.2.5 Step E – Monotonous Push: This steps involves pushing the cone by the small distance as Step A with the same speed to measure the tip resistance again. This maximum tip resistance measured during this time is saved as "TR#2".The difference of TR#2 and TR#1 shows the consequences of the first cyclic loading on the soil. A reduced tip resistance may indicate generation of pore water pressure or dilation of soil while an increased tip resistance may indicate compaction of the soil during the cyclic loading.

1.5.2.6 Step F – Application of Constant Force: This step is similar to Step B. However TR2 is used as a reference to decide the applied constant force. Therefore the applied constant force is $\alpha_{F,max}$ times TR#2. The input and the results are similar to Step B.

1.5.2.7 Step G – Application of uniform stress cycles: The second set of cyclic loading is applied. The magnitude, the time and the frequency is kept similar to Step C. The input and results are also similar to Step C. The aim of keeping a second set of cycles was to study the post liquefaction strength.

1.5.2.8 Step H – Application of Constant Force: A last waiting step applying a constant force is used and is identical to Step F.

1.6 Conclusions

This chapter provided a brief introduction to this thesis. It also introduced few of the most widely used in-situ tests for soil investigation and highlights their shortcoming for use in liquefaction analysis or determination of relevant deformation modulus. A summary of important liquefaction events and their contribution to progress of liquefaction studies was also provided. Various methods used in liquefaction analysis were introduced and the most widely used, the empirical method, is explained in greater details.

Finally the subject of this research project, a new in-situ geotechnical test : ***Cyclic CPT*** was introduced. The cone tip used for this research is described and the input parameter and key results of different steps of this test are listed.

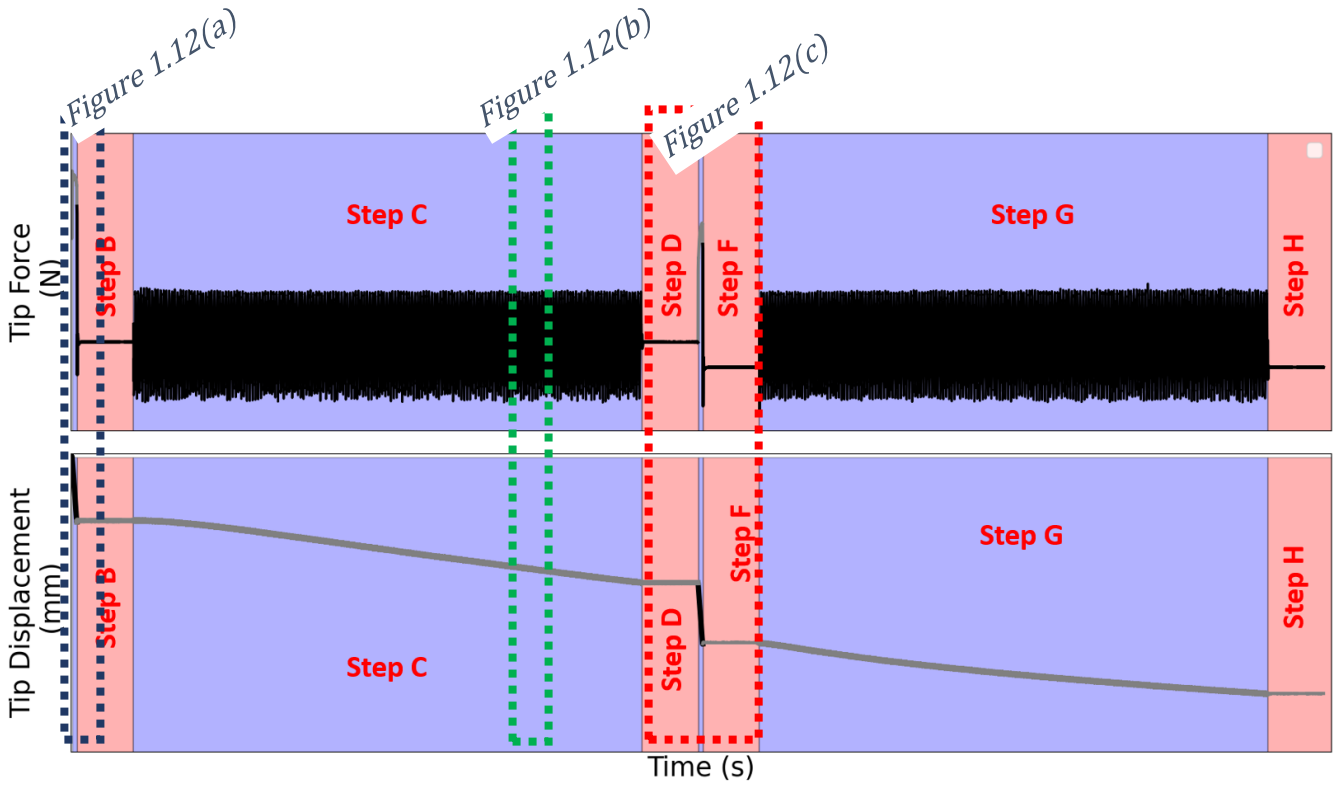

Figure 1.12 Different steps of the cyclic CPT tests performed on medium dense sand inside the calibration chamber

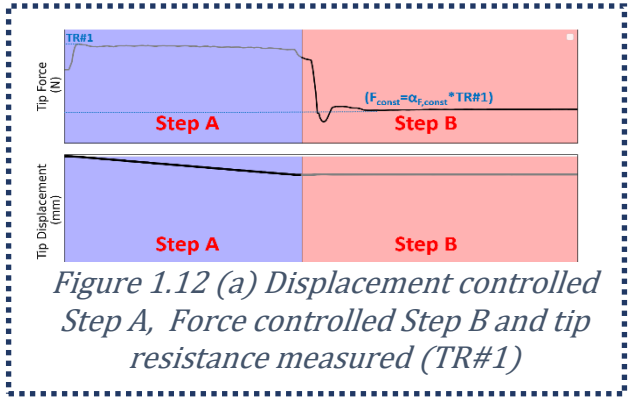

Figure 1.12 (a) Displacement controlled Step A, Force controlled Step B and tip resistance measured (TR#1)

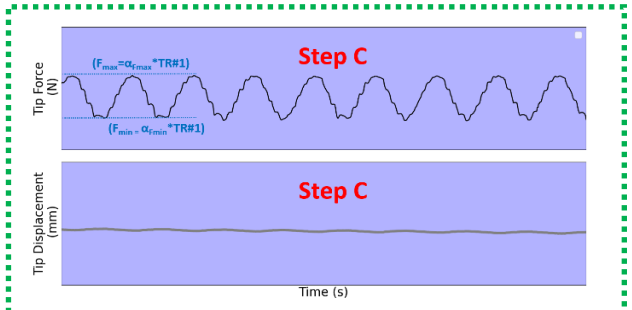

Figure 1.12 (b) Force controlled cycles during Step C

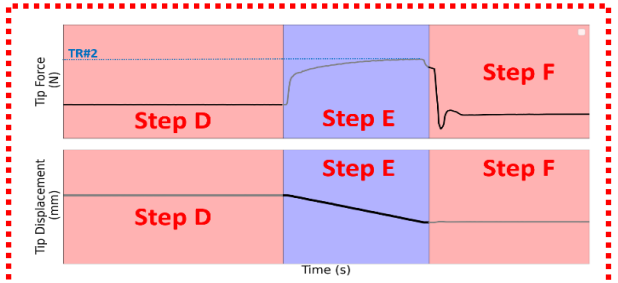

Figure 1.12 (c) Displacement controlled Step E and force controlled Step D and F and tip resistance measured (TR#2)

Step	Description	Input parameter		Key Result
			Default	
A	Monotonous push at constant speed	Speed of penetration	5 mm/s	Tip resistance (TR#1)
		Distance of penetration	1 cm	
B	Application of a constant force at a given ration of TR#1	Ratio of TR#1 to be applied as constant force ($\alpha_{F,const}$)	0.5-0.9	Displacement of tip during application of constant force
C	Applications of force cycles	Ratio of TR#1 to be applied as a maximum force($\alpha_{F,max}$)	0.1-0.5	Displacement of tip during cyclic loading
		Ratio of TR#1 to be applied as a minimum force($\alpha_{F,min}$)	0.6-1	
D	Application of a constant force at a given ration of TR#1	Ratio of TR#1 to be applied as constant force ($\alpha_{F,const}$)	0.5-0.9	Displacement of tip during application of constant force
E	Monotonous push at constant speed	Speed of penetration	5 cm/s	Tip resistance (TR#2)
		Distance of penetration	1 cm	
F	Application of a constant force at a given ration of TR#2	Ratio of TR#2 to be applied as constant force ($\alpha_{F,const}$)	0.5-0.9	Displacement of tip during application of constant force
G	Applications of force cycles	Ratio of TR#1 to be applied as a maximum force($\alpha_{F,max}$)	0.1-0.5	Displacement of tip during cyclic loading
		Ratio of TR#1 to be applied as a minimum force($\alpha_{F,min}$)	0.6-1	
H	Application of a constant force at a given ration of TR#2	Ratio of TR#2 to be applied as constant force ($\alpha_{F,const}$)	0.5-0.9	Displacement of tip during application of constant force

Table 1.1 Different steps of a cyclic CPT test

Chapter 2

2. Introduction to laboratory experiments

Experimental campaign was undertaken during this research work to develop the new **Cyclic CPT** test and demonstrate the use of this test for geotechnical investigations. The objectives of this research work can be broadly classified under three main categories.

- To improve the existing field equipment and clearly define the steps involved in the **Cyclic CPT** test, as well as to suggest changes to the test methodology and ensure its correct implementation by suggesting changes to software and hardware components involved in the test.
- To develop methods to test the **Cyclic CPT** test in the laboratory, under controlled conditions. To achieve this objective calibration chamber testing was considered the best option available. Therefore a new calibration chamber, a loading frame and a pluviator were conceptualized during this research work to perform experiments.
- To investigate the effect of saturation, density and vertical stress on the results of the **Cyclic CPT** test and use it to predict liquefaction susceptibility of soil. To achieve this objective calibration chamber tests on clean Fontainebleau GA39 silica sand are performed. Further, to better understand the properties of this sand more conventional laboratory characterizations are performed. These characterizations includes minimum and maximum void ratio calculation, hydraulic conductivity and monotonic triaxial and cone tip steel and soil interface direct shear tests.

This chapter firstly describes calibration chamber testing by discussing its history, the involved boundary conditions and the challenges faced while using this type of equipment. Then the equipment conceptualized to meet this project's need, and the closed-loop system used to apply the **Cyclic CPT** test using this equipment are discussed. Later, the sand used for calibration chamber testing is introduced. The different sample preparation methods described in the literature are discussed before explaining the sample preparation method used during this research work. Finally, the results of small-scale testing performed for the mechanical characterization of clean Fontainebleau GA39 are shown.

2.1 Calibration Chamber Testing:

The requirement for a calibration chamber originated from the need for comprehensive research on the performance of the full-size penetrometer in the laboratory, where the soil properties and its state can be accurately measured and controlled. The aim of this equipment and the research done using it was to correlate CPT measurements directly with engineering properties of the sand as internal friction angle and modulus of

deformation. Now, the scope of the calibration chamber has broadened from just the study of cone penetrometer to studying a large number of geo-investigation tools in the sand, the behaviour of piles to different loading conditions, among many other.

2.1.1 History

The first calibration chamber was designed in 1969 at the Material Research Division, Country Roads Board (CRB), Melbourne (Australia) to calibrate the friction cone penetrometer under simulated field conditions. Ron Lilley and Jim Holden are credited with the design of this chamber. Others, before this, had used rigid wall pits for the calibration. For simulating the K_0 conditions of zero lateral strain during consolidation, this calibration chamber had a cavity wall where the water pressure simulated the lateral sand pressure. As such, the inner wall of the double-walled barrel does not move, thus giving an average K_0 condition. The calibration chamber size was 0.76 m in diameter and 0.91 m high. After this, the University of Florida constructed a 1.22 m in diameter and 1.22 m high calibration chamber. This chamber had the capacity to test the sand in a saturated state also. In 1975, a third calibration chamber with a total height of 1.82 m was commissioned in Monash University. It was the first calibration chamber with a continuous automatic recording of all the pressures and a piston controlled by a displacement transducer. Norwegian Geotechnical Institute was the pioneer in Europe to have a calibration chamber and perform a calibration chamber testing program in 1974. They built a calibration chamber similar to CRB but 1.22 m in diameter and 1.5 m high. Italian Electricity Board (ENEL) in 1975 improved the calibration chamber design by using a precision servo-controlled mechanical drive for the penetrometer, a sensitive device for volume change measurement, and advanced methods for saturating samples. In early 1981, ISMES laboratory Bergamo (Italy), built the sixth calibration chamber based on CRB chamber. By this time, at least ten other calibration chambers were functional worldwide with inspiration from these initial six calibration chambers (Been and Crooks 1988).

2.1.2 Boundary Conditions

In the calibration chamber, based on the horizontal and vertical pressure applied, broadly, four different boundary conditions can be applied (Ghionna and Jamiolkowski 1991). The four different boundaries are listed below and are as shown in Figure 2.1.

- BC1 - Vertical and Lateral Stresses are kept constant.
- BC2 - Vertical and Lateral displacements are kept equal to zero.
- BC3 - Vertical Stress is kept constant while the lateral displacement is not allowed.
- BC4 - Vertical displacement is prohibited while lateral stress is kept constant.

There are some calibration chambers that are able to implement a simulated field condition of constant lateral stiffness and this boundary condition is referred as BC5. Implementation of each boundary conditions has its own challenges and its own effects on the results.

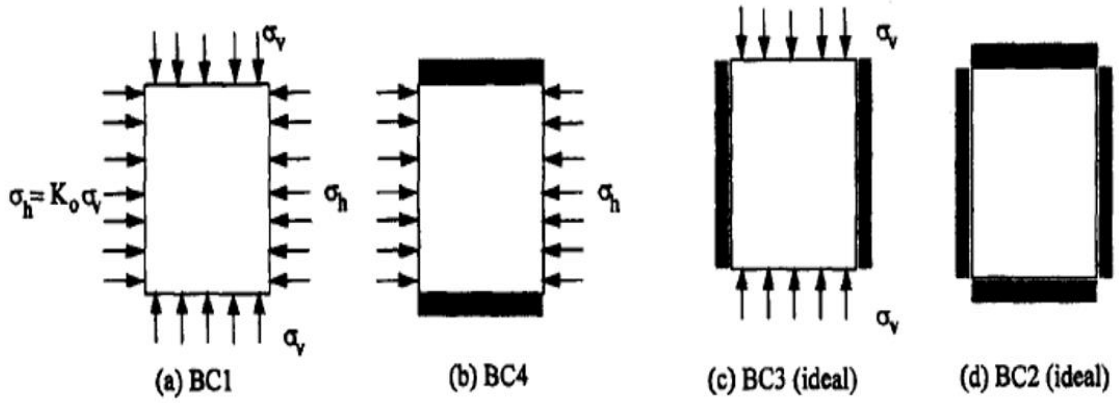

Figure 2.1 Types of boundary conditions in calibration chamber tests

2.1.3 Challenges of Calibration Chamber Research

The primary aim of calibration chamber (CC) testing is to replicate field conditions in the laboratory. Common challenges faced and their qualitative effects are discussed below:

- CC testing is performed on freshly reconstituted samples created by methods like air pluviation, dry or wet tamping, slurry deposition, vibration etc. In either of these methods, the specimen is freshly constituted, whose fabric may differ from the natural soil deposits, which have a highly developed structure. The quantification of these effects becomes of paramount importance if we want to predict the engineering properties in the field using the results from the calibration chamber tests.

- The CC tests are generally done on clean silica sands, while predominately in the field, there is a non-negligible percentage of fines in the sand, which significantly alter their behaviour. Also, there are crushable and compressible materials, such as carbonate and glauconitic sands which are usually slightly cemented in the sand. Forming a uniform and repeatable specimen of specific silt content at the desired density is challenging. It is also a challenge to have the desired degree of cementation uniformly distributed through the specimen after sample deposition. It is also challenging to know if the conditions during a test in saturated soil are drained, undrained or partially drained.

- Another problem with CC testing comes from the finite size of the chamber. This has been recognized as one of the most influential problems in CC testing. Many studies have been done specifically on the effect of chamber size on cone penetration tests. Been and Crooks 1988 argued that the influence of chamber size and applied boundary condition is complex and depends on the boundary conditions applied, the density of the sample and initial stress conditions.

  It has been well established that the size effect is more influential in denser soils than loose soils (Parkin and Lunne 1982). This effect can also be seen in Figure 2.2 where a loose soil (30% Relative Density) has almost no variations of average cone resistance with changing "Diameter Ratio" while there is significant variations for dense samples (90% Relative Density). Diameter ratio is the ratio of the diameter of the calibration chamber to the diameter of the cone. A greater value of initial density and lower values of the confining stress results in higher dilatancy and more prominent size effects. The vertical boundary conditions are less of a concern than the lateral boundary conditions.

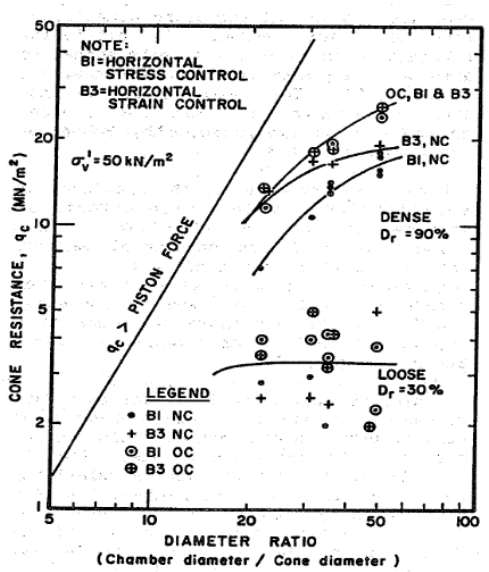

Figure 2.2 Effect of chamber size and boundary conditions on the CPT (From Parkin and Lunne 1982)

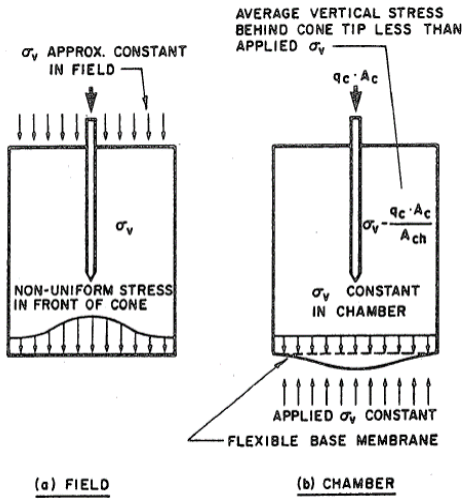

Figure 2.3 Vertical stress fields around the cone in the field and calibration chamber (From Been and Crooks 1988)

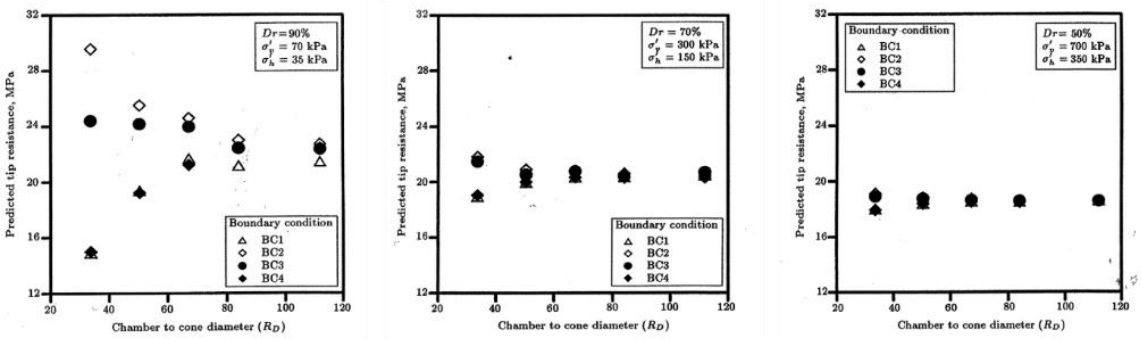

Figure 2.4 Effect of chamber size, boundary conditions, relative density and initial stresses existing in the calibration chamber (From Ahmadi 2004)

Zero strain vertical boundary condition can be expected to result in higher tip resistance values in cone penetration tests than in-situ, while constant stress vertical boundary may lead to lower tip resistance than in-situ conditions due to the difference of stress fields. The differences between the in-situ vertical stress changes and the one inside a constant stress vertical boundary are as shown in Figure 2.3. Salgado et. al. 1998 established that tip resistance under BC1 and BC4 conditions, is usually lower than in the field because a constant lateral stress during penetration underestimates the value that will develop during penetration in the field. Physically, this is because the yielding at the boundaries for these boundary conditions allows a reduction in confining pressure in comparison with free-field conditions. A numerical study (Ahmadi and Robertson 2004) pointed out that BC3 boundary conditions of fixed lateral boundaries may actually be closer to in-situ conditions than BC1 or BC4 boundary conditions of fixed lateral stresses. It was established that for a relative density of 50% the tip resistance was not affected greatly by the size effects Figure2.4 (right). **A similar trend can be seen in Figure2.2 where for a loose soil of relative density less than 30% there is no size effect visible for any of the boundary conditions tested. Since this is the range engineers are most interested to study for liquefaction studies, the size effects does not play a major role.**

Also, Been and Crooks 1988 concluded that boundary effects in most cases is less than 20% of the measured tip resistance and said that the scatter in the data from identical tests is also similar. Similarly Salgado et. al. 1998 pointed out an approximate $\pm 5\%$ uncertainty in determining the relative density and at least $\pm 10\%$ scatter of tip resistance values due to lack of sample uniformity. It was pointed out that a large number of tests were required to offset these uncertainties which owing to the large sample sizes and to labour and time requirements is generally impractical. Also, the cone tip resistance of a particular density of sand measured inside a calibration chamber can be converted to a free field tip resistance using relationships like the one described in Pournaghiazar et. al. 2012.

- There is another scale effect that can affect the results in CC tests and it depends on the ratio of grain size of the soil to the diameter of the cone, the pile or any other equipment being tested. Specifically for cone testing this effect is left insignificant if the ratio of cone diameter (d_c) to D_{50} of the soil exceeds 40.

2.1.4 Laboratory equipment used

It was necessary to perform many tests to define the test methodology clearly and to study all parameters affecting the results of a **Cyclic CPT** before the test could be used in the field. New equipment was developed for performing experiments in 3SR Laboratory during this thesis work.

It was required to design a loading mechanism that permitted penetrating at a constant speed and then stopping and performing the **Cyclic CPT** test. In addition, the cyclic loading jack had a maximum displacement amplitude of 6 cm and thus required another jack to penetrate different depths.

A few of the key challenges to be overcome for the design were:

- Isolating the cyclic loading on the front end of the mechanical cone without moving the external rods.
- Obtaining a continuous stress profile during penetration using a force sensor and using the same force cell to control the cyclic loading.
- Ensuring vertical movement of the cone during cyclic loading
- Independent measurement of the tip displacement during cyclic loading

Keeping all these challenges into consideration and taking inspiration from the requirements of field tests, a new loading frame and a new smaller calibration chamber were designed and manufactured during this research work.

Calibration Chamber

This project involved the application of cyclic loading via the cone tip at a frequency of the order of 1 Hz and a closed loop system to regulate BC1 or BC4 with a frequency greater or of similar order will be too complex. Also, no information was available based on expected expansion/contraction at the boundaries during the cyclic loading. Therefore it was decided to use *zero displacement lateral boundary conditions with a pressure membrane on top to apply a constant vertical stress*. This membrane was similar to the one used in the old calibration chamber used in 3SR and would be used to mimic the effect of depth in the soil. The membrane is connected to a pressure control unit that uses air pressure from the lab to convert it to water pressure. This pressurized water is used to fill the membrane at the desired pressure. This pressure control unit ensures the imposed boundary condition of uniform vertical stress is maintained during the calibration chamber test. The pressure control unit is as shown in Figure 2.5 and the custom made pressure membrane is as shown Figure 2.6. The calibration chamber designed for this project has a total height of 1.28 m and is composed of four identical sections, each having a height of 32 cm and empty weight of just over 200 kilograms (Figure 2.7). The chamber being in four sections allows for easier movement of the chamber and better control during the sample preparation. It was easier to ensure a uniform sample and precise positioning of the miniature stress sensors. This was also useful to adjust the height of the calibration chamber by using the required number of sections. Two sections are tied bolted together using 7 nuts to ensure a secure connection and tightening of O-rings for waterproofing. The design internal diameter of each ring is 60 cm. We used a mini cone of diameter 2.25 cm resulting in a ratio of cone tip to calibration chamber diameter of 26.7. This ratio is large enough to avoid any size effects for studying conventional cone penetration test for liquefaction susceptibility of loose soil. The presence of the miniature sensors in the soil

could also be used to study the sphere of influence for each cyclic test and changes of stresses close to the penetrating tip and also the boundary of the chamber. Moreover, a smaller size of the calibration chamber makes it easier to perform larger number of tests. The saturation of the sample can also be controlled using uniformly distributed water inlets at the base plate. Uniform distribution of water flow from bottom was ensured using a pebble layer of nearly 7.5 cm depth between two geo-membranes. This arrangement also allowed for the passage of water without allowing the sand to pass through and block the pores. The entire experimental equipment is as shown in Figure 2.7 while a zoom on the part responsible for applying the **Cyclic CPT** test is as shown in Figure 2.8.

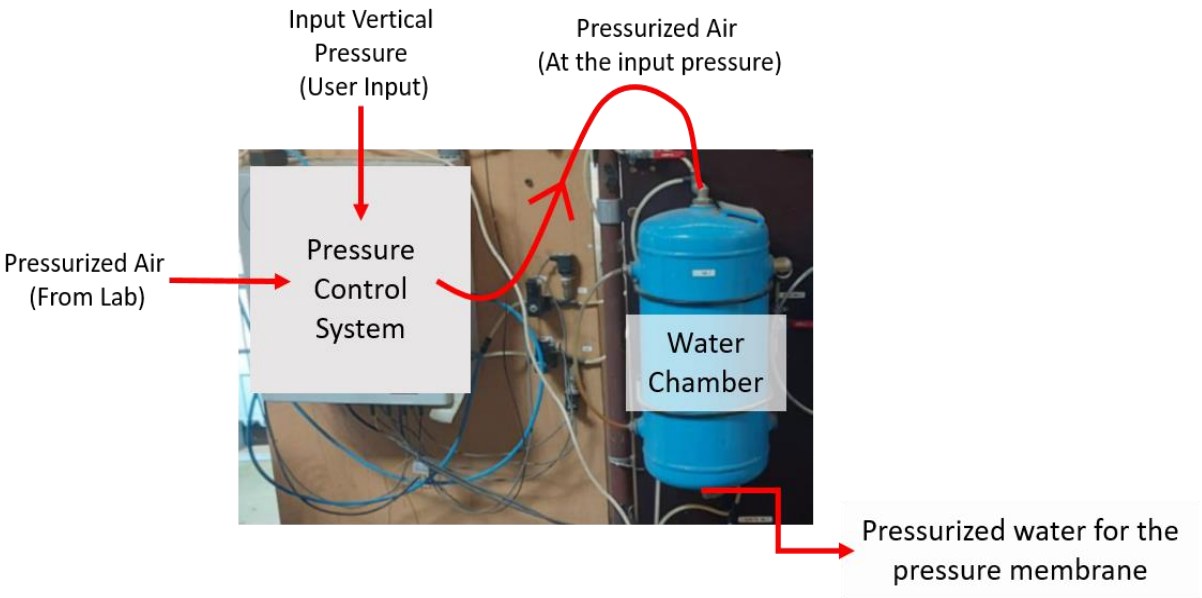

Figure 2.5 Pressure control unit

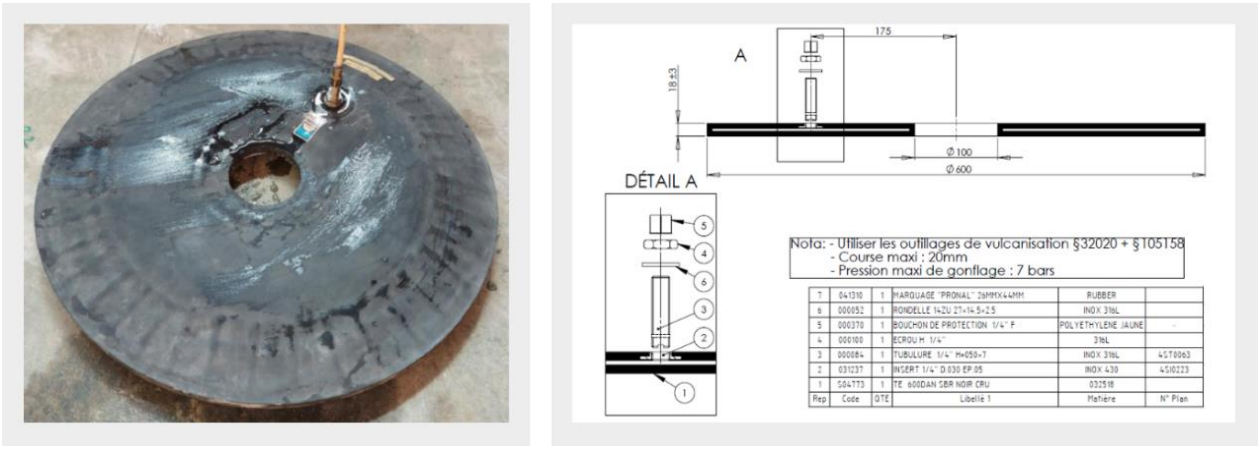

Figure 2.6 Pressure membrane: Image (Left) and Details (Right)

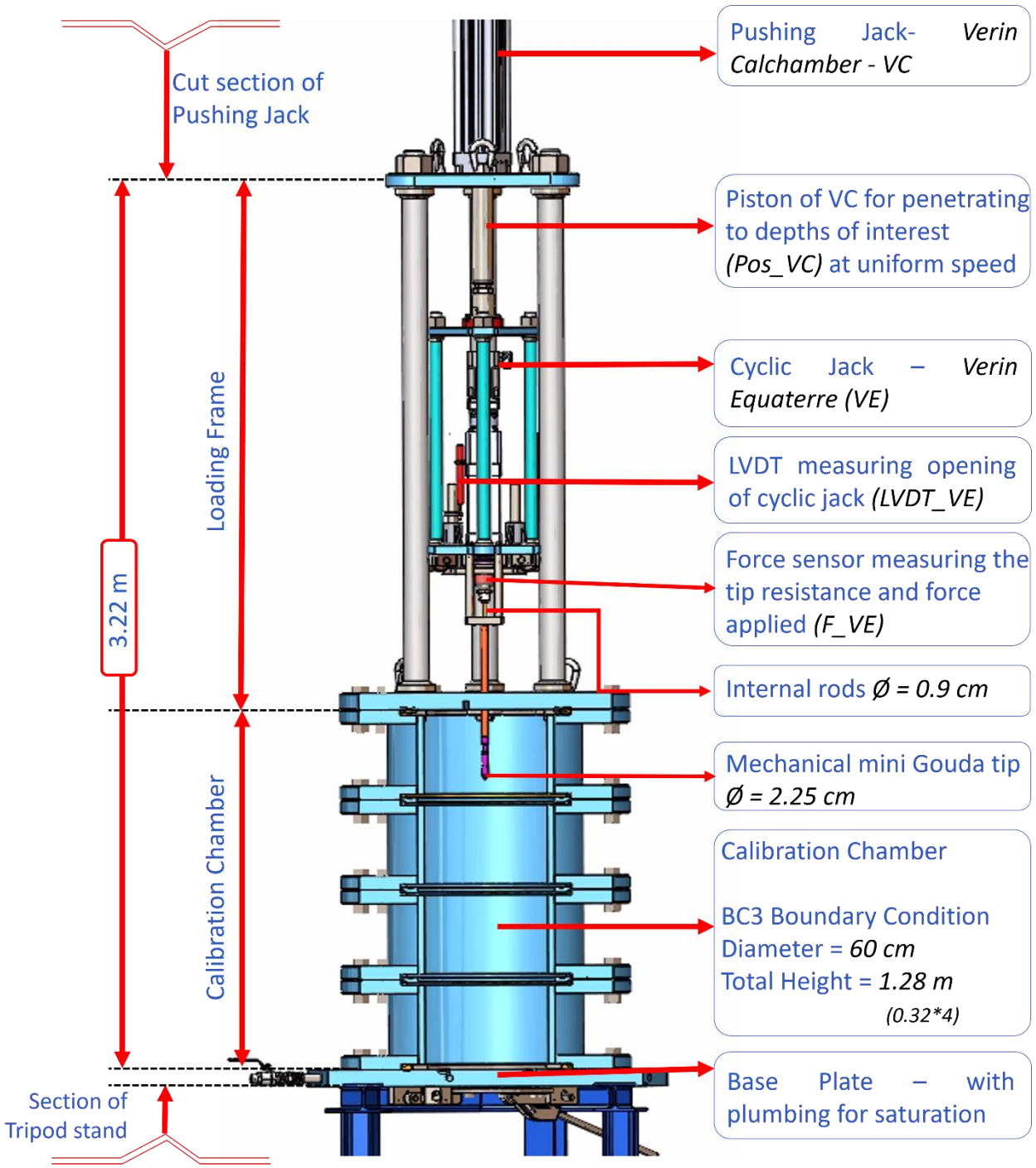

Figure 2.7 An exploded view of the calibration chamber and the loading setup used for laboratory experiments

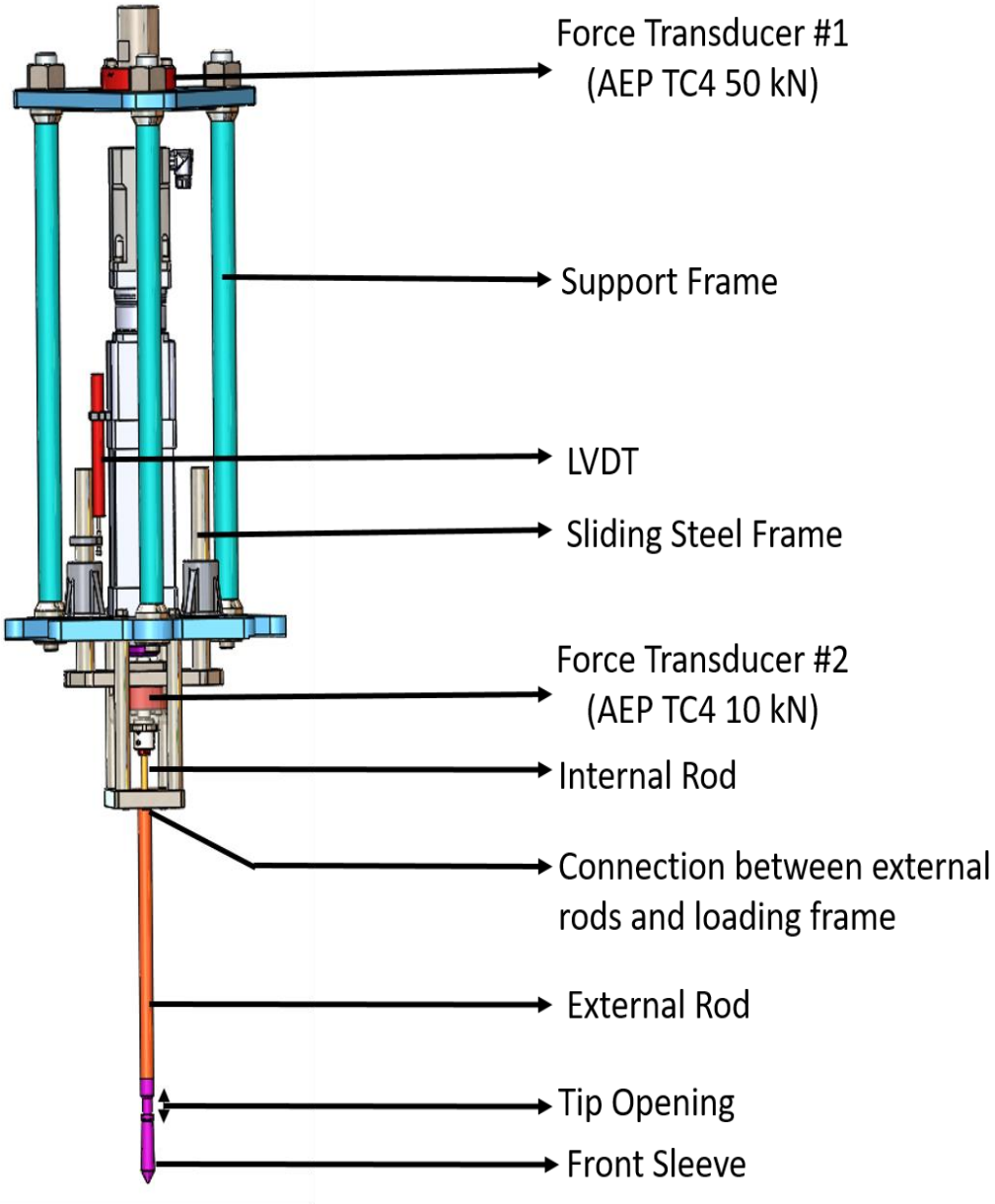

Figure 2.8 Cyclic jack and the support frame

Loading Frame

To meet the objectives of penetrating to depths of interest at a constant speed (conventional CPT test) and then stopping and performing the **Cyclic CPT** test, a new loading frame was designed to be used to perform tests inside the calibration chamber.

The loading frame has two loading jacks: an electro mechanical jack **which is referred as, "Verin Calchamber" (VC)** and another electric jack with a precision ball screw drive **which is referred as Verin Equaterre (VE).**

Verin Calchamber (VC)

The VC was also used as a pushing jack for CPT tests for the older calibration chamber in the 3SR lab (Celeste 2018). It has a maximum course of 1600 mm, a maximum force of 44.5 kN and a maximum velocity of 10 mm/s. It is manufactured by Parker (Model ETB-125-M05LA90FxB1600). In the current equipment, it is also used for the constant speed driving of the cone to depths of interest and acting as rigid support during the cyclic loading. The current design of the loading frame allows a total displacement of 510 mm of this jack. After this, to penetrate further the connection between the loading frame and the penetrating cone (Figure 2.8) is removed, the VC is retracted, and additional rods can be added. Once the connection between these newly added rods is made with the loading frame, it is possible to continue the penetration deeper inside the calibration chamber.

The piston of this jack is connected to a force transducer (Model AEP TC4 50 kN, referred as F_VC) (Appendix A). This force transducer carries the weight of the support frame (Figure 2.8) holding the cyclic jack. Thus this force transducer measures the weight of the support frame and the cyclic jack (tension). During penetration of the cone inside the chamber, this transducer is compressed by the force required to push the cone (tip resistance and friction along the outer rods). During the **Cyclic CPT** test, too, it will respond to the force changes on the tip.

Verin Equaterre

The VE was bought, calibrated and programmed during this research work. It has a total course of 6 cm and can apply constant force cycles with a maximum frequency of 5 Hz and a maximum driving force of 30 kN. The maximum speed of the jack is 70 mm/s (Manufacturer: Transtechnick, Model: PNCE-100-BS-4020-65-IP65CR) (Appendix A).

The piston of VE is connected to another force transducer (Model AEP TC4 10 kN, Referred as F_VE) (Appendix A). This force transducer can measure a maximum compressive load of 10 kN and pushes against the internal rod of the mechanical Gouda cone (Figure 1.8 & Figure Figure 2.8). The length of the internal rod is chosen, ensuring a small opening of the front sleeve of the cone at all times (Section 2.4.4).

The force transducer is connected to a conditioner (HBK clip X BM40) (Appendix A). The conditioner supplies the sensor, filters and amplifies the signal ($\pm$10V). Then, the output of the conditioner is connected to the acquisition card (analogue input). The output from this force transducer is the force applied on the front sleeve of the mechanical Gouda cone tip, that has been transferred to the force transducer via the internal rods. This force is

equivalent to tip resistance during normal driving and the tip force applied during the **Cyclic CPT** test.

A Labview program integrating PID (proportional–integral–derivative controller) allows to drive the cyclic jack (VE) in speed which is the analog output of the acquisition card. It is possible to induce a displacement of the cyclic tip (displacement control) and also apply predefined force controlled cycles guided by the values from the force transducer (force controlled).

A Linear Variable Differential Transformer (LVDT) is placed on the top of the sliding steel frame (Figure 2.8). LVDT measures the translation of the "sliding steel frame" connected to the piston of the cyclic jack. This steel frame is free to slide past the support frame. A brass alloy ensures no friction between the "sliding steel frame" and the "support frame", ensuring that the force measured by "force transducer #2" is equal to the tip resistance.

This steel frame pushes the internal rods of the cone. This ensures that the displacement of the front sleeve of the mechanical tip during the cyclic load is equivalent to the displacement of the sliding frame, which in turn is the displacement of the piston of the cyclic jack (VE). Thus, the tip opening during the **Cyclic CPT** test is equal to the relative displacement of the "sliding steel frame" and the "support frame". This relative displacement can be measured using the LVDT shown in the Figure .

To conclude, the current design of the loading frame allows a constant measure of the tip force using the "Force Transducer #2" and can also use the same force transducer to drive the VE during the **Cyclic CPT** test. Similarly, the displacement of the tip during the Cyclic CPT test is measured using the LVDT shown in Figure 2.8.

Soil Stress Transducers

A number of stress transducers were placed in the sample at two different depths while it is being built up, spaced radially at distance of 5, 10 and 20 cm from the axis of cone penetrometer. These sensors serve to establish the stress changes during the normal penetration and during the **Cyclic CPT** test. The sensors were carefully oriented so that vertical and radial stresses could be quantified.

Two type of total stress sensors are used during this research work. The first type is the commercially available miniature strain-gauged diaphragms - *KYOWA BE2KC.* These stress sensors have a upper limit ranging from 500 kPa to 7 MPa. They were purchased from Tokyo Sokki Kenkyujo Co. and Kyowa Electronic Instruments Co. These indirect sensors separate the strain gauge from the contact surface of the sensor by a thin film of mercury and using a wheatstone bridge (Berthoz 2013). These total stress sensors were

calibrated in previous works in 3SR laboratory (Silva 2006). The calibration followed the protocol established by (Zhu et. al. 2009) using a "tall oedometer" arrangement (Figure 2.9). The response of each sensor is represented by a series of hysteresis curves that depend on the history of prior loading. The cyclic nature of loading made it too complex to use different loading and unloading curves for the sensors and neither were they calibrated for such loading. It was found that a linear fit on the loading part of the sensors gave satisfactory results and was used to convert the voltage readings from the sensor to stress experienced by them.

The second type of sensors are the *EPB-PW* titanium sensors and have dimensions of 6.4 x 11.4 mm (Appendix A). The sensors were calibrated in 3SR laboratory to give a value of pressure in kPa based on the voltage output. These sensors could also be used as pore pressure sensors with a porous stone attachment added in front, which were not available for the current experimental campaign.

In total 10 *EPB-PW* miniature pressure transducers sold by TE connectivity and 8 *KYOWA BE2KC* total stress sensors were used in accordance with available 18 functional acquisition ports.

These 18 sensors were divided into six groups and were attached to laser cut thin rigid wooden pieces (Figure 2.10 & Figure 2.11). These wooden pieces acted as frames and allowed a more controlled and secure placement of the sensors when submerged in the sand. These frames also ensures required radial distance between the sensors and axis of the cone. It is also easier to control the required depth of different sensors. All frames have the same dimensions. Therefore, placing each frame so that the end touches the wall of the calibration chamber guarantees that the sensors are at the appropriate radial distances from the axis of the cone (5, 10 or 20 cm).

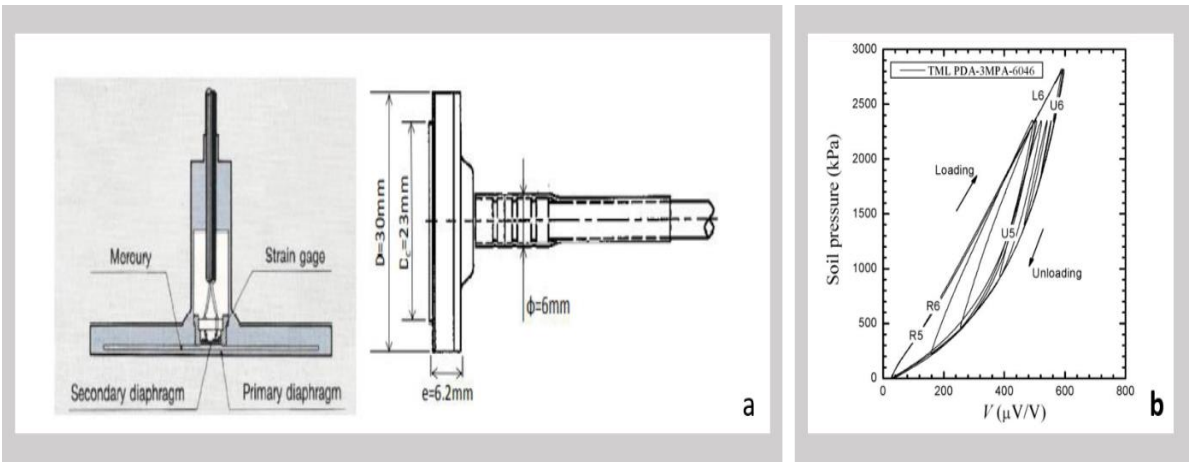

Figure 2.9 KYOWA BE2KC stress sensor (a) and graph from sensor calibration (b)

Figure 2.10 Sensor group placement in sand ensuring required radial and vertical positions of sensors.

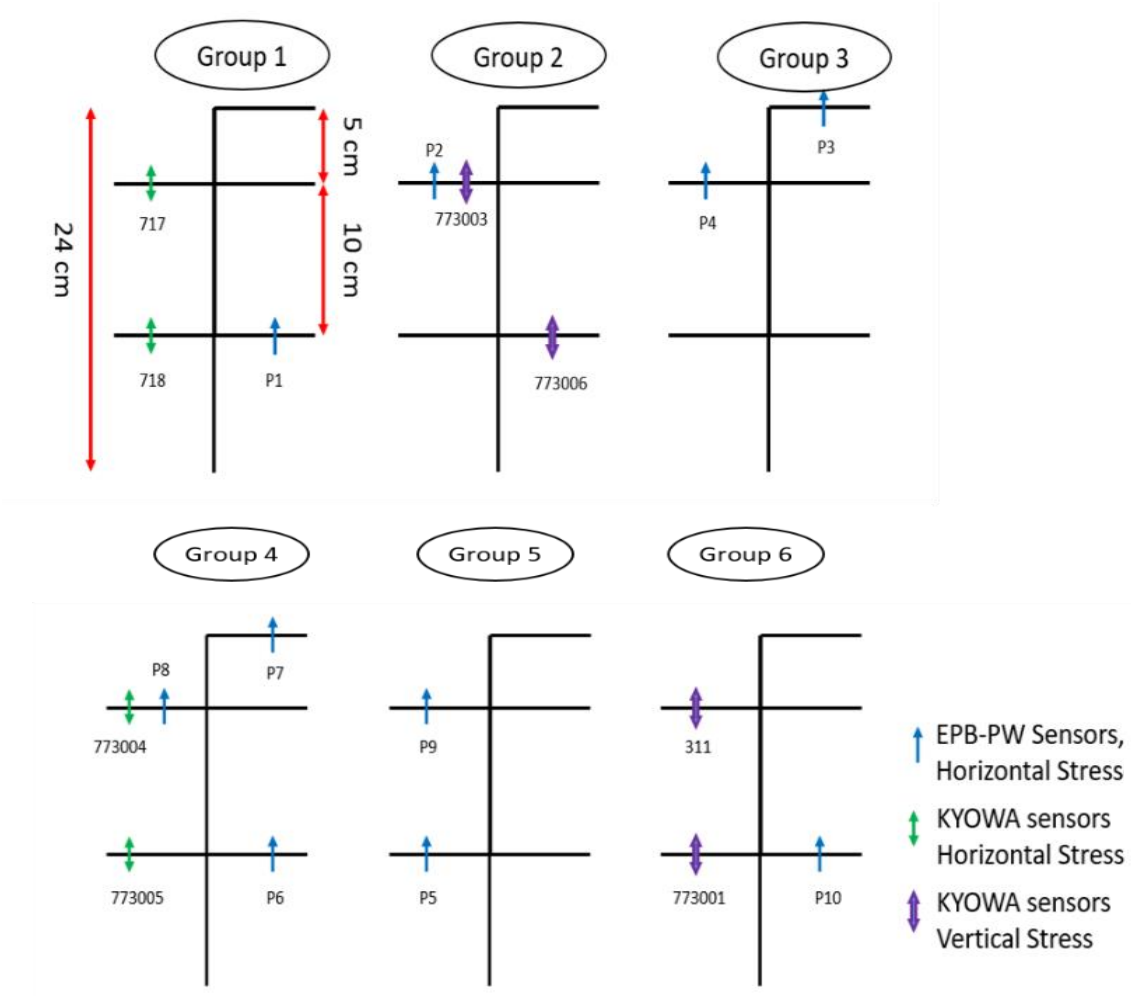

Figure 2.11 Representative image of six group of sensors

2.1.5 Force and displacement control on the tip using a closed-loop system

After defining the test methodology (Section 1.4), it was required to ensure its proper application using the cyclic jack (VE). It required a complex control system that was able to execute either force controlled or displacement controlled step. This was done using a LabView code which was developed in-house with the help of technicians at 3SR laboratory. This code depends on PID parameters to match the output and the input signals.

PID - **proportional–integral–derivative controller** is a well-established way of driving a system towards a target position or level. In other words, PID ensures that the actual output values of a closed loop system is as close to the target values as possible It is a control loop mechanism using feedback that is widely used in a large range of scientific processes as well as automation.

The working of PID control can be understood using Figure 2.12Figure . The method involves calculating an error value [*e(t)*] between the output [*y(t)*] and input value [r*(t)*] at a given time. Then a **P** (proportional) value tunes and corrects the output proportional to the error value. This correction parameter also decides how fast the actual signal reaches the target value. The other parameters (**I** and **D**) are required because as the error value will become close to zero, the applied correction will also become close to zero and hence never perfectly match the target value.

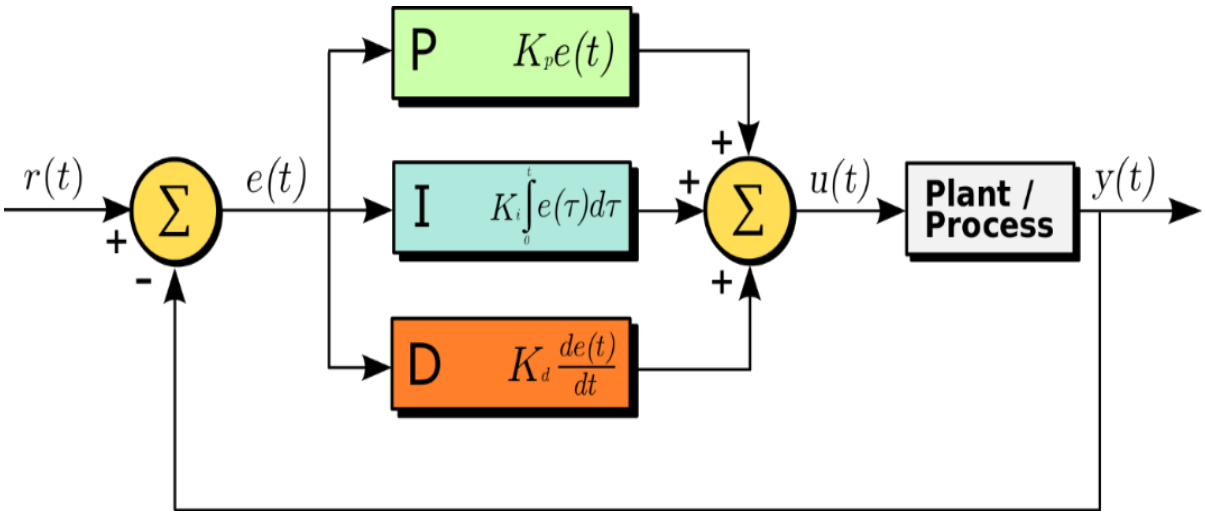

Figure 2.12 Control using PID parameters (Image by Arturo Urquizo - via Wikimedia)

Integral tuning (**I**) parameter works to rectify this problem by integrating the past error values (before the current time's error). The **I** term aims to eliminate the residual error by adding a control effect due to the historic cumulative value of the error. So if the signal is above the response value continuously, the (**I**) parameters provides a push that may result the response value to reach and even overshoot the target value.The **D**erivative

tuning is also referred as anticipatory control and calculating the rate of error change. Physically, it tries to minimize the overshoot caused by the **I** parameter.

Parameter	Rise Time	Overshoot	Settling time	Steady Stare Error	Stability
"P" Increase	Decrease	Increase	Small Change	Decrease	Degrade
"I" Increase	Decrease	Increase	Increase	Decrease	Degrade
"D" Increase	Minor Change	Decrease	Decrease	No effect	Improve if D is small

Table 2.1 Effect of change of PID parameters

The theoretical effect of change of each parameter independently on the control was discussed by Ang et al 2005 and is as summarized in Table 2.1 and the terms used are explained in Figure 2.13.

Unfortunately the LabView code did not have an auto-tuner for the PID parameters and the ideal values of PID parameters had to be found by trial and error. This was done by applying the **Cyclic CPT** test on a steel beam (Figure 2.14). The initial testing on a steel beam with different P parameters gave results as shown in Figure . The figure shows the force control part (Step C) where cycles of constant magnitude are being applied. The "Target force" is decided by $\alpha_{F,max}$ and $\alpha_{F,min}$ parameters and the force recorded during

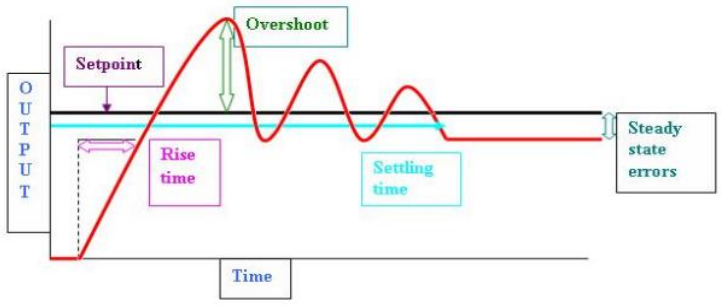

Figure 2.13 Key terms in control systems (Source: Google Images)

Figure 2.14 Cyclic CPT test being performed on a steel beam

Step A. The “Actual Force” is the force transducer’s measurement (Force transducer #2- Figure).

PID parameter of 5,0,0 gave satisfactory results to match the target values of force and displacement during different steps of the **Cyclic CPT** test. Increasing P values further did not improve the force control during cyclic loading, however made the test unstable during displacement control.

Similarly, adding an integral (**I**) and a derivative (**D**) correction made the control much worse during cyclic loading (force control), which can be explained by the changing sign of the error value [$e(t)$] due to target force reversal. Thus a PID value of 500 was thought ideal for the **Cyclic CPT** test. However, during actual calibration chamber tests, it was observed that this PID parameter was causing large vibrations during STEP B (Constant Target Force) and lead to complete tip opening during this step, even when the target tip force was 0.6 times ($\alpha_{F,const}$) the penetration resistance measured in STEP A. It can be seen in Figure that STEP A was executed as expected, causing a tip opening of 1 cm (right y axis) during the first 2 seconds (Speed = 5 mm/s) and recording the tip resistance.

However during STEP B, the applied force (left y axis) varied a lot and vibratory loading (i.e. loading/unloading force cycles on the tip with a high frequency) was applied causing the tip to open rapidly. The root cause analysis found that a constant tip force could easily be maintained on a steel beam due to its elastic properties, while in sand it was much more difficult to apply a constant force during STEP B. Even under a constant force, small settlement of the sand below the tip because of application of force, will change the recorded force value and hence the error between actual and target value of force. A very high gain parameter (**P**) results in fast movement of the tip trying to remove the error and re-establish the constant target force. In this process if the actual applied force overshot the target force, the error value changes sign and high **P** value causes the force to decrease rapidly and therefore the piston of the cyclic jack to retract. This process continues and results in strong vibrations that lead to opening of the tip during STEP B. Thus, it was established that the gain parameter (**P**) value of 5 was not ideal for an application of constant force in sand but was required for application of uniform force cycles.

A solution was found by separating the gain parameters for cyclic steps (STEP C and STEP G) and for all other steps.

A PID values of 2,0,0 were found suitable for all steps of the Cyclic CPT test apart from cyclic loading steps where PID values of 5,0,0 remain ideal. These values helped the control to maintain minimum error between target and actual force and displacement applied on the tip.

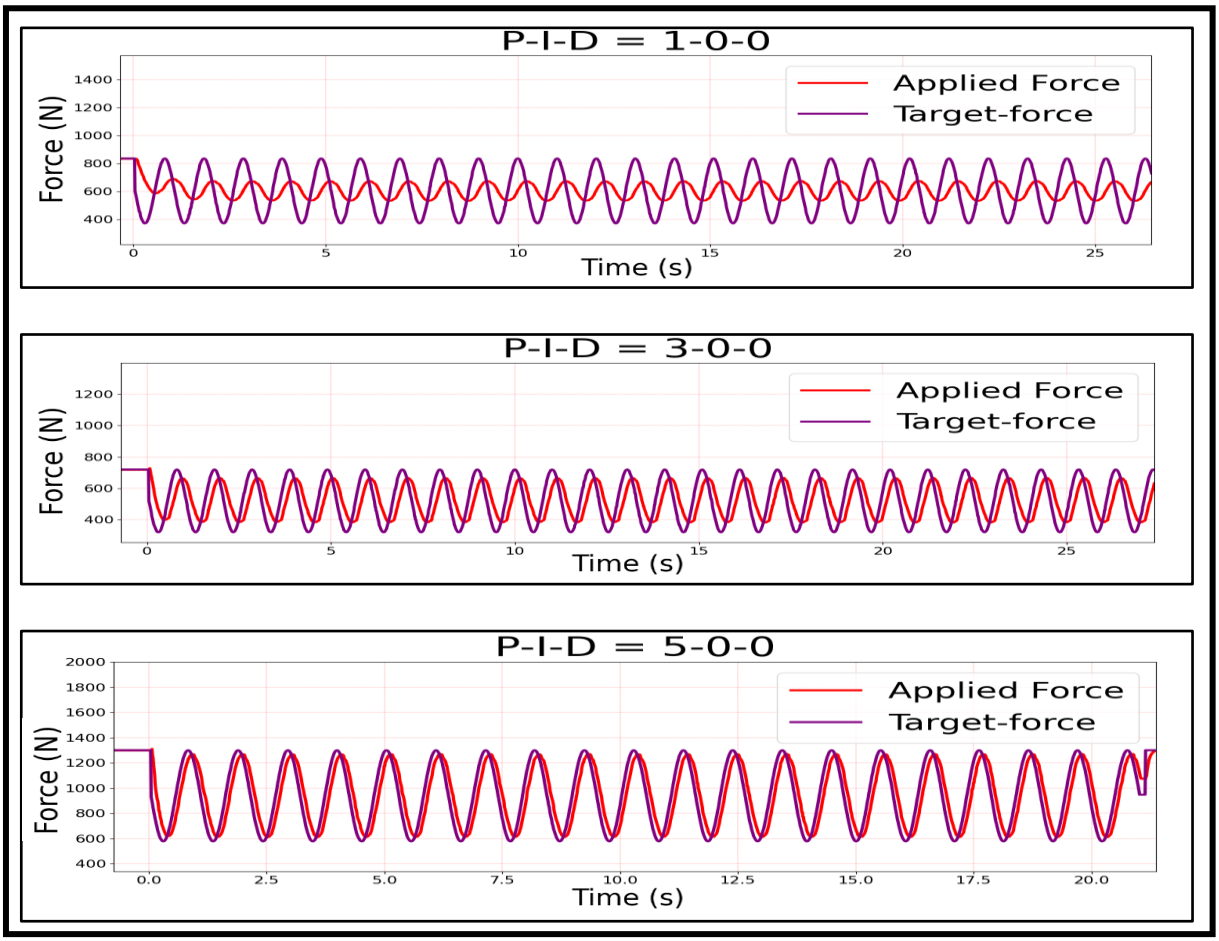

*Figure 2.15 Effect of change of **P** parameter on force applied on the steel beam by Equaterre's cyclic jack*

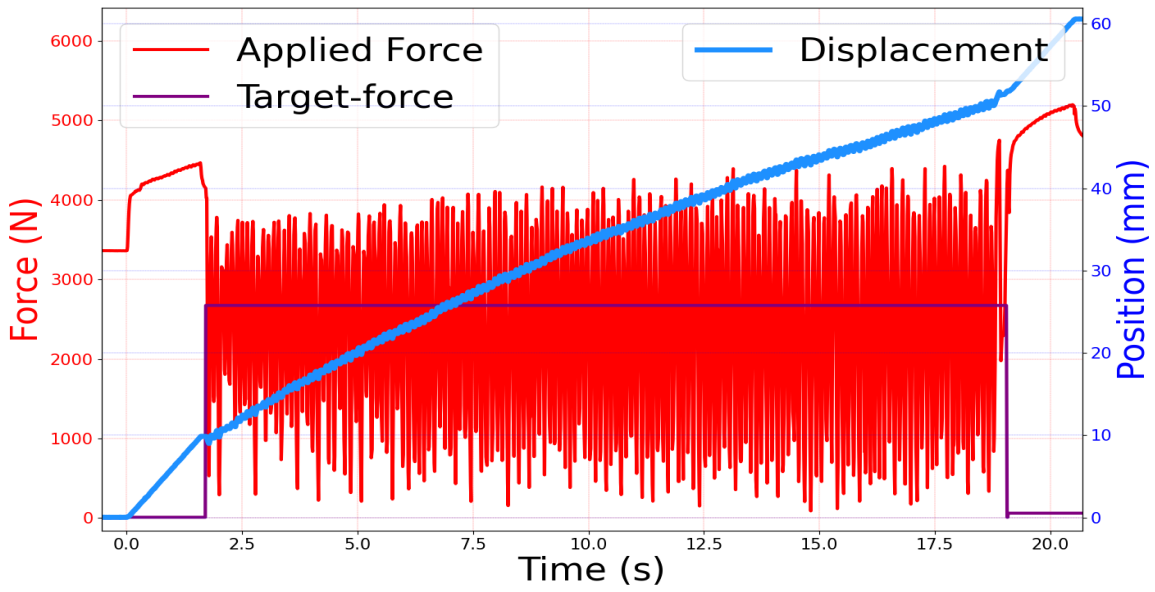

Figure 2.16 Large vibrations during Step B due to large P value (PID = 500) for a cyclic CPT test on sand inside the calibration chamber

2.2. Characterization of investigated sand

Sand investigated during this research work is Fontainebleau GA39. SIBELCO-France's quarries mines and processes the GA39 test sand at Nemours, South of Paris. It is a fine sand with the grains size distribution in the range considered most prone to liquefaction (Figure 2.17).

The grains shape is also sub-angular and sub-rounded (Figure 2.18). The same sand had been previously used during the thesis work of Silva 2006 and Rimoy 2013. However, in both these projects, NE 34 sand was the principle sand investigated which is a coarse version of the GA-39 sand. These sands match each other's mineralogy, surface roughness and grain shapes. The properties of the GA39 are detailed in Table 2.2.

SiO_2(%)	G_S(-)	d_{10}(mm)	d_{50}(mm)	d_{60}(mm)	C_u	e_{max}	e_{min}
>99.1	2.56	0.087	0.113	0.122	1.1	1.01	0.56

Table 2.2 GA39 Sand properties (From Sibelco & Silva 2006)

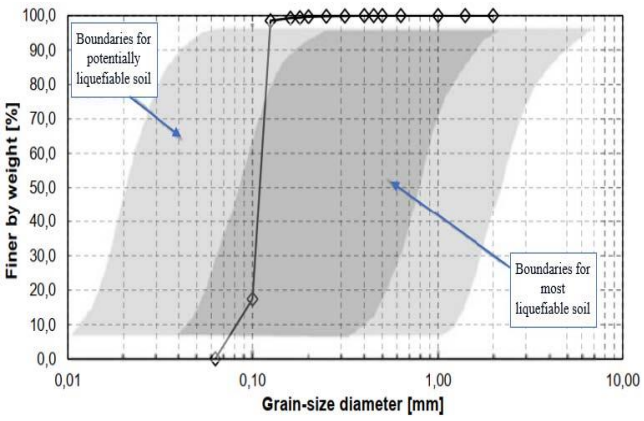

Figure 2.17 Grain Size Distribution GA39 Sand (Tsuchida 1970)

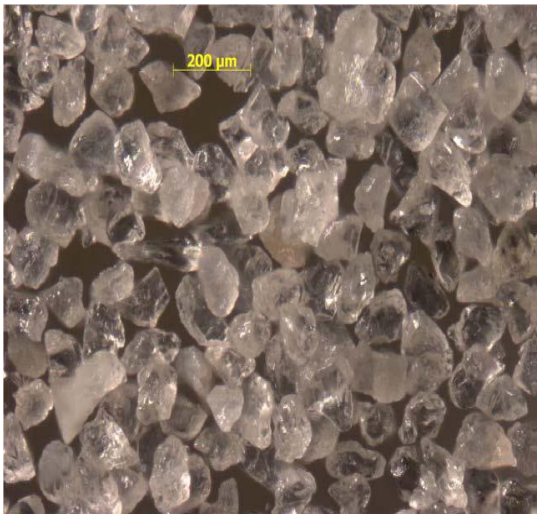

Figure 2.18 Microscope images of GA39 from Microsurf 3D Optical (From Rimoy 2013)

2.3 Sample Preparation Methods

The importance of high-quality samples for soil characterization and for measuring its mechanical properties is well documented. Undisturbed soil samples from the ground are ideal for performing laboratory experiments. While it is relatively easy to obtain undisturbed samples from traditional tube sampling methods for cohesive soils, it is challenging to retrieve samples of granular soils from the field without changing their properties. After removing the confining stresses provided by the ground, even small-scale laboratory experiments like shear tests and triaxial tests may give results different to those expected by undisturbed samples. One way around the problem is using ground freezing techniques to retrieve undisturbed sand samples. However, this method is costly and still remains an emerging one even for research activities.

Thus, there is a reliance on reconstituted representative samples for studying granular soils. In some instances, it is next to impossible to reconstitute the effect of ageing, cementation and chemical action over centuries. However, the index property most commonly used as a reference for replicating field conditions is density. An ideal reconstituted sample preparation method must have following qualities Kuerbis and Vaid 1988:

- Large range of sample density should be possible (loose to dense)
- The sample must be uniform – same void ratio throughout the sample.
- The sample must be fully saturated. (Specially for liquefaction studies)
- There should not be any segregation of fines.
- The method should mimic the actual soil deposition being modelled.

Traditionally used approaches for creating reconstituted samples involves ***dry or moist tamping, air pluviation, water sedimentation and slurry deposition***. The mechanical behaviour of sands depends predominantly on their grain shapes, grading, effective stress level, major principal stress axis orientation and density state. However, depositional fabric particle properties and orientation also affect the soil properties significantly. Thus samples created using two different methods can show variable mechanical responses of the soil during testing. Ishihara 1993 mentioned the importance of fabric dependency for a given density and discussed the sample preparation method's effect on the soil's liquefaction resistance.

2.3.1 Moist Tamping

The tamping sample preparation method is one of the oldest laboratory reconstitution technique (Lambe 1951). This technique involves adding consecutive layers of soil to the

sample and tamping it with a constant frequency and effort before adding the next layer. This method closely models the effect of landfills created by rolling over the soil.
Tamping **moist** samples with water content between 3 to 6% can result in very loose to dense samples. However, the samples created may be non-uniform with respect to density. Suits et al. 2003 studied this sample preparation method and indicated that the vertical stresses applied by tamping could be higher than the typical confining stresses in triaxial testing. They also pointed out that the bottom layer of the sample experiences greater compaction force than the layer above it. Miura et. al. 1984 performed miniature cone penetration tests for different sample preparation methods and found that moist tamped samples resulted in non-uniform samples. Casagrande, 1976 suggested that samples created using this method are more prone to liquefaction due to "honeycomb structure because of capillary forces between moist grains". Also, samples created using this technique can face large strains when saturated.

2.3.2 Air Pluviation

Mahmood & Mitchell 1976 concluded that air-pluviation produces a random orientation of grains while preferential orientation results from vibratory densification for medium-grained sand. Oda et. al. 1985 suggested that the intrinsic anisotropy and fabric obtained by pluviation method duplicate those developed in natural sediments. Other benefits of air-pluviation technique include ensuring no separation of fines across the depth of the sample and can be used to generate a wide range of densities. The sensitivity of the drop height and the possible movement of larger particles towards the specimen edge are the possible problems encountered. Air pluviation has been used to create samples varying in size from an order of ten millimetres in a triaxial test to those for creating a calibration chamber that is of an order of one meter. For a triaxial sample, the required sand is filled inside a funnel that is initially placed at the bottom of a split mould. Then, the funnel is slowly raised, and the sand particles are deposited with minimal drop heights to form very loose specimens (generally relative density, $D_r \sim 30\%$ or less). If a denser specimen is desired, vibration can be applied by tapping the split mould at constant intervals. The deposition and tapping procedures has facilitated creation of sand specimens up to 85% D_r. Similarly, for calibration chamber testing, air pluviation has been the most widely used sample preparation method.

Sample density using air pluviation is controlled by the compaction energy retained by the particles while contacting the deposition surface. The compaction energy, in turn, depends on the difference of particles' kinetic energy and energy losses on contact. The kinetic energy depends on the kinetic friction calculated using Stoke's Law and the particles' buoyancy in air. Two main factors influencing the density of the sample created are Height of Fall (HF) and Deposition Intensity (DI) or the flux. For maximum compaction energy and density, the velocity at contact is equal to terminal velocity which is achieved when HF (drop height) is equal to or exceeds the particular limiting height at which the

three particles forces (particle weight, kinetic friction and upthrust) are in equilibrium. A height lower than this maximum limiting height of fall does not increase the density, while smaller ones result in a lower density. A height of around 600 mm has generally been observed to be the limiting HF. A uniform chamber density is achieved by ensuring a uniform height of fall and uniform DI throughout the sample preparation. Pluviators generally have a reservoir with equidistant holes at the bottom to ensure constant DI throughout the cross-section of the sample. Vaid & Negussey 1984 showed varying the drop height between 0 – 0.5m has the greatest influence on the achieved density and suggested that for small containers, the density is also affected by container dimensions and wall roughness. The effect of high flow rates (i.e. high DI) inhibits compaction at the sand surface and leads to looser samples. The effect of the HF and DI can be clearly seen in Figure 2.19 as published in Tabaroei et. al. 2017. The figure shows the calibration results of an air pluviator. It is seen that for similar HF values, higher DI values (larger dia of holes or greater number of holes) lead to a lower density. Also, for a particular DI value, the density of the sample increased till a particular HF (Limiting height of fall –around 600 mm) ,after which it remained constant. This phenomenon has been widely observed and well accepted. Air pluviators vary in their design and mechanism. They can be fixed raining system of the same cross-section of the sample or may have a movable depositor.

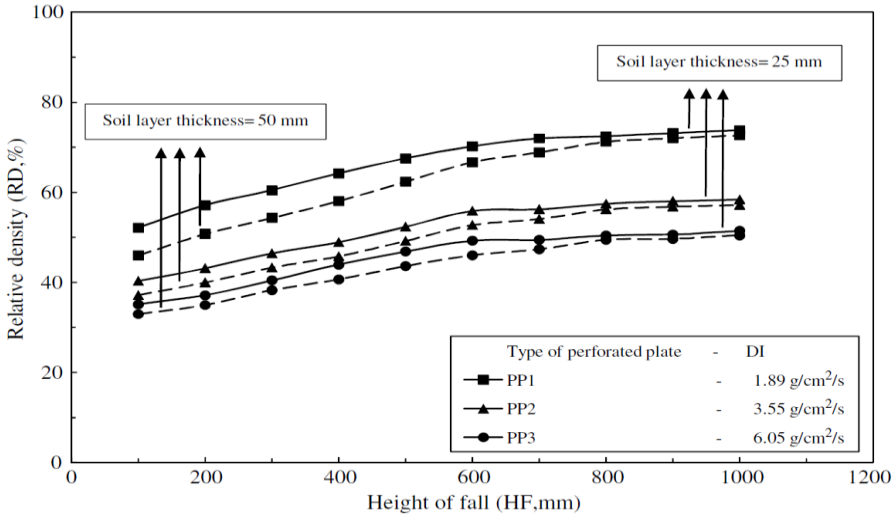

Figure 2.19 Effect of DI and HF on density of sample

2.3.3 Wet Sedimentation and Water Pluviation

This method generally involves performing pluviation in de-aired water rather than air. Water sedimentation for a tri-axial sample involves placing sand particles in a volumetric flask with de-aired water and then saturating it by either boiling or applying a vacuum. The flask is then inverted, lowered to the bottom of the split mould, and raised slowly. The benefits of this method include better saturation of the sample, even without the extra

stage of flushing CO_2 through the sample (Kwan and Mohtar 2020). However, this method may lead to separation of fines as heavier particle settle faster.

Thus water pluviation techniques should only be used to test poorly graded or clean sands. This method cannot form representative uniform samples of well graded soils or silty sand. The terminal velocity of sand in water is lower than that in the air; therefore, the energy of sand settlement and relative density of water-pluviated sands is generally lower than air-pluviated sands. Therefore, the maximum density of sample created using this method is generally lower than that of the air pluviation method. Water pluviated sand samples are also generally more compressible due to the higher radial compressibility of water pluviated fabric.

Kuerbis & Vaid, 1988 introduced a method called slurry deposition (Figure 2.20) for preparing sand samples with fines for triaxial tests aiming to overcome the shortcomings of air and wet pluviation method. Key attributes of this slurry deposition method are:

- Ensuring the saturation of the sample
- Sample preparation time between 1.5 to 3 hours
- Controlled sedimentation currents and particle size segregation during deposition.
- Loose samples created that can be compacted to higher density
- Models the soil fabric found a natural fluvial or hydraulic fill deposit

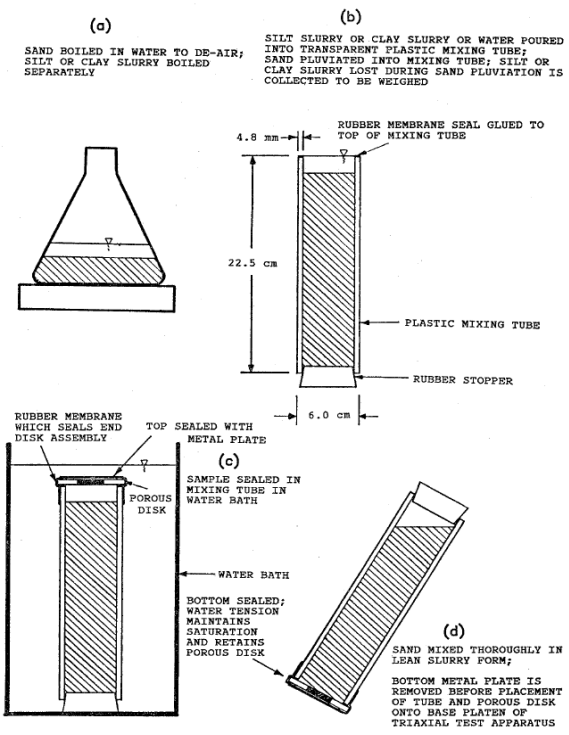

Figure 2.20 Schematic drawing of slurry deposition method for sample preparation (Kuerbis &Vaid 1988)

However, the requirement for the using of a mixing tube of diameter slightly smaller than the specimen makes it almost impossible to use this technique in its original form for calibration chamber testing. However, the benefits of slurry deposition makes it a viable option for experiments studying liquefaction probability of a sand.

2.3.4 Sample Preparation Methods Used

Samples created during this thesis work used relative densities (D_R) (Equation 2.1) as the control parameter. Samples varying from very loose state to medium dense state were tested during this PhD work.

STATE	Very loose	Loose	Medium	Dense	Very dense
D_R [%]	0 - 15	15 - 35	35 - 65	65 - 85	85 - 100

Table 2.3 State of sand according to Relative Density

$$D_R = \frac{e_{max} - e_0}{e_{max} - e_{min}} * 100\ [\%] \qquad \textit{Eq. 2.1}$$

The manufacturer provided the values of e_{max} and e_{min} which were also checked during this PhD work. The calculated values were in close agreement with the provided values (Table 2.2).

The sample preparation methods used during this work are : Dry pouring (loose state), Moist tamping (very loose) and Dry Tamping (medium dense density).

For the small scale tests: Dry pouring method depends on the funnel diameter and the fall height. A greater diameter corresponds a smaller D_R, while at higher heights of fall greater relative densities are associated. The objective of creating a sample with the dry pluviation method was to reach a density as loose as possible so as to study liquefaction of GA39 sands in triaxial tests. The dry pluviation method was used in triaxial tests (2.3.3) and the minimum relative density reached was 19%. To obtain even looser samples, moist tamping method was used to create samples with an initial water content of 5%. Relative density values obtained from this method varied from -27% to 5%. Dry tamping method with compaction was used to create samples in interface shear tests and resulted in samples around 65%.

For calibration chamber testing, a new stationary air pluviator was designed and manufactured (Figure 2.21). The use of three different deposition intensity and different height of fall were envisaged to create a broad range of possible relative densities. A silo

is used to ensure a continuous supply of sand. A rigid plate at the bottom of the silo, with uniformly distributed spaced holes can be used to control the deposition intensity. Two distribution meshes separated by 20 cm distance ensures uniform distribution of soil across the cross-section of the sample. The distance from the bottom of the distribution meshes to the top of the deposition surface is the height of fall (**HF**). The distribution meshes are attached to the silo by three steel cables running outside the silo and connected to the electric loading crane of the Laboratory 3SR. By lifting the crane, the two

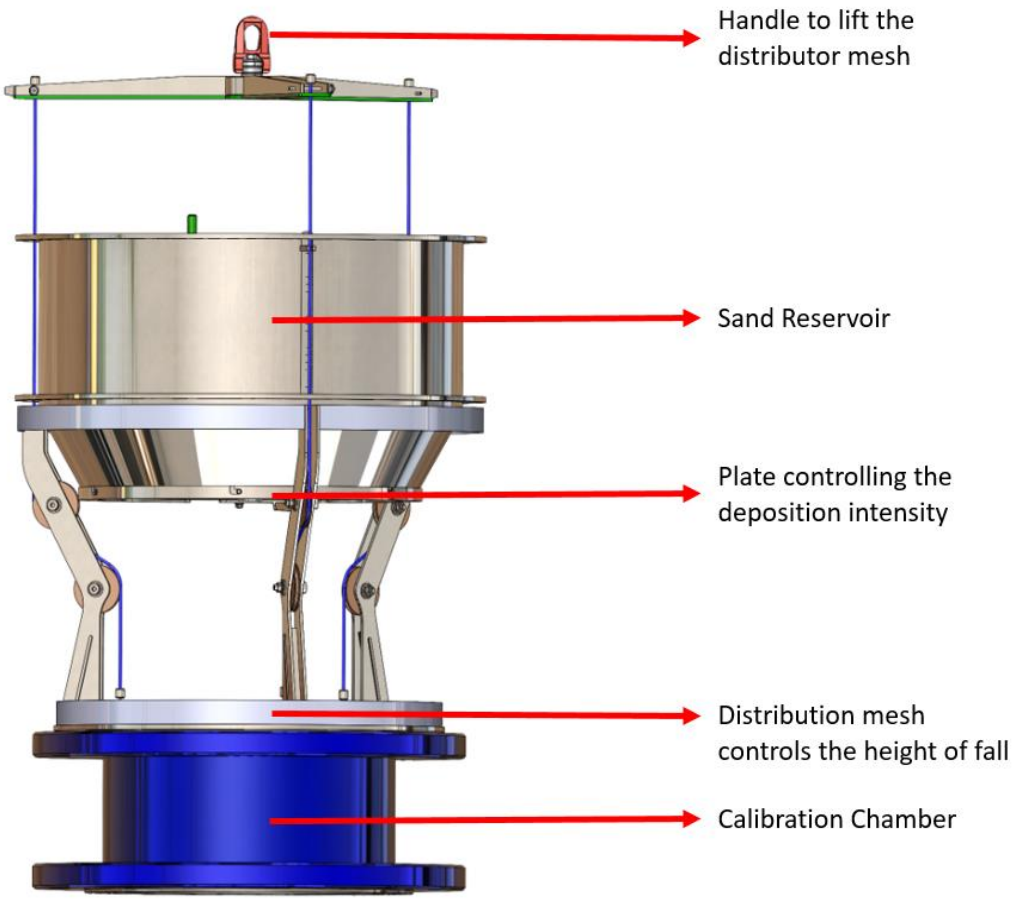

Figure 2.21 New pluviator designed for the use in 3SR Lab

distribution meshes move upward as the sand falls from the upper silo. By moving the crane upwards at the same rate as the rise of the sample inside the calibration chamber, a constant HF can be maintained ensuring uniform density of sample.
However, due to manufacturing defects, this equipment could not be made functional till the end of the experimental campaign. The defects included wrong size of the calibration chamber and a non-functioning trap to stop the sand flow while filling the reservoir. It will be used for future works in this project.

Due to lack of a pluviator and other limitations, method close to slurry deposition was used to create the saturated sample. The procedure included adding 25-30 kg quantity of moist soil in a pond of water (10~15 cm) above the top of the soil sample under preparation and using a stick to shake the slurry and letting the sample to settle down

before adding the next layer. The relative density of the samples created using this method varied between 35% to 46%.
For the dry sample at loose state, again the dry soil was added progressively using a bucket and spread uniformly without any compaction. This method resulted in a relative density of 19%. For a denser dry sample, the soil was compacted using a heavy tamper.

2.4 Small Scale Lab Experiments Performed

For characterization of the GA39 sand, a set of laboratory experiments was performed to give insight into the behavior of this sand and its liquefaction susceptibility. Also, since there will not be a possibility to apply a backpressure in the calibration chamber, the effect of backpressure on the shear behavior of this sand is studied. The performed tests are interface shear tests, permeability test and triaxial compressions tests.

2.4.1 Interface Shear Test

To study the possible friction values between the material used for manufacturing the Gouda cone and the sand used four interface shear tests were performed with a Constant Normal Load (CNL). Three different normal stress values (100, 200 and 400 kPa) were applied on medium dense GA39 sand (D_R ~ 65%) and a smooth stainless steel plate

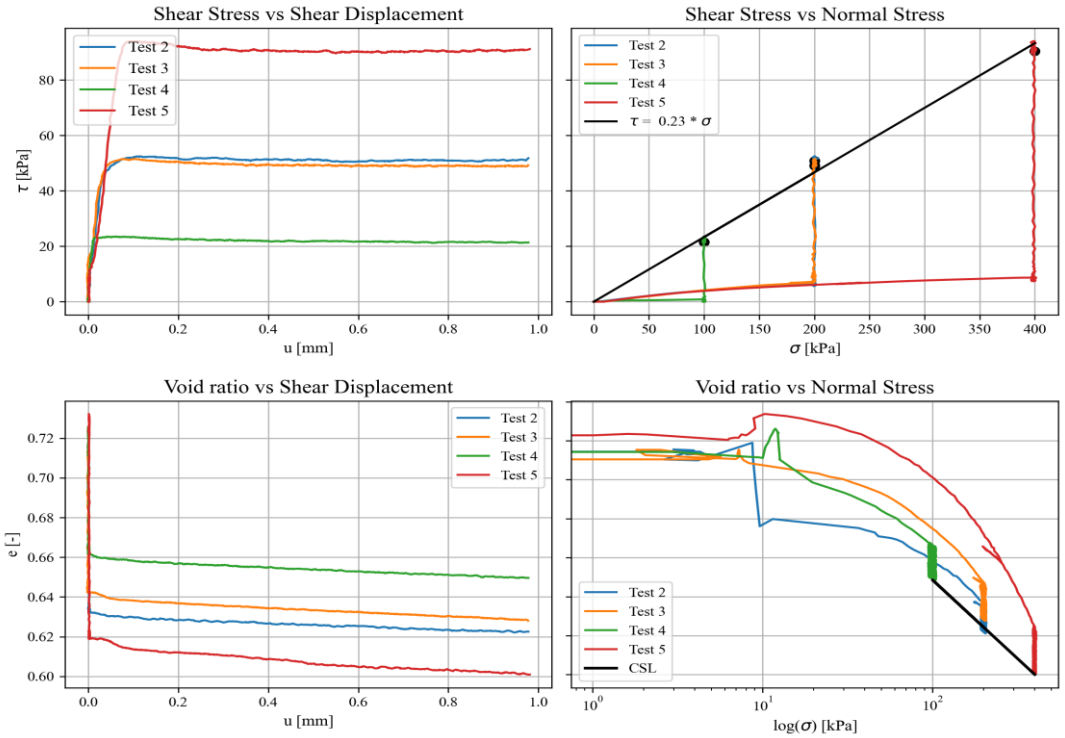

Figure 2.22 Interface shear resistance test between GA39 sand and steel plate with three different normal stress

interface. From the analysis a maximum interface friction angle equal to 13.1° was found. It was observed that the behaviour was mainly contractive with very low friction angle which was typical to smooth interface.

2.4.2 Permeability Test

Permeability tests were carried out in order to assess the drainage behaviour in GA39 soil. Empirical relations are often used to predict the permeability coefficient of sands. One commonly used expression is as shown in equation 2.2 (Hazen's formula).

$$k = (d_{10})^2 * 10^4 \qquad \textit{Eq 2.2}$$

where d_{10} is the particle size for 10% dry mass of material passing. For GA39 Fontainebleau sand, d_{10} is 87 µm. Therefore, predicted $k = 7.7 * 10^{-5}$ m/s. However, permeability coefficient depends also on the density of the sand which is not taken into account by Hazen's formula.

Constant head permeameter was used to study the effect of the sample preparation method on permeability coefficient. During this test, a constant water head is applied and water head drop at three different heights of the sample is measured via burettes (piezometers) connected at these heights. Using the rate of flow and the average drop between fixed distance, we can calculate the permeability coefficient(k).

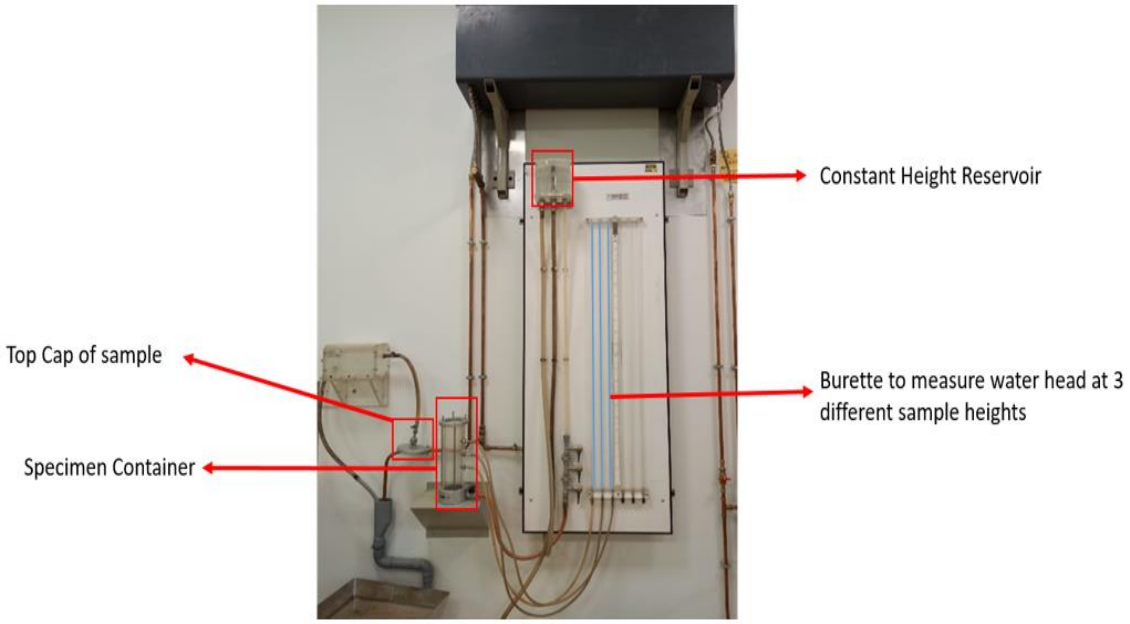

Figure 2.23 Constant Head Permeability Test (IUT, Grenoble)

Moist tamping specimens created more permeable samples than those created by dry pluviation, which were in turn more permeable than those created by dry tamping (See results in Table 2.4). In all cases, the order of magnitude of permeability was similar ($5*10^{-5}$ m/s) and corresponded to those expected from fine sand. However, the values varied between 3.4 to $7.1* 10^{-5}$ m/s. These permeability values correspond to conditions of completely drained conditions during normal cone penetration testing. (McNeilan and Bugno 1984)

S.No.	Sample Preparation Method	Density of sample (g/cm^3)	Permeability Coefficient (m/s)
1	Dry Pouring	1.38	$6.8 * 10^{-5}$
2	Dry Pouring	1.35	$6.0 * 10^{-5}$
3	Dry Tamping	1.51	$4.4 * 10^{-5}$
4	Dry Tamping	1.54	$2.5 * 10^{-5}$
5	Moist Tamping	1.183	$7.1 * 10^{-5}$

Table 2.4 Coefficient of Permeability for different sample preparation methods

2.4.3 Triaxial Testing

As a part of this study 20 tri-axial tests (6 drained, 14 un-drained) were performed to study the effect of sample preparation, back pressure and initial confining stress on very loose (Relative density<15%) or loose sand specimens (Relative density<35%). For the drained tests in Figure 2.24, we see a clear distinction in volumetric strain for tests done at similar confining stresses (200 kPa) based on sample preparation method even when all the samples fell in loose or very loose category. The relative density for the two air poured sample was 25%(±2.5%) and was the minimum we could achieve with this method of sample preparation. The moist tamped sample resulted in much looser samples. The moist tamped samples discussed in Figure 2.24 had a relative density of -13.3% (±0.3%) We observed that moist tamped loose sample contracted while shearing but the air poured sample dilated. These effects can be caused due to the density difference as well as the difference of method of sample preparation. However the shear stress were quite close at high axial strain as expected at critical state.

Also, the effect of back pressure(u) is quite small for samples prepared by same method having similar initial density and loaded in drained conditions. As such the specimen in the calibration chamber which is saturated without a back pressure should behave similarly as the one saturated using a high back pressure if we assume the soil around the tip in the calibration chamber is drained.

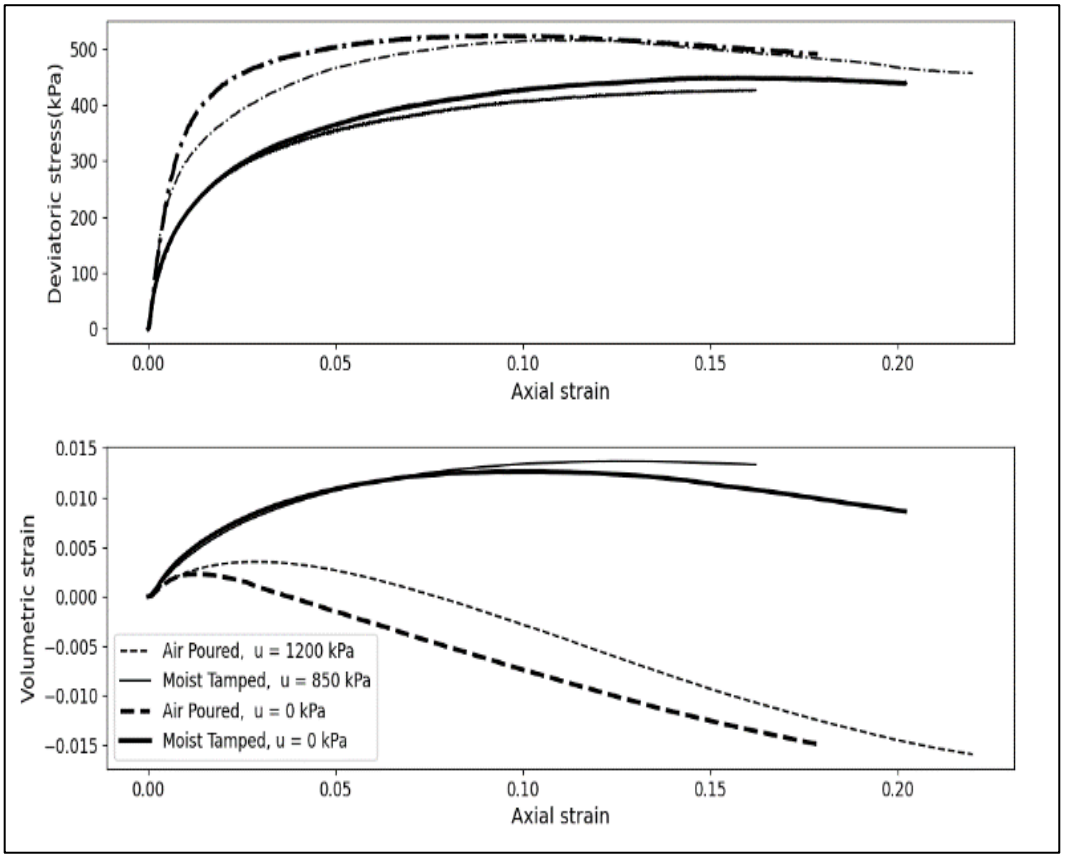

Figure 2.24 Varying drained behaviour for different sample preparation methods at 200 kPa confining stress (D_R ~ 25% for the two air poured samples and -13% for the two moist tamped sample)

For undrained tests too, the initial density of the air poured sample shown in Figure 2.25 was higher [27%(u = 2100 kPa) & 36.7%(u = 0 kPa)] as compared to moist tamped samples [-7%(u = 0 kPa) & -1%(u = 2100 kPa)]. The behaviour of the specimen even under the same initial confining pressure (200 kPa) varied depending on the method of sample preparation and the resulting relative density. It was observed that even loose air poured samples dilated (negative pore pressure) hence showing no tendency to liquefy, while very loose moist tamped sample had a development of pore pressure as the axial strain increased, as such may be prone to liquefaction. .

These results gave us the confidence that we will be able to control the initial state of the soil sample in the calibration chamber by either preparing the sample by moist tamping or air pouring. In particular the control of initial relative density can be used to create samples that are susceptible to liquefaction or not for this sand.

Lastly, in Figure 2.26 we can observe the undrained response of four moist tamped samples with relative density of -4.5±3% when initial confining stress is changed. We can observe a change of behaviour when initial confining stress changes from 200 to 300 kPa giving us an indication as to what depths on the field and what vertical stresses in the calibration chamber can be used to differentiate between liquefiable and non-liquefiable cases for these kinds of samples.

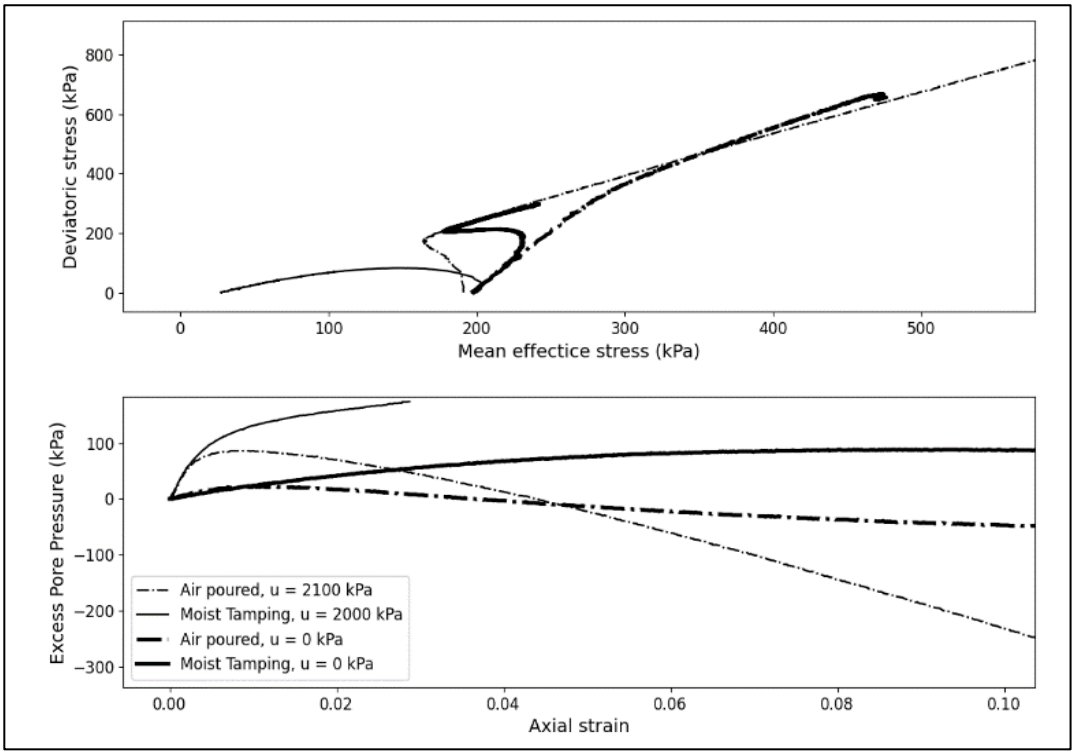

Figure 2.25 Varying behaviour of samples created using different sample preparation method and back pressure during undrained triaxial tests.
[$D_{R(air\ poured,\ u=2100\ kPa)}$=27%, $D_{R(air\ poured,\ u=0kPa\ )}$= 36.7%], [$D_{R(moist\ tamped,\ u=0\ kPa)}$=-7%, $D_{R(moist\ tamped,\ u=2000\ kPa\ )}$= -1%]

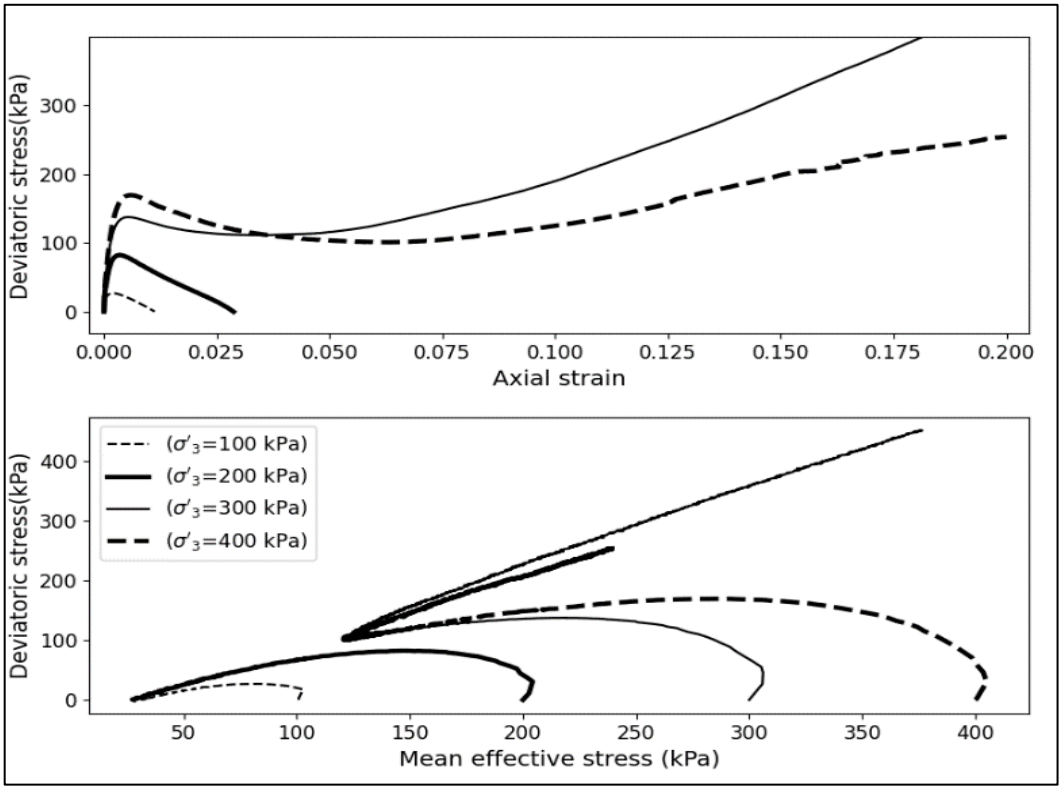

Figure 2.26 Difference of undrained behaviour of moist tamped sample based on initial confining stress during triaxial testing

2.5 Conclusions

This chapter introduced calibration chamber testing before explaining the new equipment designed for this project. Next, the sand used for the calibration chamber testing during this experimental campaign - Fontainebleau GA39 was introduced and results from small-scale tests performed for mechanical characterization of the sand are shown. It was observed that the sand saturated without backpressure showed similar shear behaviour to the ones saturated with back pressure under drained conditions. However, in undrained conditions, the moist tamped samples saturated using back pressure showed a much higher increase in pore pressure than the one tested without it. A difference in response was also observed for the air =-poured samples. The effect of applied confining stress on undrained triaxial tests was also studied. It was observed that samples demonstrated a continuous drop after the peak deviatoric stress for confining pressure of 100 and 200 kPa, while there was a dilative response after initial compression during the tests performed at 300 and 400 kPa stress. This observation is in line with liquefaction only being observed in shallower depths where the mean effective stress is low. The chapter also recommends a friction angle of -13^{o} for the modelling cone and sand interface.

Chapter 3

3. Results from Calibration Chamber Testing

More than 110 **Cyclic CPT** tests have been performed on the sand to define the test methodology, ensure a good test control, study the impact of different input parameters, and then investigate different soil conditions in GA39 sand.

The results shown in this chapter concentrates on tests done inside the calibration chamber. Ten calibration chamber tests have been performed since the equipment became functional (December 2021). An attempt was made to study different working conditions like the effect of saturation, density and vertical stress on the results of the **Cyclic CPT** test during these calibration chamber tests. Unfortunately, successful **Cyclic CPT** tests could be performed only during five out of ten calibration chamber tests. The problems were caused due to the faults caused by different hardware bugs and errors in the LabView code. The first **Cyclic CPT** test inside a calibration chamber sample was done at a depth of ten centimetres[1]. After that, it was attempted to keep a fixed distance of 16 cm between the start of two **Cyclic CPT** tests. This distance allowed for a maximum tip opening of 6 cm and a minimum distance of 10 cm between two **Cyclic CPT** tests to ensure that the result of the tests was not affected by the previous test done just above it. This allowed a total of six tests to be performed at depths of : 10, 26, 42, 58, 72 and 88 cm inside each calibration chamber sample of almost 110 cm total height.[2] **Cyclic CPT** tests with similar input parameters were tested at similar depths in different soil samples to reduce the variables to a minimum.

The current chapter discusses the results of few of the **Cyclic CPT** tests performed on these five calibration chamber samples. The details of the **Cyclic CPT** tests discussed during this chapter are as shown in Table 3.1 Details of few successful tests.[3] Each colour in this table corresponds to one of the five calibration chamber samples in which **Cyclic CPT** tests are performed. This chapter also details the stiffness parameters that can be used to study the effect of cyclic loading on the soil. Further, the effect of applied vertical stress, saturation conditions, the density of the sample and the frequency of the test on the results of **Cyclic CPT** tests are discussed. Eventually, this chapter highlights the impact of different input parameters on the control and the results of a **Cyclic CPT** test.

[1] None of the tests done at 10 cm depth are used the discussion as a greater depth was required for tip stress to stabilize. (Discussed in Section 3.2)

[2] The last test at 88 cm depth allowed for a minimum of almost 16 cm distance between the tip and the top of pebble layer at the bottom of the calibration chamber.

[3] Details of all the Cyclic CPT tests performed on sand during this research work are as shown in Appendix B.

Test ID	Saturation	Sample Preparation	R.D. (%)	σ_V (kPa)	Depth (cm)	$\alpha_{F,const}$	$\alpha_{F,max}$	$\alpha_{F,min}$	f (Hz)
51	Saturated	Slurry Deposition	34%	75	26	0.6	0.78	0.42	1
52	Saturated	Slurry Deposition	34%	75	42	0.5	0.65	0.35	1
53	Saturated	Slurry Deposition	34%	75	58	0.5	0.65	0.35	1
54	Saturated	Slurry Deposition	34%	75	74	0.6	0.85	0.35	1
55	Saturated	Slurry Deposition	34%	75	90	0.6	0.8	0.4	1
73	Saturated	Slurry Deposition	46%	150	26	0.6	0.78	0.42	1
75	Saturated	Slurry Deposition	46%	150	58	0.5	0.65	0.35	1
77	Saturated	Slurry Deposition	46%	150	82	0.6	0.8	0.4	1
84	Dry	Dry Deposition (overhanging bag)	34%	75	23.5	0.6	0.78	0.42	1
86	Dry	Dry Deposition (overhanging bag)	34%	75	44.5	0.5	0.65	0.35	1
87	Dry	Dry Deposition (overhanging bag)	34%	75	47	0.6	0.85	0.35	1
88	Dry	Dry Deposition (overhanging bag)	34%	75	57	0.6	0.85	0.35	0.1
101	Dry	Dry Deposition (buckets)	19%	85	26	0.5	0.65	0.35	1
102	Dry	Dry Deposition (buckets)	19%	85	39	0.5	0.65	0.35	1

Test ID	Saturation	Sample Preparation	R.D. (%)	σ_V (kPa)	Depth (cm)	$\alpha_{F,const}$	$\alpha_{F,max}$	$\alpha_{F,min}$	f (Hz)
103	Dry	Dry Deposition (buckets)	19%	85	55	0.6	0.85	0.35	1
104	Dry	Dry Deposition (buckets)	19%	85	63	0.6	0.85	0.35	0.1
105	Dry	Dry Deposition (buckets)	19%	85	75	0.6	0.8	0.4	1
106	Dry	Dry Deposition (buckets)	19%	85	81	0.85	0.8	0.4	1
107	Dry	Dry Deposition (buckets)	19%	85	85	0.9	0.8	0.4	1
108	Dry	Dry Deposition (buckets)	19%	85	88	0.7	0.95	0.4	1
111	Dry	Dry Compaction	53%	85	40	0.5	0.65	0.35	1

Table 3.1 Details of few successful tests in the calibration chamber

3.1 Result Processing

As discussed in Section 1.4, the only direct results during the **Cyclic CPT** tests are the force measurements during STEP A and STEP E and the displacements during the other steps.

During the cyclic loading (STEP C and STEP G) it becomes essential to study each force cycle and the changes it causes on the tip displacement. This result can be interpreted using a stiffness parameter. The definition of each cycle used and different stiffness parameters studied are discussed below:

3.1.1 Definition of a single cycle:

During the application of cyclic loading in STEP C & G, sinusoidal compressive loads between predefined ratios of tip resistance are applied. The closed loop system and acquisition frequency of the system have to be tuned to apply the desired loading.

The acquisition frequency of the current system is 100 Hz. Therefor each force cycle of 1 Hz frequency, under ideal control, 100 values are recorded for all variables e.g. force measurements on the tip, displacement of the tip measured using the LVDT, total sensor values etc.

However this was not the case in practice, especially during the application of cyclic loading as the number of recorded values per cycle of 1 Hz loading varied between 78 and 100 values.

Figure 3.1 is a zoomed view showing target and actual force applied on the tip (read on left Y axis) and tip displacement (read on right Y axis) for three cycles of one of the **Cyclic CPT** test. We can observe that the distribution of force points recorded is not uniform for the entire magnitude of the cyclic load and there is a clear concentration of recorded points near the crest and trough of the cyclic loading. It was also be seen that although the applied force and the displacement curve follow similar trends, i.e. the tip opens (moves down) when force value increases, the local actual force minima may be slightly delayed in time with respect to corresponding local displacement maxima. A similar gap can be seen between the actual and the target force values. This is because the tip started moving downwards so that the target force can be reached while it takes a small amount of time (less than 0.1 second) for the actual force to match the target force.

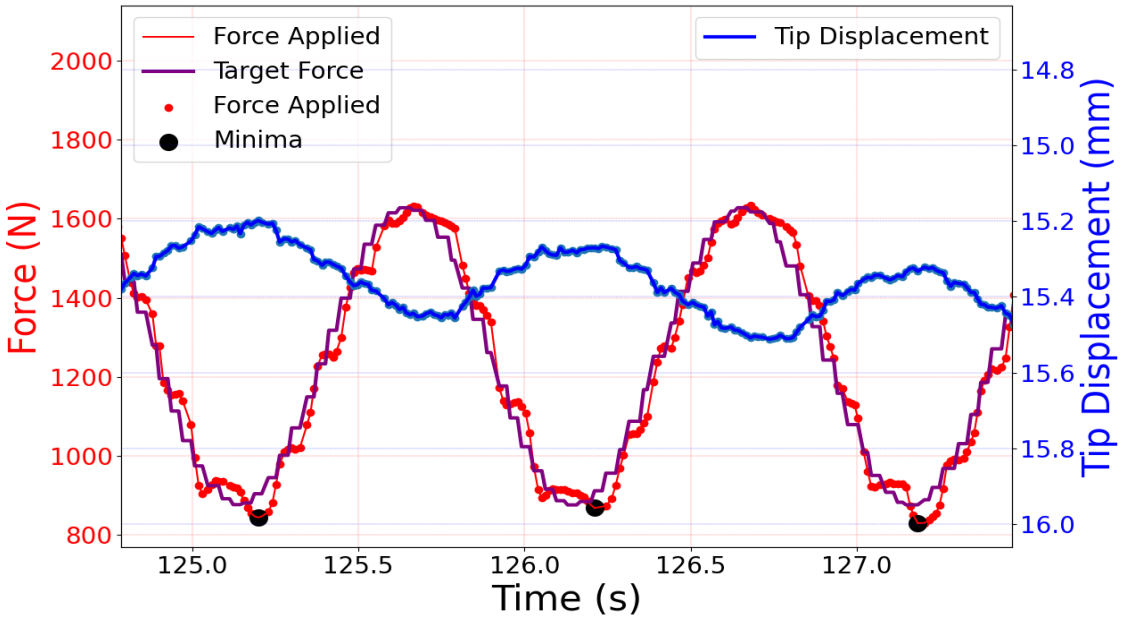

Figure 3.1 Details of force and displacement during two cycles

Thus, the definition/separation of each cycle cannot be done directly from the number of recordings. It was a complex task and the individual cycle definition can vary based on the parameter chosen. During the analysis of the collected data, each cycle is defined using the **minima of actual force** as shown in black in the time series of Figure 3.1. (The actual

force is measured using Force Transducer #2 shown in Figure 2.8). All the data gathered during the time period between two neighbouring minima's was attributed to that particular cycle.

3.1.2 Stiffness parameters

During application of force cycles, a displacement of the tip is measured using the LVDT shown in Figure 2.8. This displacement during each cycle varies depending on input parameters (e.g. $\alpha_{F,max}$, $\alpha_{F,min}$, frequency), the type of soil and the initial state conditions of the soil.

The change of displacement per cycle during the cyclic loading can be studied using stiffness changes (ΔForce/ΔDisplacement) as the force amplitude during cycles ideally remain constant. The aim of studying this stiffness value and stiffness changes was to link them to the soil properties and the stress state. Also, the objective is to make these stiffness definition independent from the choice of input parameters and constant for all the **Cyclic CPT** tests to develop its interpretation methodology.

For the definition of these stiffness values, each cycle is isolated and the total relative displacement caused during each cycle is studied. Different stiffness values can be defined for each cycle and a number of them were investigated during this research work.

Few of the stiffness values that showed promising results are as shown in Figure 3.2 and are discussed in the following sections. Figure 3.2 shows three stiffness values calculated for the 20th cycle of two different **Cyclic CPT** tests. The two CPT tests (Test No. 48 and 54) are done in the same calibration chamber test under identical state conditions but with different input parameters. During Test No 54 the $\alpha_{F,max}$ parameter (Section 1.2) is greater than the one in Test No 48 and this results in greater displacement during each cycle. It was necessary to define stiffness parameters that were consistent in tests which showed either very large or very small displacement per cycle.

Loading Stiffness (K_L):

It was desired to find a linear fit on the loading part of the graph. However, the choice of the definition of a loading stiffness can vary and affects the calculated value. Different criterions were: cut-off percentage of shear strain, using a certain number of initial values of each cycle, using a cut-off correlation coefficient or using a certain percentage of maximum force applied. Each one of these had its own associated challenges and effects. We wanted to use a method that could explain tests with large deformation per cycle as well as small deformations. (Those causing large displacement per cycle and those causing much less).

The option opted for defining this loading stiffness is using a cut-off force. The data collected during the initial 40% of the force cycles i.e. from the minima force ($\alpha_{F,min}$*Tip resistance recorded) to 40% of the difference of maximum force ($\alpha_{F,max}$*Tip resistance recorded) and minima force is used to find the best linear fit. The slope of this linear fit is referred as Loading Stiffness (Shown in blue in Figure 3.2).

Unloading Stiffness (K_U):

Similarly, the Unloading Stiffness (K_U) has been defined to characterize the force-displacement relation during the tip force decrease of the cycle. This stiffness is defined as a linear fit on relative displacement and the measured force after the maximum displacement point of each cycle (shown in black in Figure 3.2). This is a linear fit on the zone when the tip seems to move upwards to match the target force.

Secant Stiffness (K_S):

A stiffness is also defined by finding the slope of the line joining the first point of the cycle and the point of maximum relative displacement in that particular cycle in the displacement-force graph. This slope is called the Secant Stiffness (K_S).

.

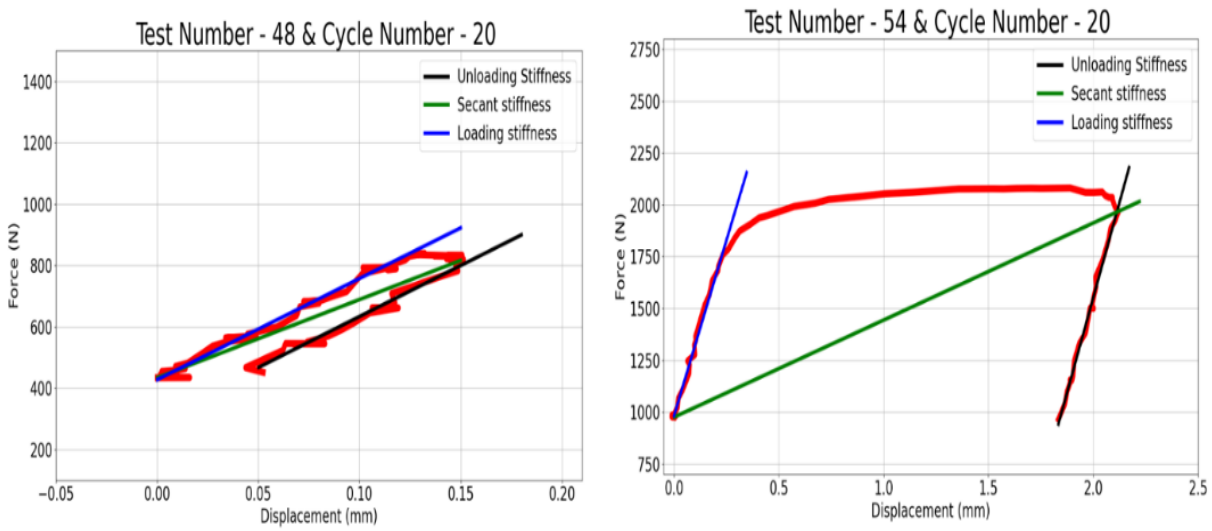

Figure 3.2 Representation of different stiffness's calculated for each cycle

3.2 Effect of vertical stress on Cyclic CPT results

To study the effect of vertical stress on the results of **Cyclic CPT** test, two calibration chamber tests were done on saturated specimens at 75 and 150 kPa vertical stress applied using the pressure membrane. The Figure 3.3 shows a scatter of the tip stress vs the depth inside the calibration chamber in these two tests. As expected, the stress profiles is

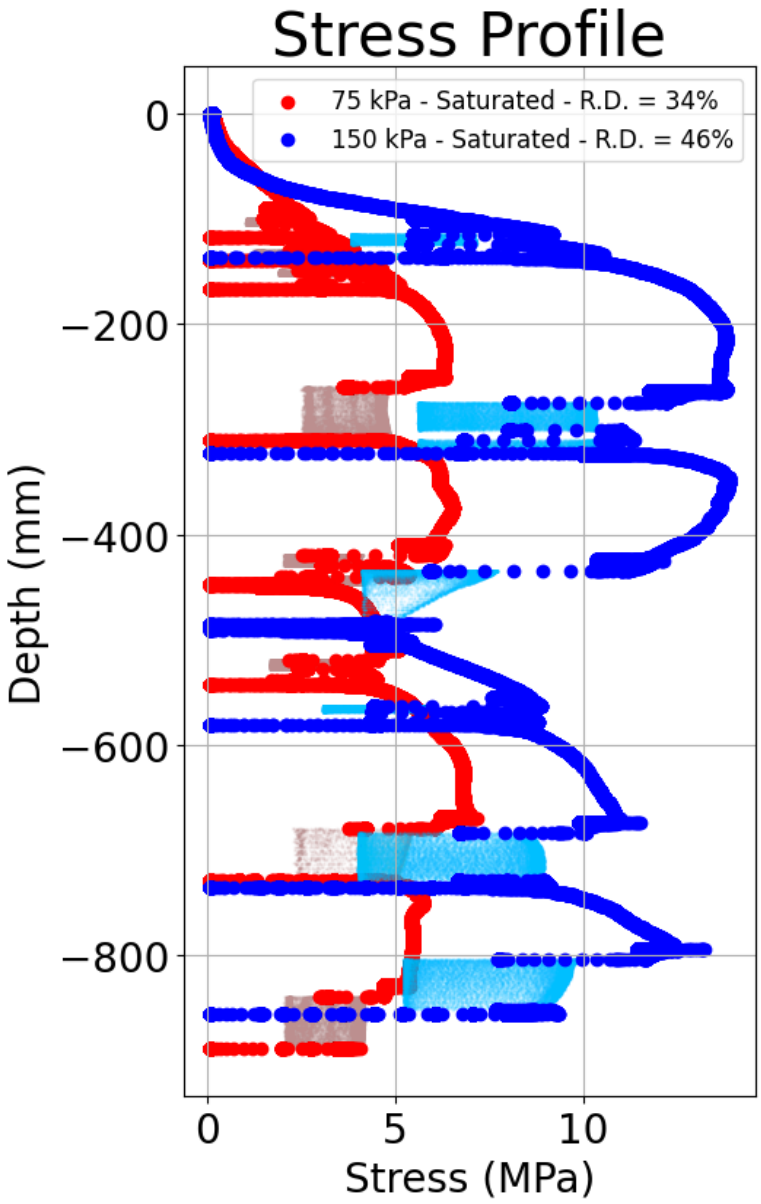

Figure 3.3 Stress profiles for two calibration chamber tests (Saturated samples at 75 & 150 kPa vertical stress)

discontinuous due to a number of **Cyclic CPT** tests being performed. The **Cyclic CPT** tests are the locations where the scatter is quite dense. As visible the applied cycling loading is always less than the penetration resistance.

Due to the central hole through the pressure membrane and the ratio of tip and chamber diameter, the tip resistance stabilize from a depth of 18 cm which is consistent with the work of Silva 2014.

The two samples were created using slurry deposition as explained in Section 2.2.4 . The relative density of both these specimens lied under medium dense category (35 and 45% R.D.). Variations in the stress profile can be attributed to heterogeneities of the sand density in the samples.

Similarly the stress sensor response during the two calibration chamber tests can be compared. Only Group 4 and Group 6 sensors (Figure 2.11Figure) were used in 75 kPa calibration chamber test and were placed at 40 cm depth from top of the sand sample. For the 150 kPa calibration chamber test, all six groups were used. Group 1, 2 and 3 are placed at depth of 26 cm while the remaining groups are placed at depth of 42 cm. The new EPB-PW miniature pressure transducers gave more consistent results and are used to study the changes in radial stress during the entire calibration chamber tests. The KYOWA stress transducers are relied on to study the changes of vertical stress during penetration.

In Figure 3.4 the radial stress sensor readings (X-axis) are plotted against the vertical distance of the cone from the sensor (Y-axis), for the two calibration chamber tests, The radial stresses are offset to zero at the start of penetration.We can observe a much bigger increase in radial stress when the tip is approaching the depth where stress sensor are installed during the 150 kPa calibration chamber test. Also, the radial stress measured at 10 cm radial distance from the centre of cone is significantly bigger as compared to the one at 20 cm radial distance. We can also observe that there is almost no change of radial stress for the 75 kPa calibration chamber test at 20 cm radial distance. Even for the 150 kPa calibration chamber test, there is a significant low value of radial stress as compared to 10 cm's value. We can expect the change of radial stress at the edge of the calibration chamber (30 cm) to be close to zero and as such the test can also be considered free from boundary effects.

A similar study showed no significant change off vertical stress at 20 cm radial distance when the tip penetrates inside the calibration chamber for 75 kPa test (Figure 3.5). There is a small decrease which increases once the tip has passed the sensor depth. For the 150 kPa calibration chamber test, an increase of vertical stress was recorded at 10 cm radial distance when the tip approaches close to the sensor depth. The change of direction of vertical stress about 160 mm above the sensor depth (i.e. zero y-tick in Figure 3.5) corresponds to the start of a **Cyclic CPT** test.

Once the tip goes below the sensor depth the vertical stress goes back to its initial value. For the sensor at 20 cm radial distance, the pressure increases when the tip crosses the sensor depth and has a bigger relative change even when the tip crosses the sensor depth.

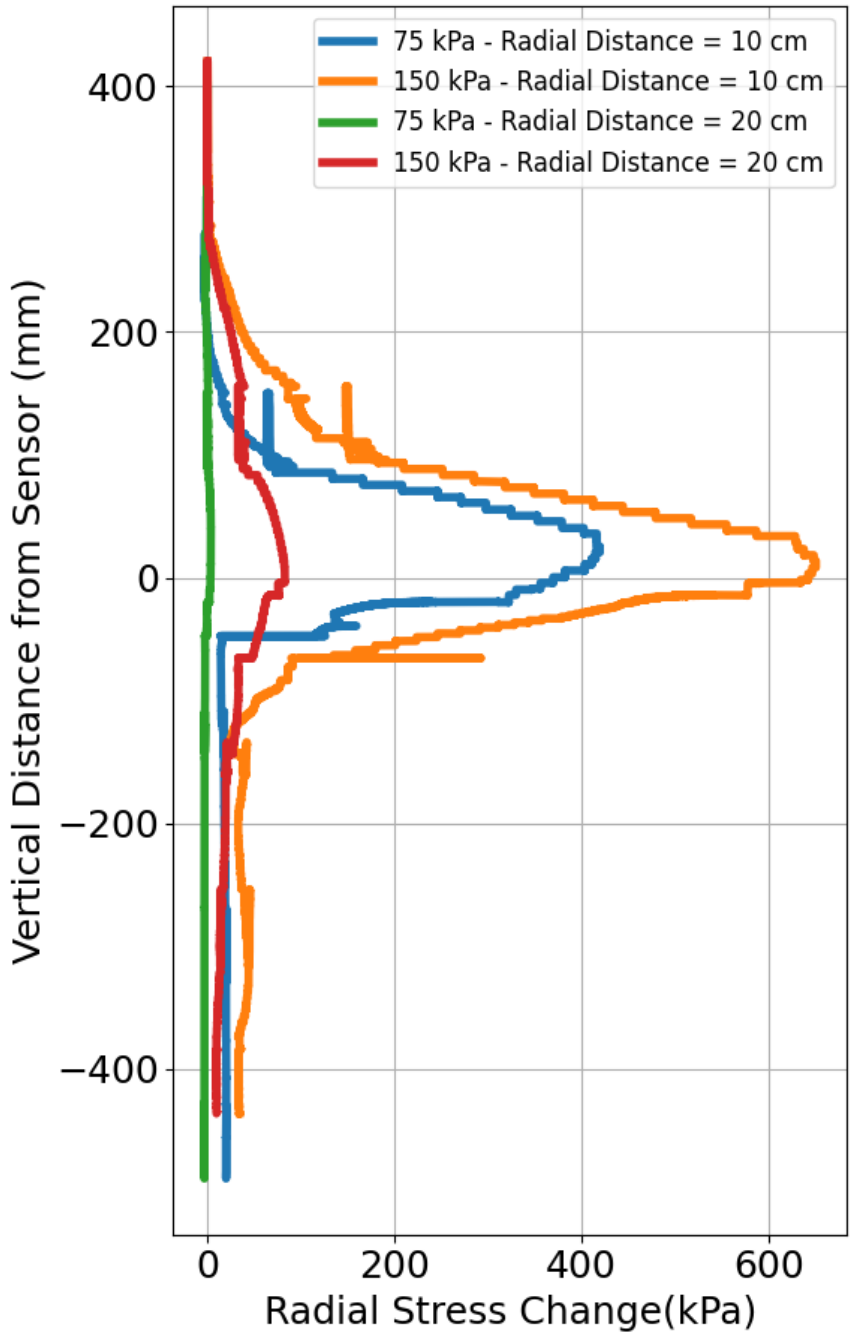

Figure 3.4 Radial Stress changes after the start of penetration for the two calibration chamber tests (75 & 150 kPa vertical stress)

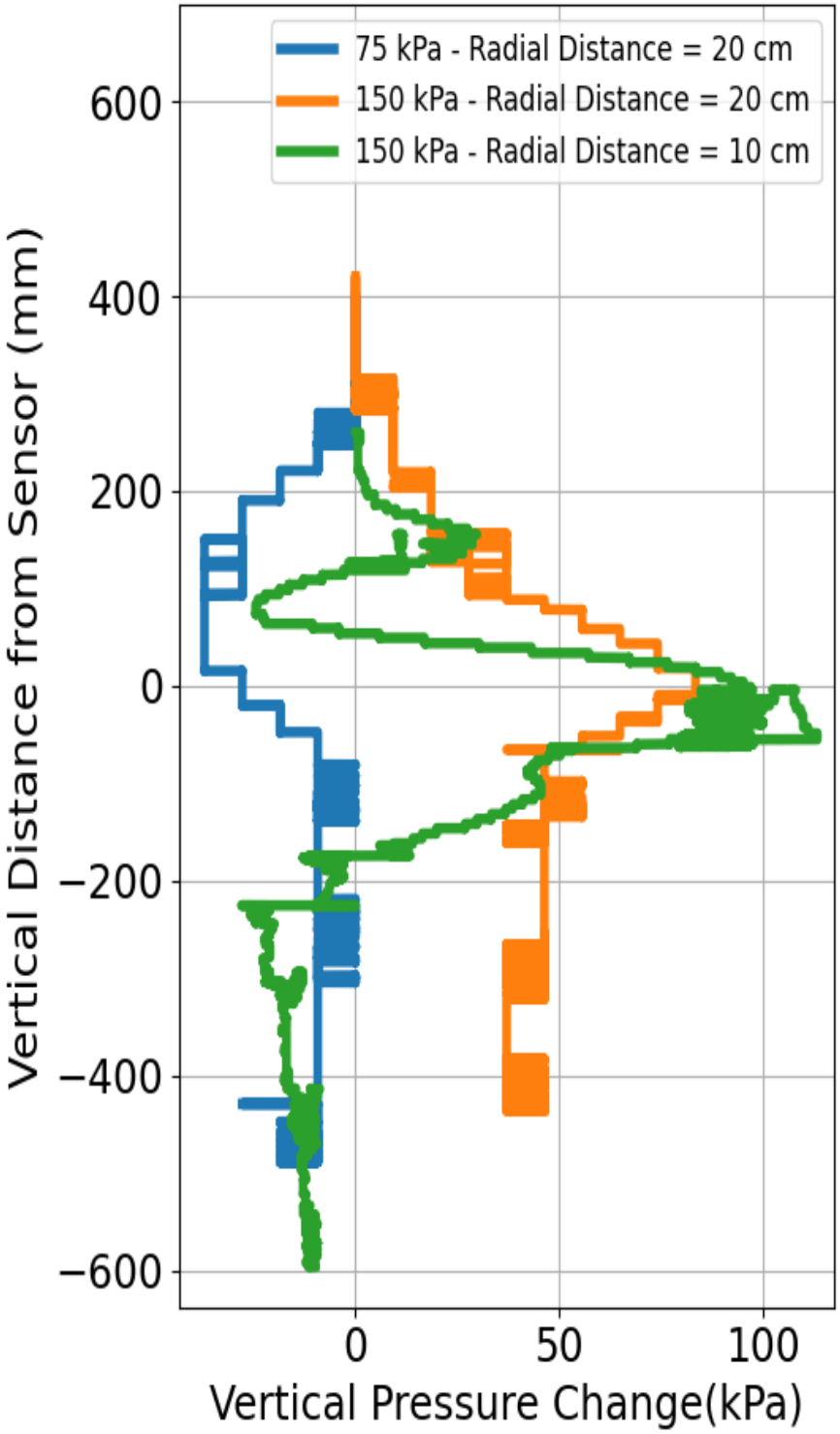

Figure 3.5 Vertical Stress changes after the start of penetration for the two calibration chamber tests (75 & 150 kPa vertical stress)

To study the **Cyclic CPT** tests it is paramount to study the effect of input parameters on the results and behaviour of tested soil. A large number of combinations of $\alpha_{F,const}$, $\alpha_{F,max}$ and $\alpha_{F,min}$ are possible for a **Cyclic CPT** test and it was required to test and fix few of them for the calibration chamber testing. Three different combinations of $\alpha_{F,const}$, $\alpha_{F,max}$ *and* $\alpha_{F,min}$ given in table 3.2 were tested at relatively similar depths, in samples of comparable densities, and for the same frequency and duration of cyclic loading. **The results of these three combinations in two different vertical stresses are as discussed below:**

S.No.	Test ID		Cyclic Loading Parameters			Depth (cm)	
	75 kPa	*150 kPa*	$\alpha_{F,const}$	$\alpha_{F,max}$	$\alpha_{F,min}$	*75 kPa*	*150 kPa*
1	53	75	0.5	0.65	0.35	58	58
2	51	73	0.6	0.78	0.42	26	26
3	55	77	0.6	0.80	0.40	90	82

*Table 3.2 Input parameters of **Cyclic CPT** tests done at different vertical stresses*

Reminder: $\alpha_{F,const}$, $\alpha_{F,max}$ *and* $\alpha_{F,min}$ *are the ratio of tip resistance to be applied as constant force during waiting periods, the ratio of tip resistance to be applied as the maximum cycle force and the ratio of tip resistance to be applied as the minimum cycle force respectively.*

3.2.1 ($\alpha_{F,const}$-$\alpha_{F,max}$-$\alpha_{F,min}$ = 0.5 – 0.65 – 0.35)

The tip stress and displacement during two **Cyclic CPT** tests (Test ID 53 and 75), done at two different vertical stresses (75 and150 kPa respectively) are shown in Figure 3.6.

The tip resistances recorded in Step A (TR#1) for 75 kPa and 150 kPa tests are 5.11 and 8.89 MPa respectively while the recorded values of tip resistance during Step E(TR#2) was 4.53 and 8.82 MPa respectively.

The magnitudes of constant tip stress at waiting steps B and D are 2.55 and 4.45 MPa which correspond to the values of $\alpha_{F,const}$ *(TR#1). The constant stress during waiting period F and H are equal to $\alpha_{F,const}$ *(TR#2). Similarly, the maximum tip stress during cycles in Step C and Step G is 3.32 and 5.78 MPa which correspond to the values of $\alpha_{F,max}$ *(TR#1). Also the minimum stress values during the cyclic loading are equal to $\alpha_{F,min}$ *(TR#2) for each test. The lines in blue show the displacement during the **Cyclic CPT** test.

It can be seen that the tip opens by 10 mm for both Step A and Step E, while other steps contribute to a total tip opening of around 7 and 13 mm respectively. The different stiffness explained in Section 3.2.2 are also calculated for these two tests and are as shown in Figure 3.7. It can be seen that the test records higher stiffness values at 150 kPa vertical stress as compared to corresponding values at 75 kPa vertical stress. For both these tests under the current input parameters, all the stiffness values remain almost constant during the 180 cycles applied at 1 Hz frequency.

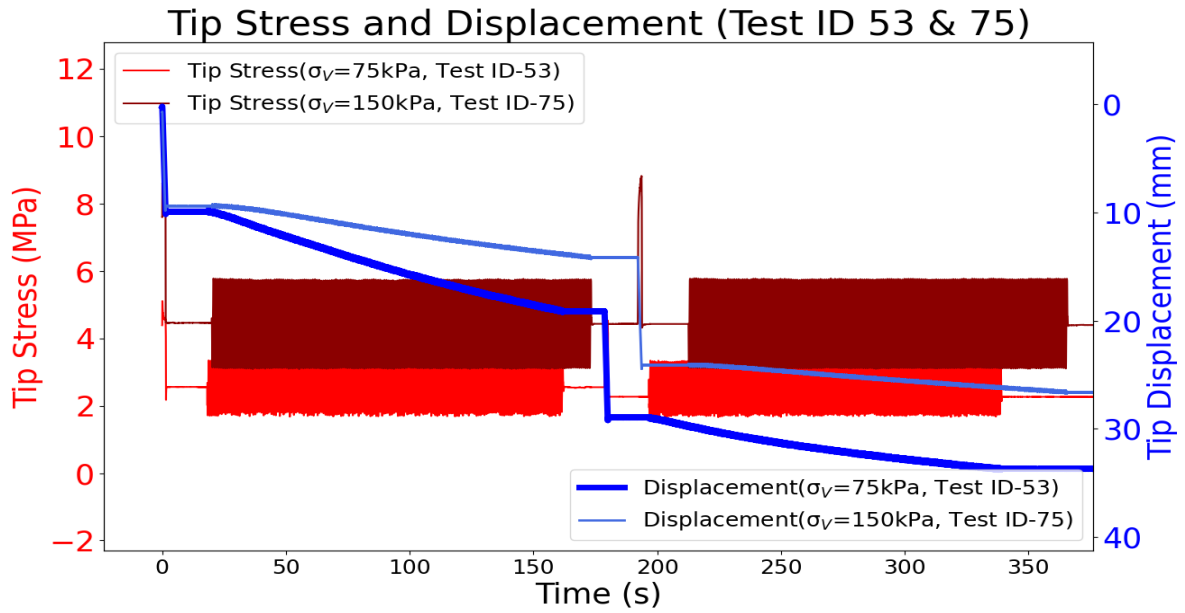

Figure 3.6 Tip Stress and Displacement ($\alpha_{F,const}$ -$\alpha_{F,max}$ -$\alpha_{F,min}$ = 0.5-0.65-0.35)

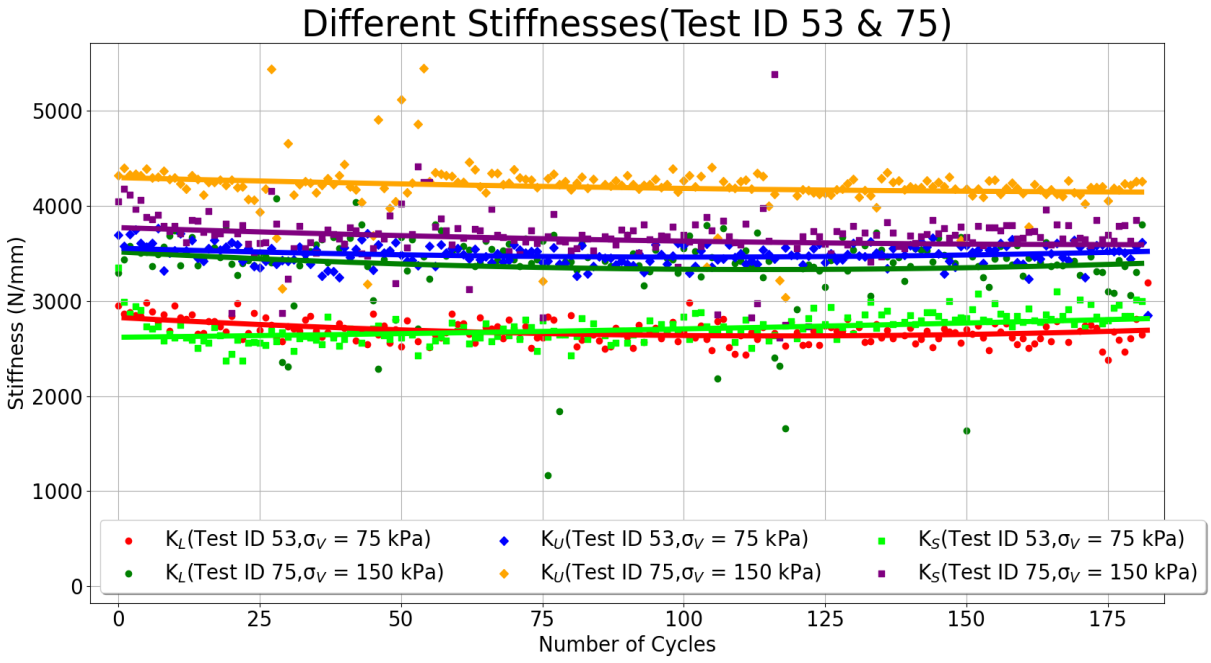

Figure 3.7 Stiffness parameters calculated for tests at different applied vertical stresses ($\alpha_{F,const}$ -$\alpha_{F,max}$ -$\alpha_{F,min}$ = 0.5-0.65-0.35)

3.2.2 ($\alpha_{F,const}$-$\alpha_{F,max}$-$\alpha_{F,min}$ = 0.60 – 0.78 – 0.42)

A higher value of $\alpha_{F,max}$ = 0.78 was applied during Test ID 51 & 73. These **Cyclic CPT** tests were done on sands samples under applied vertical stress of 75 and 150 kPa respectively and the results are as shown in Figure 3.8.

The measured tip resistance (TR#1) during the two tests were 6.35 and 13.67 MPa (respectively). Since the cyclic loading jack (Verin Equaterre or VE) opened completely (6 cm) during Step C for Test ID 51 and during Step G for Test ID 73, the **Cyclic CPT** test was not completed.

It was observed that the tip opened completely after 146 cycles of Step C during Test ID 51 done under 75 kPa applied vertical stress. Thus, 146 cycles at given input parameters caused almost 49 mm displacement under 75 kPa stress. While similar number of cycles caused 20 mm displacement under 150 kPa stress. Under an applied stress of 150 kPa, the tip opens up by a total of 37 mm after 292 cycles applied during Step C and Step G.

The calculated stiffness parameters for these two tests are as shown in Figure 3.9. We again observe lower stiffness values for test done at 75 kPa as compared with test done at 150 kPa. The secant stiffness (K_S) values show the least scatter around the second degree

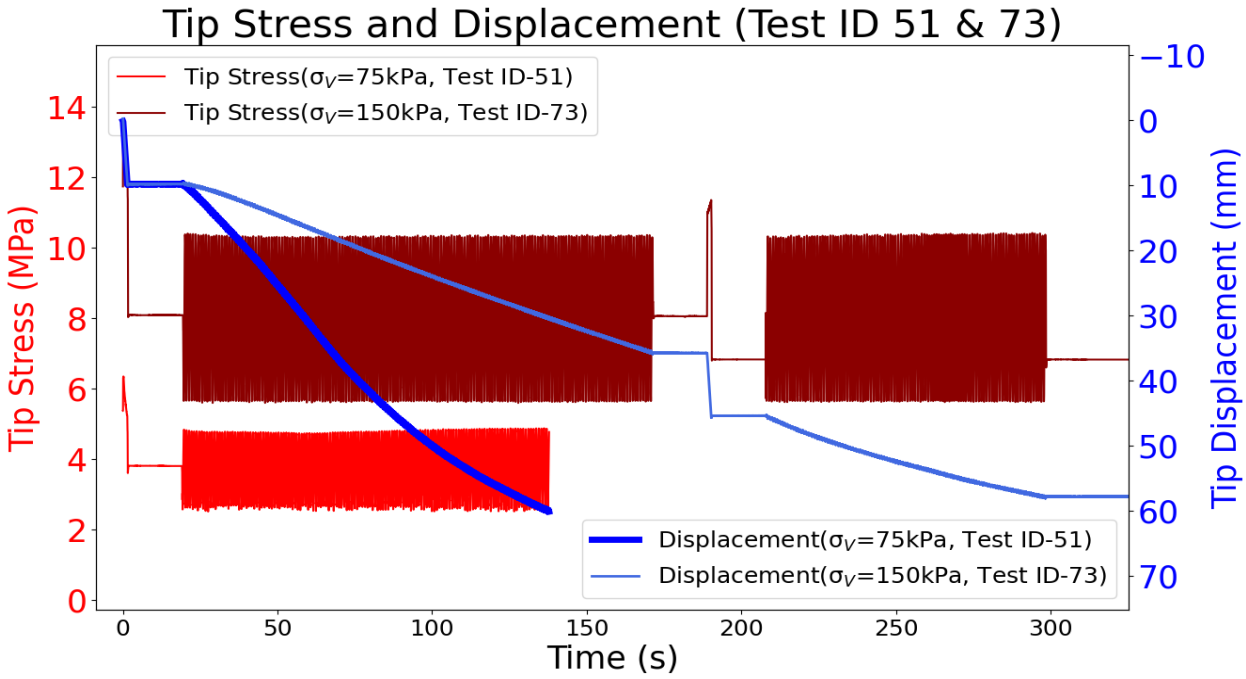

Figure 3.8 Tip Stress and Displacement ($\alpha_{F,const}$ -$\alpha_{F,max}$ -$\alpha_{F,min}$ =0.6-0.78-0.42)

polynomial fit. However, stiffnesses increase with cycles for test done at 75 kPa while they are relatively constant for the test done at 150 kPa.

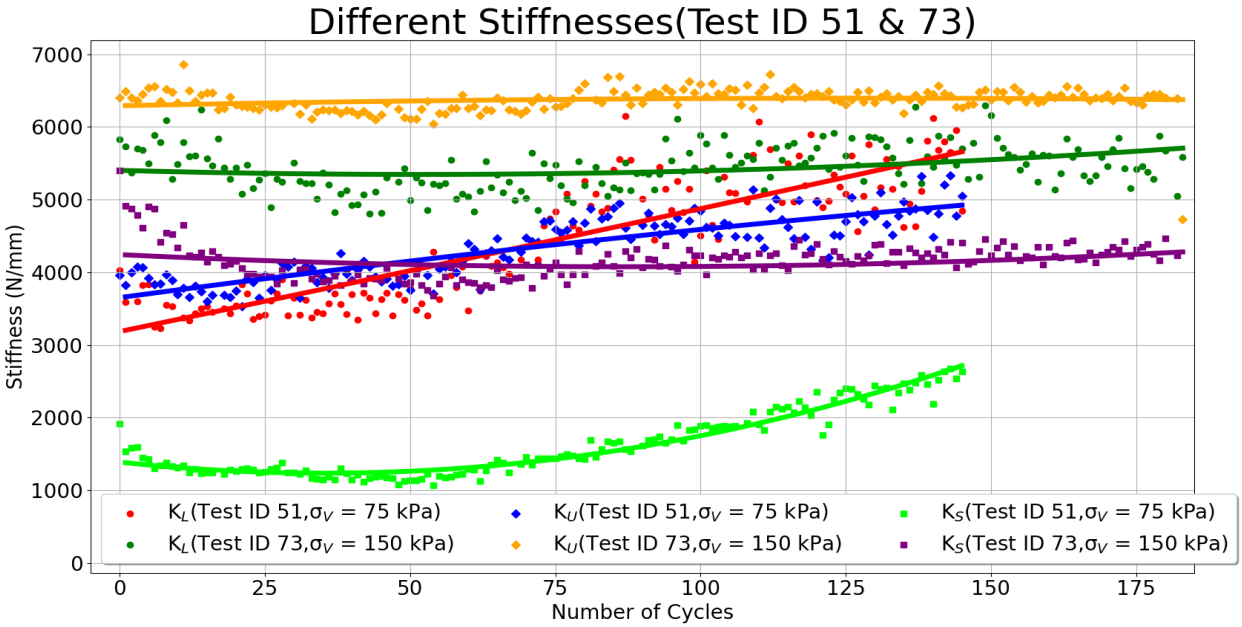

Figure 3.9 Stiffness parameters calculated for tests at different applied vertical stresses ($\alpha_{F,const}$ -$\alpha_{F,max}$ -$\alpha_{F,min}$ =0.6-0.78-0.42)

3.2.3 ($\alpha_{F,const}$-$\alpha_{F,max}$-$\alpha_{F,min}$ = 0.60 - 0.85 – 0.35)

Even a further increase of ratio of maximum cyclic force of cyclic loading to tip resistance was tried in Test ID 54 and 76 ($\alpha_{F,max}$ = 0.85). These tests were performed on similar samples at 75 and 150 kPa vertical stress respectively.

The results are as shown in Figure 3.10. The tip resistance measured during Step A (TR#1) are equal to 7.19 and 10.98 MPa. It can be seen that during both these tests, the cyclic jack opened completely before the completion of Step C. For the test done under 75 kPa vertical stress, 27 cycles with maximum tip stress of 0.85 times the tip resistance were required for 40 mm displacement while for the test done at 150 kPa it required 169 cycles.

It was also observed that as the displacement per cycle was large, the maximum target stress could not be reached and the actual maximum of cyclic tip stress applied decreased with respect to the number of cycles, while the cyclic loading for test under 150 kPa was relatively stable.

This is an indication of stiffness change for the first test and can also be observed in Figure 3.11. The different calculated stiffnesses change during the cyclic loading for the first test (Test 54) while they remain almost constant for the second test (Test 76). However the

loading and the unloading stiffnesses (K_L & K_U) appear to first decrease and then increase for this test while there is a constant decrease of secant stiffness parameter(K_S).

The secant stiffness seems to be a good indicator of the loss of strength of the soil as it becomes progressively easier to penetrate the soil during cyclic loading i.e. the total displacement per cycle increases for this test.

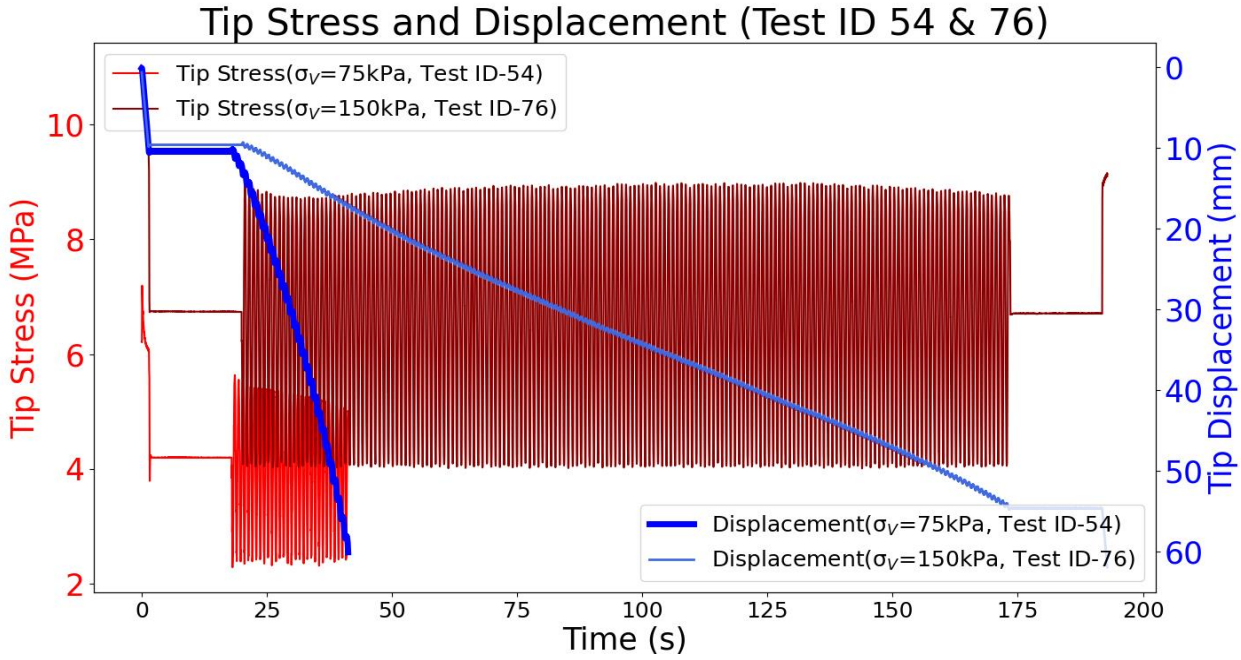

Figure 3.10 Tip Stress and Displacement ($\alpha_{F,const}$ -$\alpha_{F,max}$ -$\alpha_{F,min}$ =0.6-0.85-0.35)

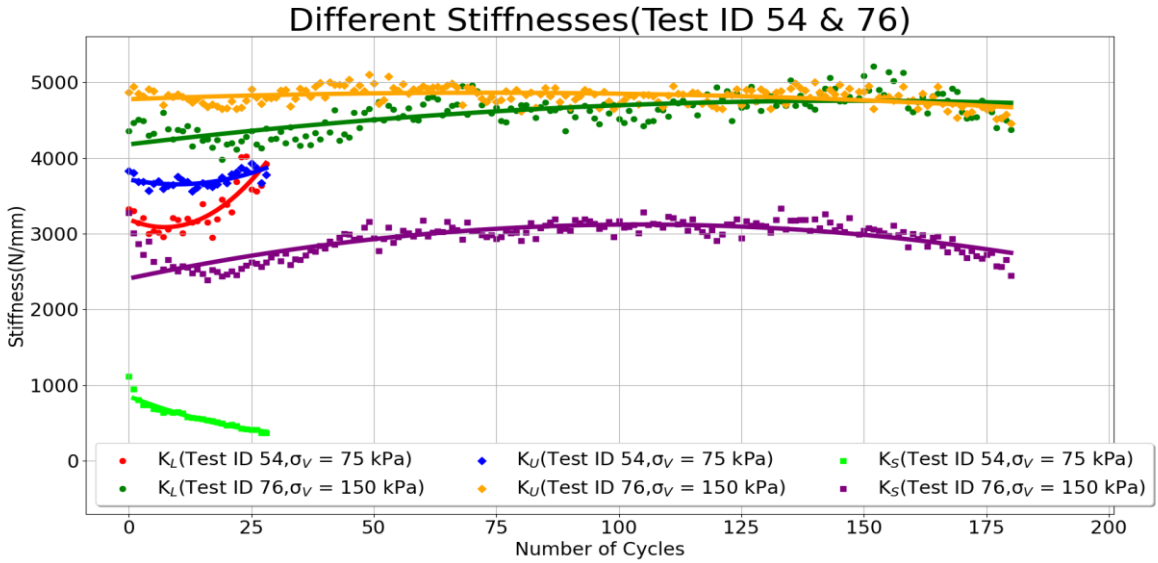

Figure 3.11 Stiffness parameters calculated for tests at different applied vertical stresses ($\alpha_{F,const}$ -$\alpha_{F,max}$ -$\alpha_{F,min}$ =0.6-0.85-0.35)

3.3 Effect of saturation conditions on cyclic CPT results

To study the effect of saturation, we needed to prepare two calibration chamber samples with similar dry density and test them under similar stresses but different saturation conditions. Ideally, the method of sample preparation should also be identical. This was not possible during the time duration of this PhD thesis. However, the calibration chamber sample created using slurry deposition and tested under 75 kPa stress, and the sample created using dry deposition of sand using an overhanging bag, tested under identical vertical stress had similar dry relative density (34 %). This dry density was based on a global measurement taken for the first two rings of the calibration chamber. [4] Details of few of the **Cyclic CPT** tests done inside these two calibration chamber samples are as listed in Table 3.3 and the results from tests done under different saturation conditions with similar input parameters of $\alpha_{F,const}$, $\alpha_{F,max}$ and $\alpha_{F,min}$ are discussed in the following subsections.

S.No.	Saturation Condition		Relative Density (%)	Applied vertical stress (kPa)	$\alpha_{F,const}$-$\alpha_{F,max}$-$\alpha_{F,min}$	
	Saturated	*Dry*			*Saturated*	*Dry*
1	52	86		75	0.5 – 0.65 – 0.35	
2	51	84		75	0.6 – 0. 78 – 0.42	
3	54	87		75	0.6 – 0. 85 – 0.35	

Table 3.3 Details of Cyclic CPT tests used to study the effect of saturation

3.3.1 ($\alpha_{F,const}$-$\alpha_{F,max}$-$\alpha_{F,min}$ = 0.5 – 0.65 – 0.35)

Test ID 52 and Test ID 86 were performed with $\alpha_{F,const}$, $\alpha_{F,max}$ and $\alpha_{F,min}$ values equal to 0.5,0.65 and 0.35 respectively. Both these tests were done at depth of nearly 42 cm inside the calibration chamber. The tip stress and displacement during these two tests is as shown in Figure 3.12. It can be observed that measured tip resistance during Step A is much more for the test done on saturated sand as compared to the dry one. Also, similar number of cycles applied at same values of $\alpha_{F,max}$ lead to greater displacement in the saturated soil as compared to the dry soil (Even if the tip resistance was lower for dry soil). Figure 3.13 shows the three different stiffness measurement for these two tests. It can be seen that there is no significant change in the stiffness parameters during the first

[4] The weighing scale was used to lift and measure the weight of the empty calibration chamber and the one filled with sand. However, the maximum limit of this weighing scale limited us to lift only the initial two out of the four calibration chamber rings. These measurements were used to calculate the density of the sample.

180 cycles applied. The unloading stiffness (K_U) for both these specimens is greater than the corresponding loading (K_L) and secant stiffness (K_S) values.

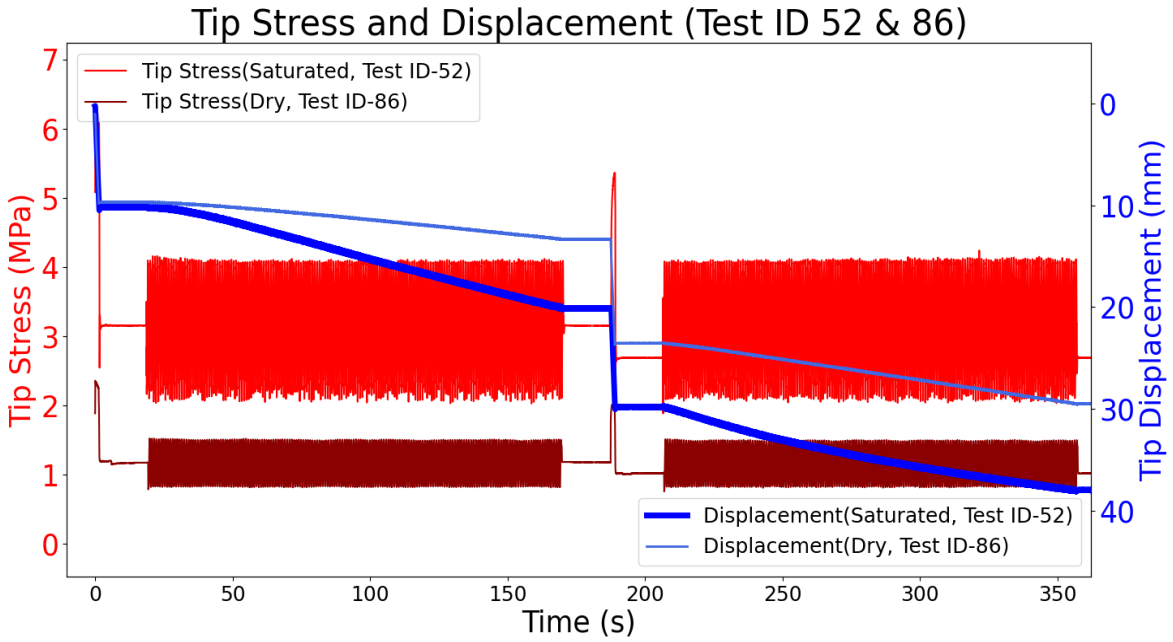

Figure 3.12 Tip Stress and Displacement - Effect of saturation conditions ($\alpha_{F,const}$ -$\alpha_{F,max}$ -$\alpha_{F,min}$ = 0.5-0.65-0.35)

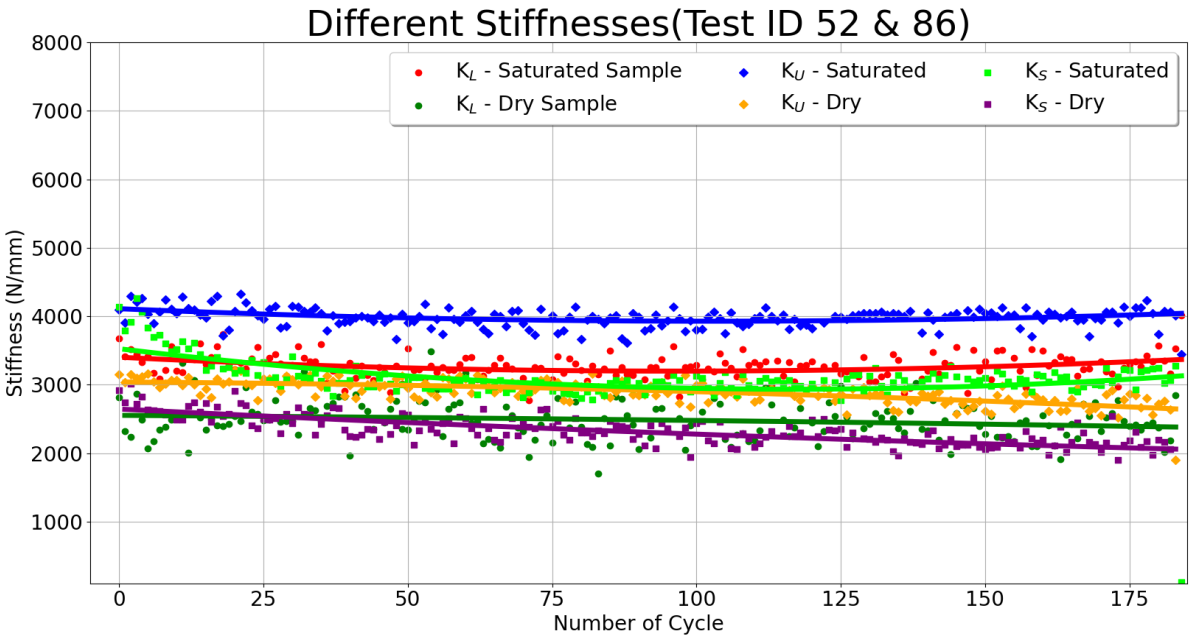

Figure 3.13 Stiffness parameters calculated for different saturation conditions ($\alpha_{F,const}$ -$\alpha_{F,max}$ -$\alpha_{F,min}$ = 0.5-0.65-0.35)

3.3.2 ($\alpha_{F,const}$-$\alpha_{F,max}$-$\alpha_{F,min}$ = 0.6 – 0. 78 – 0.42)

Test ID 51 and Test ID 84 were both done at depths of 26 cm below the top of the calibration chamber under 75 kPa applied vertical stress, with a higher $\alpha_{F,max}$ values as compared to tests discussed in section 3.3.1. The tip stresses and displacement observed during these tests are as shown in Figure 3.14. It can be clearly seen it was much easier to penetrate the saturated sample during cyclic loading as compared to the dry one. It can also be seen that the slope of displacement curve is almost constant for the dry sample while it changes for the saturated sample indicating change in stiffness.

The actual changes in calculated stiffness parameters ae shown in Figure 3.15. All the three stiffness parameters clearly increase with cycles for the saturated samples while they remain almost constant for the dry sample.

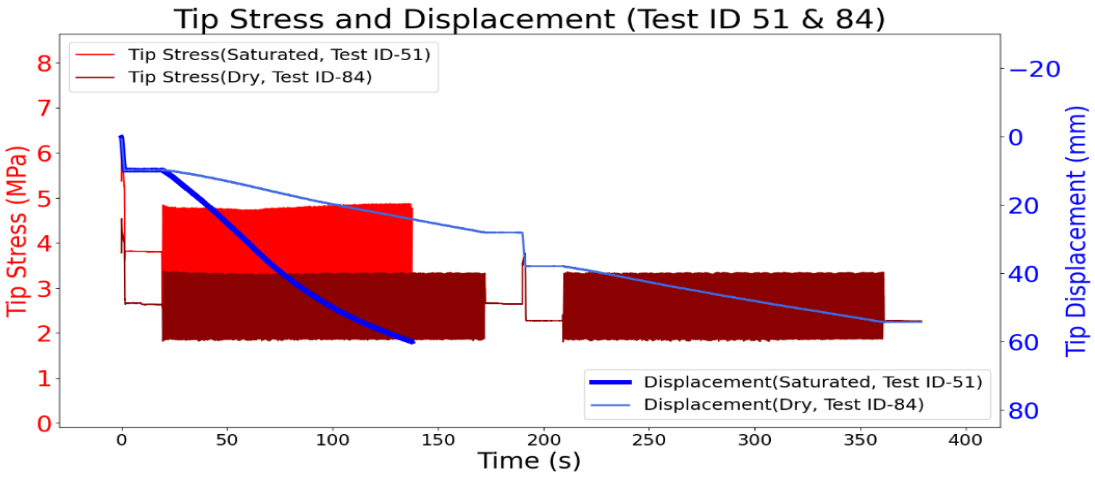

Figure 3.14 Tip Stress and Displacement - Effect of saturation conditions ($\alpha_{F,cyclic}$ -$\alpha_{F,max}$ -$\alpha_{F,min}$ = 0.6-0.78-0.42)

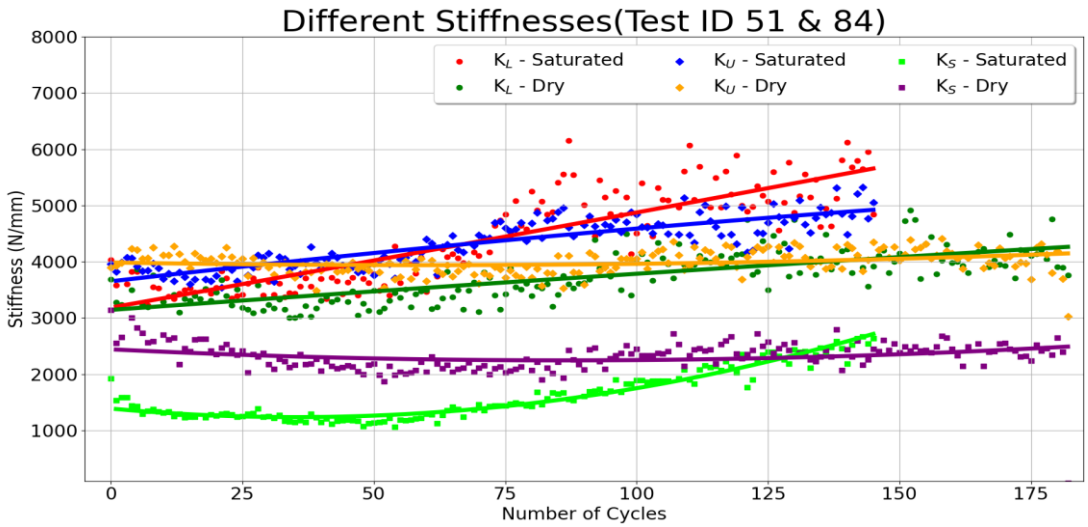

Figure 3.15 Stiffness parameters calculated for different saturation conditions ($\alpha_{F,const}$ -$\alpha_{F,max}$ -$\alpha_{F,min}$ = 0.5-0.65-0.35)

3.3.3 ($\alpha_{F,const}$-$\alpha_{F,max}$-$\alpha_{F,min}$ = 0.6 – 0. 85 – 0.35)

Similarly for Test ID 54 and 87, i.e. tests done with $\alpha_{F,max}$ =0.85 at two different saturations, there was a marked difference of the response to the **Cyclic CPT** test. Figure 3.16 shows that while the tip opened completely after 28 cycles for the saturated sample, it took 178 cycles in dry sample to open the tip with a similar distance.

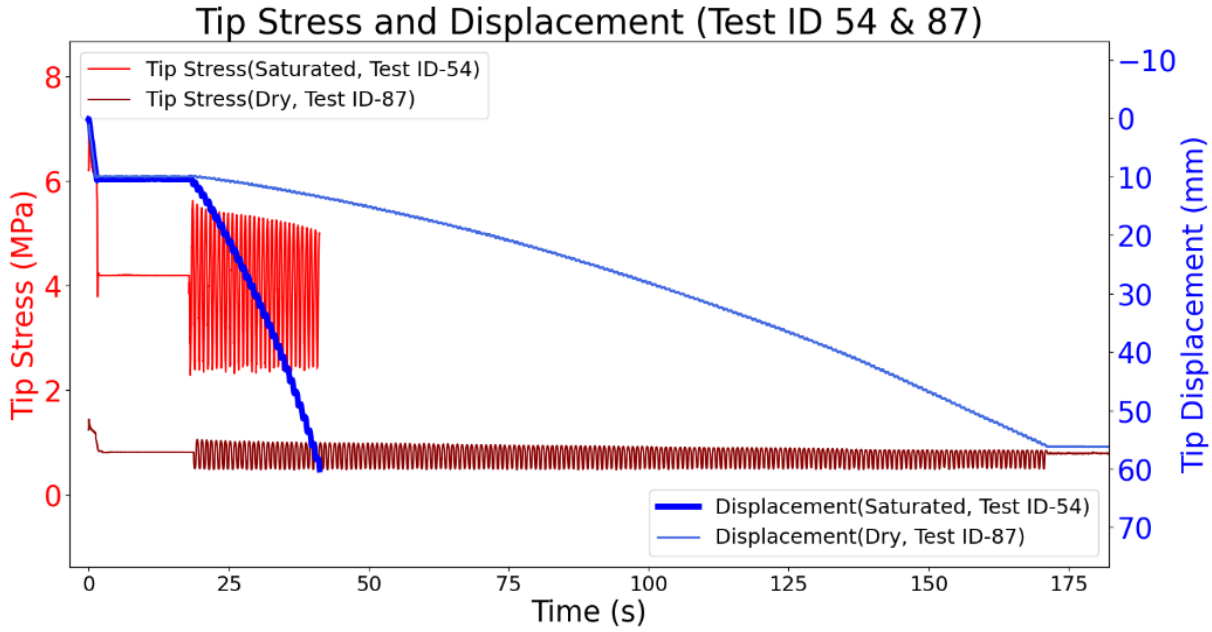

Figure 3.16 Tip Stress and Displacement - Effect of saturation conditions ($\alpha_{F,const}$ -$\alpha_{F,max}$ -$\alpha_{F,min}$ = 0.6-0.85-0.35)

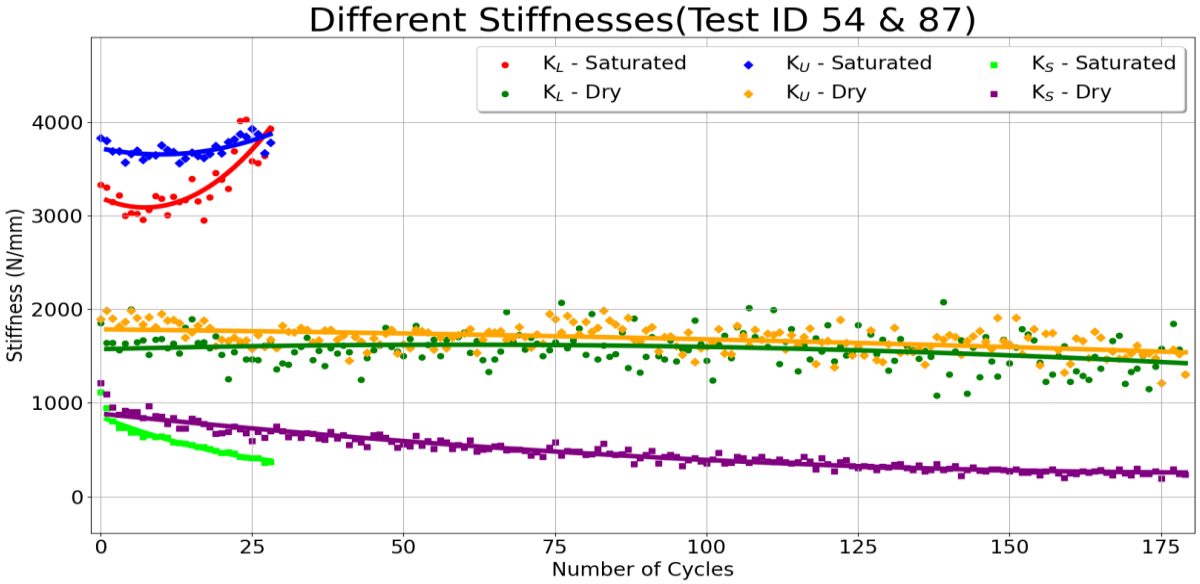

Figure 3.17 Stiffness parameters calculated for different saturation conditions ($\alpha_{F,const}$ -$\alpha_{F,max}$ -$\alpha_{F,min}$ = 0.6-0.85-0.35)

Another important difference is that even at high $\alpha_{F,max}$ value of 0.85, during application of the cyclic load on dry sample, the applied force matched closely the target force and there was no loss of the control. However, in saturated samples at all the tests done at such high $\alpha_{F,max}$ values (higher than 0.8), it became progressively difficult for the closed control loop to match the target and the actual tip stress. The stiffness changes are as shown in Figure 3.17 and it can be seen that secant stiffness values drop faster for saturated sample as compared to the dry sample Also, there are almost no change for loading and unloading stiffness for the dry sample while for the saturated sample, they appear to first decrease and then increase.

The secant stiffness measured for all the **Cyclic CPT** tests discussed previously in Section 3.3 are shown in Figure 3.18. It was observed that for tests done at $\alpha_{F,max}$ values of 0.65 and 0.85, saturated samples had lower values of secant stiffness (K_S) as compared to corresponding dry samples. However, this was not true for the tests done at $\alpha_{F,max}$ values of 0.78. It is interesting to note that during cyclic loading, all the saturated samples demonstrated significantly greater changes in the values of secant stiffness with respect to the corresponding tests done on dry sample.

More tests on identical samples with different saturation conditions should be performed to understand the effect of saturation on the results of **Cyclic CPT** tests.

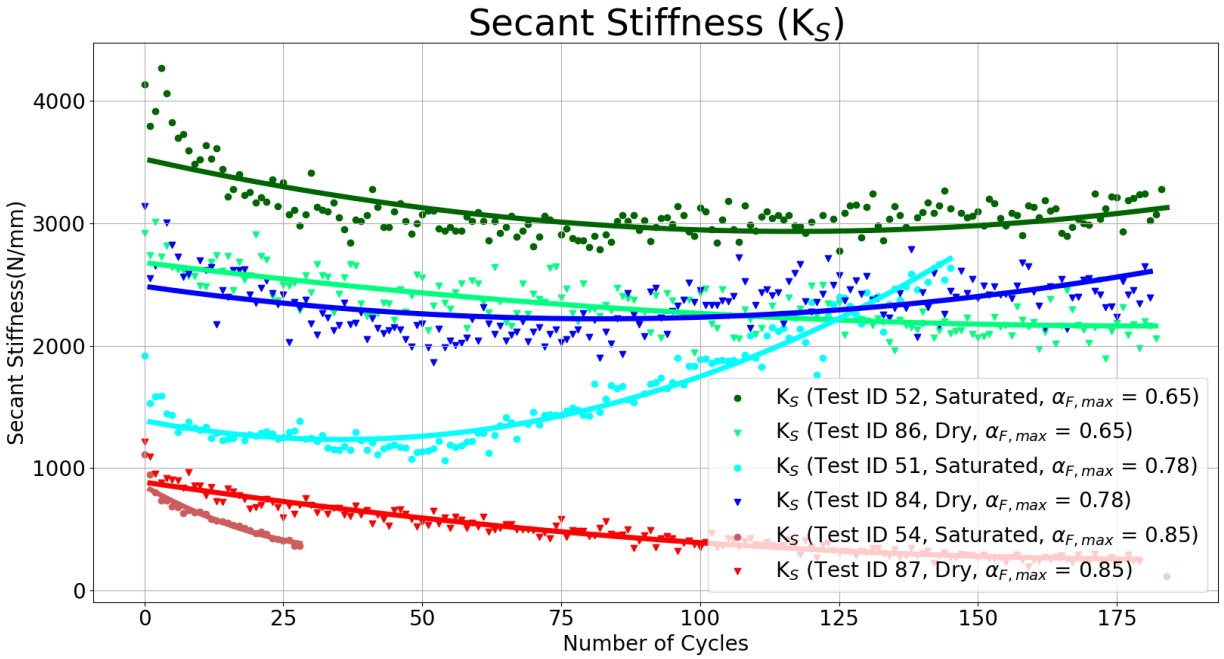

Figure 3.18 Secant stiffness changes for saturated and dry sample of similar density

3.4 Effect of density on Cyclic CPT results on dry samples

Two calibration chamber tests were done at similar vertical stresses but using samples of significantly different densities. The samples were created using dry sand. For the loose sample, dry sand was uniformly added to the calibration chamber using small buckets without any tamping. For the denser sample, after every 15 cm of deposition the sand was compacted using a tamper. Figure 3.19 shows large differences of tip resistances recorded between loose and dense samples tested with similar values of $\alpha_{F,const}$, $\alpha_{F,max}$ and $\alpha_{F,min}$. Even thought there is a huge difference between the magnitude of cyclic loading applied for the two tests the observed final displacement after same duration of cyclic loading varies less than 1 cm (Figure 3.19).

However there is a marked difference between the stiffness parameters calculated from these tests and is as shown in Figure 3.20. This was true for all the **Cyclic CPT** tests done with these two soil samples. The observed differences in stiffness can therfore be used for predicting density of soils during in-situ tests.

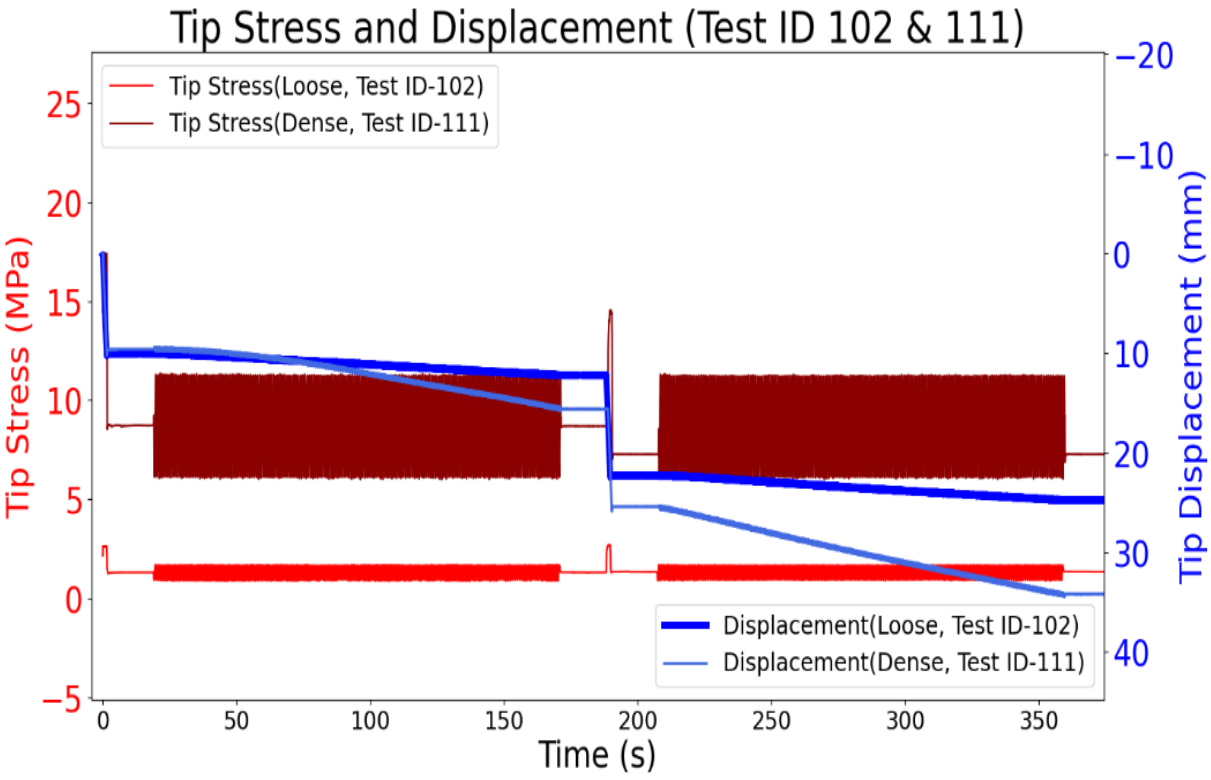

Figure 3.19 Tip Stress and Displacement – Different densities of dry sample

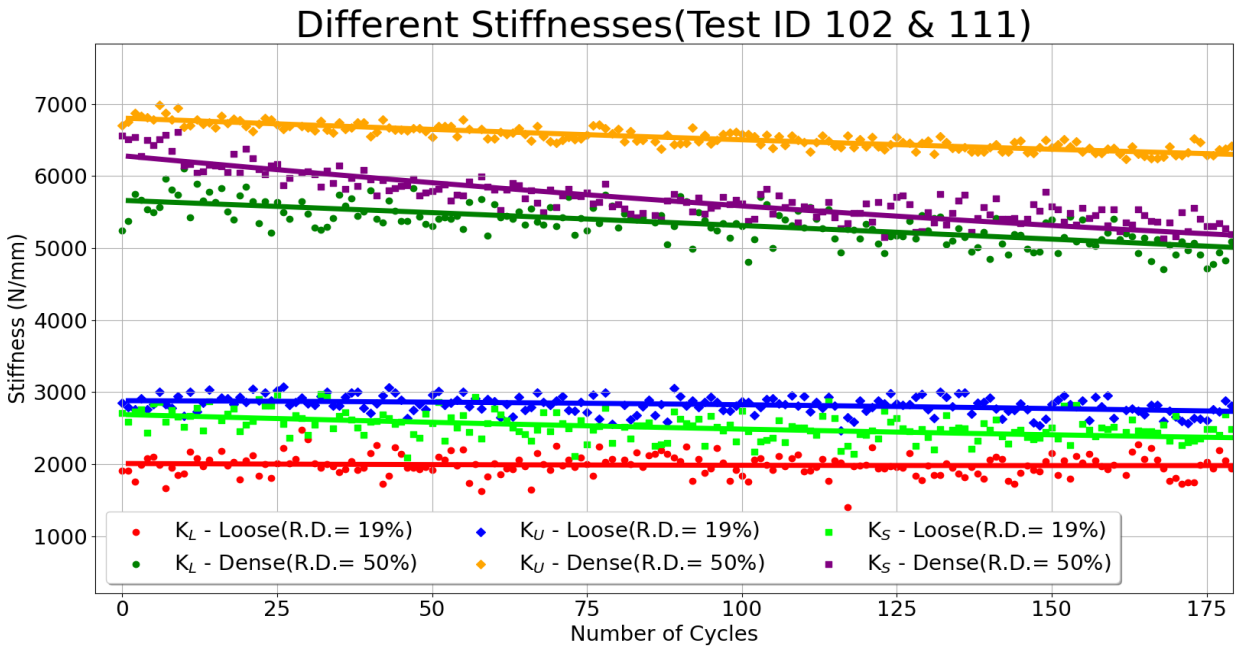

Figure 3.20 Stiffness parameters calculated for different densities of dry samples

3.5 Effect of frequency on Cyclic CPT results on dry samples

Two tests (Test ID – 103 & 104) were done with similar input of $\alpha_{F,const}$, $\alpha_{F,max}$ and $\alpha_{F,min}$ values at frequency of 1 and 0.1 Hz to study the effect of frequency on the results of **Cyclic CPT** test. Both these tests were performed in the same dry sand sample with a relative density of 19% and a vertical stress of 85 kPa. The tip stress and tip displacement are as shown in Figure 3.21. Both these tests were done at high $\alpha_{F,max}$ value of 0.85. During Test ID 103 was performed at 1 Hz frequency and did not witness a complete opening of the tip even after two sets of 180 cycles. However, for the same values of $\alpha_{F,max}$, Test ID 104 ($v = 0.1$ Hz) saw a complete opening of tip in less than 120 cycles (Figure 3.22).

The change of stiffness parameters calculated are as shown in Figure 3.23 There was no significant change of stiffness for either of these tests done on dry samples. The effect of loading frequency on results of cyclic loading and on soil liquefaction is not well understood. The test results in literature have often been non-conclusive. Mostly the effects are studied using cyclic triaxial tests which do not simulate the shear loading caused by an earthquake. However, even for these tests, some researchers like Tatsuoka et al. 1986 and Yoshimi and Oh-Oka 1975 found no effect of frequency on number of cycles required for an accumulated shear strain of 5%. These two papers tested frequencies in the range of 0.05 to 1 Hz and 1 to 12 Hz respectively but recommended a lower frequency loading for better control of stress cycles in large strains. However, a recent study by Zhu et al. 2021 found contradictory results. In this research it has been observed that there is no difference of behaviour of dry sand based on frequency of loading, while the response

of saturated sands in alternating stress controlled cycles is dependent on frequency. Lower frequency loading (0.01 Hz) has been observed to require lower number of cycles to cause liquefaction than a frequency of loading of 1 Hz. Inertia force opposing the applied loading in the axial direction is considered the main reason for this observation. However, the same study found no clear effect of frequency in case of pure compressive loading. A significant increase in the liquefaction resistance was also observed by Nong et al. 2020 for an increase of frequency of loading for cyclic direct simple shear tests which more closely represent the earthquake loading.

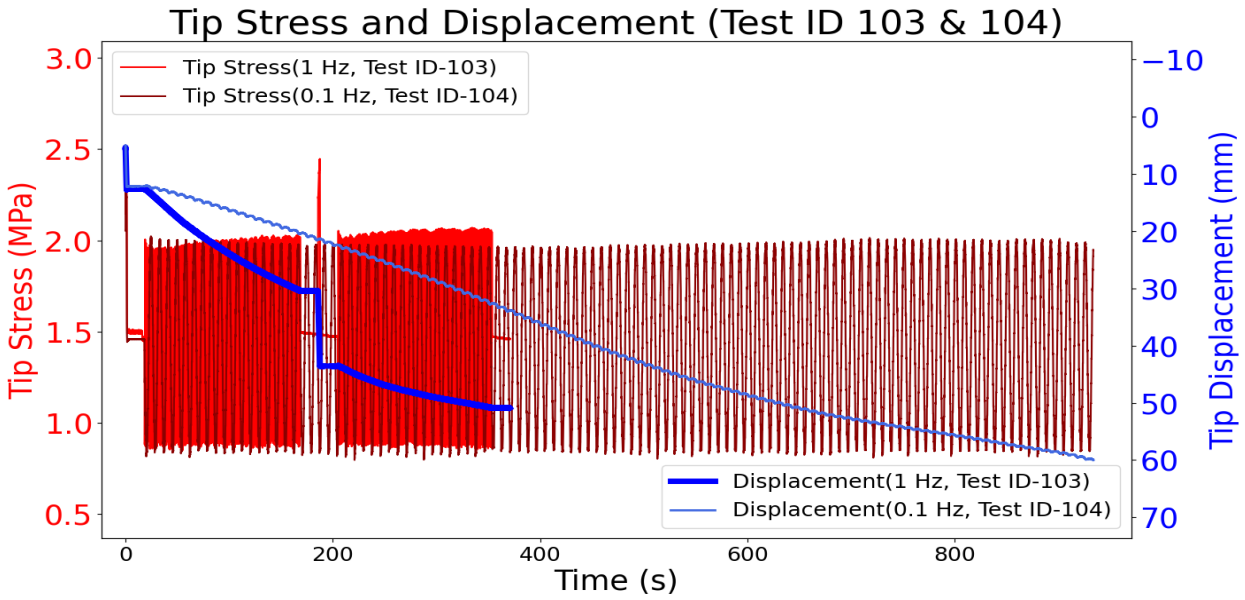

Figure 3.21 Tip Stress and Tip Displacement (Effect of Frequency)

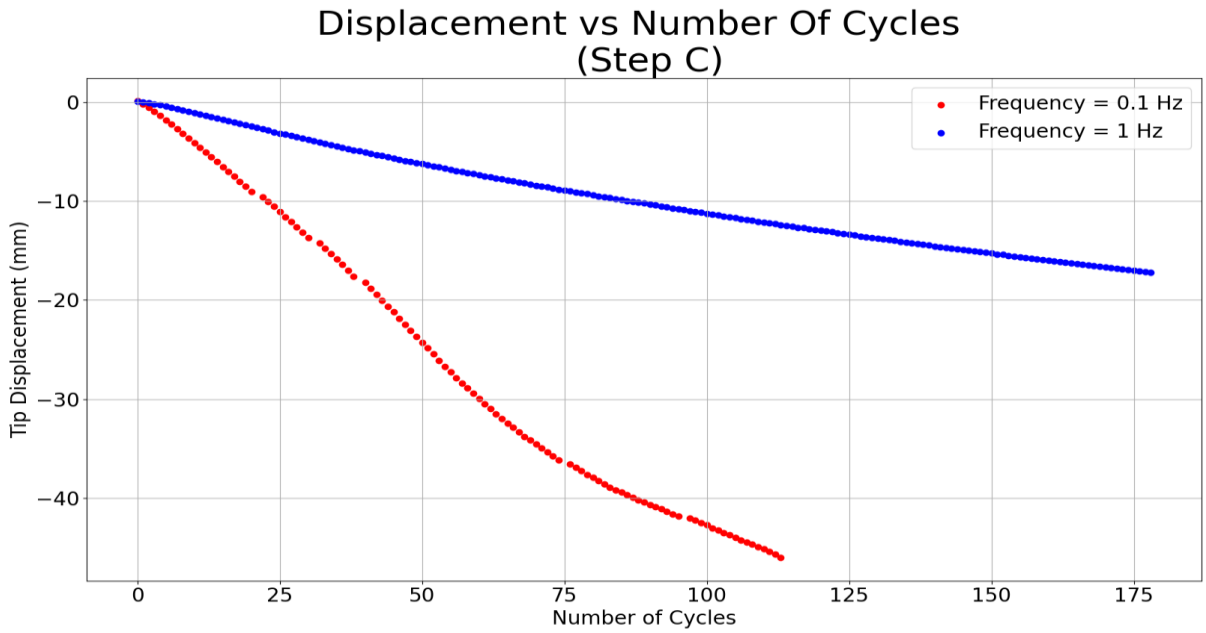

Figure 3.22 Displacement of Tip vs Number of Cycles (Effect of Frequency)

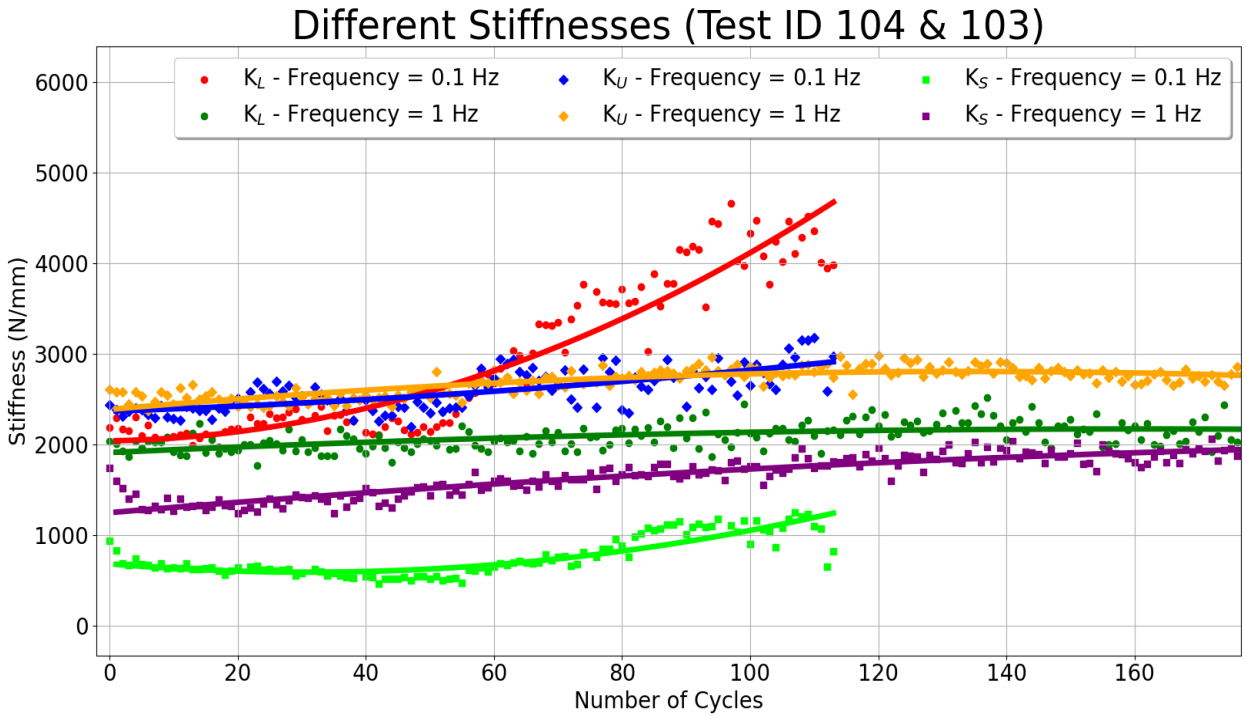

Figure 3.23 Stiffness Parameters changes w.r.t. number of cycles (Effect of Frequency)

3.6 Effect of $\alpha_{F,const}$ parameter on displacement during Step B

Another input parameter that will affect the information extracted from the cyclic CPT test is $\alpha_{F,const}$. $\alpha_{F,const}$ is the ratio of tip stress applied as constant force during Step B, Step D, Step F and Step H.

Constant force application steps are expected to be useful for differentiating between different soil types as displacement at a given value of $\alpha_{F,const}$ can be expected to be different for different soil types. However during the calibration chamber tests, different $\alpha_{F,const}$ values were tested on GA39 sand to find the best $\alpha_{F,const}$ value to be used for field tests. The results from different cyclic CPT tests done in the same calibration chamber test under dry conditions and 85 kPa vertical stress are as shown in Figure 3.24.

The closer $\alpha_{F,const}$ value is to one, the greater is the displacement during the application of constant tip stress. However, till $\alpha_{F,const}$ value of 0.7, the tip has to retract to apply a constant force after the initial penetration (Step A) for GA39 sand under dry conditions. In any case, it is expected that the choice of $\alpha_{F,const}$ value will not affect the results of cyclic loading as long as tip is not moving at a speed close to 1 mm/s during the start of cyclic loading.

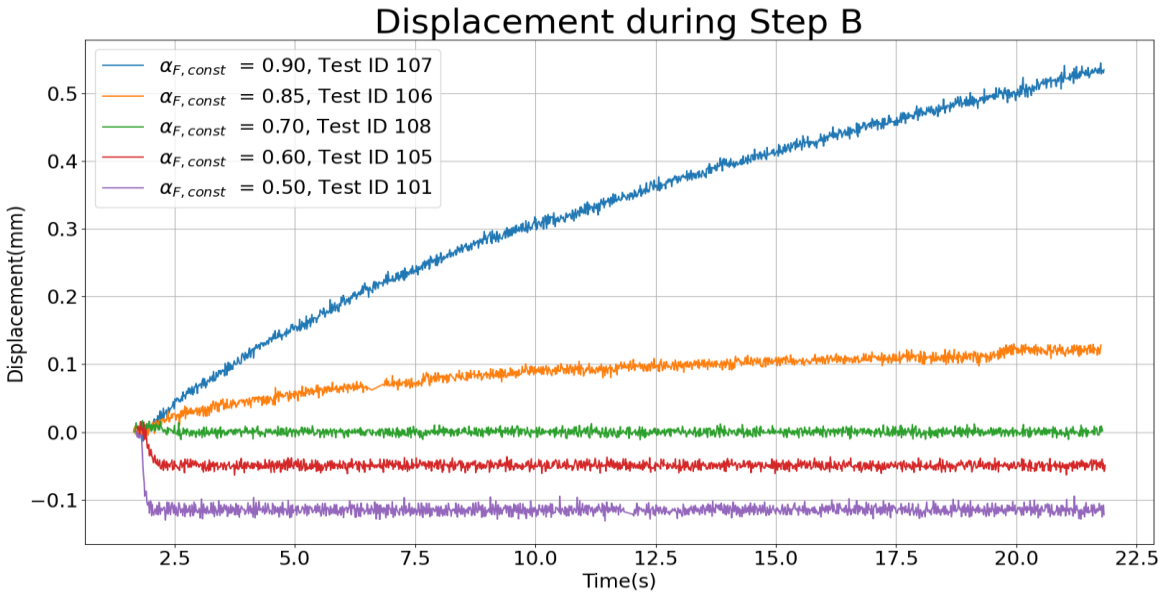

Figure 3.24 Tip displacement - Effect of $\alpha_{F,const}$ parameter

3.7 Conclusions

This chapter provides details about the stiffness parameters that can be used for interpretation of the results from **Cyclic CPT** test. It also discusses the effect of vertical stress, saturation conditions, density of tested sample and frequency of the applied cyclic loading on the results of a **Cyclic CPT** test. It highlights the dependency of results on the values of input parameters: $\alpha_{F,const}$, $\alpha_{F,max}$ *and* $\alpha_{F,min}$.

It was observed that secant stiffness parameter demonstrated the most significant changes during the application of cyclic loading. It was demonstrated that a greater number of cycles were required to observe the same tip displacement for tests done under higher applied vertical stress. It was observed that these secant stiffness value for saturated samples changes much more than for the corresponding dry samples indicating that the **Cyclic CPT** test may not be a completely drained test. For the tests discussed in Section 3.4, it was observed that for similar values of $\alpha_{F,max}$ *and* $\alpha_{F,min}$, denser samples of dry soil observed lower tip opening even when magnitude of cyclic loading was significantly higher. Section 3.5 discussed the effect of frequency of cyclic loading on the results of dry samples. It was observed that higher tip opening was observed for lower frequency loading in dry samples. It was also observed that $\alpha_{F,const}$ value of at least 0.7 was required to prevent any upward movement of tip during the waiting period after application of monotonous tip penetration.

Chapter 4

4. Site Investigation

During the first half of this research work, two field campaigns were performed for the development of the **Cyclic CPT** test and the field equipment. The test campaigns were performed at the university campus of Grenoble and Chambéry. The strategy adopted was to perform a CPTu test to find information about subsoil and then perform a **Cyclic CPT** test using Equaterre's equipment at different depths already knowing the expected tip resistance and the soil type.

The expected soil type and their liquefaction susceptibility at different depths are predicted using the CPTu data analysis. The methodology used for finding soil type and liquefaction susceptibility using the CPTu test is explained in sections 4.1 and 4.2. Later, the two field campaigns are discussed in sections 4.3 and few conclusions from this chapter are mentioned in Section 4.4.

4.1 Soil Classification

4.1.1 Traditional Soil Classification Systems

The most widely used soil classification system is the United Soil Classification System (USCS) which broadly distinguishes the soil into two types : Coarse-Grained and Fine-Grained Soil. However, the actual in situ soil behaviour depends on factors such as geologic processes related to origin, environmental factors, as well as physical and chemical processes. Therefore, studying the volumetric changes, strength and stiffness changes, and non-linear behaviour after a minimal threshold strain is essential. Apart from this, deposit scale (macrostructure) and particle scale (microstructure) factors also greatly affect the soil behaviour and cannot be explained by the traditional USCS soil characterization.

Soils are often classified based on their response in shear prior to failure. This classification can be used to divide the soil among those that dilate under large strains and those that contract at large strains. For example, saturated soils that contract at large strains under shear stress have lower undrained shear strength than drained shear strength. This can be attributed to an increase in pore pressure, leading to a decrease in effective stress during shear loading. Similarly, saturated soils that dilate at large strains tend to have greater or equal undrained shear strength than drained shear strength. Another possible classification can be behavioural in nature where soil can be classified in terms of sand-like or clay-like behaviour (Boulanger and Idriss 2007). Saturated soils that are primarily sand-like generally show a drained response to static loading, while

clay-like soil shows mostly an undrained response to the same. This classification is similar to the UCSC classification of coarse and fine-grained soil. However, there are some fine-grained soils that show predominately sand-like behaviour.

A more widely used method to differentiate different soil types is to use a modified classification system based on behavioural soil classification but further divided into groups that show dilative or contractive behaviour. This classification system better defines soil types in the transition zone from sand-like to clay-like behaviour.

Soil behaviour can be very complex, and predicting soil properties based on any soil classification system is challenging. Multiple measurements should provide information about different in-situ soil behaviour features. Any test required for such a soil classification must be repeatable and easy to use. Therefore, the continuous, rapid, highly accurate and repeatable data logging of tip resistance, friction sleeve measurement and pore pressure make CPTu an ideal geotechnical test for accurately determining soil type.

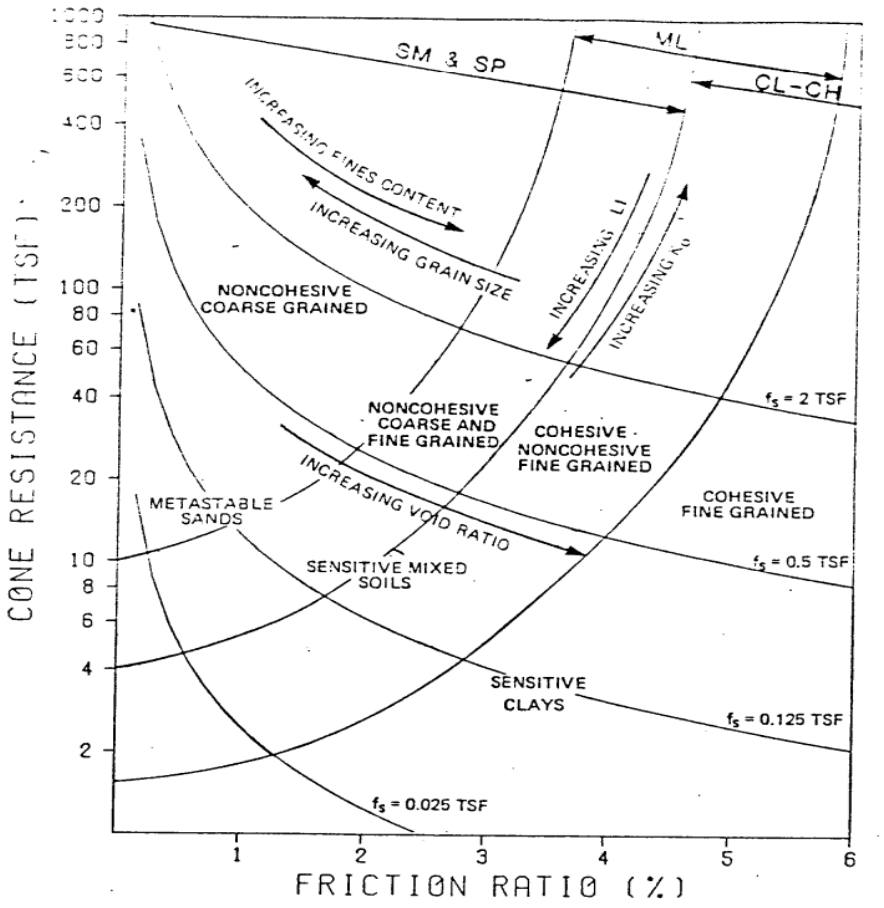

Figure 4.1 Soil classification based on tip resistance and local friction measurement (from Douglas and Olsen, 1981)

4.1.2 Soil classifications using Cone Penetration tests

One of the earliest soil classifications using the CPT measurements used only the cone tip resistance(q_c) values. It was considered that a high tip resistance (over 100 MPa) generally indicates dense sand or layers of gravel, while a low tip resistance (0 to 3 MPa) indicates soft young clays, layers of peat or a mixture of the two. However, it was almost impossible to forecast the soil type for values between the two solely based on tip resistance.

In the mid-1950s, a friction sleeve was added to the cone penetrometer and measured the local friction (f_s) caused by the soil on a small area. It was then extensively used in the soil classification graphs and formulas. Begemann 1965 provided a soil classification based on the tip resistance and the local friction measurement, as shown in Figure 4.1. Olsen and Joseph 1995 provided a famous soil classification system that used the electric cone penetrometer data and gathered extensive data to create correlations to suggest the soil behaviour classification chart (Figure 4.2). It was found that the friction ratio (%), i.e. the ratio of measurement from the friction sleeve to the tip resistance, is an excellent parameter to differentiate different soil behaviour. However, the cone resistance (in TSF = Ton per square feet) used for making this graph did not account for pore pressure effects. A similar soil classification using the mechanical cone was provided by Searle 1979.

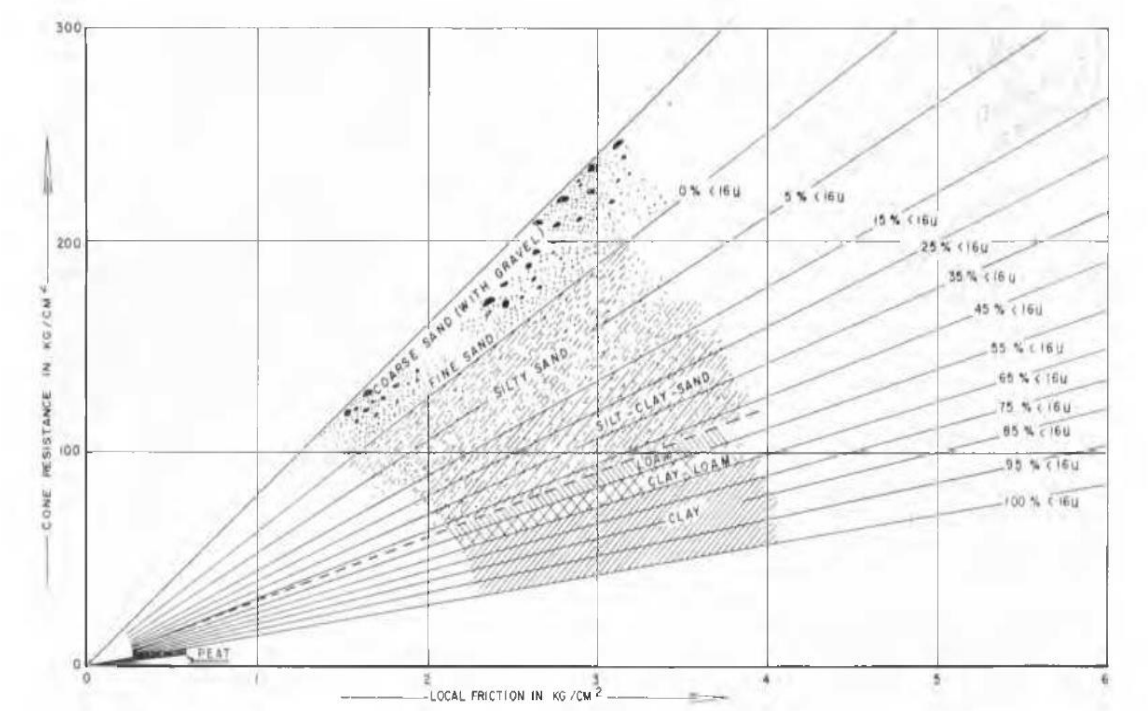

Figure 4.2 Soil classification based on tip resistance and local friction measurement (from Begemann, 1965)

Even further advancement in the stratification and detailed information about the soil was found using the pore pressure sensor in the cone (Jones et. al. 1981, Baligh et. al 1980). This further strengthened the position of the CPT tool for its use in predicting soil stratification. These classifications used cone measurements to respond to the in-situ mechanical properties of the soil.

4.1.3 Robertson methods for soil classification using CPT data

One of the most widely used soil classification criteria using the CPTu data was initially suggested by Robertson et al. 1986 and has been modified a number of times since then. The original paper provided the soil behaviour chart as shown in Figure 4.3 and had twelve soil behaviour types based on the combination of corrected tip resistance (q_t) and friction ratio (FR) values. Corrected tip resistance (q_t) is the cone resistance corrected for water effects [$q_t = q_c + u_2(1\text{-}a)$]; a is the cone area ratio.

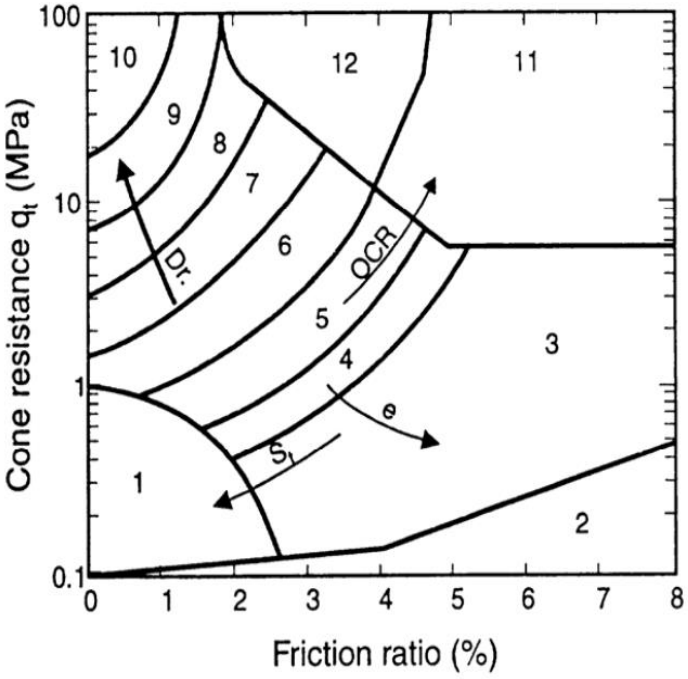

Zone	Soil Behavior Type
1	Sensitive fine grained
2	Organic material
3	Clay
4	Silty Clay to clay
5	Clayey silt to silty clay
6	Sandy silt to clayey silt
7	Silty sand to sandy silt
8	Sand to silty sand
9	Sand
10	Gravelly sand to sand
11	Very stiff fine grained*
12	Sand to clayey sand*

Figure 4.3 SBT chart from Robertson 1986

Robertson 1990 modified the above graph and used the three normalized parameters to identify soil type. These parameters are calculated as shown in equation 4.1, 4.2 and 4.3.

$$Q_t = (q_t - \sigma_{vo})/\sigma'_{vo} \qquad \textit{Eq. 4.1}$$

$$F_r = \frac{f_s}{q_t - \sigma_{vo}} * 100\% \qquad \textit{Eq. 4.2}$$

$$B_q = (u_2 - u_o)/(q_t - \sigma_{vo}) \qquad \textit{Eq. 4.3}$$

Where:
σ_{vo} is in situ total vertical stress;

σ_{vo}' is in situ effective vertical stress;
u_2 is the penetration pore pressure (immediately behind cone tip);
u_0 is the current in situ equilibrium water pressure.

Graphs made with normalized parameters embody the effect of depth and are more consistent with the in-situ soil behaviour. The normalized graph Figure 4.4 also divided the soil behaviour type in nine types rather than original twelve zones. The 1990 paper also gave a soil characterization chart using the tip resistance and a normalized pore pressure measurement called B_q which did not become as popular as the one shown in Figure 4.4 due to pore pressure measurement (u_2) problems.
Robertson and Wride 1998 used Figure 4.4 to define a soil behaviour type index (I_C) calculated as in Equation 4.4.

$$I_C = [(3.47 - \log Q_t)^2 + (1.22 + \log Q_t)^2]^{0.5} \qquad \textit{Eq. 4.4}$$

The contours described by this formula are approximately the normalized Soil Behaviour Type (SBTn) chart boundaries. The I_C value of 2.6 was an approximate boundary between soils that are either sandlike or claylike.

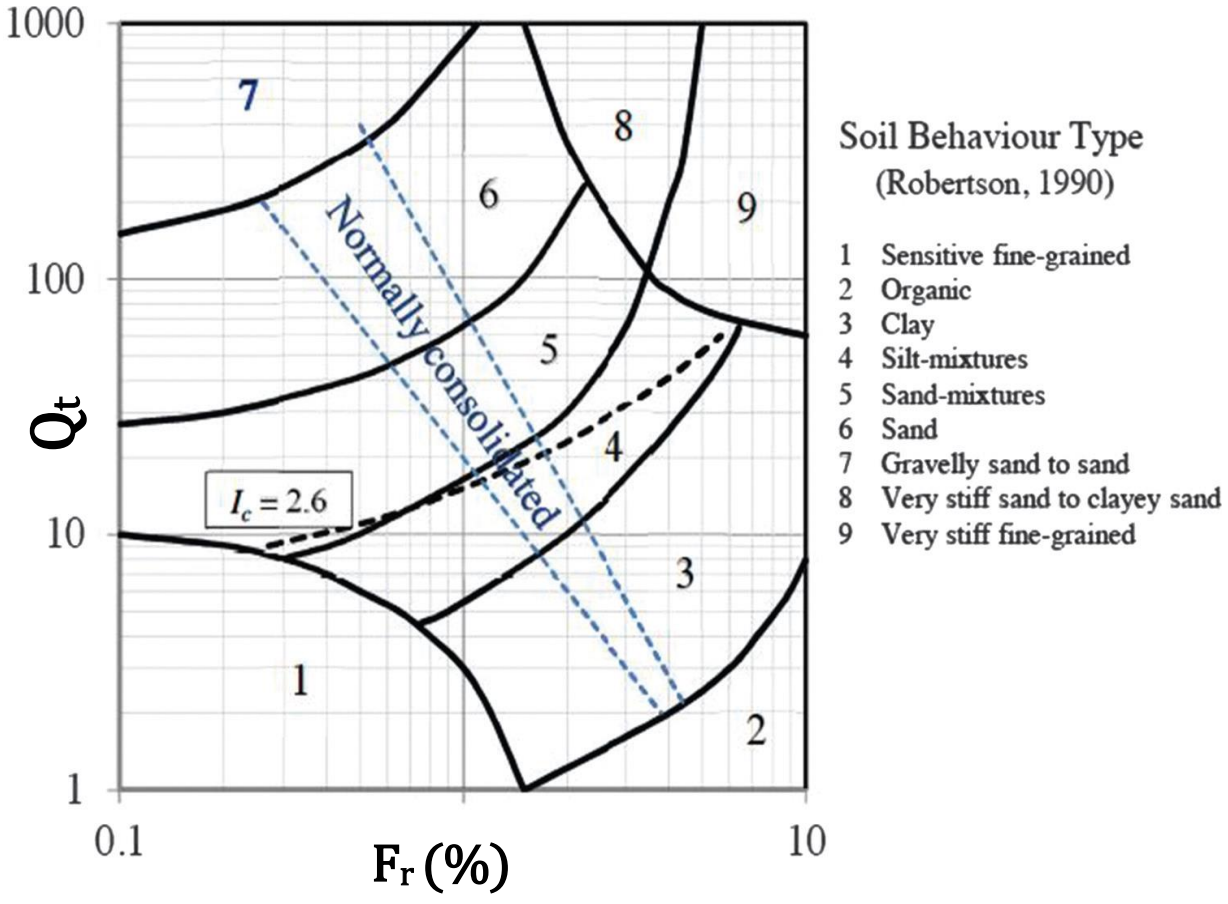

Figure 4.4 Normalized soil behaviour chart (Robertson, 1990)

Initially introduced by Robertson and Wride 1998 and updated by Zhang, Robertson, and Brachman 2002 the normalized tip resistance (Q_{tn}) is calculated as shown in Eq 4.5.

$$Q_{tn} = [(q_t - \sigma_{vo})/p_a](p_a/\sigma'_{vo})^n \qquad Eq\ 4.5$$

Where n is the shear stress exponent.

Robertson and Wride 1998 gave three values of n based on I_c values (0.5, 0.75 & 1). Robertson 2004 explained an iterative process to calculate n for I_C values between 1.64 and 3.3 and the process is explained as in Figure 4.5. It was further modified and equation 4.5 was suggested in Robertson et al. 2008. It was claimed that this new stress exponent "would capture the correct in situ state for soils at high stress level and that this would also avoid any additional stress level correction for liquefaction analyses".The suggested formula for the calculation of stress component "n" is shown in equation 4.6.

$$n = 0.381\ (I_C) + 0.05(\sigma'_{vo}/p_a) - 0.15 \qquad Eq\ 4.6$$

The resulting contours of n values for effective stress value equal to atmospheric pressure are as shown in Figure 4.6. It can be observed that $n = 1$ for most fine grained soils and it varies from 0.5 to 0.9 for most coarse grained soil. The $n = 1$ contour will move upwards for region with high in-situ stress i.e. $(\sigma'_{vo}/p_a) > 1$.

Robertson 2016 stressed the importance of predicting the effect of post deposition processes resulting in microstructure and proposed graphs to predict microstructure in soil using seismic CPT (SCPT). The paper also introduced another soil behaviour chart and a modified soil behaviour type index (I_B) (Figure 4.7). The CD value (calculated as shown in Figure 4.7) of 70 was used as a boundary for most geotechnical interpretations, as anything above this line could be considered dilative and hence not prone to liquefaction. The recommended procedure highlighted in this paper is to continue using the value of I_c to calculate stress component and normalized tip resistance (Q_{tn}) and then use the new I_B value to define the main boundaries between sand-like and clay-like behaviour.

However, even now, most of liquefaction prediction methods use the soil behaviour index definition from Robertson and Wride 1998 paper.

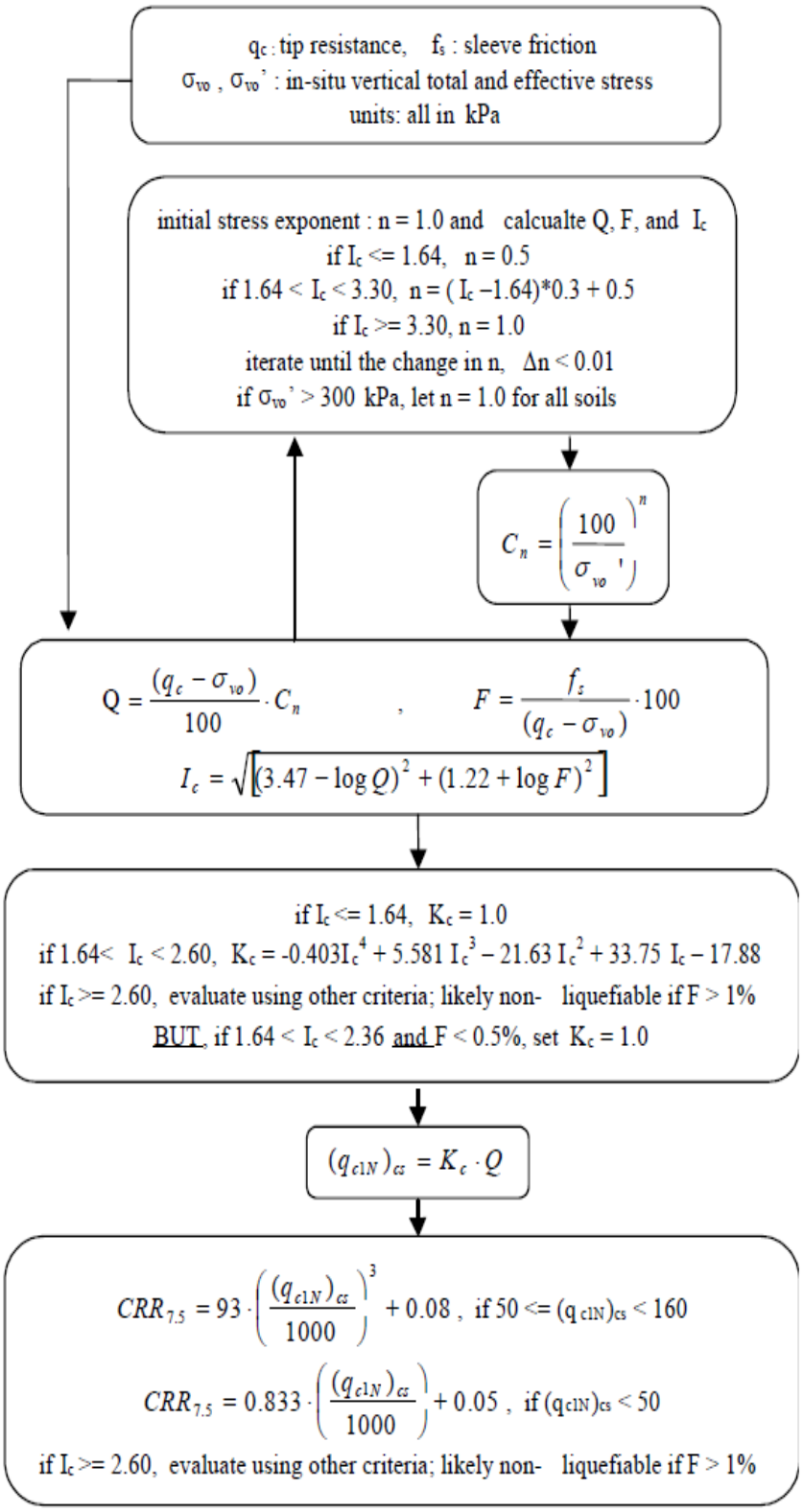

Figure 4.5 Flow chart of Robertson method to evaluate CRR (From Robertson 2004)

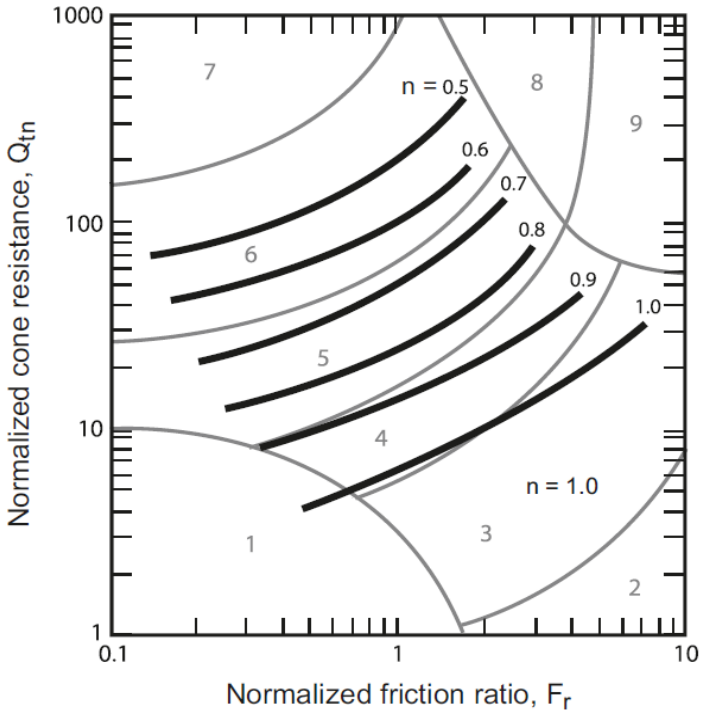

Figure 4.6 Contours of stress exponent imposed on SBTn chart

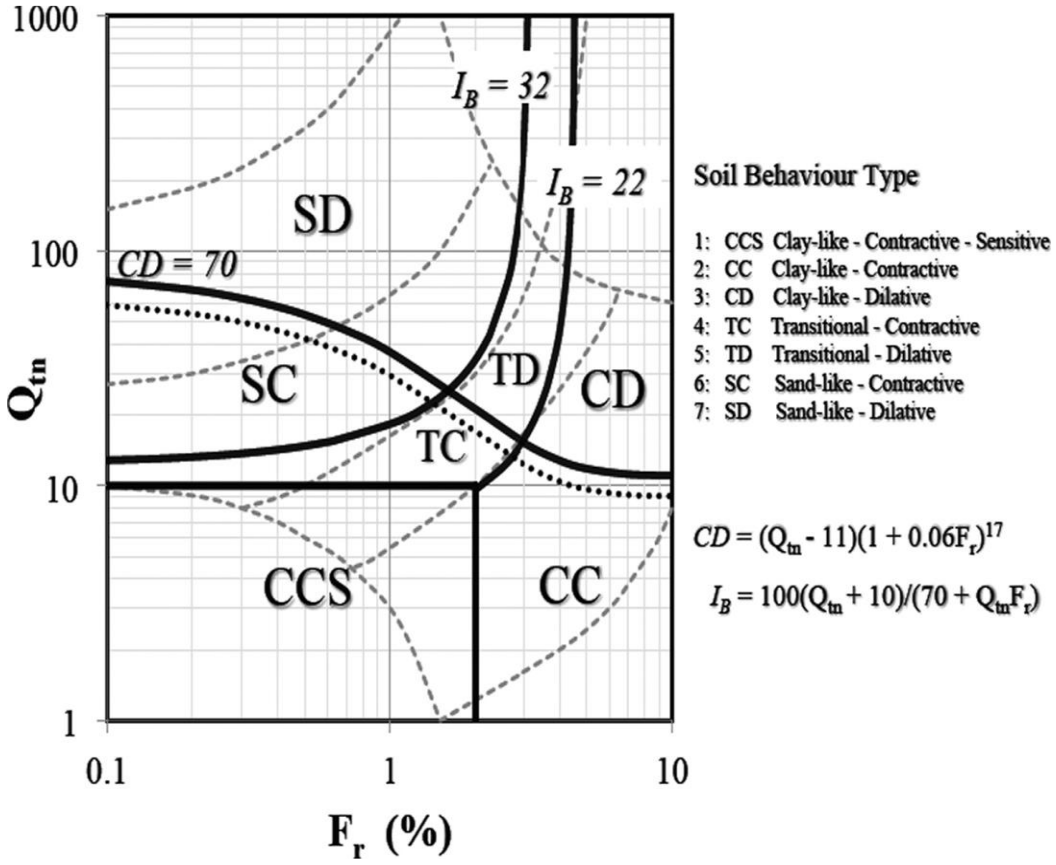

Figure 4.7 SBTn chart proposed in Robertson 2016 (dark lines)

4.2 Liquefaction susceptibility prediction from CPTu test

The prediction of resistance to liquefaction using CPT tests has been attempted for over 40 years now. A number of contributions have helped the growth of liquefaction prediction using penetration tests. A few of them are Christian and Swiger 1975, Olsen and Joseph 1995, Robertson and Wride 1998, Boulanger and Idriss 2007 and Boulanger and Idriss 2016.

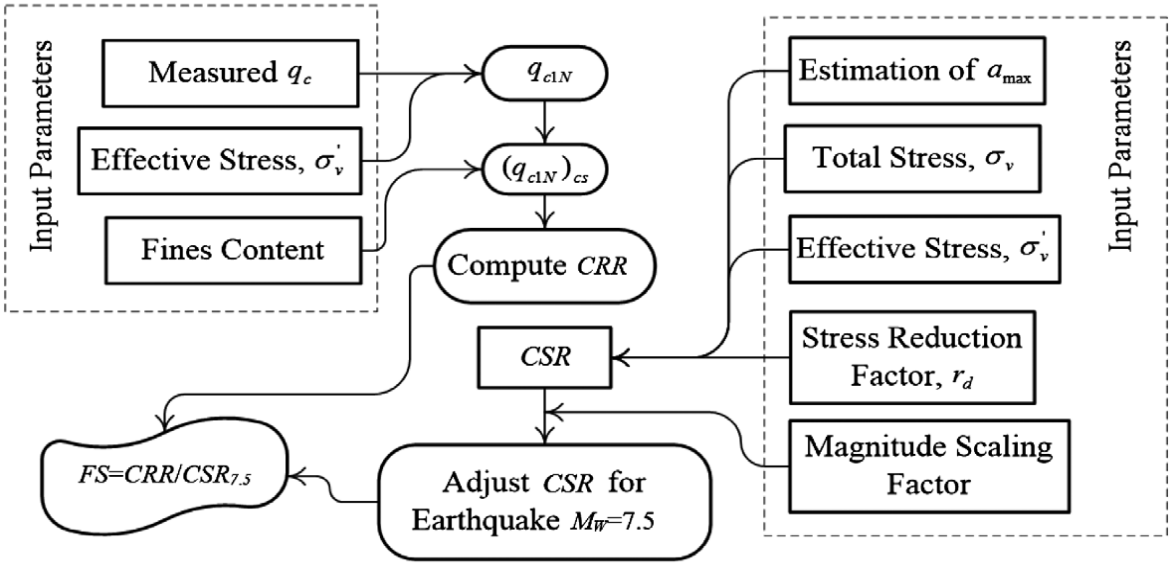

Figure 4.6 General approach to predict liquefaction susceptibility using CPT test (From Mola-abasi et. al. 2017)

Most current methods estimate a normalized tip resistance (Q_{tn}) using the CPT measurements (q_c , f and u_2). Next, the soil behaviour index predictions are used to predict the fine percentage in the soil and then provide the corrected clean sand equivalent of normalized tip resistance [$(Q_{tn})_{CS}$] and then calculate the cyclic resistance ratio (CRR). The complete process is as summarized in Figure 4.6 from Mola-abasi et. al. 2017. (Q_{tn} and q_{c1N} are identical and represent normalized tip resistance).

Most of these methods recommend their own relationships to calculate the CSR and all the associated parameters like stress reduction factor (r_d - to account for changes of shear stress caused by an earthquake w.r.t depth) or magnitude scaling factor (to account for change of shear stresses caused by different magnitude of earthquakes and find equivalent stress for 7.5 magnitude earthquake). Each method also has its own relationships to predict the resistance to liquefaction (CRR). It depends on the methods used to normalize the tip resistance, the methods to find the equivalent clean sand resistance [$(q_{c1N})_{CS}$] by predicting the fine content (F.C.), which in turn often requires soil behaviour prediction.

Two of the most widely used simplified methods to predict liquefaction using CPTu testing are explained in Robertson and Wride 1998 and Boulanger and Idriss 2016. They are also used for finding the liquefaction susceptibility of CPTu sites in this research work.

4.2.1 Robertson Method

It is a simplified method to predict liquefaction susceptibility and involves quantifying the earthquake shear loading in terms of a normalized parameter called Cyclic Stress Ratio (CSR). The resistance to the earthquake is predicted using empirical relationships and is then adjusted for an earthquake of the same magnitude causing the loading. The resistance parameter is called Cyclic Resistance Ratio (CRR).

CSR prediction: The paper mentions the use of site-specific seismicity analysis based on the probability of occurrence of an earthquake to determine the cyclic stress ratio profile with depth. For a simplified method, Robertson's method recommends the use of the procedure explained in Seed and Idriss 1971.

$$CSR = \frac{\tau_{av}}{\sigma'_{vo}} = 0.65(\frac{a_{max}}{g})(\frac{\sigma_{vo}}{\sigma'_{vo}})r_d \qquad \textit{Eq 4.7}$$

where:
τ_{av} is the average cyclic shear stress;
a_{max} is the maximum horizontal acceleration at the ground surface;
g is the acceleration due to gravity;
σ_{vo} and σ'_{vo} are the total and effective vertical overburden stresses, respectively;
r_d is a stress-reduction factor which is dependent on depth.

Equation 4.7 is derived from the assumption that shear stresses during an earthquake are caused due to the inertial forces and by assuming a homogenous rigid soil column that deforms together. "r_d" accounts for deformation of the soil column and changes of movement with respect to depth. A number of formulas are suggested to predict r_d in the literature. Robertson and Wride 1998, suggested the formula shown in equation 4.8.

$$r_d = \begin{cases} 1.0 - 0.00765z & if\ z < 9.15m \\ 1.174 - 0.0267z & if\ z = 9.15\ to\ 23\ m \\ 0.744 - 0.008\ z & if\ z = 23\ to\ 30\ m \\ 0.5 & if\ z > 30\ m \end{cases} \qquad \textit{Eq 4.8}$$

where z is the depth in meters.

CRR prediction:

As indicated in Figure 4.8 the first step for calculating the CRR value is to correct the cone resistance values from the effect of vertical stress. This correction accounts for the change of tip resistance for the same soils at different depths.

The Robertson method uses equation 4.5 for finding the normalized tip resistance(Q_{tN}). After calculating normalized tip resistance and the soil behaviour index (I_C) discussed in section 4.1, the next step is to account for the tip resistance changes for sands with fines. The tip resistance for such soils is generally lower due to increased compressibility and decreased permeability. This would result in apparent decrease of calculated liquefaction resistance which in reality is not true. Therefore the normalized tip resistance (Q_{tN}) values have to be corrected and converted to equivalent clean sand values [$Q_{tN,CS}$](Equation 4.9).

$$Q_{\text{tn,cs}} = K_C * Q_{\text{tn}} \qquad \textit{Eq 4.9}$$

K_C is a correction factor and depends on grain characteristics. The recommended formula to predict the K_C is as shown in equation 4.10 and depends on the calculated soil behaviour index I_C. It was originally proposed in Robertson and Wride 1998.

$$K_C = \begin{cases} 1 & if\ I_C \leq 1.64 \\ 5.581I_C^3 - 0.403I_C^4 - 21.63I_C^2 + 33.75I_C - 17.88 & if\ I_{C.} > 1.64 \end{cases} \qquad \textit{Eq 4.10}$$

Whenever possible, it is recommended to use sampling to find the fines content and not rely on these correlations.

After calculation of the clean sand equivalent the relationships suggested for the calculation of resistance of soil to an earthquake of magnitude 7.5 ($CRR_{7.5}$) and for soils with I_C value less than 2.6 is as shown in Equation 4.11.

$$CRR_{7.5} = \begin{cases} 93\left(\dfrac{Q_{\text{tn,cs}}}{1000}\right)^3 + 0.08 & if\ 50 \leq Q_{\text{tn,cs}} < 160 \\ 0.833\dfrac{Q_{\text{tn,cs}}}{1000} + 0.05 & if\ Q_{\text{tn,cs}} < 50 \end{cases} \qquad \textit{Eq 4.11}$$

Soils with I_C value greater than 2.6 are generally considered non-liquefiable if F.C. $> 1\%$. Resistance to an earthquake with a magnitude different from 7.5 is calculated using a magnitude scaling factor (MSF) and is as shown in equation 4.12.

$$CRR_M = CRR_{7.5} * MSF = CRR_{7.5} * 174/M^{2.56} \qquad \textit{Eq 4.12}$$

By comparing the CRR_M to the calculated CSR value (which depends on the design earthquake and site's ground movement) the liquefaction susceptibility of the soil can be

identified. The entire process is explained in the flowchart from Robertson 2004 (Figure 4.5).

4.2.2 Boulanger and Idriss Method

Boulanger and Idriss used latest case histories from events like Canterbury earthquake and Tohoku earthquake and an updated case history to give a new probabilistic CPT based liquefaction triggering procedure. The method is similar to Robertson's in terms of definition of a normalized tip resistance, a clean sand equivalent resistance and then calculation of a CRR value. The calculated resistance value is compared to a loading parameter (CSR) to find liquefaction probability.

CSR prediction

The method to calculate the loading caused by an earthquake is quite similar to Robertson method discussed before. Equation 4.7 is used to calculate CSR caused by an earthquake.

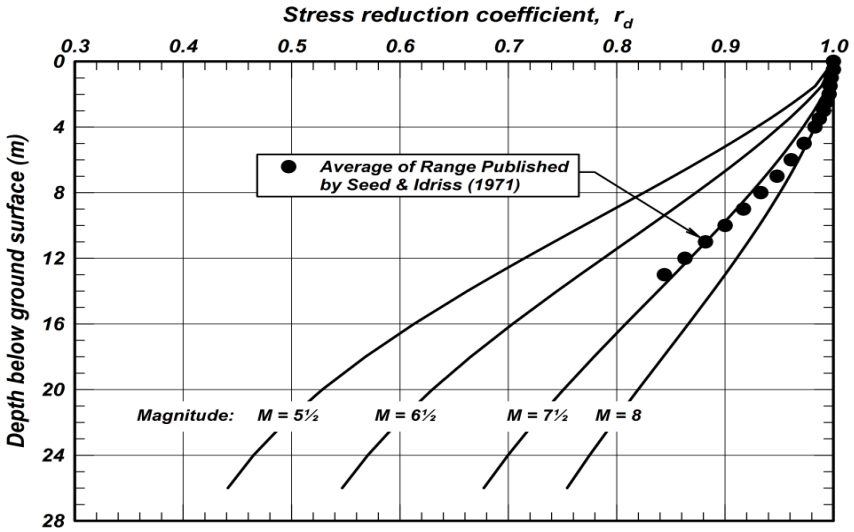

Figure 4.9 Shear stress reduction factor suggested for Boulanger's method

However, the suggested reduction factor (r_d) for this method is different and is calculated as shown in Equation 4.13.

$$r_d = exp[\alpha(z) + \beta(z)]. \qquad \textit{Eq 4.13}$$

where:

$$\alpha(z) = -1.012 - 1.126 \sin(\frac{z}{11.73} + 5.133) \qquad \textit{Eq 4.13 (a)}$$

$$\beta(z) = 0.106 + 0.118 \sin\left(\frac{z}{11.28} + 5.133\right) \qquad Eq\ 4.13\ (b)$$

Above relation results in a reduction factor as shown in Figure 4.9 and is in accordance with the values published by Seed and Idriss 1971.

CRR prediction

The method to predict CRR remains similar to the one explained in Figure 4.8. The normalized tip resistance, referred as q_{c1N} has corrections for overburden stress effects and is calculated as:

$$q_{c1N} = C_N q_{cN} = C_N \frac{q_c}{P_a} \qquad Eq\ 4.14$$

Where C_N is the overburden correction factor and is limited to a maximum value of 1.7. The suggested formula for calculating C_N is discussed in Boulanger 2003 and is calculated using equation 4.14(a); q_{cN} is the normalized tip resistance or the tip resistance that will be observed at an overburden stress of 1 atm (others parameters remaining similar) ; P_a is the atmospheric pressure.

$$C_N = \left(\frac{P_a}{\sigma'_v}\right)^m \qquad Eq\ 4.14\ (a)$$

where m is calculated as:

$$m = 1.338 - 0.249(q_{c1Ncs})^{0.264} \qquad Eq\ 4.14\ (b)$$

q_{c1Ncs} is the equivalent clean sand normalized penetration resistance and is calculated as shown in Equation 4.15.

The lower and upper limits of m are 0.264 and 0.782 respectively.

$$q_{c1Ncs} = q_{c1N} + \Delta q_{c1N} \qquad Eq\ 4.15$$

Δq_{c1N} is the correction for the normalized tip resistance that accounts for the fine content in the soil. The formula suggested for the calculation of this correction is:

$$\Delta q_{c1N} = \left(11.9 + \frac{q_{c1N}}{14.6}\right) exp\left[1.63 - \frac{9.7}{FC + 2} - \left(\frac{15.7}{FC + 2}\right)^2\right] \qquad Eq\ 4.16$$

Fine content (FC) calculation for this method is calculated using the Robertson's soil behaviour index (I_C) and the formula:

$$FC = 80(I_C + C_{FC}) \qquad Eq\ 4.17$$

where C_{FC} is a fitting parameter with default value of 0 and can vary within the range $\pm$ 0.29 and is site specific. The Cyclic Resistance Ratio for a 7.5 magnitude earthquake for an overburden stress of 1 atm $\left(CRR_{M=7.5,\sigma'_v=1atm}\right)$ is calculated as shown below:

$$CRR_{M=7.5,\sigma'_v=1atm} = exp\left[\frac{q_{c1Ncs}}{113} + \left(\frac{q_{c1Ncs}}{1000}\right)^2 - \left(\frac{q_{c1Ncs}}{140}\right)^3 + \left(\frac{q_{c1Ncs}}{137}\right)^4 - 2.80\right] \quad \textit{Eq 4.18}$$

The calculated $CRR_{M=7.5,\sigma'_v=1atm}$ value can be used to calculate the CRR for a given earthquake (M) and at any given overburden stress using equation 4.19.

$$CRR_{M,\sigma'_v} = CRR_{M=7.5,\sigma'_v=1atm} * MSF * k_\sigma \quad \textit{Eq 4.19}$$

Where MSF is the magnitude scaling factor and has been discussed in Boulanger and Idriss 2015 (Equation 4.20) and k_σ is the factor added to account for different effective vertical stresses. (Equation 4.21). These formulas have been derived using laboratory experiments, analysis of ground motion recordings and its dependency on soil characteristics.

$$MSF = 1 + (MSF_{max} - 1)\left[8.64\, exp\left(\frac{-M}{4}\right) - 1.325\right] \quad \textit{Eq 4.20}$$

Where MSF_{max} is calculated as per Equation 4.20(a)

$$MSF_{max} = 1.09 + \left(\frac{q_{c1Ncs}}{180}\right)^3 \leq 2.2 \quad \textit{Eq 4.20(a)}$$

The k_σ relationship from Boulanger 2003 is suggested for this method.

$$k_\sigma = 1 - C_\sigma \ln\left(\frac{\sigma'_v}{P_a}\right) \leq 1.1 \quad \textit{Eq 4.21}$$

where:

$$C_\sigma = \frac{1}{37.3 - 8.27(q_{c1Ncs})^{0.264}} \leq 0.3 \quad \textit{Eq 4.21(a)}$$

Finally, just like the Robertson's method, we can find the liquefaction susceptibility for a particular soil at a particular depth, and for a given magnitude by comparing CRR_{M,σ'_v} to the CSR.

4.2.3 Liquefaction susceptibility indexes

A conventional cone penetration test generally has one data entry for every two centimetres of penetration. Therefore, every two centimetre of soil can have a CRR value that can be compared to CSR value expected at that depth. Therefore a Factor of Safety (FS) value can be defined every two centimetres.

$$FS = CRR/CSR \qquad \textit{Eq 4.22}$$

However, it is hard to summarize the liquefaction susceptibility of a site using FS and a number of different liquefaction susceptibility indexes have been suggested. Few important ones are discussed below.

Cumulative thickness of liquefaction:

It is an important index to know what depth of soil layers can be expected to liquefy in case of an earthquake and is the sum of all depths where FS is less than one. Even if the FS values are quite low, if the cumulative thickness of liquefiable layers is not large, we can expect no significant damages on the surface.

Liquefaction Potential Index (LPI):

Iwasaki et al. 1978 introduced one of the most widely used liquefaction susceptibility index. It was the first published index to assess the vulnerability of sites to liquefaction. It is calculated as shown in equation 4.23.

$$LPI = \int_0^{20} F_1 * W(z)\, dz \qquad \textit{Eq 4.23}$$

Where $W(z) = 10 - 0.5z$, z is the depth and $F_1 = 1 - FS$ if $FS < 1$ or $F_1 = 0$. Its popularity is also attributed to its ease of application to differentiate **"low"**, **"high"** and **"very high"** risk locations. Sites with an LPI of more than 5 have a **high** liquefaction risk and more than 15 indicates **very high** risk (Iwasaki, 1982). In this index the effect of depth on liquefaction is considered to linearly decrease with depth. However Van Ballegooy et al. 2012 showed that the correlation between LPI and land damage or foundation damage is event specific. The paper introduced a new index known as Liquefaction Severity Number.

Liquefaction Potential Index (LSN):

It is similar to LPI but instead of FS, this index uses the expected volumetric densification strain and instead of a linear function, this index accounts for the decrease of effect on liquefaction damage by depth using a hyperbolic function (1/z). This resulted in more weightage to layers closer to surface. Expected volumetric densification was suggested to be calculated by method described in Zhang et. al. 2002. LSN has benefits that it also accounts for deformation in layers with FS between 1 and 2 and the maximum contribution to the potential damage caused by a layer is limited to the predicted volumetric strain. LSN is calculated as per equation 4.24

$$LSN = \int \frac{\varepsilon_v}{z} dz \qquad \textit{Eq 4.24}$$

It has been observed that a LSN value less than 20 will have no expression of liquefaction on the surface, a value between 20 and 40 may have some moderate expressions like cracking of ground surface while a LSN value greater than 40 always was accompanied with widespread damage.

4.3 In-situ campaign

For the development of the **Cyclic CPT** test, two field campaigns were performed during the first half of this PhD. The first site was close to 3SR Laboratory in the university campus of Grenoble, while the second was performed in front of a student residence in Chambéry. The location of the two sites can be seen in Figure 4.10. The CPTu tests at these sites were performed by external contractors while the CPT tests with the mechanical cone for the **Cyclic CPT** and double measurement tests were performed using the in-house CPT rig shown in Figure 4.11. The rig has six hydraulic jacks capable of being driven at 2 cm/s with a maximum combined thrust of 18 tonnes i.e. 18 MPa tip stress on a standard cone (ignoring friction). The maximum opening of the rig is sufficient to hold 2 m of penetration rods. The cone tip used in the experimental campaign was a mechanical Gouda cone with a 10 cm^2 cross-section.

4.3.1 Site #1 – Grenoble

The first test series was performed on an open field near 3SR laboratory. The CPTu test was performed on 27th August 2019 while the tests around it were performed on 11th March 2020. The location of the site and the planned layout of the tests around CPTu is as shown in Figure .

It was decided to perform **Cyclic CPT** tests at location P1, P2 and P3 while regular penetration tests using the mechanical cone at P4, P5 and P6. This test series was

hampered by a number of hardware and software problems and only 38 **Cyclic CPT** test performed at P-1 and P-3 locations were recorded. [5]

4.3.1.1 CPTu Analysis

The raw data of the CPTu test is shown in Figure 4.14 CPTu measurements- Site#1 4.14. The tip resistance slowly increased up to a depth of about three meters and remained above 10 MPa for almost thirteen meters. Then, there was a sudden drop of tip resistance between 14 and 18 meters. For the same depth, there was a sudden increase of pore pressure and the measured pore pressure values exceeded the hydrostatic pressure line indicating a clay-like soil. The water depth was found to be 4 m for this site, and hydrostatic pressure(u_0) is plotted with the measured pore pressure (u_2)(Figure 4.14(c)).

Using the data shown in Figure 4.14, the soil stratigraphy was found using methods described in sections 4.1. A python code "py-CPT" was developed during this thesis work to use the CPTu data to extract important information about the soil substrata. Robertson's method was implemented to calculate the I_C value (Figure 4.15). Different values of I_C correspond to clean sand-like behaviour. There existed a layer of clay-like soil between 14 and 18 m depth. ($2.95 < I_C < 3.60$) correspond to different groups of soil behaviour types. (Table 4.1) It was observed that the majority of the soil till 14 m depth had I_C values between 1.31 and 2.05 which

Liquefaction susceptibility is calculated using the two methods discussed in Section 4.2.3 and the results are as shown in Figure 4.16. The earthquake loading (CSR) is considered for an earthquake of magnitude 6.5 and for a ground acceleration of 2.24 m/s^2 (Recommended ground acceleration in Zone 4 for important structures in category 4). Corresponding resistance CRR values for such an event is calculated using the two different methods. CSR and the two CRR values are as seen in Figure 4.16(b).

The values of CSR and CRR(s) calculated are used to find factor of safety (FS) for different depths. FS is only calculated for depths with I_C values less than 2.6, considering soils with higher I_C values as non-liquefiable. This I_C value is recommended by Robertson's method, in the absence of data from laboratory testing. Layers with FS less than one are used to calculate the Liquefaction Potential Index (LPI) and cumulative depth of liquefaction. The LPI values of 1.72 and 4.47 and cumulative depth of liquefaction of 3.4 and 8.7 meters were calculated for the Robertson and Boulanger method, respectively. The LPI values for the sites are less than 5, indicating very small chances of liquefaction even in the

[5] Based on the problems encountered during this campaign, hardware and software corrections were suggested. A number of these suggestions were implemented during the Chambéry test campaign. It was envisaged to perform further tests at this locations after hardware and software corrections. However, these tests could not be performed during this work and will be performed during future works in this project

extreme loading event considered. However, the cumulative depth seems quite high and may be caused by a large number of points having FS just slightly below one, not contributing significantly to the LPI measurements.

Figure 4.10 Location of two in-situ campaigns

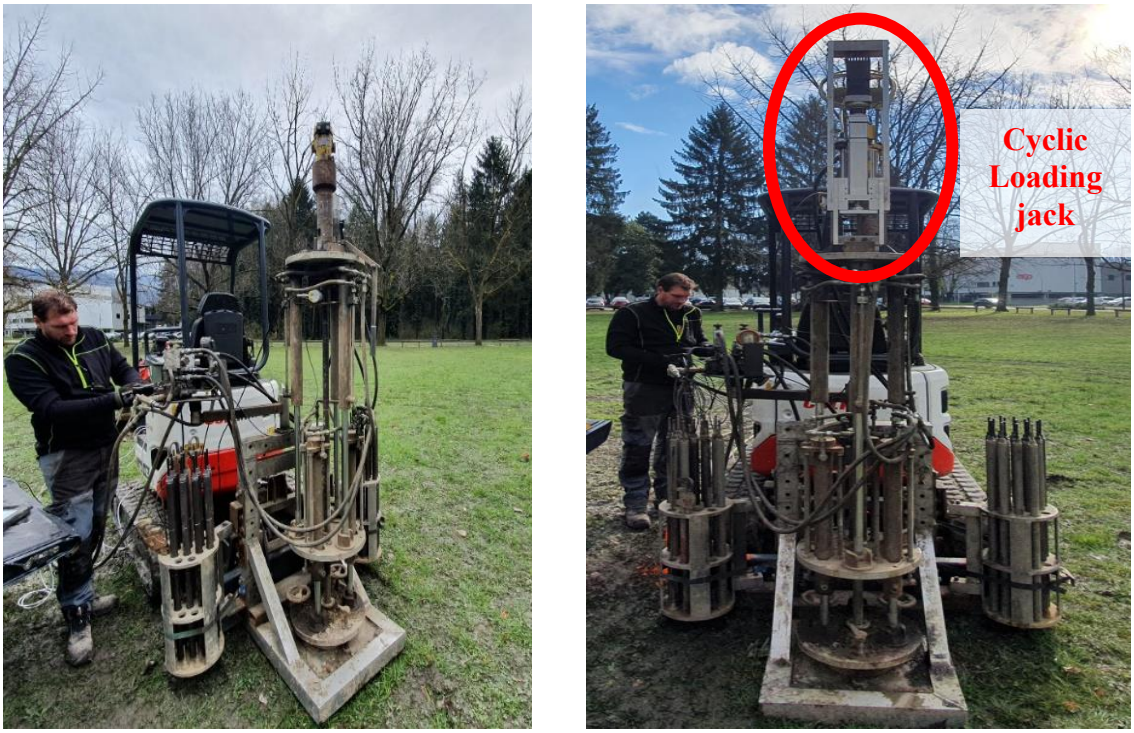

Figure 4.11 CPT pushing rig - Setup for normal driving (left) and for cyclic CPT test (right)

Soil Behaviour Index (I_C)	Soil Behaviour Type
$I_C < 1.31$	Gravelly Sand
$1.31 < I_C < 2.05$	Sands : clean sand to silty sand
$2.05 < I_C < 2.60$	Sand Mixtures : silty sand to sandy silt
$2.60 < I_C < 2.95$	Silt Mixtures : Clayey silt to silty clay
$2.95 < I_C < 3.60$	Clays
$I_C > 3.60$	Organic soils: peats

Table 4.1 Soil behaviour type based on I_c values

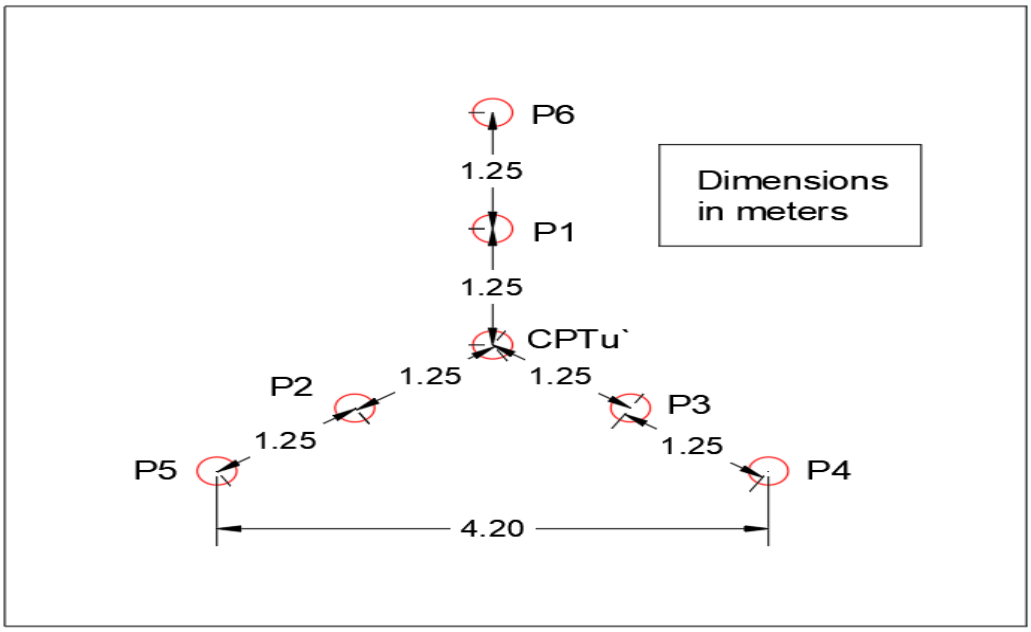

Figure 4.12 Layout of planned experiments around the CPTu test

4.3.1.2 Cyclic CPT test performed

This test campaign was the first time a **Cyclic CPT** test was undertaken on the field. The new cyclic loading jack was able to apply stress-controlled cycles. However, during this phase of testing, the loading device could not apply Equaterre's test methodology completely (Section 1.4). The cyclic loading jack was still under development and the tests conducted only applied a push force till the input displacement was reached (STEP A) and started applying the stress controlled cycles (STEP C) immediately after that (i.e. zero waiting time for STEP B). The push force was limited to 5000 N, while the cyclic loading was limited to 3500 N. This forced us to perform the tests at shallow depths or in layers

between 14 and 18 m where the tip resistance was less than 3500 N. Also, the cycles were applied using predefined input values of maximum and minimum amplitude of the cyclic compressive force. This made it impossible to test fixed $\alpha_{F,max}$ and $\alpha_{F,min}$ values as it was not possible to know the tip resistance recorded during Step A without performing the test. It was attempted to anticipate the tip resistance from layers just above the one tested and apply a maximum cyclic force that was close to the tip resistance.

Table 4.2 shows the tip resistance recorded during Step A, the input values of maximum and minimum amplitude of cyclic load and the resulting $\alpha_{F,max}$ and $\alpha_{F,min}$ values, the depth at which the cyclic test was done, the I_C value calculated at a similar depth using the CPTu test , the total number of cycles (N_{cycles}) applied and the displacement during cyclic loading (Δ_{cyclic}). The force measurement in the field tests was derived using the torque required by the rotating motor to apply the target cyclic loading and lacked an external force sensor. The displacement measurements were also from the internal system of the cyclic loading jack. It can be seen from table 4.2 that for every $\alpha_{F,max}$ value less than 0.8, there was no displacement observed during the cycling loading. A vital comparison from this campaign is the behaviour of the cyclic CPT test just before and after the start of clay layer at 14 m depth. As can be seen in table 4.2, Test #18 was performed at a depth of 13.7 m, while Test #19 was performed at a depth of 14.2 m depth. The I_C values for the tested depth at these two tests were 1.5 (sand-like) and 3 (clay-like) respectively. The tip resistance and the $\alpha_{F,max}$-$\alpha_{F,min}$ values were very close to each other (Similar loading). However, the observed displacement during the cyclic loading varied quite a lot from one another (Figure 4.13). The test done in the sand-like soil, resulted in a cumulative tip opening that was quite low (7 mm), while it reaches 43 mm for the test done in clay-type soil.

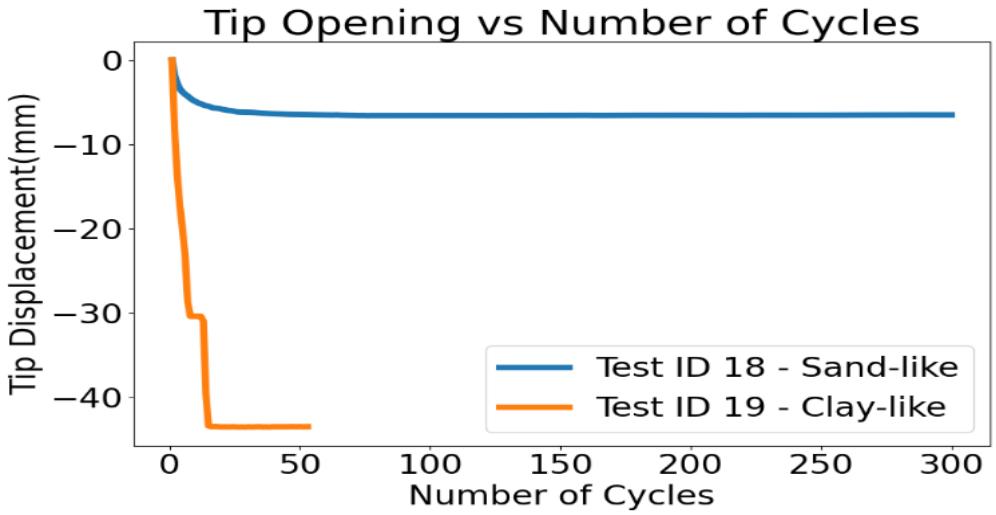

Figure 4.13 Tip opening for different SBT values - Site #1

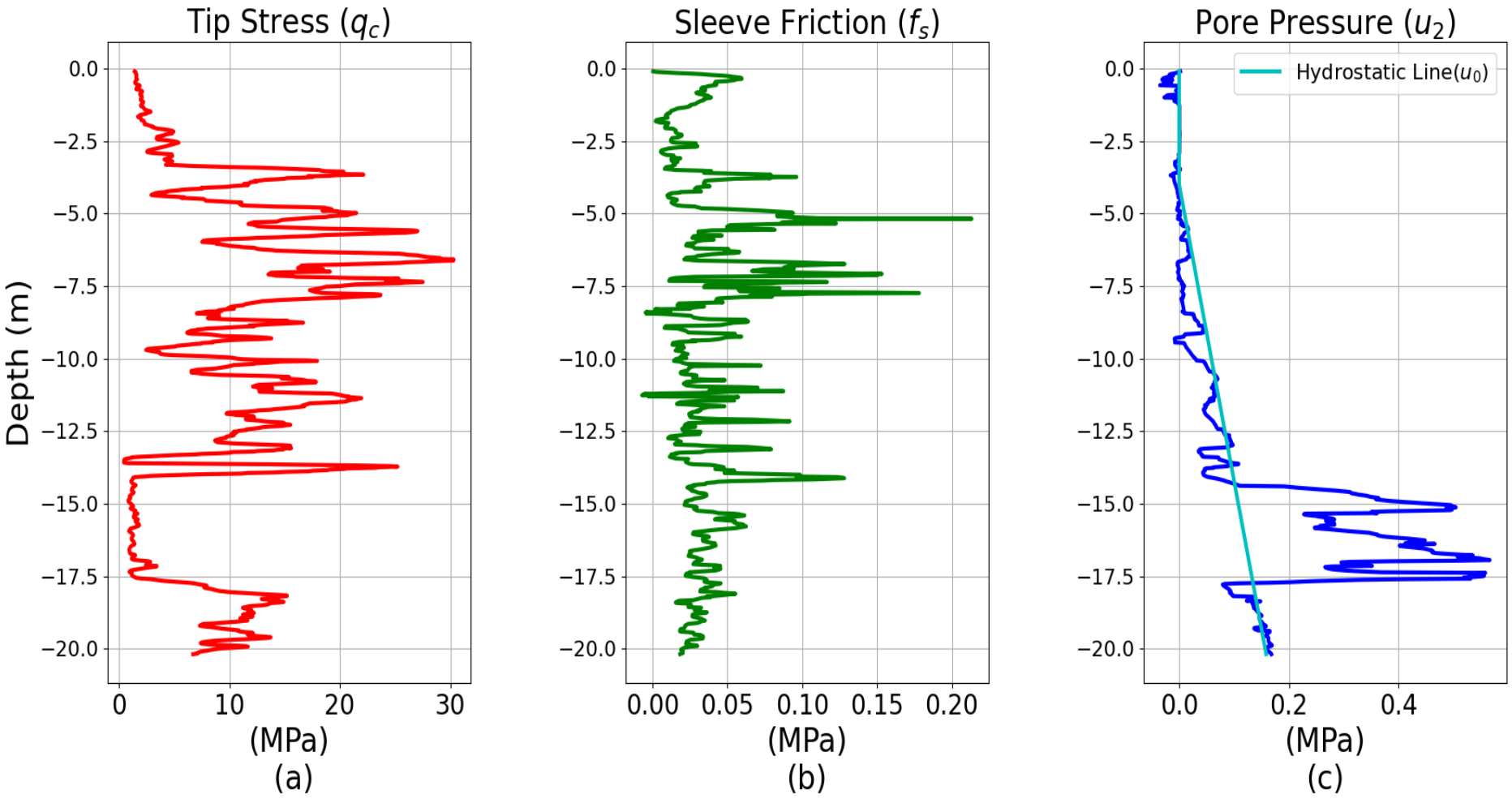

Figure 4.14 CPTu measurements- Site#1

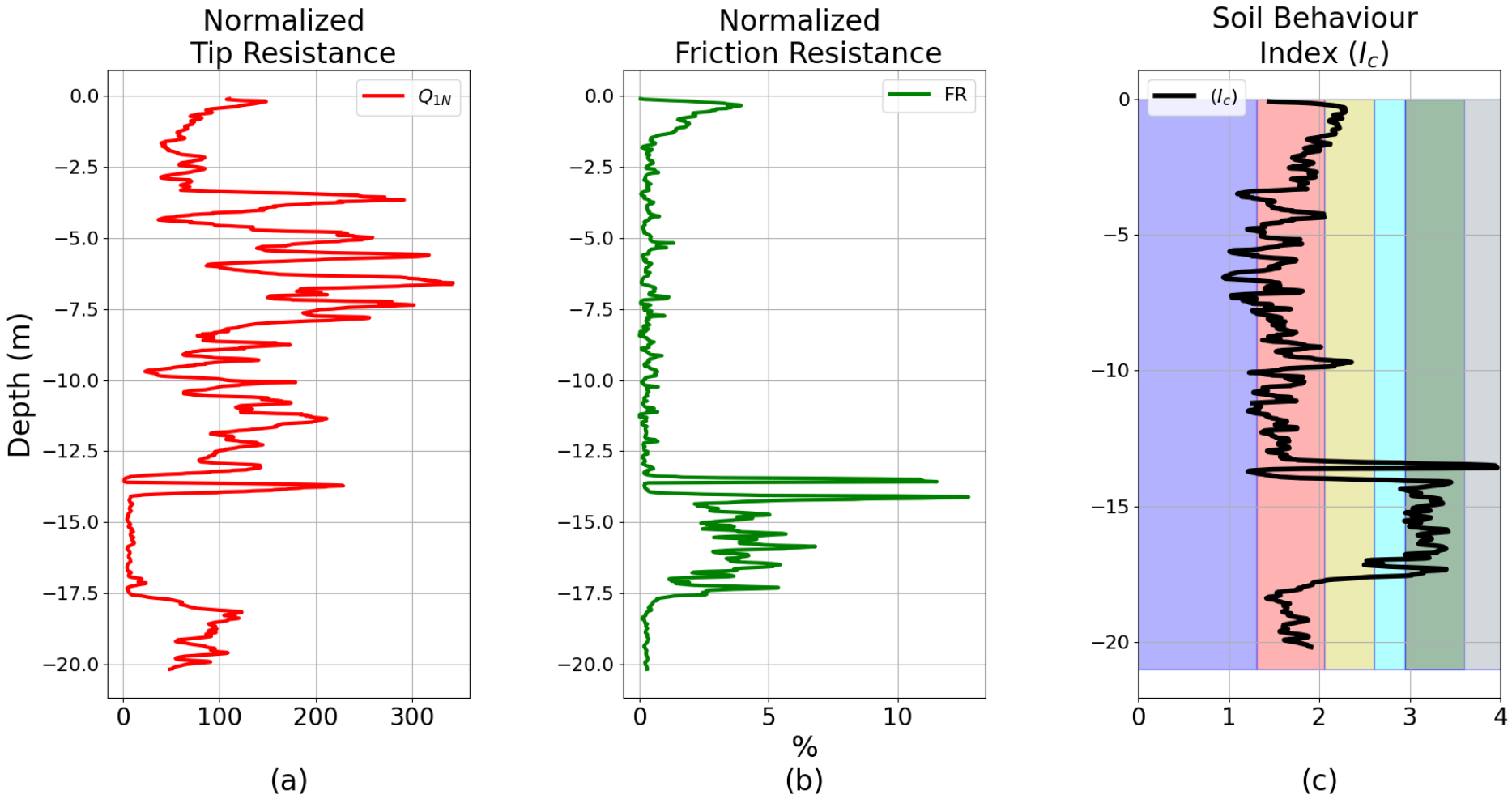

Figure 4.15 CPTu analysis to find I_c values - Site #1

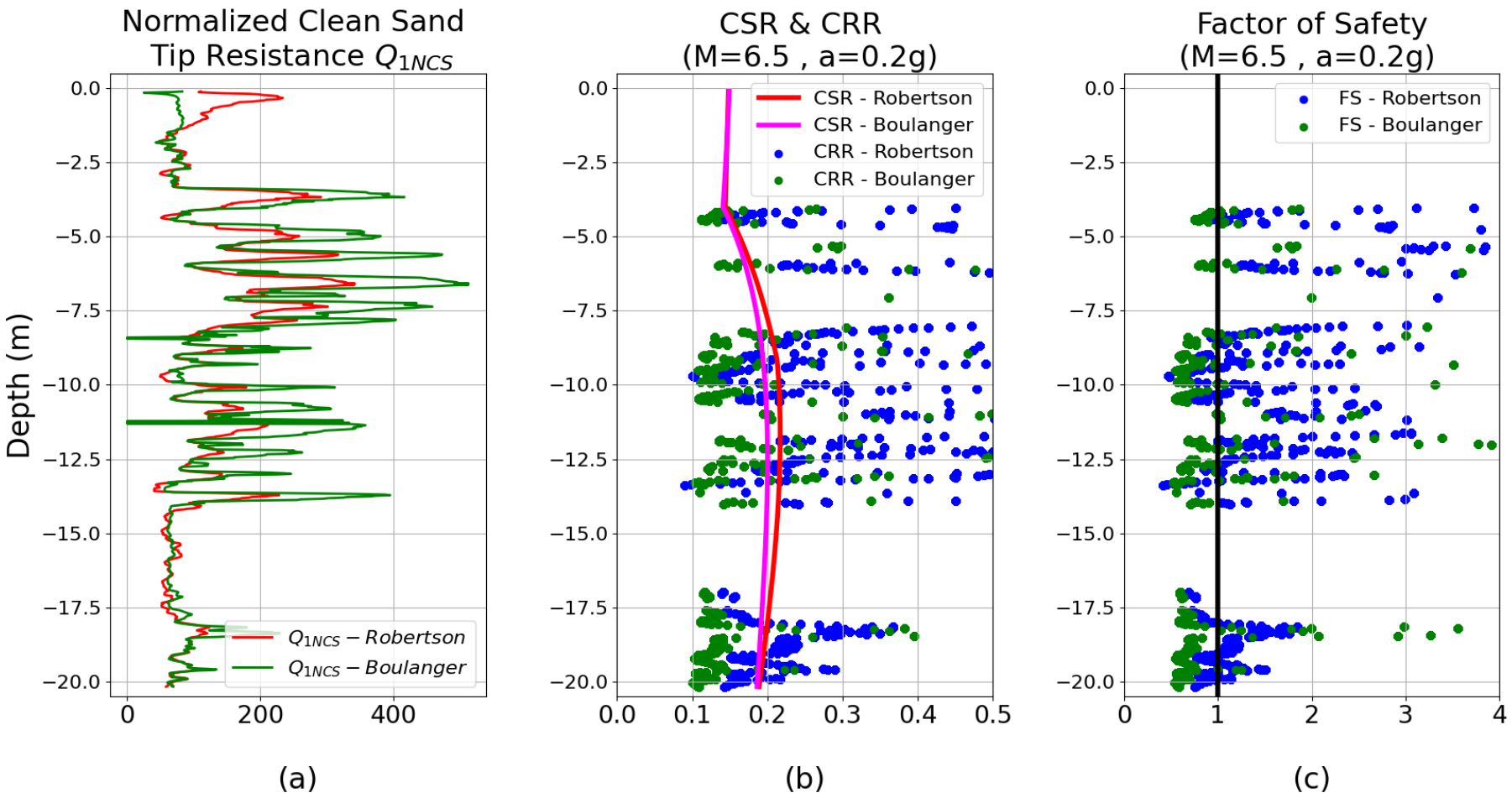

Figure 4.16 Liquefaction susceptibility based on CPTu test - Site#1

S.No.	Loca-tion	Depth (m)	Ic (CPTu)	V (Hz)	F-max (Step A)	Minimum force	Maximum force	$\alpha_{F,max}$	$\alpha_{F,min}$	N_{cycles}	Δ_{cyclic}
G_1	P1	0.8	2.1	1	2393.0	600	2500	1.0	0.3	10	60
G_2	P1	1.2	2.2	1	2661.7	600	2500	0.9	0.2	300	4
G_3	P1	1.8	1.8	1	3186.4	600	2500	0.8	0.2	300	0
G_4	P1	2.2	1.7	1	4990.7	600	-500	0.7	0.1	300	0
G_5	P1	2.4	1.9	1	4811.5	600	3500	0.7	0.1	300	0
G_6	P1	2.6	1.9	1	>5000						
G_7	P1	2.8	1.9	1	>5000						
G_8	P1	3	1.8	1	>5000						
G_9	P1	3.2	1.8	1	>5000						
G_10	P1	3.4	1.3	1	>5000						
G_11	P1	3.8	1.4	1	>5000						
G_12	P1	9.6	2.0	1	>5000						
G_13	P1	9.8	2.2	1	>5000						
G_14	P1	10	1.5	1	>5000						
G_15	P1	10.6	1.5	1	>5000						
G_16	P1	13.4	3.0	1	>5000						
G_17	P1	13.6	3.4	1	3122.4	600	3500	1.1	0.2	8	20
G_18	P1	13.7	1.2	1	2393.0	600	2500	1.0	0.3	300	7
G_19	P1	14.2	3.3	1	2495.3	600	2500	1.0	0.2	53	43
G_20	P1	14.8	3.3	1	2853.6	600	2000	0.7	0.2	97	0
G_21	P1	14.9	3.4	1	2943.2	600	2500	0.8	0.2	67	55
G_22	P1	15.2	3.0	1	2789.7	600	2200	0.8	0.2	300	12
G_23	P1	15.4	3.3	2	3237.5	600	2200	0.7	0.2	376	0
G_24	P1	15.6	3.1	2	3237.5	600	2500	0.8	0.2	443	9
G_25	P1	15.8	3.2	4	3903.0	600	2500	0.6	0.2	384	0
G_26	P1	16	3.2	1	3275.9	600	3000	0.9	0.2	323	52
G_27	P1	16.4	3.2	2	3736.6	600	3000	0.8	0.2	565	49
G_28	P1	16.6	3.4	3	3736.6	600	3000	0.8	0.2	588	0
G_29	P1	16.6	3.4	2	3992.5	600	3500	0.9	0.2	434	48
G_30	P3	0.2	2.0	2	2303.4	600	1200	0.5	0.3	200	0
G_31	P3	0.3	2.2	2	2508.1	600	2000	0.8	0.2	200	9
G_32	P3	0.4	2.3	2	2853.6	600	2200	0.8	0.2	200	3
G_33	P3	0.6	2.2	2	2648.9	600	2400	0.9	0.2	228	50
G_34	P3	0.8	2.1	2	2418.6	600	2200	0.9	0.2	200	22
G_35	P3	1.2	2.2	2	3595.8	600	2200	0.6	0.2	51	0
G_36	P3	1.2	2.2	2	4069.3	600	3300	0.8	0.1	200	26
G_37	P3	1.4	2.0	2	>5000						
G_38	P3	1.6	2.0	2	>5000						

Table 4.2 Details Cyclic CPT tests - Site #1

4.3.2 Site #2 Chambéry

The second test campaign was done at 9 Rue du Lac Saint-Andre, 73370 Le Bourget-du-Lac. This is a student residence building in the university campus that is facing a large settlement. Before the construction of the building, 1.5 m of original soil was replaced by compacted subgrade material. As a part of the analysis, initially, a CPTu was done to know the details of the underlying strata. Later **Cyclic CPT** tests were performed on 10th March 2020 with improvement made to the software and the hardware of the cyclic loading device. In total 53 cyclic CPT tests were performed at 2 different locations close to the CPTu borehole (within 2 m distance).

4.3.2.1 CPTu Analysis

The CPTu measurements are shown in Figure 4.19. The top 1.5 layer of the soil corresponds to huge values of tip resistance and friction values. The same region also corresponds to negative pore pressure, which may have resulted in the unsaturation of the porous stone. The soil was found saturated immediately below the compacted layer, and the hydrostatic water line assuming 1.5 m water depth is also shown in Figure 4.19(c).

The soil behaviour index (I_C) was calculated using the normalized tip resistance and Friction Ratio (FR) values as explained in Section 4.1. The resulting I_C values corresponded to gravel-type soil for the first 1.5 m, followed by clay/organic type soil behaviour till 8.5 meters depth characterized by very low tip resistance and high FR. After this depth the next 16 m of soil fell entirely in the clean sand type soil (Figure 4.20).

The liquefaction analysis of this site using the two methods discussed in Section 4.2 is as shown in Figure 4.21. There is a significantly larger number of depths with FS less than one. The LPI values of 9.1 and 12.5 from Robertson and Boulanger method also indicate "**high**" risk of liquefaction.

4.3.2.2 Cyclic CPT test performed

With the modifications made to the control system, it was possible to specify the $\alpha_{F,max}$ and $\alpha_{F,min}$ parameters before the **Cyclic CPT** tests. However, the maximum force for the cyclic loading was still limited to 3500 N (3.5 MPa with 10 cm^2 tip) while almost the entire sand type soil had tip resistance greater than 7.5 MPa. Therefore, majority of tests were done in clay type soil. The I_C values at corresponding depth and other details of **Cyclic CPT** tests are shown in Table 4.3.

Tests C_10, C_11, C_12 and C_13 can be used to study the effect of $\alpha_{F,max}$ values on measured displacement during the application of cyclic load. The results of these tests are as shown in Figure 4.17. No tip opening was observed for $\alpha_{F,max}$ values of 0.6, while the rate of tip opening increased rapidly for $\alpha_{F,max}$ increasing from 0.7 to 0.9. All these tests were done in soil layers with almost identical I_C values.

Tests C_29 and C_30 can be used to study the effect of frequency on the results of **Cyclic CPT** tests. The two tests have very similar tip resistance measured during Step A and have same $\alpha_{F,max}$ input values. It was observed that the tip opens much faster for a frequency of 1 Hz (Test C_30) as compared to 2 Hz (Test C_29). This can be possible due to the fact that

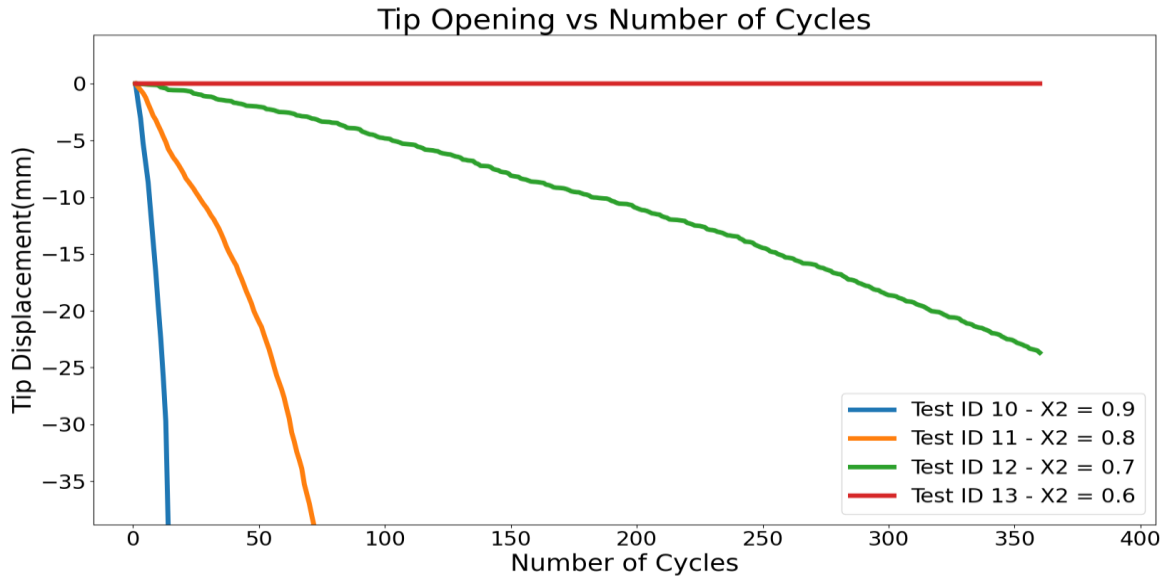

Figure 4.17 Effect of $\alpha_{F,max}$ value on clay type soil - Site#2

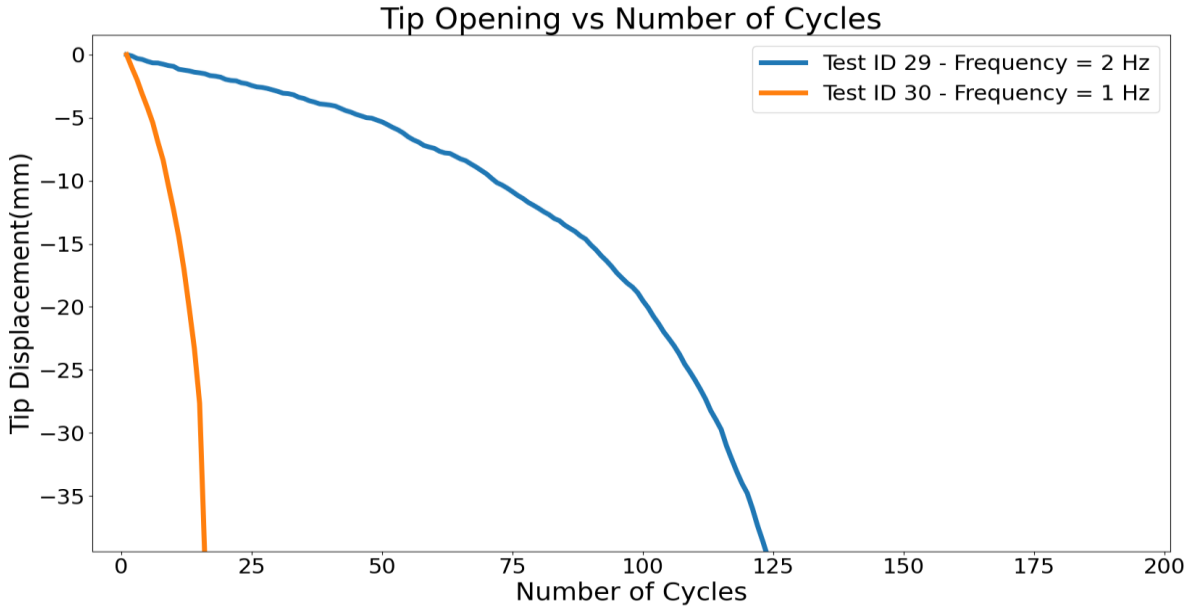

Figure 4.18 Effect of frequency on clay type soil - Site#2

a lower frequency ensures application of higher tip stress for a longer duration of time. The results of these two tests is as shown in Figure 4.18.

S.No	Loca-tion	Depth (m)	Ic (CPTu)	V (Hz)	F-max (Step A)	Minimum force	Maximum force	$\alpha_{F,max}$[6]	$\alpha_{F,min}$[7]	N_{cycles}	Δ_{cyclic}
C_1	P1	1.6	2.9	2							
C_2	P1	1.8	2.8	2	2085.8	280.5	1262.2	0.6	0.1	600	0.2
C_3	P1	1.9	2.9	2	2124.2	283.7	1276.6	0.6	0.1	600	0.0
C_4	P1	2	2.9	2	2137.0	304.9	1524.3	0.7	0.1	607	38.2
C_5	P1	2.2	2.9	2	2021.8	289.1	1445.7	0.7	0.1	360	15.5
C_6	P1	2.3	3.0	2	2175.4	272.2	2041.3	0.9	0.1	61	48.9
C_7	P1	2.5	3.1	2	2034.6	285.3	2139.6	1.1	0.1	59	48.4
C_8	P1	2.7	3.2	2	2047.4	269.4	1616.5	0.8	0.1	149	39.4
C_9	P1	2.9	3.3	2							
C_10	P1	3	3.1	2	1829.9	270.7	1623.9	0.9	0.1	101	39.4
C_11	P1	3.2	3.1	2	1778.7	260.4	1432.1	0.8	0.1	126	39.5
C_12	P1	3.4	3.0	2	1945.0	276.6	1383.1	0.7	0.1	360	23.7
C_13	P1	3.5	3.1	2	1957.9	286.4	1145.6	0.6	0.1	360	0.0
C_14	P1	3.6	3.2	2	1957.9	261.4	1307.2	0.7	0.1	360	0.0
C_15	P1	3.7	3.3	2	2085.8	292.5	1608.5	0.8	0.1	360	4.6
C_16	P1	3.8	2.7	2	2444.1	348.9	1919.0	0.8	0.1	360	8.5
C_17	P1	4	2.3	2	2226.6	328.0	1804.2	0.8	0.1	360	4.9
C_18	P1	4.1	2.4	2	2226.6	323.0	1937.7	0.9	0.1	82	49.5
C_19	P1	4.3	2.9	2	2482.5	376.1	2068.4	0.8	0.2	103	50.8
C_20	P1	4.5	3.1	2	2456.9	330.8	1819.5	0.7	0.1	205	39.9
C_21	P1	4.7	3.1	2	2124.2	287.2	1436.2	0.7	0.1	360	1.4
C_22	P1	4.7	3.1	2	2124.2	287.2	1436.2	0.7	0.1	360	1.4
C_23	P1	5.1	3.1	2	2034.7	296.2	1628.9	0.8	0.1	84	39.8
C_24	P1	5.3	3.3	2	2392.9	365.8	1646.1	0.7	0.2	360	0.0
C_25	P1	5.5	3.3	2	2085.8	288.4	1442.1	0.7	0.1	360	0.0
C_26	P1	5.7	3.5	2	1996.3	252.7	1390.0	0.7	0.1	360	0.7
C_27	P1	5.9	3.4	2	2124.2	266.1	1596.8	0.8	0.1	80	49.9
C_28	P1	6.1	3.4	2	2098.6	323.0	1857.2	0.9	0.2	104	25.5
C_29	P1	6.3	3.0	2	1932.3	268.0	1474.0	0.8	0.1	200	39.9
C_30	P1	6.5	3.3	1	1842.7	279.8	1539.1	0.8	0.2	33	40.0
C_31	P1	6.7	3.3	1	2009.1	262.1	1310.5	0.7	0.1	180	0.0
C_32	P1	6.8	3.3	1	2034.6	268.8	1478.3	0.7	0.1	176	50.9
C_33	P1	7	3.4	1	2034.6	296.7	1632.0	0.8	0.1	51	39.8
C_34	P1	7.2	3.3	1	2252.2	328.6	1478.6	0.7	0.1	90	0.3

[6,7] $\alpha_{F,max}$ and $\alpha_{F,min}$ values were recalculated after the tests as the recorded tip resistance during penetration (TR#1) was different from the maximum values of force during Step A (Software Error)

S.No	Loca-tion	Depth (m)	Ic (CPTu)	V (Hz)	F-max (Step A)	Minimum force	Maximum force	$\alpha_{F,max}$[6]	$\alpha_{F,min}$[7]	N_{cycles}	Δ_{cyclic}
C_35	P1	7.4	3.4	1	3493.4	621.6	3107.9	0.9	0.2	30	38.1
C_36	P1	7.6	3.3	1	2956.0	472.2	2361.1	0.8	0.2	180	9.7
C_37	P1	7.8	3.4	1	3224.7	503.2	2516.2	0.8	0.2	90	16.5
C_38	P1	8	3.1	2	2623.3	416.6	2291.3	0.9	0.2	62	38.7
C_39	P1	8.2	3.5	2	3160.7	484.6	2180.6	0.7	0.2	360	0.4
C_40	P1	8.4	2.8	2	3493.4	698.7	3842.8	1.1	0.2	37	10.2
C_41	P2	2.2	2.9	2	1996.2	249.6	1248.1	0.6	0.1	360	0.0
C_42	P2	2.5	3.1	2	2201.0	292.9	2196.6	1.0	0.1	60	38.1
C_43	P2	2.7	3.2	2	2444.1	287.0	1722.1	0.7	0.1	83	39.5
C_44	P2	2.9	3.3	2	2098.6	288.0	1728.1	0.8	0.1	75	39.0
C_45	P2	3.2	3.1	2	1855.5	257.6	1416.7	0.8	0.1	360	0.0
C_46	P2	3.4	3.0	2	2034.6	249.4	1246.9	0.6	0.1	360	0.0
C_47	P2	3.8	2.7	2	2290.5	338.4	1861.1	0.8	0.1	360	0.7
C_48	P2	4	2.3	2							
C_49	P2	4.3	2.9	2	2367.3	341.7	1879.1	0.8	0.1	147	39.3
C_50	P2	4.5	3.1	2							
C_51	P2	4.7	3.1	2	2175.4	281.6	1407.9	0.6	0.1	360	0.0
C_52	P2	4.9	3.5	2	2277.7	289.2	1590.6	0.7	0.1	192	50.6

Table 4.3 Details of Cyclic CPT tests - Site#2

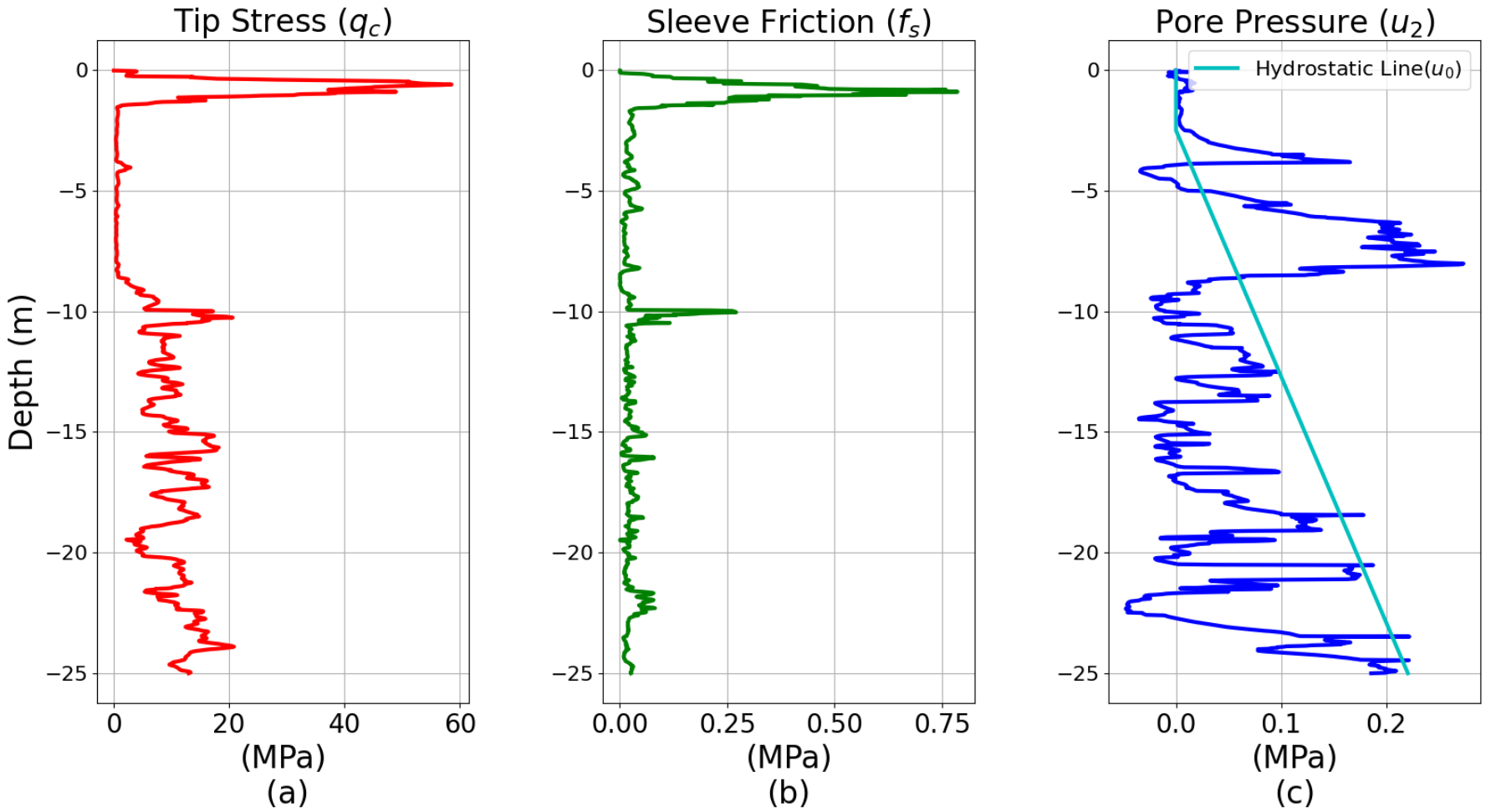

Figure 4.19 CPTu measurements - Site#2

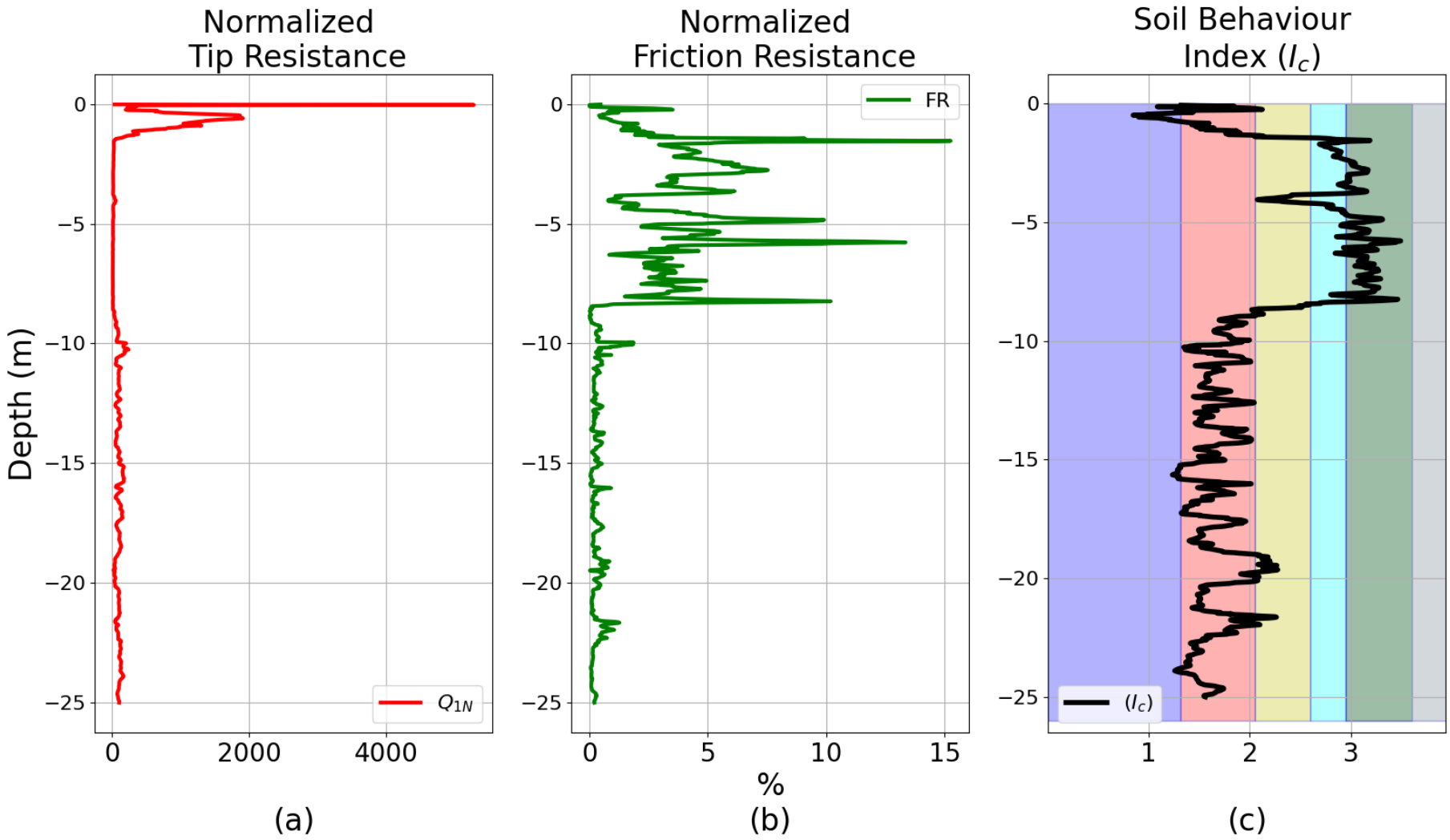

Figure 4.20 CPTu analysis to find Ic values - Site#2

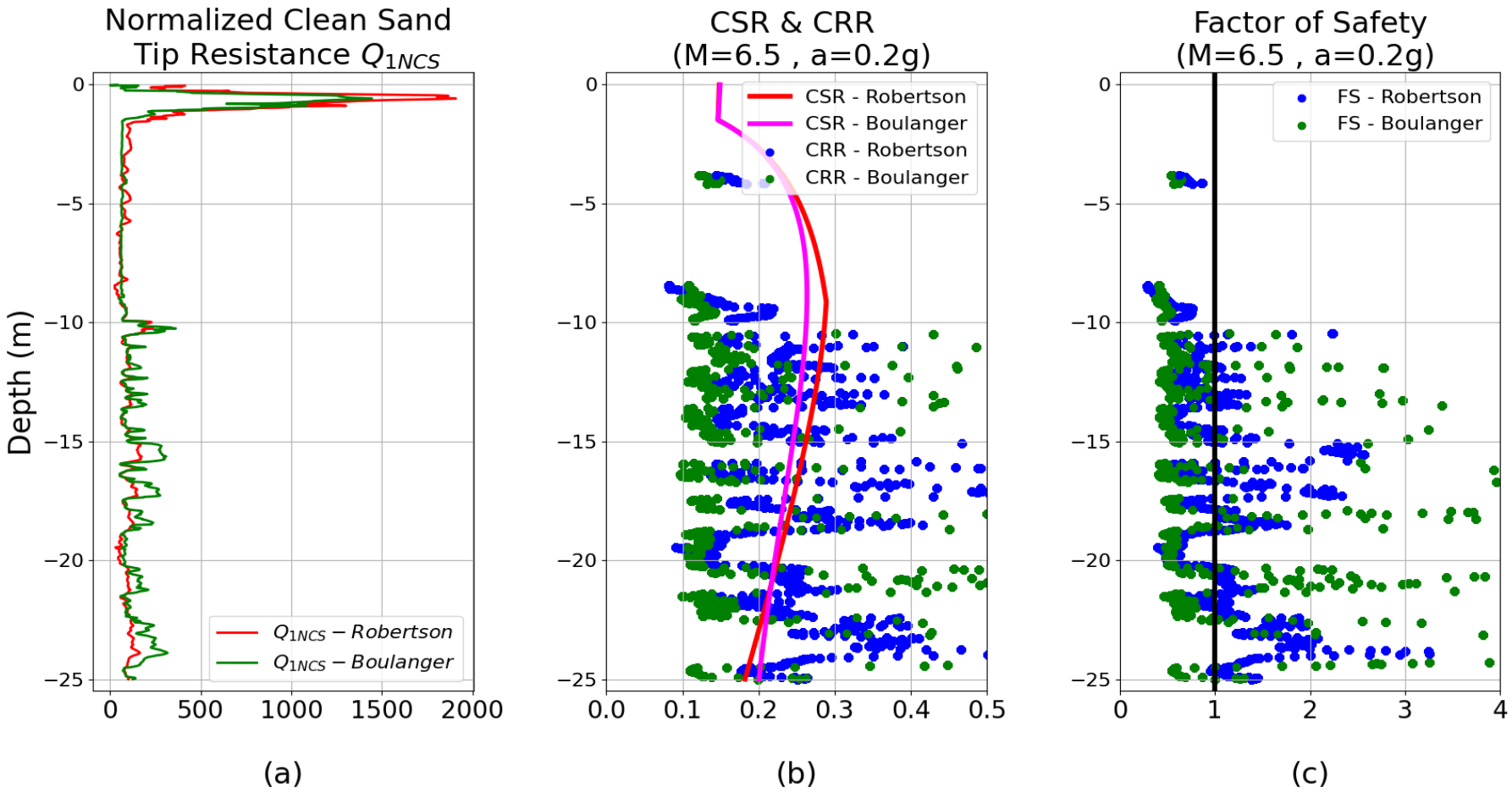

Figure 4.21 Liquefaction susceptibility using CPTu - Site#2

4.4 Conclusions

During this research work, it was not possible to perform **Cyclic CPT** tests after making all the modifications required for a proper application of the **Cyclic CPT** test in the field. Moreover, none of the **Cyclic CPT** tests done in situ were performed in liquefiable layers.

However, the two campaigns performed successfully demonstrated the suitability of a small Equaterre CPT rig for performing **Cyclic CPT** tests. The CPTu tests were analysed using a new in-house code (py-CPT). This python code implements several methods suggested by different researchers to extract information about the subsoil using the CPTu measurements. The py-CPT also makes it possible to compare results from these methods.

The preliminary results demonstrate that different soil types (predicted using results of py-CPT) will show different response to the **Cyclic CPT** tests. Therefore this new **Cyclic CPT** test could be successfully used to predict the properties of subsoil. For example, during the Chambéry test campaign, out of three **Cyclic CPT** tests performed in soils with soil behaviour index (I_C) less than 2.7 (sand-like soil) and with $\alpha_{F,max}$ values equal to 0.8, none of the tests led to complete tip opening during the cyclic loading (Test IDs C_16, C_17 & C_47).

On the other hand, out of fourteen tests in soils with I_C values greater than 2.7 i.e. in clay type soils, only four of the test did not witness a complete tip opening. (Test IDs C_8, C_11, C_15, C_19, C_23, C_27, C_29, C_30, C_33, C_36, C_37, C_44, C_45 and C_49). Also, all of the four tests that did not result in complete tip opening were performed at depths very close to the dense sand layers. In other words, they may actually be performed in sand type soil since the exact depths of soil layers at the site of the **Cyclic CPT** test may slightly differ from those at the CPTu site.

Similar to the results done inside the calibration chamber for dry soil, tests done below the water table in clay type soil demonstrated that a lower frequency cyclic loading requires less number of cycles for a given tip displacement opening. (Figure 4.18 and Figure 3.22). Also a cyclic loading with maximum amplitude closer to the tip resistance led to faster opening of the tip (Figure 4.17). All these results demonstrate the suitability of this test to differentiate between different soil type and also its possibility to predict liquefaction susceptibility.

Chapter 5

5. Discussion and Conclusion

During this research work, the test methodology of **Cyclic CPT** test was refined and two loading devices were calibrated to apply this methodology to identify soil properties. The equipment used in the field and the associated control system were rectified for better control of the test. New equipment was designed and built for the laboratory experiments to perform the **Cyclic CPT** tests in well-defined conditions of stress and density of the sample. This included the design of a new calibration chamber and the loading mechanism to apply the **Cyclic CPT** test and the design of a pluviator to create the required density of samples. Experiments were performed to better understand the effect of vertical stress, saturation conditions and density of the tested samples on the results of **Cyclic CPT** tests.

The displacement and the force on the front sleeve of the Gouda tip are the only two information being recorded during the actual **Cyclic CPT** test and make it necessary to study stiffness changes to extract information about the soil conditions and eventually liquefaction susceptibility. Three definitions of stiffness parameters were used to study the effect of cyclic loading during the calibration chamber testing. Among the different stiffness parameters discussed in chapter 3, the secant stiffness parameters(K_S) was most responsive to the cyclic loading. It was demonstrated that this stiffness parameter depend on ratio of tip resistance that is used for the maximum and minimum amplitude of the cycles **($\alpha_{F,max}$-$\alpha_{F,min}$).** It was also witnessed that the displacement of the tip even for dry samples, depended on the frequency of applied cyclic loading. Therefore any interpretations using the **Cyclic CPT** tests, will vary with the input test parameters (e.g. $\alpha_{F,max}$, $\alpha_{F,min}$, frequency etc) used during testing.

This chapter recommends the various inputs for the future **Cyclic CPT** tests. It also highlights the suitability of our test for liquefaction prediction while recommending derived results that can be used for predicting liquefaction susceptibility.

5.1 Suggested input parameters for testing:

5.1.1 Distance of push (Steps A & E)

One cm push has been proven sufficient to achieve a plateau of tip stress in most of the tests performed with GA39 sand in the calibration chamber (Figure 5.1) and also during the field tests (Figure 5.2). The maximum force during the push time is saved as the tip resistance (TR#1 and TR#2). For field experiments, there is a scope of increasing the maximum tip opening and as such a greater push distance will also be investigated in future research.

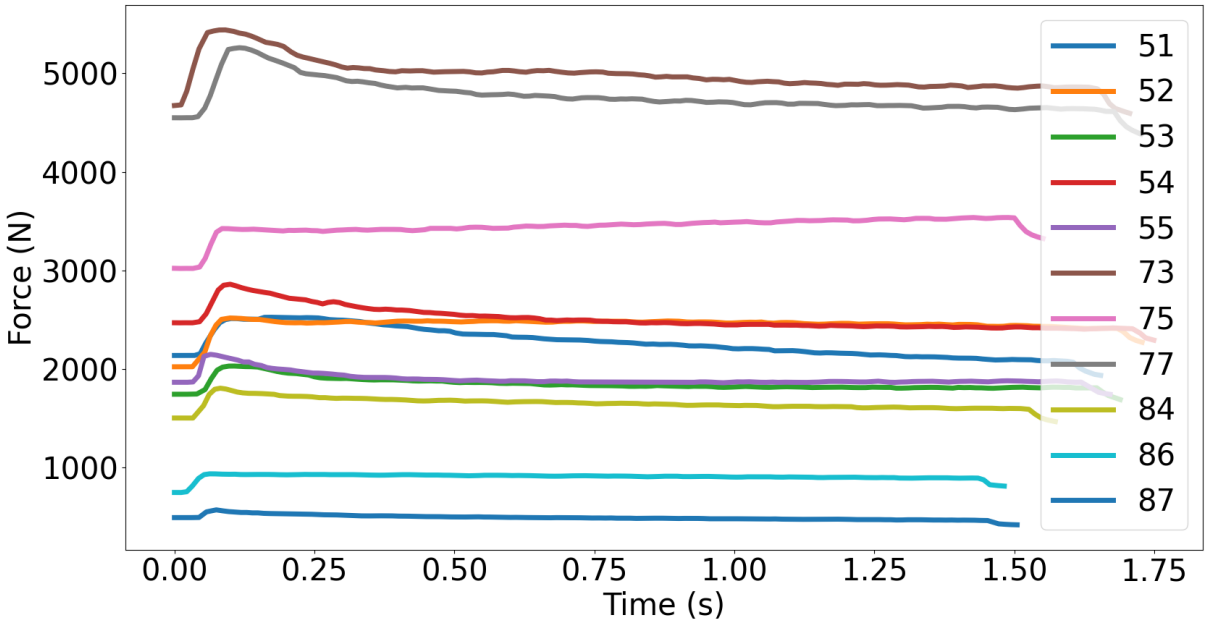

Figure 5.1 Tip Resistance measured during Step A inside the calibration chamber

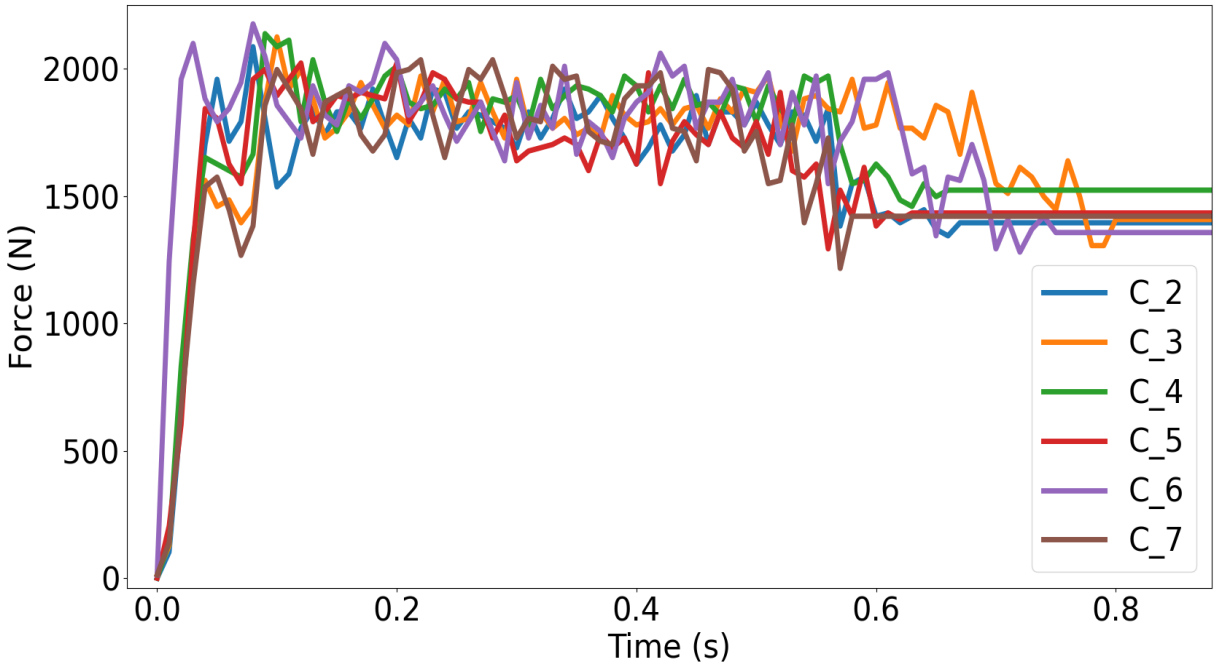

Figure 5.2 Tip Resistance measured during Step A during field tests

5.1.2 Ratio of tip resistance to be applied as constant force and waiting time during waiting steps (Step B,D,F & H)

The effect of $\alpha_{F,const}$ values on test results is as seen in Figure 3.18. It is suggested to use a $\alpha_{F,const}$ value equal to or higher than 0.75 for future experiments. This will result in minor deformation even in dense sand like soil and will lead to higher displacement in clay type soils.

During majority of tests, 20 second waiting time was used. A waiting time after the push(Step B & F) is aimed to allow dissipation of pore water pressure caused by the penetration of the tip, while the waiting period after the cyclic loading helps to differentiate the tip displacement caused by the cycling loading and the monotonous push. It also allows to check, if it becomes relatively easier or difficult to penetrate the sand after cyclic loading under application of load, lower than the tip resistance. A twenty second period is considered sufficient to achieve these goals at the recommended $\alpha_{F,const}$ value of 0.8.

5.1.3 Ratio of tip resistance to be applied as maximum and minimum amplitude of cyclic loading, frequency and mumber of Cycles of cyclic loading (Step C & G)

The $\alpha_{F,max}$ and $\alpha_{F,min}$ values significantly impact the results of a **Cyclic CPT** test. As expected, higher values of $\alpha_{F,max}$ causes greater tip displacement. Apart from the tip displacement, the stiffness parameters calculated are also influenced by the choice of these parameters. Table 5.1 lists three sets of two **Cyclic CPT** tests. The two tests in each set are performed under almost identical conditions with similar values of the tip resistance (TR#1) measured during the step A of the test. The resulting secant stiffnesses are presented in Figure 5.3. For each set, an higher value of $\alpha_{F,max}$ leads to a lower secant stiffness,

S.No.	Vertical Stress (kPa)	Saturation Condition	Cyclic CPT		
			Test ID	TR#1 (N)	$\alpha_{F,max}$-$\alpha_{F,min}$
1	75	Saturated	51	2526	0.78 - 0.42
			52	2518	0.65 - 0.35
2	85	Dry	101	1267	0.65 - 0.35
			103	1003	0.85 - 0.35
3	85	Dry	111	6931	0.65 - 0.35
			112	6733	0.85 - 0.35

Table 5.1 Cyclic CPT tests used to study the effect of $\alpha_{F,max}$ and $\alpha_{F,min}$ on stiffness parameters

whatever the initial relative density (ranging from 19% to 53% depending on the set of tests) and the saturation condition.

The $\alpha_{F,max}$ for **Cyclic CPT** tests should be high enough to measure significant tip displacement even for higher relative density samples tested under relatively higher stresses. It should also be lower than the tip resistance to ensure the stability of tests.

Nevertheless, it was observed that the test became unstable with very high $\alpha_{F,max}$ values of 0.85, and it was not possible to reach the target tip stress. This response was much rare for tests performed with a $\alpha_{F,max}$ value equal or lower than 0.8. In all the tests performed with $\alpha_{F,max}$ values 0.78 or 0.80 there was progressively increasing measured displacement during cyclic loading even for the tests done under the higher value of vertical stress and on higher relative densities sample. Also, in certain tests, there was a significant change in the secant stiffness parameter (K_S) which could be expected for soils prone to liquefaction. Therefore, a value of 0.8 for $\alpha_{F,max}$ parameter is recommended for field experiments.

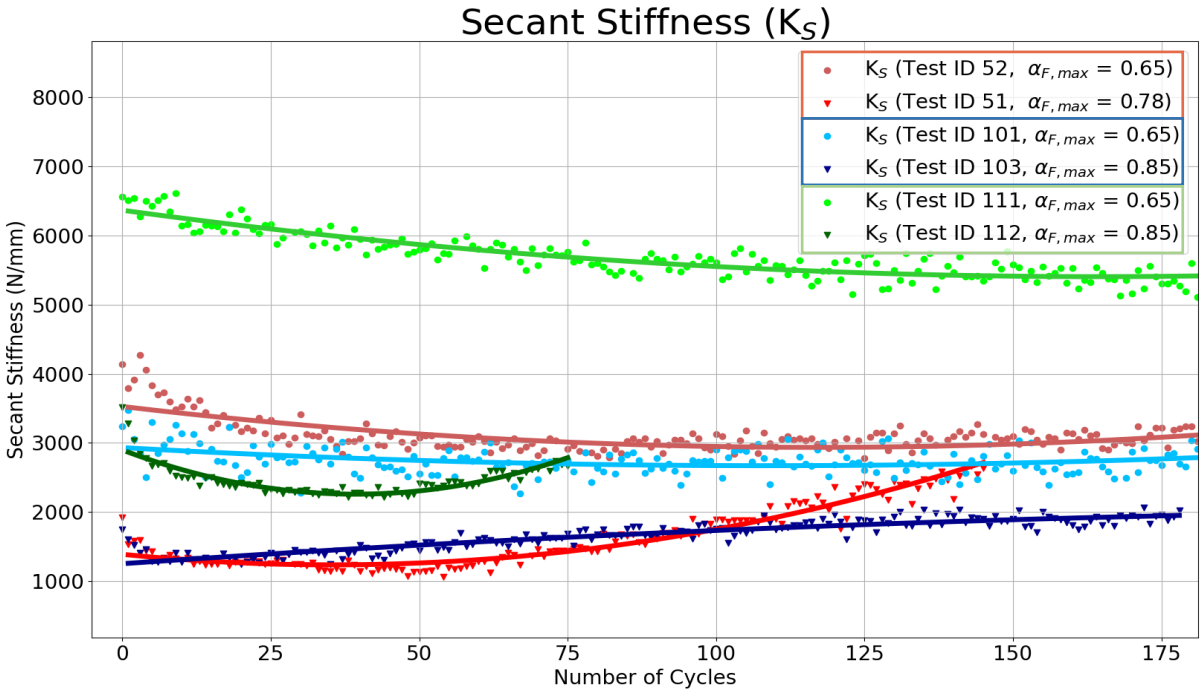

Figure 5.3 The effect of $\alpha_{F,max}$-$\alpha_{F,min}$ on stiffness parameters

The effect of lower amplitude($\alpha_{F,min}$) was not studied during this research and will be studied in future works. However, a lower bound of 0.4 seemed satisfactory and resulted in good control of the cycles. On the other hand, a lower value sometimes resulted in faster movement of the tip and lead to control problems.

As discussed in Section 3.5, the effect of frequency on liquefaction resistance and on the results of **Cyclic CPT** tests needs further research. However, a **frequency of 1 Hz** showed

acceptable control during cyclic stress loading even in cases of high strain during cycles. This frequency is also ideal as there are a large number of cyclic triaxial and direct simple shear tests performed at this frequency, whose results can be used for correlations while interpretation of the **Cyclic CPT** test. This frequency of 1 Hz also leads to a much shorter test time per test as compared to lower frequency like 0.1 Hz which is of prime importance during in-situ investigation.

The number of cycles required to observe significant displacement during the **Cyclic CPT** test depends on the $\alpha_{F,max}$ parameter. For the recommended value of 0.8 there were tests performed which witnessed a complete opening of the miniature Gouda tip (6 cm) before the application of the 180 cycles. Also, the same number of cycles were sufficient to observe some displacement (10 mm) even in dense and dry specimens during cyclic loading after two sets of 180 cycles (Step C and Step G). Thus, the choice of 180 cycles during each cyclic loading step is recommended to be continued for the future tests.

5.2 Suitability for predicting liquefaction susceptibility

Traditionally to develop the interpretation methodology of the results of any new in-situ test the result from such a test are compared with well-established laboratory experiments. It was using the same methodology that was used to define correlations between CPTu results and soil mechanical properties.

Even in case of tests to identify liquefaction susceptibility, often comparisons are made with the results from laboratory cyclic triaxial tests. Dupla and Canou 2003 have suggested one such CRR formula for cyclic pressuremeter loading. In this paper, an analogy between the results of homogeneous cyclic triaxial test and the non-homogeneous cyclic cylinder expansion test motivated them to find quantitative correlations between the CRR formulas from the two tests. The analogies between the test results were based on three basic results:

- Samples with different densities tested under similar conditions gave different results. During both type of tests, the samples with higher density showed a decreased accumulated strain.
- Samples with the same density tested under different stress conditions gave different results. During both tests, the samples tested under higher confining stress conditions resulted in increased resistance to deformation.
- The different magnitudes of cyclic loading gave different results for both these tests. For both types of tests, a higher magnitude of cyclic loading resulted in higher values of cumulative strains as compared to the same test done on a similar sample under the similar condition of stresses but with a lower magnitude.

Since all these responses were also observed during the **Cyclic CPT** test, it is a positive indication for using this test for finding quantitative values of liquefaction susceptibility. However, it is difficult to give meaningful correlations between the liquefaction susceptibility of the soil and the results of the **Cyclic CPT** test based on the current dataset. We need to perform more tests, especially on loose liquefiable sand.

However, a liquefaction criterion using the **Cyclic CPT** test could be based on the elements detailed in the following sub-sections.

5.2.1 Number of cycles required for a given displacement of the tip

Liquefiable soils loose their shear strength and behaves as a liquid during the applications of shear loading from an earthquake. Based on this behaviour, it can be expected that liquefiable sand layers will result in faster tip opening during the applications of cyclic loading as compared to non-liquefiable sand layers tested under similar conditions of vertical stress and density. Therefore, **higher the number of cycles required for a given displacement of the tip, higher would be the liquefaction resistance.**

5.2.2 Range of stiffness values for a particular $\alpha_{F,max}$

The stiffness parameters identified during this research work can be useful to differentiate between different soil types. It is demonstrated from calibration chamber testing that the stiffness parameters can also be used to distinguish different conditions of density and saturation in sands. For example, Figure 5.4 represents the secant stiffness changes of 5 different **Cyclic CPT** tests done using the similar input parameters ($\alpha_{F,max}$-$\alpha_{F,min}$ = 0.65-0.35) on five different calibration chamber samples.

- For dry samples tested at similar vertical stress (Test ID 101 & 111) the samples with higher density showed higher stiffness values.
- Although Test ID 85 was performed on a denser sample than Test ID 101, it had a slightly lower value as the applied vertical stress for the looser sample was higher.
- Also, even a saturated medium dense sample tested at a high vertical stress of 150 kPa (Test ID 75), showed significantly lower stiffness values than the medium dense dry sample tested at much lower vertical stress (Test ID 111).
- For two saturated samples (Test ID 52 & 75), stiffness values of the tests are significantly higher for the test done under higher applied vertical stress.

In other words, there is a combined effect of the density and the vertical stress. There is probably the need to normalized the measurements of the stiffness with respect to the vertical stress in order to produce a corrected stiffness that would be representative of the density of the soil whatever the depth of realisation of the **Cyclic CPT** test.

More tests have to be performed in varying density of samples and under different vertical stresses to better understand the changes of these observed stiffness values. And then, different cut-offs can be suggested to differentiate samples that are prone to liquefaction from the ones that are not. But for sands it can be expected that **lower the stiffness values, more prone is that sand to deformation by cyclic shear loading.**

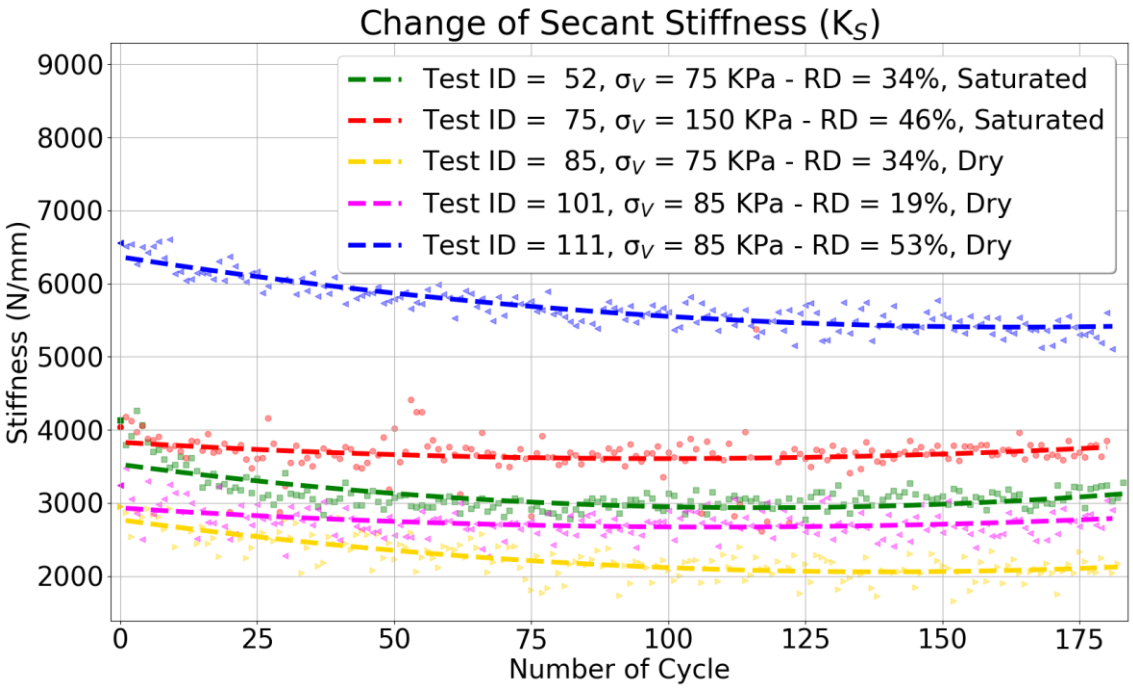

Figure 5.4 Range of stiffness values for tests done with $\alpha_{F,max} = 0.65$

5.2.3 Stiffness parameter changes during cyclic loading

For identifying liquefiable soils, in addition to the absolute value of stiffness parameters, it will be useful to study their changes during the cyclic loading. A liquefaction prone soil can be expected to demonstrate decreasing stiffness values during the **Cyclic CPT** test. Also, as discussed in Section 3.3, the secant stiffness parameter can also be expected to change more for saturated soil samples as compared to the dry ones.

Chapter 6

6. Perspectives

This research work was successful in defining a test methodology and conceptualizing the equipment required to apply that loading inside the calibration chamber. We were also able to suggest changes to ensure a better control of the test during the field campaigns. Key effects of density, saturation and vertical stress are studied during the calibration chamber tests. However, due to significant challenges associated with developing a new test and equipment, accompanied by a fire in the laboratory and a pandemic, a lot more research work remains to be done in this project. The main areas that requires further research are discussed below:

6.1 Study of Drainage Conditions:

The uncertainty of drained nature and stress conditions existing around the tip, make the interpretation of this test a difficult task. The speed of the tip penetration and the permeability of the soil are two main controlling parameters for the drainage condition of the soil. Generally for a sand like Fontainebleau GA39 with hydraulic conductivity (k) in

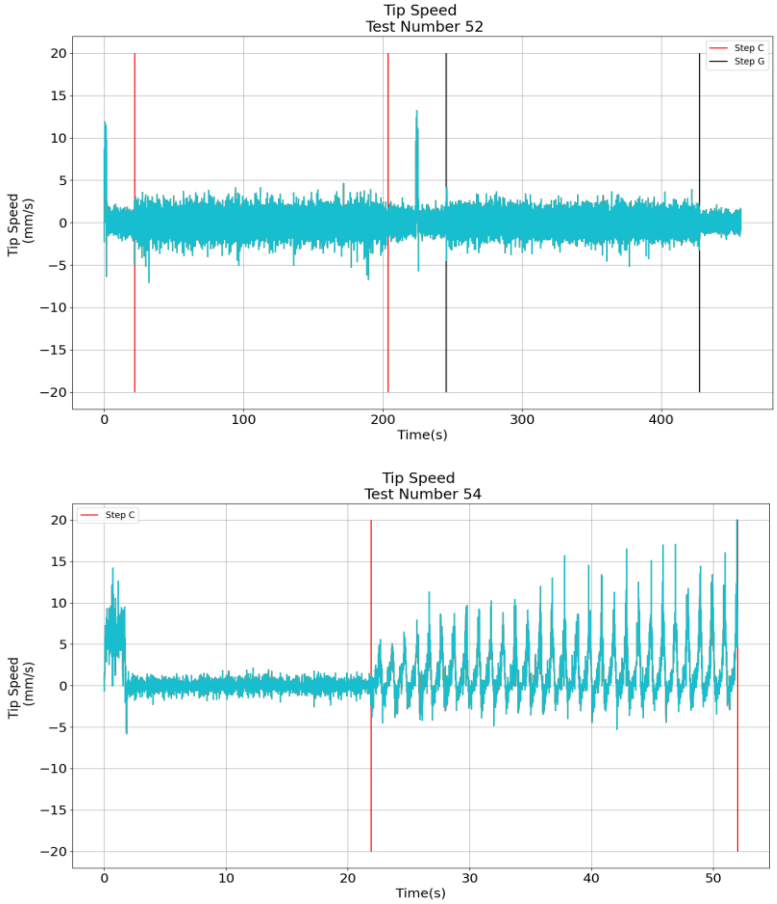

Figure 6.1 Tip speed during the cyclic CPT test

the order of 10^{-5} m/s the conventional CPTu test is considered drained. Since the speed of the tip varies during the application of cyclic loading the drainage conditions can vary during the **Cyclic CPT** test. The tip speed can depend on the soil tested, the $\alpha_{F,max}$ and $\alpha_{F,min}$ values, and the tip resistance measured during **Step A**.

The speed of penetration during two of the tests done on the same calibration chamber sample with different values of $\alpha_{F,max}$ and $\alpha_{F,min}$ is as shown in Figure 6.1. Test ID 52 was performed at $\alpha_{F,max}$ and $\alpha_{F,min}$ value of 0.65 and 0.35 while Test ID 54 was performed at 0.85 and 0.35. Therefore, a larger displacement was measured at much smaller number of cycles during Test ID 54. This is why higher tip velocities are observed for test 54 than for test 52 during the step C.
It can be clearly seen that, the tip speed varies during the application of stress cycle. The value mostly lies between +5 to -5 mm/s for test ID 52 while it lies from -5 to +20 mm/s for test ID 54. Since the speed always lies below 20 mm/s, the test could be considered drained based on previous research on conventional cone penetration testing. However, the direction of velocity continuously changes and such non monotonous loadings may change the state of drainage of the surrounding soil. This point will require further investigation including the use of pore pressure sensors around the tip inside the calibration chamber. The study of the soil drainage in the vicinity of the tip can also be studied using numerical modelling. This was attempted in the research work Sadrabadi 2019 where he used DEM (Discrete Element Method) to describe the solid phase of soil and PFV (Pore Finite Volume) for the fluid medium. However, the question specific to the soil drainage condition could be advantageously and more easily investigated via a conventional continuous model involving hydromechanical coupling as long as soil failure below the penetrometer tip is discarded.

6.2 Compression of the internal rods during cyclic loading:

The displacement measured using the LVDT sensor during the cyclic loading includes the compression of the internal rods. The internal rods are built using toughened steel with high value of Young's modulus. However, a small axial deformation can still be expected while applying the compressive load. Assuming perfectly horizontal contacts between different internal rods (Ø = 9 mm) and a Young's modulus of 210 GPa, the length of one meter of internal rod is shortened 0.37 mm when the load changes by an amount of 5000 N. This small compression is not accounted into the stiffness calculation during the current research work and can be incorporated in the results using the force values applied on the given section of the internal rod. Knowing the value of Young's modulus of elasticity of the material, the component from shortening or elongation of internal rods can be separated. It can also be interesting to add a displacement sensor inside the tip to measure the opening of the front sleeve of Gouda tip during the **Cyclic CPT** test and avoid the effects caused by changing length of internal rods.

6.3 Double Measurement Testing

Equaterre is also interested to use the current tip to perform another test, called **Double Measurement**. This test involves stopping the cone penetration at a given depth and measure the changes of the tip resistance with time. The difference of drainage conditions around the tip are expected to cause different tip stress changes for different types of soil. It is aimed to use these differences to define the soil type.

90 Double Measurement Experiments were performed using the equipment shown in Figure and the results can be summarized using Figure 6.2. The red lines represent the tests done in depths with clay type soils while the blue represents the sand type soils. It was seen that there was significantly larger and mostly faster drop of tip stress in sands as compared to clay type soils. However, further investigation found that the drop of the tip stress was also caused by the relaxation of the loading device and also the tip stress measuring cell. A much more advanced equipment was required to perform this test to ensure that the decrease of tip stress depends only on the soil type tested. Based on the learnings from this experimental campaign, Equaterre made the required changes and

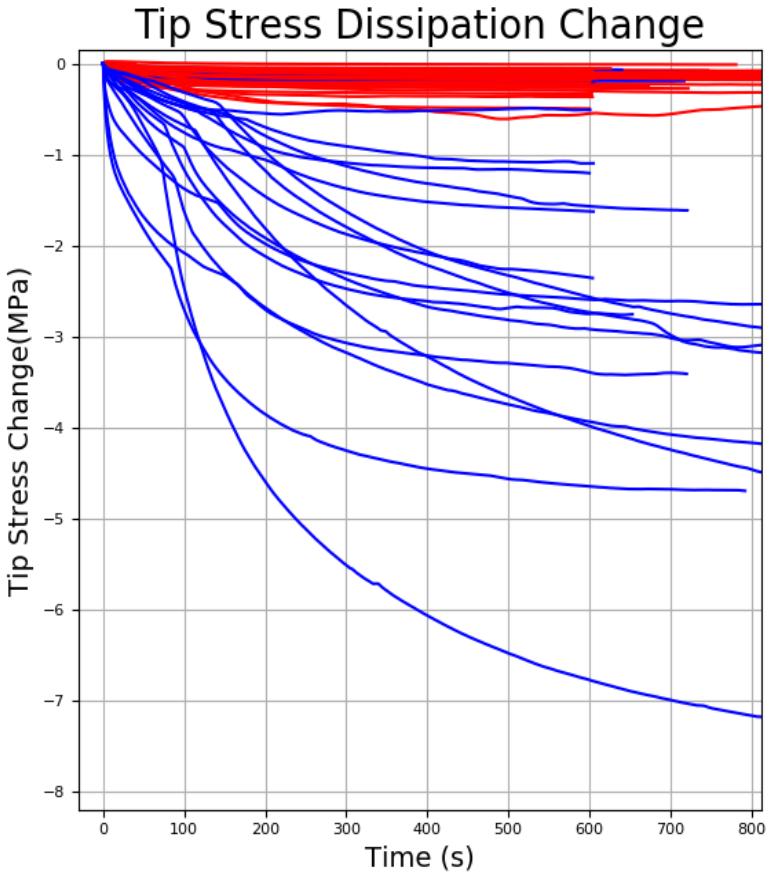

Figure 6.2 Double Measurement Tests

built a new equipment to perform the tests on field (Figure 6.3). The hydraulic force sensors and the hydraulic jacks were replaced by electric versions.

The Unfortunately, no test could be performed after making all the required changes to the field equipment. Testing using this equipment will be undertaken during the next research work.

Figure 6.3 Equaterre's new CPT rig

6.4 Laboratory Experiments

Due to a number of problems, the pluviator could not be used during this research work. It is envisaged to make the pluviator functional and use it for creating more uniform samples. It is also envisaged to use imbedded pore pressure sensors around the tip to differentiate the total and effective stress changes during the application of the cyclic loading.

Besides, due to the limited expansion of the pressure membrane applying the vertical stress, it was not possible to test very loose samples presenting a settlement of more than five centimetre during the application of the vertical loading. A new mechanism to apply

the vertical loading capable of expanding and ensuring application of constant vertical stress even during the large consolidation of the sample is required to test liquefaction prone loose sand specimens inside the calibration chamber. The current pressure membrane could only expand by two centimetres which was not sufficient to apply the vertical stress on loose soils. Also, a smaller and water tight central hole on the membrane applying the vertical stress is required to ensure a shorter distance for the stabilizing of tip stress.

An experimental campaign of cyclic triaxial testing performed using Fontainebleau GA39 sand will help to have CRR curves for different densities of this sand based. The CRR value of this sand can also be found using CPTu testing inside the calibration chamber. These tests will help in the development of CRR formulas using the results of **Cyclic CPT** test and also act as validation for the same.

7. References

Ahmadi M.M., and Robertson P.K.. 2004. "Calibration Chamber Size and Boundary Effects for CPT Qc Measurements." In ISC-2 on Geotechnical and Geophysical Site Characterization: 541-553

Ali, Elfatih M., Mohammed A. Osman, and Mohammed B. Abuelhassan. 2012. "Field Measurement of Shear Modulus of Hard Clays Field Measurement of Shear Modulus of Hard Clays." *Jounrnal of BRR*: 37–44.

Ameratunga, Jay, Nagaratnam Sivakugan, and Braja M. Das. 2016. "Vane Shear Test." In *Correlations of Soil and Rock Poperties in Geotechnical Engineering*, , 193–205.

Andrus, R.D. 1994. "In Situ Characterization of Gravelly Soils That Liquefied in the 1983 Borah Peak Earthquake." Ph.D. Dissertation, University of Texas at Austin.

Ang, K.H., Gregory Chong, and Li Yun. 2005. "PID Control System Analysis , Design and Technology." *IEEE transactions on control systems technology (13)*: 559–76.

Baligh, M.M., V. Vivatrat, and C.C. Ladd. 1980. "Cone Penetration in Soil Profiling." *ASCE Journal of Geotechnical Engineering*: 447–453.

Been, K., and J.H.A. Crooks. 1988. "A Critical Appraisal of CPT Calibration Chamber Tests." In *1st Intenational Conference on Cone Penetration Testing*, 651-660.

Begemann, H.K.S. 1965. "The Friction Jacket Cone as an Aid in Determining the Soil Profile." In *6th International Conference of Soil Mechanics and Foundations*, 17-20.

Benoit, J., and J.A. Howie. 2014. "A View of Pressuremeter Testing in North America." *Soils and Rocks* (3): 211–231.

Berthoz, Nicolas. 2013. "Modélisation Physique et Théorique Du Creusement Pressurisé Des Tunnels En Terrains Meubles Homogènes et Stratifiés Modélisation Physique et Théorique Du Creusement Pressurisé Des Tunnels En Terrains Meubles Homogènes et Stratifiés." Ph.D. Dissertation, INSA de Lyon.

Boulanger, Ross W. 2003. "High Overburden Stress Effects in Liquefaction Analyses." *Journal of Geotechnical and Geoenvironmental Engineering* 129(12): 1071–1082.

Boulanger, Ross W., and I. M. Idriss. 2007a. "Evaluation of Cyclic Softening in Silts and Clays." *Journal of Geotechnical and Geoenvironmental Engineering* 133(6): 641–652.

Boulanger, Ross W., and I. M. Idriss. 2015. "CPT-Based Liquefaction Triggering Procedure." *Journal of Geotechnical and Geoenvironmental Engineering* 142(2): 1–11.

Briaud, Jean-Louis, and Jordan Gerald. 1983. Report for Texas Transporation Institute *Design of Shallow Foundations*.

"BS 5930:2015." 2015. Code of Practise for ground investigation, BSI Standards Publication.

Campanella R, and Lim B. 1981. "Liquefaction Characteristics of Undisturbed Soils." In *International Conferences on Recent Advances in Geotechnical Earthquake Engineering and Soil Dynamics*, , 227–30.

Casagrande A. 1976. *Liquefaction and Cyclic Deformation of Sands: A Critical Review*.

Celeste F. 2018. "Engineering and Risks Probing Liquefiable Soils by Cyclic Cone Penetration." Master Dissertation, University of Grenoble Alpes.

Christian J.T., and W.F. Swiger. 1975. "Statistics of Liquefaction and SPT Results." *Journal of Geotechnical Engineering Devision, ASCE* 101: 1135–1150.

Crapps D.K. 2006. "Brief History of the Flat Plate Dilatometer in North America." In *Second International Flat Dilatometer Conference*, 4–6.

Cudmani R. 2014. "Soil Liquefaction: Mechanism and assessment of liquefaction susceptibility." In Conference of *Seismic Design of Industrial Facilities.*

Dupla J, and Canou J. 2003. "Cyclic Pressuremeter Loading and Liquefaction Properties of Sands." *Soils and Foundations, Japanese Society of Soil Mechanics and Foundation Engineering* 43(2): 17–31.

Finn W.D.L. 1981. "Liquefaction Potential: Developments since 1976." In *International Conferences on Recent Advances in Geotechnical Earthquake Engineering and Soil Dynamics*, , 655–81.

Ghionna V.N., and Jamiolkowski M. 1991. "A Critical Appraisal of Calibration Chamber Testing of Sands." In *First International Symposium on Calibration Chamber Testing*, New york, USA, 13–39.

Hazen A. 1920. "Hydraulic Fill Dams." In *Transactions of the Americal Society of Civil Engineers*: 1717–1745.

HousnerG.W. 1958. "The Mechanism of Sandblows." *Bulletin of Seismological Society of America* 48(April): 155–161.

Ishihara K. 1993. "Liquefaction and Flow Failure during Earthquakes." *Geotechnique* (43): No. 3, 351-415.

Ishihara K, and Koga Y. 1981. "Case Studies of Liquefaction in the 1964 Niigata Earthquake." *Soil and Foundation* 21(3): 33–52.

Iwasaki T., Tatsuoka F., Tokida K., and Yasuda S. 1978. "A Practical Method of Assessing Soil Liquefaction Potential Based on Case Studies at Various Sites in Japan." In *2nd International Conference on Microzonation,National Science Foundation,*.

Iwasaki T., Tatsuoko F., Tokida K., and Yasuda S. 1978. "A Practical Method for Assessing Soil Liquefaction Potential Based on Case Studies at Various Site in Japan." In *5th Japan Earthquake Engineering Symposium*, , 641–48.

Jones G.A., Van Zyl D., and Rust E. 1981. "Mine Tailing Characterization by Piezometer Cone." In

Symposium on Cone Penetration Tersting and Experience.

Kamura A., and Kazama M. 2020. "Assessment of Stiffness Degradation of Soil by In-Situ Cyclic Loading Using Pressuremeter." In *6th International Conference on Geotechnical and Geophysical Site Characterization*.

Karagiannopoulos, P.G. 2020. "Apport de La Mesure de La Pression Interstitielle à l'essai Pressiométrique. Chargements Cycliques et Monotones Soutenue." PhD Dissertation Université Gustave Eiffel.

Kramer S. 1996. *Geotechnical Earthquake Engineering*. Prentice-Hall internation series.

Kuerbis R., and Vaid Y.P. 1988. "Sand Sample Preparation -The Slurry Deposition Method." *Japanese Society of Soil Mechanics and Foundation Engineering* 28(No.4): 107–18.

Kuribayanshi E. and Tatsuoka F. 1975. "Brief Review of Liquefaction during Earthquakes in Japan." *Soils and Foundation* 15(4): 81–92.

Kwan W.S. and Mohtar C. 2020. "A Review on Sand Sample Reconstitution Methods and Procedures for Undrained Simple Shear Test." *International Journal of Geotechnical Engineering* 14 (No.8)

Lambe T.W. 1951. *Soil Testing for Engineer*. John Wiley & Sons, Inc., New York

Lancellotta R. 2009. *Geotechnical Engineering*. Second Edition. Taylor & Francis

Mahmood A, and J Mitchell. 1976. "Effect of Specimen Preparation Method on Grain Arrangement and Compressibility in Sand." *ASTM STP* 599.pp.169-192.

McNeilan T.W., and Bugno W.T. 1984. "Cone Penetration Test Results in Offshore California Silts" In *Proceedings of the Symposium on Strength Testing of Marine Sediments: Laboratory and In-Situ Measurements, San Diego*, 55–71.

Ménard L. 1957. "An Appratus for Measuring the Strength of Soils in Place." PhD Dissertation, University of Illinois.

Miura S., Toki S. and Tanizawa F. 1984. "Cone Penetration Characteristics and Its Correlation to Static and Cyclic Deformation-Strenght Behaviour of Anisotropic Sand." *Soils and Foundations, Japanese Society of Soil Mechanics and Foundation Engineering* 24(No. 2): 58–74.

Mola-abasi H., Kordtabar B. and Kordnaeij A. 2017. "Liquefaction Prediction Using CPT Data by Triangular Chart Identification" *International Journal of Geotechnical Engineering* : 12(4),377-382

Moon V., Tobias M., Jorat E. and Kreiter S. 2013. "Vibrocone CPTu Testing as a Tool for Enhanced Definition of Liquefaction-Prone Soil Layers." *NZ Geomechanics News* (86): 105–107.

Muir S.G. and Scott R.F. 1979. "Earthquake Generated Sand Blows Formed during the 15 October 1979 Imperoal Valley Main Shock." *U.S. Geological Survey professional paper 1254*.

Nong Z., Park S.S, Jeong S.W., and Lee D. 2020. "Effect of Cyclic Loading Frequency on Liquefaction

Prediction of Sand." *Applied Sciences.* 10(13):4502: 1–15.

Oda M., Nemat-Nasser S. and Konishi J. 1985. "Stress-Induced Anisotropy In Granular Masses." *Japanese Society of Soil Mechanics and Foundation Engineering* Vol. 25(September): No. 3, 85-97.

Olsen R.S., and Joseph P.K.. 1995. "Prediction of Liquefaction Resistance Using the CPT." In Internation conference of *Cone Penetration Testing*. 251–56.

Parkin A.K. and Lunne T. 1982. "Boundary Effects in the Laboratoy Calibration of a Cone Penetrometer for Sand." *2nd (European Symposium on Penetration Testing (ESOPT II), Amsterdam.* 138.

Peuchen J., and Mayne P. 2007. "Rate Effects in Vane Shear Testing." In *Offshore Site Investigation and Geotechnics: Confronting New Challenges and Sharing Knowledge*,.

Potter S.H., Becker J. S., Johnston D. M., and Rossiter K. P. 2015. "An Overview of the Impacts of the 2010-2011 Canterbury Earthquakes." *International Journal of Disaster Risk Reduction* 14(1): 6–14.

Pournaghiazar M., Russell A.R., and Khalili N. 2012. "Linking Cone Penetration Resistances Measured in Calibration Chambers and the Field" . Géotechnique letteres 2, 29–35.

Puri V.K. 1984. "Liquefaction Behavior and Dynamic Properties of Loessial (Silty) Soils." Ph.D. Dissertattion, University of Missouri.

Reiffsteck P., Thorel L., Bacconnet C., Gourvés R. and Graaf H. 2009. "Measurements of Soil Deformation by Means of Cone Penetrometer." *Soils and Foundation* 49(3): 397–408.

Reigel P. 2017. "Pénétromètre Statique Pour l'évaluation Du Caractère Liquéfiable d'un Sol et Procédés Associés."

Rimoy S.P. 2013. "Ageing and axial cyclic loading wtudies of displacement piles in sands." *PhD Dissertation, Imperial College London*.

Robertson P. K., Campanella R. G., Gillespie D., and Rice A. 2008. "Seismic Cpt to Measure in Situ Shear Wave Velocity." *Journal of Geotechnical Engineering* 112(8): 791–803.

Robertson P.K., Campanell R.G., Gillespie D., and Greig J. 1986. "Use of Piezometer Cone Data." *Use of in-situ testing in Geotehcnical Engineering, GSP 6, ASCE* SM 92: 1263–80.

Robertson P K. 2004. "Evaluating Soil Liquefaction and Post-Earthquake Deformations Using the CPT." *Proceedings of ISC2 on Geotechnical and Geophysical Site Characterization*: 233–49.

Robertson P K. 2016. "Cone Penetration Test (CPT) -Based Soil Behaviour Type (SBT) Classification System — an Update." *Canadian Geotechnical Journal* (53(12)): 1910–27.

Robertson P K, and Wride C.E.. 1998. "Evaluating Cyclic Liquefaction Potential Using the Cone Penetration Test." Canadian Geotechnical Journal. 35(3):442-459

Sadrabadi H.H. 2016. "Identificiation In-Situ Des Sols Liquéfiables Par Pénétromètre Statique Cyclique : Modélisations Physiques et Numériques In-Situ Identification of Liquefiable Soils

by Cyclic Static Penetrometer : Physical and Numerical Modelling." University of Grenoble Alpes.

Salgado R., Mitechell J.K., and Jamiolkowski M. 1998. "Calibration Chamber Size Effects on Penetration Resistance in Sand." Journal of Geotechnical and Geoenvironmental Engineering, 124 (9), 878–888.

Sarker D., and Abedin Z. 2015. "Applicability of Standard Penetration Test in Bangladesh and Graphical Representation of SPT-N Value." *International Journal of Science and Engineering Investigations* 4(41): 55–59.

Sassa S. and Takagawa T. 2019. "Liquefied Gravity Flow-Induced Tsunami: First Evidence and Comparison from the 2018 Indonesia Sulawesi Earthquake and Tsunami Disasters." *Landslides* 16(1): 195–200.

Scott R.F. and Zuckerman K.A. 1964. *Sand Blows and Liquefaction*. In the Great Alaskan Earthquake of 1964 -Engineering Volume, Committee on the Alaska Earthquake, Division of Earth Sciences, National Research Council, National Academy of Sciences, Washington, 197 3, 179-189.

Searle I.W. 1979. "The Interpretations of Begemann Friction Jacket Cone Reaults to Give Soil Types and Design Paramters." *In 7th European Conference on Soil Mechanics and Foundation Engineering,Brighton*. 265–270.

Seed H.B. and Idriss I.M. 1971. "Simplified Procedure for Evaluating Soil Liquefaction Potential." *Journal of Soil Mechanics and Foundation Design*.:Vol 97(9), 1249–1273.

Seed H.B., Idriss I.M., Makdisi F. and Banerjee. 1975. *Representation of Irregular Stress Time Histories by Equivalent Uniform Stress Series in Liquefaction Analyses*. EERC 75-29, University of California, Berkeley.

Seed H.B., and Idriss I.M. 1968. "Seismic Response of Horizontal Soil Layers." *Journal of the Soil Mechanics and Foundations Division* 96(1): 1003–31.

Seed H.B. 1971. "Simplidied Procedure for Evaluating Soil Liquefaction Potential." *Journal of the Soil Mechanics and Foundations Division* 97(9).

Silva M. 2006. "Experimental Study of Ageing and Axial Cyclic Loading Effect on Shaft Friction along Driven Piles in Sands." *PhD Dissertation, University of Grenoble Alpes.*

Skempton A.W. 1986. "Standard Penetration Test Procedures and the Effect in Sands of Overburden Pressure, Relative Density, Particle Size, Aging and Over-Consolidation." *Geotechnique* 36: 425–47.

Soga, K. 1998. "Soil Liquefaction Effects Observed in the Kobe Earthquake of 1995." In *Procedeeings of the Instituion of Civil Engineers: Geotechnical Engineering* 131(1): 34–52.

Suits L, Sheahan T.C., Frost J, and Park J-Y. 2003. "A Critical Assessment of the Moist Tamping Technique." *Geotechnical Testing Journal: 26(1)*

Tabaroei A., Abrishami S., and Hosseininia E.S.. 2017. "Comparison between Two Different

Pluviation Setups of Sand Specimens." *Journal of Materials in Civil Engineering* (29).

Tatsuoka F. et al. 1986. "Some Factors Affecting Cyclic Undrained Triaxial Strength of Sand." *Soils and Foundations* 26(3): 99–116.

Tsuchida H. 1970. "Prediction and Countermeasure Against the Liquefaction in Sand Deposits." *Abstract of the Seminar in the Port and Harbor Research Institute*.

Vaid Y P, and Negussey D.. 1984. "Relative Density of Pluviated Sand Samples." *Japanese Society of Soil Mechanics and Foundation Engineering* 24(No. 2): 101–5.

Van Ballegooy S, Malan P, Lacrosse V, et al. Assessment of Liquefaction-Induced Land Damage for Residential Christchurch. Earthquake Spectra. 2014;30(1):31-55. Bardet, J.P., and M. Kapuskar. 1993. "Liquefaction Sand Boils in San Francisco During 1989 Loma Prieta Earthquake." Jornal of Geotechnical Engineering 119(3): 543–62.

Wang, W.S. 1979. "Some Findings in Soil Liquefaction". Water Conservancy and Hydroelectric Power Scientific Research Instiute, Beijing, China.

Whitman R.V. 1971. "Resistance of Soil to Liquefaction and Settlement." *Japanese Society of Soil Mechanics and Foundation Engineering* 11(4): 59–68.

Widyaningrum R. 2012. "*Geological Investigation of Liquefaction Potential in Palu Area, Central Sulawesi Province*". Center fro groundawater resources and environmental geology.

Yoshimi Y., and Oh-Oka H. 1975. "Influence of Degree of Shear Stress Reversal on the Liquefaction Potential of Saturated Sand." *Soils and Foundations* 15(3): 27–40.

Youd T. L. 1999. "Physics and Mechanics of Liquefaction from Field Records and Experience." In *Physics and Mechanics of Soil Liquefaction*, , 325–34.

Zhang G., Robertson P.K., and Brachman R.W.I.. 2002. "Estimating Liquefaction-Induced Ground Settlements from CPT for Level Ground." *Canadian Geotechnical Journal* 39(5): 1168–80.

Zhu B. T., Jardine R. and Foray P.. 2009. "The Use of Miniature Soil Stress Measuring Cells in Laboratory Applications Involving Stress Reversals." *Soils and Foundations, Japanese Society of Soil Mechanics and Foundation Engineering*. 49(5):675-688.

Appendix A

(Sensors used)

1) Miniature Stress Sensors – EPB - PW

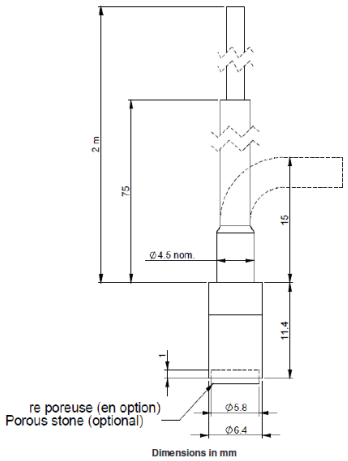

STANDARD RANGES

Ranges (FS)		Pressure Reference Sealed	Pressure Limit	Sensitivity "FSO" (nom.)	CNL&H (%FS)	Thermal Zero Shift "TZS" (/50°C)
bar	psi					
1	15	•	4.5 x FS	5 mV/V	±1%	±4% FSO
1.5	25	•	3 x FS	7.5 mV/V	±1%	±2% FSO
3.5	50	•	2 x FS	10 mV/V	±1%	±2% FSO
7	100	•	2 x FS	12.5 mV/V	±0.5%	±1.5% FSO
15	250	•	2 x FS	12.5 mV/V	±0.5%	±1.5% FSO
35	500	•	2 x FS	12.5 mV/V	±0.5%	±1.5% FSO
70	1K	•	2 x FS	12.5 mV/V	±0.5%	±1.5% FSO

PERFORMANCE SPECIFICATIONS (typical values at temperature 23±3ºC)

PARAMETERS	VALUES
Supply Voltage	1 to 10Vdc regulated
Input Resistance	1000Ω nom.
Output Resistance	400Ω nom.
Non-Repeatability	±2.5% FSO
Thermal Sensitivity Shift "TSS" in CTR	±2% / 50°C [/100 ° F]
Operating Temperature Range (OTR)	-40°C to 80°C [-40 to 170 ° F]
Compensated temperature Range (CTR)	0°C to 60°C [32 to 140 ° F]
Zero Offset	±10 mV
Ingress Protection	IP68 – 10 meters (1bar)
CE conformance according to	EN 61010-1, EN 50081-1, EN 50082-1

Sensors are calibrated with 10Vdc power supply as standard.
For custom configurations, consult factory.

2) Stress sensors - KYOWA

PS

Miniature Pressure Sensors

●For Pressure Distribution Measurement ●50 kPa to 7 MPa

Thin Size Compact Lightweight

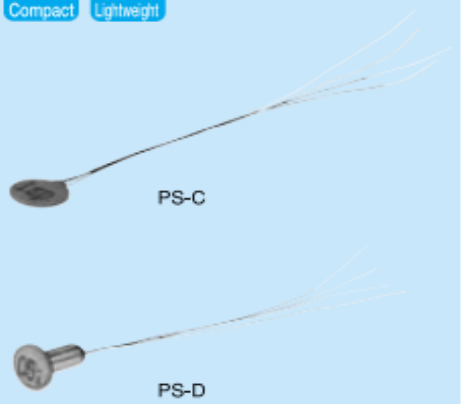

PS series is the strain gage pressure transducers having the bridge formed in the ultra-thin miniature structure. Installation is made with adhesive. Suitable for pressure distribution measurement by using multiple units.

Features

- Ultra-thin design
- Compact
- Wide range of rated capacities

Specifications

Performance

Rated Capacity:

Model		Rated Capacity	Natural Frequency (Approx.)
Cable Direction to Sensing Surface			
Horizontal	Vertical		
PS-05KC	PS-05KD	50 kPa	10 kHz
PS-1KC	PS-1KD	100 kPa	10 kHz
PS-2KC	PS-2KD	200 kPa	14 kHz
PS-5KC	PS-5KD	500 kPa	20 kHz
PS-10KC	PS-10KD	1 MPa	37 kHz
PS-20KC M2	PS-20KD M2	2 MPa	46 kHz
PS-30KC M2	PS-30KD M2	3 MPa	58 kHz
PS-50KC M2	PS-50KD M2	5 MPa	71 kHz
PS-70KC M2	PS-70KD M2	7 MPa	86 kHz

Measuring liquids of PS-20 to 70KC/D M2 are limited to oils.

Nonlinearity: Within ±1% RO
Hysteresis: Within ±1% RO
Rated Output:
0.25 mV/V (500 μm/m) or more (PS-05KC/D)
0.5 mV/V (1000 μm/m) or more (PS-1KC/D)
0.85 mV/V (1700 μm/m) ±30% (PS-2KC/D)
1 mV/V (2000 μm/m) ±20% (PS-5 to 70KC/D)
Note: Rated output is sorted to one of the classes divided by every 2% difference in output value. Since the rated output stated in the Test Data Sheet is the center value of the class, it may have a maximum error of ±1%.

Environmental Characteristics
Safe Temperature Range: −20 to 70°C
Compensated Temperature Range: 0 to 50°C
Temperature Effect on Zero Balance:
Within ±0.8% RO/°C (PS-05KC/D)
Within ±0.4% RO/°C (PS-1KC/D)
Within ±0.3% RO/°C (PS-2KC/D)
Within ±0.2% RO/°C (PS-5 to 70KC/D)
Temperature Effect on Output:
Within ±0.3%/°C (PS-05 to 2KC/D)
Within ±0.2%/°C (PS-5to 70KC/D)

Electrical Characteristics
Safe Excitation Voltage: 3 VAC or DC
Recommended Excitation Voltage: 1 to 2 VAC or DC
Input Resistance: 350 Ω ±10%
Output Resistance: 350 Ω ±10%
Cable: Polyurethane coated copper wires, 0.1 mm diameter (0.08 mm diameter with PS-05KD & 1KD) by 5 cm long, soldering finish at each tip (Shield wire is not connected to mainframe.)

Mechanical Properties
Safe Overload Rating: 150% (100% with PS-70KC/D M2)
Materials: Metallic finish
Weight: Approx. 0.5 g ±20% (including cable)
Dedicated Adhesive: RC-19 (Request when ordering, charge-free)

Dimensions

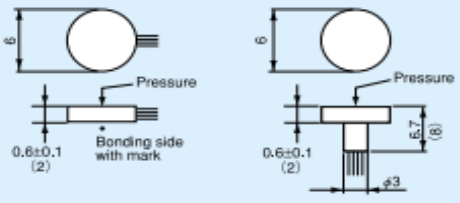

PS-C PS-D

Figures in parentheses are for PS-20 to 70KC/D M2.

3) LVDT_VE

Fiches produits VJT/0270-0271

CAPTEURS DE DEPLACEMENT
Type LSCT

SPECIFICATIONS

- ***Capteurs analogiques***
- ***Courses de 10 à 100mm***
- ***Grande précision 0.1% EM***
- ***Résolution infinie***

Code	Course	Précision
VJT /0270	10 mm	+/-0.01 mm
VJT /0271	25 mm	+/-0.025 mm
VJT / 0272	50 mm	+/-0.05 mm
VJT / 0273	100 mm	+/-0.1mm

Description :

L'instrument est constitué d'un corps de section circulaire de courses variées.

Il est utilisé dans différentes applications et nécessite un support approprié :

- monté sur le piston d'une cellule triaxiale : dia.25 ou 15,5 mm,
- monté dans un anneau dynamométrique en parallèle au comparateur,
- installé sur un appareil de mesure de variations de volume...
- Nous consulter !

Caractéristiques techniques :

Courses :	10-25-50-100mm
Précision :	+/- 0.1% EM
Effet de la température :	négligeable
Conditions d'utilisation :	de -10°C à +60°C
Alimentation :	entre 2 et 10 VDC
Signal de sortie PE :	de 3.6 à 7mV/V
Force du ressort :	250g pour les 10-25mm
Force du ressort :	300g pour les 50-100mm
Construction :	robuste en acier inox
Poids :	de 140 à 200g
Câble :	de 2m
Connecteur :	DIN 5 broches

1) Force Sensor (F_VC and F_VE)

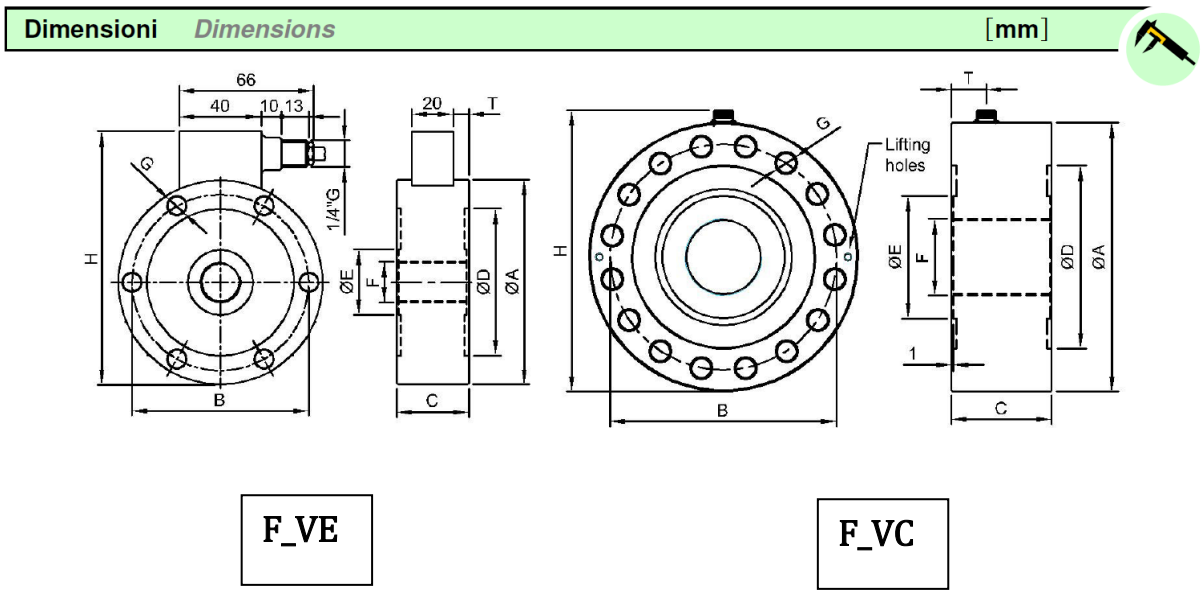

Dati Tecnici — *Technical Data*

Classe di precisione: **ISO 376**	*Accuracy class: ISO 376*	1					
CARICO NOMINALE	*NOMINAL LOAD*	5-10-25-50[1] kN	50 kN 100 kN	200 kN 300 kN	500 kN	750kN 1 MN	2 MN	3 MN[2] 5 MN[2]
ERRORI RELATIVI (**al valore letto**)	*RELATIVE ERRORS (at reading)*							
a) ripetibilità 0°-120°-240° (b)	*a) repeatability 0°-120°-240° (b)*	≤ ±0.145%[3]						
b) interpolazione (fc)	*b) interpolation (fc)*	≤ ±0.090%[3]						
c) reversibilità (u)	*c) reversibility (u)*	≤ ±0.240%[3]						
d) zero (fo)	*d) zero (fo)*	≤ ±0.030% F.S.						
LINEARITA'	*LINEARITY*	≤ ±0.05% F.S.						
ISTERESI	*HYSTERESIS*	≤ ±0.05% F.S.						
EFFETTO DELLA TEMPERATURA (10°C)	*TEMPERATURE EFFECT (10°C)*							
a) sullo zero	*a) on zero*	≤ ±0.028% F.S.						
b) sulla sensibilità	*b) on sensitivity*	≤ ±0.024% F.S.						
EFFETTO CARICO TRASVERSALE:	*EFFECT OF TRANSVERSE LOAD:*							
a) al 10% del carico nominale	*a) at 10% of nominal load*	≤ ±0.030% F.S.						
SENSIBILITA' NOMINALE	*NOMINAL SENSITIVITY*	2mV/V[4]						
TOLLERANZA DI CALIBRAZIONE	*SENSIVITY TOLERANCE*	≤ ±0.1% F.S.						
CARICO NOMINALE	*NOMINAL LOAD*	**5-10-25-50-100-200-300 kN**						
RESISTENZA DI INGRESSO	*INPUT RESISTANCE*	800 ± 20Ω						
RESISTENZA DI USCITA	*OUTPUT RESISTANCE*	705 ± 2Ω						
CARICO NOMINALE	*NOMINAL LOAD*	**500-750-1000-2000-3000-5000 kN**						
RESISTENZA DI INGRESSO	*INPUT RESISTANCE*	430 ± 20Ω						
RESISTENZA DI USCITA	*OUTPUT RESISTANCE*	352 ± 2Ω						
RESISTENZA DI ISOLAMENTO	*INSULATION RESISTANCE*	> 5 GΩ						
BILANCIAMENTO DI ZERO	*ZERO BALANCE*	≤ ± 1% F.S.						
ALIMENTAZIONE DI RIFERIMENTO	*RECOMENDED SUPPLY VOLTAGE*	10 V						
ALIMENTAZIONE NOMINALE	*NOMINAL SUPPLY VOLTAGE RANGE*	1-15 V						
ALIMENTAZIONE MAX.	*MAXIMUM SUPPLY VOLTAGE*	18 V						
VALORI MECCANICI LIMITE	*MECHANICAL LIMIT VALUES*							
RIFERITI AL CARICO NOMINALE :	*REFERRED TO NOMINAL LOAD :*							
a) carico di servizio	*a) service load*	120%						
b) carico limite	*b) max permissible load*	150%						
c) carico di rottura	*c) breaking load*	>300%						
d) massimo carico trasversale	*d) max transverse load*	100%						
e) carico dinamico limite	*e) max permissible dynamic load*	75%[5]						
Freccia max. al carico nominale (mm)	*Displacement at nominal load (mm)*	~0.06	~0.09	~0.17	~0.17	~0.23	~0.21	~0.21
TEMPERATURA DI RIFERIMENTO	*REFERENCE TEMPERATURE*	+23°C						
CAMPO NOMINALE DI TEMPERATURA	*TEMPERATURE NOMINAL RANGE*	-10 / +40 °C						
TEMPERATURA DI ESERCIZIO	*SERVICE TEMPERATURE*	-10 / +70 °C						
TEMPERATURA DI STOCCAGGIO	*STORAGE TEMPERATURE*	-20 / +80 °C						
PESO (kg)	*WEIGHT (kg)*	1.60	2.45	5.80	6.80	16.5	35	63
CLASSE DI PROTEZIONE (EN 60529)	*PROTECTION CLASS (EN 60529)*	IP67						
MATERIALE DINAMOMETRO	*EXECUTION MATERIAL*	Acciaio Inox / *Stainless Steel*						
LUNGHEZZA CAVO	*CABLE LENGTH*	5 m						
VITI DI FISSAGGIO:	*FIXING SCREWS:*							
a) diametro	*a) diameter*	M8	M10	M16	M16	M24	M24	M27
b) classe di resistenza	*b) resistance class*	12.9	12.9	12.9	12.9	12.9	12.9	12.9
c) coppia di serraggio (Nm)	*c) tightening torque (Nm)*	40	70	368	368	460	460	1500

2) Conditioner (Connected with F_VE)

ClipX®

BM40, BM40PB, BM40IE
Amplificateur de mesure industriel

Caractéristiques spécifiques

- Voie de mesure librement configurable avecparamétrage de la voie par TEDS
- Raccordement de 7 types de capteurs avec fréquence d'échantillonnage de 19,2 kHz
- Classe de précision jusqu'à 0,01 avec conversion A/N 32 bits
- 4 E/S numériques et 1 sortie analogique (tension/courant commutable)
- Jusqu'à 6 modules juxtaposables avec transfert de données par bus ClipX
- Voies de calcul internes (fonctions intelligentes)
- OPC UA, Profinet (IRT/RT), EtherCAT®, EtherNet/IP™, PROFIBUS (DPV1)
- Utilisation simple par serveur Web intégré avec 3 niveaux d'utilisateurs
- Boîtier métallique robuste et compact à monter sur rail DIN

Caractéristiques techniques

Synoptique

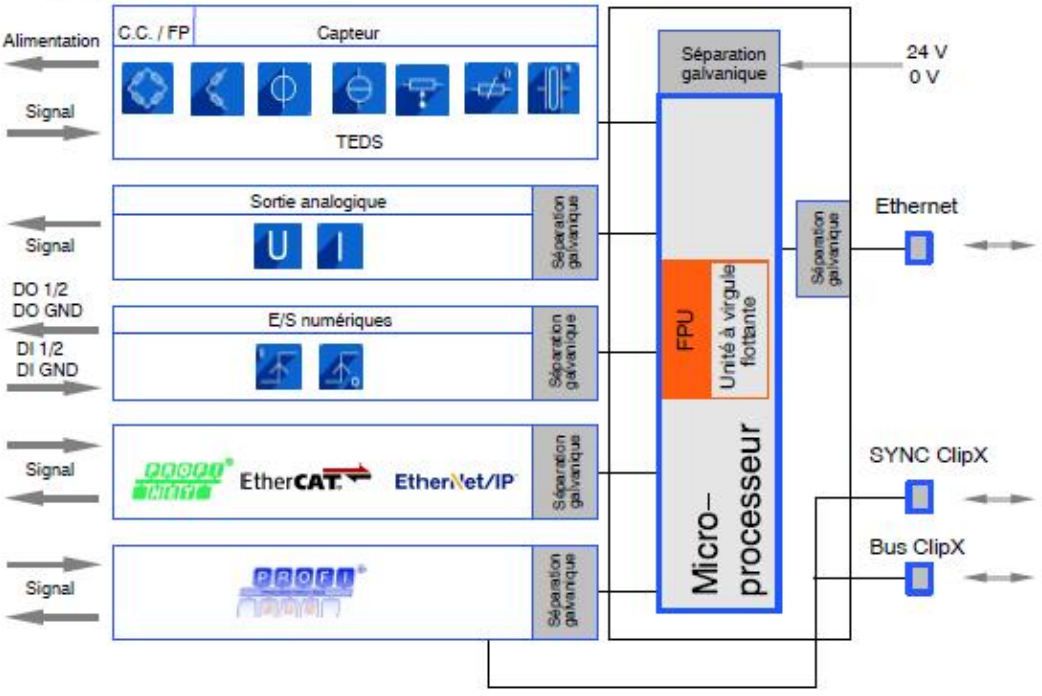

Appendix B

List of Cyclic CPT tests performed on sand

Test ID	Saturation	Location	Sample Preparation	RD (%)	Stress kPa	Depth cm	$\alpha_{F,Const}$	$\alpha_{F,max}$	$\alpha_{F,min}$	f (hZ)
1	Dry	Small bucket	Dry Deposition	-	-	5	0.8	1	0.6	1
2	Saturated	Small bucket	Dry Deposition	-	-	5	0.8	1	0.6	1
3	Saturated	Small bucket	Dry Deposition	-	-	5	0.8	1	0.6	1
4	Saturated	Small bucket	Dry Deposition	-	-	5	0.8	1	0.6	1
5	Dry	Small bucket	Dry Deposition	-	-	5	0.8	1	0.6	1
6	Dry	Small bucket	Dry Deposition	-	-	5	0.8	1	0.6	1
7	Dry	Small bucket	Dry Deposition	-	-	5	0.8	1	0.6	1
8	Dry	Small bucket	Dry Deposition	-	-	5	-	-	-	-
9	Dry	Small bucket	Dry Deposition	-	-	5	0.7	0.7	0.4	1
10	Dry	Small bucket	Dry Deposition	-	-	5	0.7	0.7	0.4	1
11	Dry	Small bucket	Dry Deposition	-	-	5	-	-	-	-
12	Saturated	Small bucket	Dry Deposition	-	-	5	0.7	0.7	0.4	1
13	Saturated	Small bucket	Dry Deposition	-	-	5	0.8	1	0.6	1
14	Saturated	Small bucket	Dry Deposition	-	-	5	0.8	1	0.6	1
15	Saturated	Small bucket	Dry Deposition	-	-	5	0.6	cm	0.4	1
16	Saturated	Small bucket	Dry Deposition	-	-	5	0.5	0.7	0.4	1
17	Saturated	Small bucket	Dry Deposition	-	-	5	0.5	0.7	0.4	1
18	Saturated	Small bucket	Dry Deposition	-	-	5	0.8	0.7	0.4	1
19	Saturated	Small bucket	Dry Deposition	-	-	5	0.8	0.7	0.5	1
20	Saturated	Small bucket	Dry Deposition	-	-	5	0.8	0.7	0.5	1

Test ID	Saturation	Location	Sample Preparation	RD (%)	Stress kPa	Depth cm	$\alpha_{F,Const}$	$\alpha_{F,max}$	$\alpha_{F,min}$	f (hZ)
21	Saturated	Small bucket	Dry Deposition	-	-	5	0.8	0.8	0.4	1
22	Saturated	Small bucket	Dry Deposition	-	-	5	0.6	0.6	0.4	1
23	NA	Small bucket	Dry Deposition	-	-	5	-	-	-	-
24	Saturated	Small bucket	Dry Deposition	-	-	5	0.7	0.7	0.4	1
25	Saturated	Small bucket	Dry Deposition	-	-	5	0.7	0.7	0.4	1
26	Saturated	Small bucket	Dry Deposition	-	-	5	0.7	0.7	0.4	1
27	Saturated	Small bucket	Dry Deposition	-	-	5	0.7	0.7	0.4	1
28	Saturated	Small bucket	Dry Deposition	-	-	5	0.7	0.7	0.4	1
29	Saturated	Small bucket	Dry Deposition	-	-	5	0.6	0.78	0.42	1
30	Saturated	Small bucket	Dry Deposition	-	-	5	0.6	0.78	0.42	1
31	Saturated	Small bucket	Dry Deposition	-	-	5	0.6	0.78	0.42	1
32	Saturated	Small bucket	Dry Deposition	-	-	5	0.6	0.78	0.42	1
33	Saturated	Small bucket	Dry Deposition	-	-	5	0.6	0.78	0.42	1
34	Saturated	Small bucket	Dry Deposition	-	-	5	0.6	0.78	0.42	1
35	Saturated	Small bucket	Dry Deposition	-	-	5	0.6	0.78	0.42	1
36	Saturated	Small bucket	Dry Deposition	-	-	5	-	-	-	-
37	Saturated	Small bucket	Dry Deposition	-	-	5	-	-	-	-
38	Saturated	Small bucket	Dry Deposition	-	-	5	-	-	-	-
39	Saturated	Small bucket	Dry Deposition	-	-	5	-	-	-	-
40	Saturated	Small bucket	Dry Deposition	-	-	5	-	-	-	-
41	Saturated	Calibration Chamber	Slurry Deposition	30%	75	15	0.45	0.75	0.15	1
42	Saturated	Calibration Chamber	Slurry Deposition	30%	75	25	0.6	0.78	0.42	1
43	Saturated	Calibration Chamber	Slurry Deposition	30%	75	31	0.6	0.78	0.42	1

Test ID	Saturation	Location	Sample Preparation	RD (%)	Stress kPa	Depth cm	$\alpha_{F,Const}$	$\alpha_{F,max}$	$\alpha_{F,min}$	f (hZ)
44	Saturated	Calibration Chamber	Slurry Deposition	30%	75	41	0.6	0.78	0.42	1
45	Saturated	Calibration Chamber	Slurry Deposition	30%	75	59	0.6	0.78	0.42	1
46	Saturated	Calibration Chamber	Slurry Deposition	30%	75	65	0.6	0.78	0.42	1
47	Saturated	Calibration Chamber	Slurry Deposition	30%	75	75	0.6	0.78	0.42	1
48	Saturated	Calibration Chamber	Slurry Deposition	34%	75	10	0.6	0.78	0.42	1
49	Saturated	Calibration Chamber	Slurry Deposition	34%	75	13	0.6	0.85	0.35	1
50	Saturated	Calibration Chamber	Slurry Deposition	34%	75	15	0.6	0.85	0.35	1
51	Saturated	Calibration Chamber	Slurry Deposition	34%	75	26	0.6	0.78	0.42	1
52	Saturated	Calibration Chamber	Slurry Deposition	34%	75	42	0.5	0.65	0.35	1
53	Saturated	Calibration Chamber	Slurry Deposition	34%	75	58	0.5	0.65	0.35	1
54	Saturated	Calibration Chamber	Slurry Deposition	34%	75	74	0.6	0.85	0.35	1
55	Saturated	Calibration Chamber	Slurry Deposition	34%	75	90	0.6	0.8	0.4	1
56	Saturated	Calibration Chamber	Slurry Deposition	34%	-	-	-	-	-	-
57	Saturated	Calibration Chamber	Slurry Deposition	40%	150	10	0.8	0.8	0.4	1
58	Saturated	Calibration Chamber	Slurry Deposition	40%	150	28.5	0.6	0.78	0.42	1
59	Saturated	Calibration Chamber	Slurry Deposition	40%	150	42	0.5	0.65	0.35	1
60	Saturated	Calibration Chamber	Slurry Deposition	40%	-	-	-	-	-	-
61	Saturated	Calibration Chamber	Slurry Deposition	40%	150	58	0.5	0.65	0.35	1
62	Saturated	Calibration Chamber	Slurry Deposition	40%	150	74	0.6	0.85	0.35	1
63	Saturated	Calibration Chamber	Slurry Deposition	40%	150	82	0.3	0.5	0.4	1

Test ID	Saturation	Location	Sample Preparation	RD (%)	Stress kPa	Depth cm	$\alpha_{F,Const}$	$\alpha_{F,max}$	$\alpha_{F,min}$	f (hZ)
64	Saturated	Calibration Chamber	Slurry Deposition	40%	150	90	0.6	0.8	0.4	1
65	Saturated	Calibration Chamber	Slurry Deposition	40%	150	-	-	-	-	-
66	Dry	Calibration Chamber	Dry Compaction	55%	75	7.5	0.6	0.78	0.42	
67	Dry	Calibration Chamber	Dry Compaction	55%	75	-	-	-	-	-
68	Dry	Calibration Chamber	Dry Compaction	55%	75	-	-	-	-	-
69	Saturated	Calibration Chamber	Dry Compaction	50%	75	10	0.6	0.78	0.42	1
70	Saturated	Calibration Chamber	Dry Compaction	50%	75	25	0.6	0.65	0.35	1
71	Saturated	Calibration Chamber	Dry Compaction	50%	75	35	0.6	0.85	0.35	1
72	Saturated	Calibration Chamber	Slurry Deposition	46%	150	10	0.6	0.78	0.42	1
73	Saturated	Calibration Chamber	Slurry Deposition	46%	150	26	0.6	0.78	0.42	1
74	Saturated	Calibration Chamber	Slurry Deposition	46%	150	42	0.5	0.65	0.35	1
75	Saturated	Calibration Chamber	Slurry Deposition	46%	150	58	0.5	0.65	0.35	1
76	Saturated	Calibration Chamber	Slurry Deposition	46%	150	70	0.6	0.85	0.35	1
77	Saturated	Calibration Chamber	Slurry Deposition	46%	150	82	0.6	0.8	0.4	1
78	Saturated	Calibration Chamber	Moist Tamping	10%	75	10±5	0.6	0.78	0.42	1
79	Saturated	Calibration Chamber	Moist Tamping	10%	75	20±5	0.6	0.78	0.42	1
80	Saturated	Calibration Chamber	Moist Tamping	10%	75	32±5	0.5	0.65	0.35	1
81	Saturated	Calibration Chamber	Moist Tamping	10%	75	46±5	0.5	0.65	0.35	1
82	Saturated	Calibration Chamber	Moist Tamping	10%	75	56±5	0.6	0.85	0.35	1

Test ID	Saturation	Location	Sample Preparation	RD (%)	Stress kPa	Depth cm	$\alpha_{F,Const}$	$\alpha_{F,max}$	$\alpha_{F,min}$	f (hZ)
83	Dry	Calibration Chamber	Dry Deposition - (overhanging bag)	34%	75	10	0.6	0.78	0.42	1
84	Dry	Calibration Chamber	Dry Deposition - (overhanging bag)	34%	75	23.5	0.6	0.78	0.42	1
85	Dry	Calibration Chamber	Dry Deposition - (overhanging bag)	34%	75	38.5	0.5	0.65	0.35	1
86	Dry	Calibration Chamber	Dry Deposition - (overhanging bag)	34%	75	44.5	0.5	0.65	0.35	1
87	Dry	Calibration Chamber	Dry Deposition - (overhanging bag)	34%	75	47	0.6	0.85	0.35	1
88	Dry	Calibration Chamber	Dry Deposition - (overhanging bag)	34%	75	57	0.6	0.85	0.35	0.1
89	Dry	Calibration Chamber	Dry Deposition - (overhanging bag)	34%	75	67	0.6	0.85	0.35	1
90	Dry	Calibration Chamber	Dry Deposition - (overhanging bag)	34%	75	72	0.6	0.85	0.35	1
91	Dry	Calibration Chamber	Dry Deposition - (overhanging bag)	34%	75	77	0.85	0.85	0.3	1
92	Dry	Calibration Chamber	Dry Deposition - (overhanging bag)	31%	150	10	0.6	0.78	0.42	1
93	Dry	Calibration Chamber	Dry Deposition - (overhanging bag)	31%	150	40.5	0.5	0.65	0.35	1
94	Dry	Calibration Chamber	Dry Deposition - (overhanging bag)	31%	150	45.5	0.5	0.65	0.35	1

Test ID	Saturation	Location	Sample Preparation	RD (%)	Stress kPa	Depth cm	$\alpha_{F,Const}$	$\alpha_{F,max}$	$\alpha_{F,min}$	f (hZ)
95	Dry	Calibration Chamber	Dry Deposition - (overhanging bag)	31%	150	50.5	0.6	0.78	0.42	0.1
96	Dry	Calibration Chamber	Dry Deposition - (overhanging bag)	31%	150	58.5	0.6	0.84	0.36	0.1
97	Dry	Calibration Chamber	Dry Deposition - (overhanging bag)	31%	150	67	0.6	0.85	0.35	1
98	Dry	Calibration Chamber	Dry Deposition - (overhanging bag)	31%	150	72	0.6	0.85	0.35	0.5
99	Dry	Calibration Chamber	Dry Deposition (buckets)	19%	85	10	0.6	0.78	0.42	1
100	Dry	Calibration Chamber	Dry Deposition (buckets)	19%	85	16	0.6	0.78	0.42	0.1
101	Dry	Calibration Chamber	Dry Deposition (buckets)	19%	85	26	0.5	0.65	0.35	1
102	Dry	Calibration Chamber	Dry Deposition (buckets)	19%	85	39	0.5	0.65	0.35	1
103	Dry	Calibration Chamber	Dry Deposition (buckets)	19%	85	55	0.6	0.85	0.35	1
104	Dry	Calibration Chamber	Dry Deposition (buckets)	19%	85	63	0.6	0.85	0.35	0.1
105	Dry	Calibration Chamber	Dry Deposition (buckets)	19%	85	75	0.6	0.8	0.4	1
106	Dry	Calibration Chamber	Dry Deposition (buckets)	19%	85	81	0.85	0.8	0.4	1
107	Dry	Calibration Chamber	Dry Deposition (buckets)	19%	85	85	0.9	0.8	0.4	1
108	Dry	Calibration Chamber	Dry Deposition (buckets)	19%	85	88	0.7	0.95	0.4	1

Test ID	Saturation	Location	Sample Preparation	RD (%)	Stress kPa	Depth cm	$\alpha_{F,Const}$	$\alpha_{F,max}$	$\alpha_{F,min}$	f (hZ)
109	Dry	Calibration Chamber	Dry Compaction	53%	85	10	0.6	0.78	0.42	1
110	Dry	Calibration Chamber	Dry Compaction	53%	85	26	0.6	0.78	0.42	1
111	Dry	Calibration Chamber	Dry Compaction	53%	85	40	0.5	0.65	0.35	1
112	Dry	Calibration Chamber	Dry Compaction	53%	85	50	0.6	0.85	0.35	1
113	Dry	Calibration Chamber	Dry Compaction	53%	85	66	0.6	0.8	0.4	1
114	Dry	Calibration Chamber	Dry Compaction	53%	85	82	0.85	0.85	0.4	1
115	Dry	Calibration Chamber	Dry Compaction	53%	0	92	0.6	0.6	0.3	1